Engineering Materials

Woon Siong Gan

New Acoustics Based on Metamaterials

Springer

Engineering Materials

The “Engineering Materials” series provides topical information on innovative, structural and functional materials and composites with applications in optical, electronical, mechanical, civil, aeronautical, medical, bio and nano engineering. The individual volumes are complete, comprehensive monographs covering the structure, properties, manufacturing process and applications of these materials. This multidisciplinary series is devoted to professionals, students and all those interested in the latest developments in the Materials Science field.

More information about this series at http://www.springer.com/series/4288

Woon Siong Gan

New Acoustics Based on Metamaterials

Springer

Woon Siong Gan
Acoustical Technologies Singapore Pte Ltd
Singapore
Singapore

ISSN 1612-1317 ISSN 1868-1212 (electronic)
Engineering Materials
ISBN 978-981-10-6375-6 ISBN 978-981-10-6376-3 (eBook)
https://doi.org/10.1007/978-981-10-6376-3

Library of Congress Control Number: 2017952002

Printed on acid-free paper

This Springer imprint is published by Springer Nature
The registered company is Springer Nature Singapore Pte Ltd.
The registered company address is: 152 Beach Road, #21-01/04 Gateway East, Singapore 189721, Singapore

To My Parents

Foreword

Acoustics is a classic field of inquiry that has enjoyed a strong revival during the past two decades, propelled mainly by the advent of phononic crystals and acoustic metamaterials, two newly developed research areas that focused on man-made structures with acoustic properties not commonly found in nature. Whereas phononic crystals denote periodic structures exhibiting frequency bandgaps in which there can be no propagating acoustic/elastic waves, acoustic metamaterials acquire their exotic characteristics as collective manifestations of local resonators. Both phononic crystals and acoustic metamaterials are composite structures comprising materials of different mass densities and hardness. In the case of acoustic metamaterials, however, the response of the composite to external excitations can differ from a rigid solid by having internal relative motions between the different material components. The past fifteen years have witnessed the novel capabilities that can arise from such locally resonant sonic materials, which are characterized not only by their subwavelength physical size, but also by their effective mass density and bulk modulus that can exhibit negative values. The unusual phenomena exhibited by the phononic crystals and acoustic metamaterials, as well as their underlying physics, are the subjects of the present volume—New Acoustics.

The author, Dr. Woon Siong Gan, was trained as a physicist, with a Ph.D. degree in acoustics from Imperial College London. After doing postdoc at International Centre for Theoretical Physics, Trieste, Italy, he returned to Singapore and taught at Nanyang University from 1970 to 1979. He was a practicing acoustic consultant for ten years, from 1979 to 1989, and after that he founded Acoustical Technologies Singapore Pte Ltd. The contents of the present volume very much reflect this rather unique background of the author—a combination of basic theory and practical applications. The initial few chapters lay the theoretical basis of the "new acoustics", a term coined to denote the recent developments enabled by acoustic metamaterials, followed by chapters with each one devoted to some specific application. Underlying these applications are some unifying principles, such as the coordinate transformation of the acoustic wave equation and its one-to-one equivalence to a system where the material constants of the transformed system can be point-wise determined by those of the original untransformed system, plus the Jacobian matrix

of the coordinate transformation. This mathematical equivalence, denoted transformation acoustics, offers tremendous freedom in designing structures that can, for example, "cloak" objects and achieving effects that were thought impossible previously. However, a basic requirement for the successful implementation of such a structure, with mathematically transformed material constants, is the availability of material properties that can take all possible values. That is where metamaterials come in—they offer the freedom of material design not available before, such as negative refractive index and negative (dynamic) mass density. The latter may seem counter-intuitive at first, but the effect can be easily demonstrated with a mechanical system comprising local resonators, so that when the external forcing is out of phase with the internal resonances, large relative motion of the components can result, with the momentum of the internal resonators opposing the externally exerted force. Similarly, in an array of Helmholtz resonators, the overall bulk modulus can appear negative. Such negative values of the material properties have to be interpreted in an effective medium sense, where the intend structure of the system are "homogenized", i.e. averaged over. As far as an external observed is concerned, this may not be a problem since only the external response of the system is sensed. And if one can realize a system where both the effective mass density and bulk modulus are simultaneously negative, then negative index becomes possible. As shown by the Russian physicist Veselago in 1967, if a material possesses negative index, then the phase velocity and group velocity would be in opposite directions. His prediction was realized experimentally about four decades later, with the realization of structures that can exhibit the strange behaviours implied by the negative index, one of which is that an obliquely incident plane wave will bend to the same side of the (planar) interfacial normal as the incident wave. Subsequently, J. Pendry at Imperial College London predicted the possibility of using negative index materials to break the classical resolution limit that is imposed by the finite wavelength. This work has stimulated a great deal of experimental interests in both optics and acoustics, and various schemes, some of them not even involving the negative index materials, were devised to show that resolution beyond the classical limit is indeed possible. In fact, it may be said that the greatest contribution of metamaterials lies in their liberating effect on thinking about what is possible in the manipulation of electromagnetic and acoustic waves. Above are just few of the many developments that can be traced to this effect, and the present volume gives a selection of those topics judged by the author to reflect not only the novelty, as advertised by the title of the book, but also their potential importance in applications. With the very fast advance of this whole area, this book can give the readers not only a timely vignette of the current landscape, but also serve as the basis for further development.

August 2016

Ping Sheng
HKUST, Clear Water Bay
Hong Kong

Contents

Chapter 1
Symmetry Properties of Acoustic Fields

Abstract W S Gan introduced symmetry properties of the acoustic field in 2007. This has been confirmed by the successful fabrication of the acoustical metamaterials, diverse applications of time reversal acoustics and that phonon is a Goldstone mode. The form invariance of the linear acoustic field equation demonstrates the symmetry properties of acoustic fields. Likewise, form invariance is also applicable to nonlinear acoustic field equations such as Burgers equation, Westervelt equation and Shapiro–Thurstone equation. The symmetry between the acoustic velocity field and stress field is a further demonstration of the symmetry properties of acoustic fields. Symmetry is the theoretical framework of acoustical metamaterials. The propagation of sound waves in fluids obeys both translational and rotational symmetry, whereas propagation of sound waves in solids obeys rotational symmetry but broken translational symmetry due to the discrete and periodic nature of the crystal gives rise to phonons. The scale invariance or symmetry property of the turbulence field also supports the symmetry properties of acoustic fields as turbulence field is intrinsically acoustic field considering that turbulence is the source of the aerodynamic noise.

1.1 Introduction

In 2007, Gan [1] proposed gauge invariance approach to acoustic this means introducing symmetry properties to acoustic fields. This has been confirmed by the successful fabrication of the acoustical metamaterials [2], the various applications of the time reversal symmetries of the acoustic fields [3], that phonon is a Goldstone mode [4] and the symmetry properties of the turbulence field which is basically acoustic field [5]. In the past, most works have been on the symmetry properties of the medium, e.g. the crystal and not on the symmetry property of the propagating sound wave. This will give a better understanding of the property of sound wave.

W.S. Gan, *New Acoustics Based on Metamaterials*, Engineering Materials,
https://doi.org/10.1007/978-981-10-6376-3_1

1.2 Sound Propagation in Solids

1.2.1 Derivation of Linear Wave Equation of Motion and Its Solutions

Our work will emphasize the mechanical and elastic properties of sound waves. We will start with the propagation of linear sound waves or infinitesimal amplitude sound waves in solids. First, the acoustic field equations of motion will be derived. There are two basic field equations. These will involve Newton's law of motion from mechanics and Hooke's law of the theory of elasticity. The first field equation is Newton's law of equation of motion given as

$$\nabla.\mathbf{T} = \rho \frac{\partial^2 \mathbf{u}}{\partial t^2} - \mathbf{F} \tag{1.1}$$

where **T** = stress, **u** = displacement, **F** = body force.

The second field equation is the strain-displacement relation related to Hooke's law given as

$$\mathbf{S} = \nabla_s \boldsymbol{u} \tag{1.2}$$

where **S** = strain.

In order to solve the two variables, u and **T**, a second equation is necessary and this is given by Hooke's law from the theory of elasticity states that the strain is linearly proportional to the stress. That is

$$T_{ij} = c_{ijkl}\mathrm{S}_{kl} \tag{1.3}$$

where $i, j, kl = x, y, z$

with summation over the repeated subscripts k and l. The microscopic spring constants c_{ijkl} in (1.3) are called elastic stiffness constants.

We consider source-free region, so **F** = 0. The next step is to eliminate **T** from (1.1) and (1.3). From (1.2) and (1.3), $\mathbf{T} = c_{ijkl} \nabla_s \mathbf{u} = c_{ijkl} \frac{\partial u}{\partial x}$, if only one dimension, x-direction is chosen. Substituting in (1.1), we obtain

$$c_{ijkl} \frac{\partial^2 u}{\partial x^2} = \rho \frac{\partial^2 u}{\partial t^2} \tag{1.4}$$

The above equation is also known as the Christoffel equation.

Equation (1.4) is the equation of a travelling wave and the solution can be given as

$$u = u_0 e^{i(\omega t \pm kx)} \tag{1.5}$$

which gives

$$\rho\omega^2 = c_{ijkl}k^2 \tag{1.6}$$

Phase velocity is given by v = ω/k. Thus for transverse (or shear) waves, the velocity is

$$v_s = \sqrt{\frac{c_{ijkl}}{\rho}} \tag{1.7}$$

1.2.2 *Symmetries in Linear Acoustic Wave Equations and the New Stress Field Equation*

Equation (1.2) can be written in terms of the particle velocity and compliance as

$$\nabla_s \mathbf{v} = s : \frac{\partial \mathbf{T}}{\partial t} \tag{1.8}$$

where s = compliance.

Acoustic wave equations can be obtained by eliminating either T or v from the acoustic field equations. Usually the stress field is eliminated since it is a tensor quantity and consists of six field components rather than three like a vector field.

For infinitesimal amplitude sound waves, the lossless acoustic field equations are given by (1.1) and (1.2). We will now eliminate the velocity field from (1.1) and (1.8).

Differentiating (1.8) with respect to t:

$$\nabla_s \frac{\partial v}{\partial t} = s : \frac{\partial^2}{\partial t^2}\mathbf{T} \tag{1.9}$$

with $\mathbf{F} = 0$ for source-free region, and taking the divergence of both sides of (1.1):

$$\nabla_{\mathbf{s}}(\nabla.\mathbf{T}) = \rho\nabla_s \frac{\partial \boldsymbol{v}}{\partial \boldsymbol{t}} \tag{1.10}$$

By the insertion of (1.9), we also have

$$\nabla_s(\nabla.\mathbf{T}) = \rho s : \frac{\partial^2}{\partial t^2}\mathbf{T}$$

or

$$\mathrm{c}\nabla_s(\nabla.\mathbf{T}) = \rho\frac{\partial^2}{\partial t^2}\mathbf{T} \tag{1.11}$$

This is a new stress equation. The potential and the applications of this equation have yet to be explored.

We also discover an important property. That is the acoustic wave Eqs. (1.4) and (1.11) are symmetrical in u and T. This symmetrical property can give rise to several simplications in the solving of acoustic wave equations.

1.3 Use of Gauge Potential Theory to Solve Acoustic Wave Equations

As analogous to the electromagnetic wave fields, we can also represent the acoustic particle velocity field in terms of the gauge potentials of gauge theory, that is in terms of the scalar potential ϕ and the vector potential $\mathbf{A}$. For isotropic media, which are always nonpiezoelectric, the Christoffel equation can be written as

$$c_{44}k^2\mathbf{v} + (c_{11} - c_{44})\mathbf{k}(\mathbf{k}.\mathbf{v}) = \omega^2\rho v \tag{1.12}$$

for an isotropic medium. This governs plane wave solutions with harmonic time variation. To obtain the general equation for plane wave solutions, the substitutions

$$\nabla \to -ik, \qquad \frac{\partial}{\partial t} \to i\omega$$

are inverted. This gives

$$c_{44}\nabla^2 v + (c_{11} - c_{44})\nabla(\nabla.v) = \rho\frac{\partial^2 v}{\partial t^2} \tag{1.13}$$

or

$$c_{11}\nabla(\nabla.v) - c_{44}\nabla\times\nabla\times v = \rho\frac{\partial^2 v}{\partial t^2} \tag{1.14}$$

where the vector identity

$$\nabla\times\nabla\times A = \nabla(\nabla.A) - \nabla^2 A \tag{1.15}$$

has been used to rearrange terms.

Solutions of (1.14) are obtained by using a gauge theory formulation of expressing **v** in terms of the gauge potentials, the scalar potential ϕ and the vector potential **A**

$$\mathbf{V} = \nabla\varphi + \nabla \times \boldsymbol{A} \tag{1.16}$$

Substitution of (1.16) in (1.14) gives

$$\nabla\left(c_{11}\nabla^2\varphi - \rho\frac{\partial^2\varphi}{\partial t^2}\right) - \nabla \times \left(c_{44}\nabla \times \nabla \times A + \rho\frac{\partial^2 A}{\partial t^2}\right) = 0 \tag{1.17}$$

Since $\nabla.\nabla \times A = 0$ and $\nabla \times \nabla\varphi = 0$

For the second term, the quantity in brackets is set equal to the gradient of an arbitrary function f:

$$c_{44}\nabla \times \nabla \times A + \rho\frac{\partial^2 A}{\partial t^2} = c_{44}\nabla f \tag{1.18}$$

Application of the identity (1.15) will convert (1.18) into:

$$\nabla(\nabla.A - f) - \nabla^2 A + \frac{1}{v_s^2}\frac{\partial^2 A}{\partial t^2} = 0 \tag{1.19}$$

where $v_s = \sqrt{\frac{c_{44}}{\rho}}$. Since f is arbitrary, it can always be chosen to cancel ∇. **A** in the first term on the left. The vector potential can thus be taken as a solution to the vector potential wave equation

$$\nabla^2\boldsymbol{A} - \frac{1}{v_s^2}\frac{\partial^2 A}{\partial t^2} = 0 \tag{1.20}$$

The first term in (1.17) is made zero by simply requiring that the scalar potential φ satisfies the following scalar potential wave equation:

$$\nabla^2\varphi - \frac{1}{v_s^2}\frac{\partial^2\varphi}{\partial t^2} = 0 \tag{1.21}$$

Equations (1.20) and (1.21) show that the linear wave equations are symmetrical in φ and **A**, same as for the case of the electromagnetic waves. Equations (1.20) and (1.21) are also of the same form as the Helmholtz wave equation, which confirms the analogy.

1.4 Gauge Theory Formulation of Sound Propagation in Solids

1.4.1 Translational Symmetry

So far the acoustic equations of motion derived are for the case of a stationary medium. In real world situations, usually the medium is moving. This is applied to the case when sound wave is propagating in solids and the unstressed state of the material is moving with time. Galilean transformation or Galilean symmetry is the type of gauge transformation which is applicable to sound wave propagation in solids. Gauge theory or gauge transformation includes both translational symmetry and rotational symmetry. Galilean transformation is translational symmetry. Kambe [6] derived gauge theory formulation for ideal fluid flows based on Galilean transformation and covariant derivative which are properties of gauge transformation and intrinsic properties of acoustic equation of motion. Here, we extended the gauge principles to sound propagation in solids. Kambe's [6] work involves only translational symmetry or Galilean transformation. Here, we cover also rotational symmetry. The analogy in the electromagnetic counterpart is that covariant derivative is also intrinsic properties of Maxwell's equations. However, due to the different nature of sound waves and electromagnetic waves, covariant derivative for Maxwell's equations leads to Lorentz transformation and covariant derivative for acoustic equation of motion leads to Galilean transformation. In fact, the Lorentz transformation reduces to the Galilean transformation when the medium is moving at a velocity much less than the velocity of light.

First, we have a brief description of the gauge principle. In gauge theory, there is the global gauge invariance and the local gauge invariance. Local gauge invariance is more stringent than the global gauge invariance. There is Weyl's gauge principle which states that when the original Lagrangian is not locally gauge invariant, the principle of local gauge invariance requires a new gauge field to be introduced in order to acquire local gauge invariance, and the Lagrangian is to be altered by replacing the partial derivative with the covariant derivative. Covariant derivative is necessary for local gauge invariance as well as to fulfil Galilean transformation. This can be illustrated as follows:

$$D_t := \partial_t + G \tag{1.22}$$

where D_t = covariant derivative, and G the new gauge field.

We will use Galilean transformation which describes sound propagation in solids. The symmetries to be investigated here are the translational symmetry and the rotational symmetry. First, we consider translational symmetry without local rotation. A translational transformation from one coordinate system A to another A' moving with a relative velocity R is called a Galilean transformation in Newtonian mechanics. The transformation law is defined by

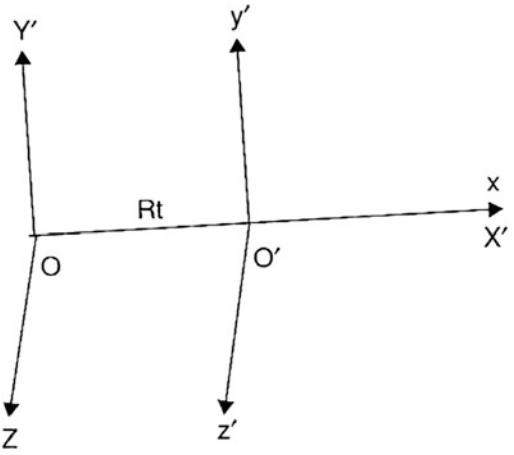

Fig. 1.1 Coordinate system moving with velocity R translationally

$$x = (t, x) \rightarrow \quad x' = (t', x') = (t, x - Rt) \tag{1.23}$$

Please refer to Fig. 1.1.

Kambe [6] has derived for local Galilean transformation, the covariant derivative given as

$$D_t = \partial_t + (v.\nabla) \tag{1.24}$$

1.4.2 Introduction of Covariant Derivative to the Infinitesimal Amplitude Sound Wave Equation

Replacing the partial derivative in (1.1) by the covariant derivative given by (1.24), we have

$$\nabla.\boldsymbol{T} = \rho\left(\frac{\partial v}{\partial t} + (\boldsymbol{v}.\nabla)\mathbf{v}\right) - \mathbf{F} \tag{1.25}$$

If only one direction, x-direction is chosen, and with $\mathbf{F} = 0$ for source-free region, (1.25) can be reduced to a simpler form as shown below:

$$\frac{\partial^2 u}{\partial x'^2} = \rho\frac{\partial^2 u}{\partial t^2} + \rho\frac{\partial u}{\partial t}\frac{\partial^2 u}{\partial x' \partial t} \tag{1.26}$$

where x' = moving coordinate given by $x' = x - Rt$.

We realize that with the introduction of the covariant derivative, there is the additional second term on the right-hand side of the equation. So far no one has attempted on the exact analytical solution of this equation yet.

1.4.3 Introduction of Covariant Derivative to the Large Amplitude Sound Wave Equation

We apply the covariant derivative (1.24) to the nonlinear wave equation given by

$$\ddot{u} = \frac{M_2}{\rho}\frac{\partial^2 u}{\partial x^2}\left[1 + \frac{M_3}{M_2}\frac{\partial u}{\partial x}\right] \tag{1.27}$$

we obtain

$$C_{ijkl}M_2\frac{\partial^2 u}{\partial x'^2}\left[1 + \frac{M_3}{M_2}\frac{\partial u}{\partial x'}\right] = \rho\left(\frac{\partial^2 u}{\partial t^2} + \frac{\partial u}{\partial t}\frac{\partial^2 u}{\partial x'\partial t}\right) \tag{1.28}$$

The introduction of the covariant derivative only introduces the same additional term on the right-hand side of the equation as in the case for the linear wave equation in (1.26). Again, so far no one has obtained the exact analytical solution of this equation yet.

1.4.4 Local Rotational Symmetry

Kambe's [6] work does not include the local rotational symmetry. Here, we include the rotational symmetry. This is described by Weyl's [7] gauge transformation which involves at every spacetime point, also called $U(1)$ rotation essentially a simple rotation in the complex plane. This can be illustrated by the invariance of the compliance and stiffness of an isotropic solid under same coordinate rotation at every point in the spacetime. For an isotropic solid, the form of coordinate rotation is different at different points in the spacetime. For an isotropic solid, the sound velocity and the stress field are the same in all directions. This is a consequence of the rotational symmetry of the velocity field.

1.5 Symmetry Is the Theoretical Framework of Acoustical Metamaterial

The symmetry in acoustical metamaterials can be manifested in two aspects: one is the intrinsic symmetry property of the medium and another is the symmetry property of the acoustic field. Metamaterials are artificial materials with periodic and repetitive structures and hence can be considered as artificial crystals. Since crystals, they will have symmetry properties. Metamaterials were first proposed by Veselago [8] in 1968 as materials with negative permeability and negative permittivity and electromagnetic wave was used as the propagating wave. His concept

was originating from the dispersion relation for isotropic material, n = index of refraction = $\pm\sqrt{\mu\varepsilon}$ where μ = permeability, ε = permittivity which has form invariance irrespective of positive or negative values of μ and ε. However, both positive and negative signs occur in front of the square root sign and there is ambiguity on whether the positive or negative sign has to be chosen. This type of metamaterial with negative μ and ε is also known as left-handed material or negative material. This is because the Poynting vector will be in the negative direction, and the phase velocity will be opposite in direction to the Poynting vector. The idea of left-handed metamaterial was subsequently extended to acoustic wave in 2004 by Li et al. [9]. However, bandgap metamaterials were first proposed in the form of photonic crystals [10] and phononic crystals [11] in the 1990s. They are artificial crystals.

The symmetry property of the acoustic fields was given in Sect. 1.4.

1.5.1 Rotational Symmetry and Theory of Elasticity

The concept of negative mass density and negative bulk modulus is an extension of the positive mass density and positive bulk modulus of the theory of elasticity to the negative mass density and negative bulk modulus depending on rotational symmetry and coordinate transformations with 180° coordinates rotation in the clockwise direction. In Hooke's law, within the linearity limit, stress/strain = elastic constant, c_{ij}. c_{ij} has rotational symmetry and is invariant with coordinates transformation. It has global $U(1)$ symmetry for isotropic solids where the velocity field and the stress field are the same in all directions. For anisotropic solids, there is local symmetry where each point in spacetime has its own rotational symmetry and independent of each other but governed by the acoustic equation of motion.

1.6 Local Gauge Invariance

A gauge theory is a type of field theory in which the Lagrangian is invariant under a continuous group of local transformation. Many powerful theories in physics are described by Lagrangians that are invariant under a transformation identically perform at every point in the space in which the physical processes occur. These are said to have a local symmetry. The requirement of local symmetry, the cornerstone of gauge theory is a stricter constraint. In fact, a global symmetry is just a local symmetry whose group's parameters are fixed in spacetime. So far most of the theories and applications of acoustical metamaterials and phononic crystals are all based on global gauge invariance.

The application of gauge invariance or gauge symmetry concept has the advantage of being able to extend to local symmetry unlike the Veselago [8] paper

which is based on the dispersion relation and unable to extend to local symmetry. Local gauge invariance is an important topic, shown in the Yang Mills theory [12], the theoretical foundation of the Standard Model of particle physics is an example of extending global transformation to local transformation. The first equation of Yang Mills paper [12], the equation of global transformation is the same as the equation used in the elastic fields transformation in crystals. Hence by extending global gauge transformation to local symmetry for acoustic fields will also yield remarkable consequences.

1.7 Covariant Derivative

First, we shall give a brief description of the gauge principle. In gauge theory, there are global gauge invariance and local gauge invariance. Global gauge invariance requires symmetry of the object as a whole, whereas in local gauge invariance demands symmetry of each point in spacetime. Hence, local gauge invariance is more stringent than global gauge invariance. Maxwell's equations of electromagnetic theory are an example of local gauge invariance. Weyl's [7] gauge principle states that when the original Lagrangian is not locally gauge invariant, a new gauge field must be introduced in order to satisfy local gauge invariance, and the Lagrangian is then to be altered by replacing the partial derivative with the covariant derivative. The introduction of a covariant derivative is necessary for local gauge invariance. It is the theoretical framework of local gauge invariance. The well-known Yang Mills theory [12] and the Higgs theory [13] can both be derived by using covariant derivative approach [14].

In acoustics, there are two types of covariance, the Galilean covariance and the manifest covariance. The Galilean covariance is a form of local gauge invariance which takes account of continuous translational symmetry for sound propagation in solids. The broken translational symmetry gives rise to the Goldstone mode which is phonon for acoustics. Manifest covariance, on the other hand, takes account of nonlinear interaction and coupling of sound wave with the lattice resulting in nonlinear phonon-phonon interaction.

For manifest covariance, the coupling between the sound wave and the crystal lattice has to be considered. This will be in the form of phonon-phonon interaction and the form of the covariant derivative will be given by:

$$D = \partial + i\varepsilon\vec{A} \tag{1.29}$$

where ε = coupling constant, and $\vec{A}$ = vector potential or vector gauge field.

In the global transformation or global gauge invariance, we have

$$\varphi' = G\varphi \tag{1.30}$$

where φ is a vector of fields and φ' is the vector of fields after transformation and G = transformation matrix. For local gauge transformation or local transformation or demanding the Lagrangian to have local gauge invariance requires that the G matrix which were earlier constant should be allowed to become function of the spacetime coordinate χ. Unfortunately, the G matrix does not pass through the derivative when $G = G(\chi)$:$\partial_\mu(G) = G(\partial_{\mu\varphi})$. The failure of the derivative to commute with G introduces an additional term (in keeping with the product rule), which spills the invariance of the Lagrangian. In order to rectify this we define a new derivative operator, the manifest covariant derivative such that the derivative of a Gauge transformation will be identical with φ:

$$(D_\mu \varphi)' = \mathrm{G} D_\mu \varphi \tag{1.31}$$

where $D_\mu = \partial_\mu + i\varepsilon \vec{A}$.

Here, we would like to mention that Pauli called gauge transformation of the first kind to the one applied to scalar field only while the compensating transformation in the vector gauge field is said to be a transformation of the second kind. Gauge transformation of the first kind is in fact, the global transformation and gauge transformation of the second kind in fact is local transformation.

1.8 Discovery of Anisotropy as a Form of Local Symmetry

Crystal, both natural crystal and phononic crystal have repetitive patterns and periodic structures and so have symmetry properties. Their symmetry is microscopic symmetry. For anisotropic crystals, the symmetry changes at every point in spacetime and so is local symmetry. This is different from isotropy which is global symmetry such as symmetry of elastic properties in isotropic solids. There are two basic kinds of symmetry operations that transform a crystal lattice into itself:

1. Translations, which displace the lattice as a whole. This is global symmetry.
2. Point transformations, which leave at least one point in the lattice unchanged. This is local symmetry.

Since the compliance and stiffness matrices relate stress and strain fields at the same point in a crystal, their symmetry properties can be obtained from the point symmetry transformation alone. These transformations include rotation, reflection, inversion, rotation-inversion and rotation-reflection symmetries for anisotropic media are local and so are much more complicated than that for the isotropic case.

1.9 Role of Symmetry Properties of Acoustic Field in the Design of a Phononic Structure

Phononic crystals are periodic structures which possess spectral gaps primarily based on avoided crossing due to the Bloch symmetry. The spectral gaps that occur are due to the Bragg like scattering. The Bloch's theorem is mathematically actually a manifestation of discrete translational symmetry. The creation of phononic metamaterial possessing multiple complete spectral gaps is very interesting both from a fundamental and application perspective, allowing for the study of nonlinear phonon-phonon interaction processes to development as a structured material for shaping and moulding nonlinear waves such as solitons and shock waves. The local design principle takes into account the propagation behaviour of the classical phonons and identifies the category of the geometrical structure of the phononic crystal which we need to control the relative placement of energy eigenvalues of the dispersion bands. By utilizing two general design principles, one governing the global properties and one governing the local wave interactions of phonons within the structure, it is possible to impose controls over spectral gaps in a rational fashion and even control the band curvature. In the design of phononic crystals, one main challenge has been the control of the dispersion of bands along general directions, i.e. low symmetry directions. This is, especially important when one wishes to optimize complete gaps. These details are spectral position of our bands which require the details of the phonons propagation dynamics. The imprint of the symmetry of the system on the eigenmodes affords a powerful alternative to its usage as a tool to guide design of phononic crystal, cavities and waveguides, etc. Symmetry has proven here its power as an elegant language with which to design not just analysing the dispersion relation because it laid the foundation with which to apply all the subsequent design principles which we have had to involve to arrive at our final design of dispersion relation depending on symmetry. By building on the symmetry of the phononic structure and the symmetry property of the acoustic fields and conservation principles places the design of various phononic structures on the same footing. This relies on two fundamental principles: global group symmetry which governs the allowed degeneracy of the eigenfunctions at specific positions and along specific directions vis a vis the plane group and point group symmetry. The global symmetry imparts on the structure the second principle, namely the eigenmodes are classified by a set of irreducible representation shaping the dispersion relation and forming the spectral gaps. These two symmetry principles control the possibility of interaction and provide the framework and the language which we utilize to design the dispersion relation. This is in our symmetry language which governs the physical propagation of phonons within the structure. This is derived from conservation and continuous principle enabling us to develop the concept of the dynamic mechanical bond and our lattice classification of the topology of the phononic structure. In the dispersion relation, in the linear phonon regime, we noted the ability to control the interaction between phonons of different frequencies, i.e. phonon-phonon interaction. While the phonon-phonon scattering

process is inelastic and often nonlinear the intrinsic material nonlinearities which govern the phonon-phonon scattering process are embodied in the material constitutive relations and hence do not alter the fundamental continuity and flux equation.

1.10 Phonon as a Goldstone Mode

The phonon as a Goldstone [4] mode is another demonstration of the symmetry property of acoustic fields. In a lattice, both longitudinal and rotational symmetries are broken which give rise to longitudinal and transverse phonons which are the Goldstone bosons of this symmetry breaking. However, one cannot link, e.g. longitudinal modes to translational symmetry breaking and transverse to rotational. Everything is mixed and the relationship between symmetry breaking and the different Goldstone phonons depend on the symmetry of the lattice. Goldstone modes are present in any system with a broken continuous symmetry. Phonons are an example of Goldstone modes, corresponding to the breaking of translation and rotation symmetry by a crystal structure.

Crystals are rigid because of the broken translational symmetry. The elementary excitations in crystal are the sound waves. In crystals, the broken translational symmetry introduces a rigidity to shear deformations and low frequency phonons.

Goldstone's [4] theorem examines a generic continuous symmetry which is spontaneously broken; that is, its currents are conserved, but the ground state is not invariant under the action of the corresponding charges. Then, necessarily, new massless scalar particles appear in the spectrum of possible excitations. There is one scalar particle called a Nambu-Goldstone boson for each generator of the symmetry that is broken, i.e. that does not preserve the ground state. The Nambu-Goldstone mode is a long-wavelength fluctuation of the corresponding order parameter. In fluids, the phonon is longitudinal and it is the Goldstone of the spontaneously broken Galilean symmetry. In solids, the situation is more complicated. The Goldstone bosons are the longitudinal and transverse phonons and they happen to be the Goldstone bosons of spontaneously broken Galilean, translational and rotational symmetry with no simple one-to-one correspondence between the Goldstone modes and the broken symmetries.

1.11 Symmetry Property of Turbulence Field

Kolmogorov's [5] theory of turbulence is based on scale invariance or symmetry of the turbulence field. The turbulence field is basically acoustic field [15] and this demonstrates symmetry property of the acoustic field. Kolmogorov's [5] idea was an extension of Richardson's [16] concept. Richardson's [16] notion of turbulence flow is composed of "eddies" of different sizes. The sizes define a characteristic

length scale for the eddies which are also characterized by flow velocity scales and time scales dependent on the length scale. The large eddies are unstable and eventually break up originating smaller eddies, and the kinetic energy of the initial large eddy is divided into the smaller eddies that stemmed from it. These smaller eddies undergo the same process, giving rise to even smaller eddies which inherit the energy of their predecessor eddy, and so on. In this way, the energy is passed down from the large scales of the motion to smaller scales until reaching a sufficiently small length scale such that the viscosity of the fluid can effectively dissipate the kinetic energy into internal energy. In his original theory of 1941, Kolmogorov [5] postulated that for very high Reynolds numbers, the small scale turbulent motions are statistically isotropic. In general, the large scales of a flow are not isotropic, since they are determined by the particular geometrical features of the boundaries (the size characterizing the large scales will be denoted by L). Kolmogorov's [5] idea was that in Richardson's energy cascade this geometrical and directional information is lost, while the scale is reduced, so that the statistics of the small scales has a universal character. They are the same for all turbulent flow when the Reynolds number is sufficiently high.

Thus, Kolmogorov [5] introduced a second hypothesis: for very high Reynolds numbers the statistics of small scales are universally and uniquely determined by the kinematic viscosity (ν) and the rate of energy dissipation (ε). With only these two parameters, the unique length that can be formed by dimensional analysis is

$$\eta = \left(\frac{\nu^3}{\varepsilon}\right)^{1/4} \tag{1.32}$$

This is also known as the Kolmogorov length scale.

A turbulent flow is characterized by a hierarchy of scales through which the energy cascade takes place. Dissipation of kinetic energy takes place at scales of the order of Kolmogorov length η, while the input of energy into the cascade comes from the decay of the large scales, of order L. These two scales at the extremes of the cascade can differ by several order of magnitude at high Reynolds numbers. In between there is a range of scales (each one with its own characteristic length r) that has formed at the expense of the energy of the large ones. These scales are very large compared with the Kolmogorov length but still very small compared with the large scale of the flow. Since eddies in this range are much larger than the dissipative eddies that exist at Kolmogorov scales, kinetic energy is essentially not dissipated in this range, and it is merely transferred to smaller scales until viscous effects become important as the order of the Kolmogorov scale is approached. Within this range inertial effects are still much larger than viscous effects, and it is possible to assume that viscosity does not play a role in their inertial dynamics.

Hence, a third hypothesis of Kolmogorov was that at very high Reynolds number the statistics of scales in the range r much smaller than L and much larger than η are universally and uniquely determined by the scaled r and the rate of energy dissipation ε.

1.12 Time Reversal Symmetry in Acoustics

Acoustic fields have time reversal (TR) symmetry property. This can be demonstrated by the solutions of the acoustic equation of motion. It implies that changing the time variable into a –t for the solution for a given field produces another field which is also solution of the same equation. In other words, if within a given medium there exists a solution of the wave equation denoted $S(t)$, then another dual solution, namely the time reversed one $S(-t)$, necessarily exists as well. For instance, if one is able to record the entire field created by a diverging source placed inside a reversible medium, time reversing and reemitting the latter generates a wave field that converges toward the initial source. Such an ideal TR experiment, however, requires the knowledge of the field throughout the medium, which is impossible in most practical environments. In practice, TR is made possible with the use of the Helmholtz-Kirchhoff integral theorem. The latter states that a wave field and its normal derivative known on the boundaries of a closed surface holds the knowledge of the field inside the whole volume the solution denoted $S(t)$, then another dual solution, namely the time reversed one $S(-t)$, necessarily exists as well. For instance, if one is able to record the entire field created by a diverging source placed inside a reversible medium, time reversing and reemitting the latter generates a wave field that converges toward the initial source. Such an ideal TR experiment, however, requires the knowledge of the field throughout the medium, which is impossible in most practical environments. In practice, TR is made possible by using the Helmholtz-Kirchhoff integral theorem. The latter states that a wave field and its normal derivative known on the boundaries of a closed surface hold the knowledge of the field inside the whole volume contained by the surface. Hence, a more realistic TR experiment can be imagined as follows: a source generates a brief pulsed inside a heterogeneous medium that is surrounded by sensors which record the corresponding time varying fields until all the energy has exited the closed surface. In a second step, the sensors play the recorded fields in a reversed chronology, which generates the time reversed wave field on the boundary of the closed surface.

References

1. Gan, W.S.: Gauge invariance approach to acoustic fields. In: Akiyama, I. (ed.) Acoustical Imaging, vol. 29, pp. 389–394. Springer, The Netherlands (2007)
2. Gan,W.S.: Acoustical Imaging: Techniques & Applications for Engineers. Wiley 343–368 (2012)
3. Fink, M.: Time reversed acoustics. Phys. Today **50**, 34–40 (1997)
4. Goldstone, J.: Field theory with superconductor solution. Nuovo Cimento **19**, 154–164 (1961)
5. Kolmogorov, A. N.: The local structure of turbulence in incompressible viscous fluid for very large reynolds numbers. In: Proceedings of the USSR Academy of Sciences(in Russian), **30**, 299–303 (1941)

6. Kambe, T.: Variational formulation of ideal fluid flows according to gauge principle, Preprint accepted by Fluid Dynamics Research. Elsevier Science, The Netherlands, 2007
7. Weyl, H.: Gravitation and the electron. Proc. Nat. Acad. Sci **15**, 323–334 (1929)
8. Veselago, V.G.: The electrodynamics of substances with simultaneous negative values of ε and μ. Soviet Physics Uspekhi **10**(4), 509–514 (1968)
9. Li, J., Chan, C.T.: Double-negative acoustic metamaterial. Phys. Rev. E **70**, 055602(R) (2004)
10. Yablonovitch, E.: Inhibited spontaneous emission in solid state physics and electronics. Phys. Rev. Lett. **58**(20), 2059–2062 (1987)
11. Kushwaha, M.S., Halevi, P., Dobrzvnski, L., Djafrari-Rouhani, B.: Acoustic band structure of periodic elastic composites. Phys. Rev. Lett. **71**, 2022 (1993)
12. Yang, C.N., Mills, R.: Conservation of isotopic spin and isotopic gauge invariance. Phys. Rev. **96**(1), 191–195 (1954)
13. Higgs, P.: Broken symmetries and the masses of gauge bosons. Phy. Rev. Lett. **13**(16), 508–509 (1964)
14. Gan, W.S.: A unified Yang Mills field and Higgs field-towards a superfluid model for particles of the universe. J. Basic Appl. Phys. **3**(2), 105–109 (2014)
15. Lighthill, M.J.: On sound generated aerodynamically,II. Turbulence as a source of sound. Proc. R. Soc. Lond. A222, 1–32 (1954)
16. Richardson, L.F.: Weather prediction by numerical process. Cambridge Univefrsity Press, UK (1922)

Chapter 2
Negative Refraction and Acoustical Cloaking

Abstract Negative refraction is not only the consequence of the negative mass density and negative bulk modulus of the acoustical metamaterial but also can produce phononic crystal's band gap. Acoustical cloaking is an application of the form invariance of the acoustic field equation. It is the first application of sound propagation in curvilinear space-time. It enables the bending and the manipulation of the direction of the sound wave to our requirement. Both negative refraction and acoustical cloaking can be derived from coordinates transformation of the acoustic field equation. In fact, negative refraction is a special case of acoustical cloaking when the value of the determinant of the coordinates transformation equals -1. Negative refraction enables the production of super-resolution lens and acoustical cloaking can be used for shielding objects.

2.1 Introduction

The phenomenon of negative refraction was first theoretically mentioned in Veselago's 1968 [1] paper with idea taken from Mandel'stam's [2] 1945 paper. This is the outcome of the two key parameters of electromagnetic waves: permittivity and permeability having negative values. The material having these properties is known as double negative metamaterial (DNG). It is a special type of metamaterial. This paper did not receive much attention because it was not possible to fabricate double negative metamaterial (DNG) although the other important form of metamaterial, the band gap metamaterial such as photonic crystals and phononic crystals was fabricated much earlier in the 1980s and in the early 1990s, respectively, and photonic crystals were known more than 100 years ago by Lord Rayleigh. In 1999 Pendry et al. [3] of Imperial College London successfully introduced the theoretical concept of split-ring resonator (SRR). This was a great contribution to the field of double negative metamaterial (DNG) as his theoretical concept enabled Smith [4] of Duke University USA to successfully fabricate experimentally the double negative metamaterial (DNG) using the concept of SRR. Then, there was great increase in interests in double negative metamaterials.

W.S. Gan, *New Acoustics Based on Metamaterials*, Engineering Materials,
https://doi.org/10.1007/978-981-10-6376-3_2

Metamaterials are artificial materials engineered to have properties that may not be found in nature. Metamaterials usually gain their properties from structure rather than composition, using small inhomogeneities to create effective macroscopic behaviour. It is a high-level form of composite material with periodic structure. Double negative metamaterials (DNG) also known as left-handed material because the negative directions of the permittivity, the permeability and the Poynting vector will form an anticlockwise rotation.

The phenomenon of negative refraction of left-handed symmetry can be considered and explained in the light of gauge theory. Maxwell's equation is the oldest gauge theory, Left-handed symmetry and the negative values of permeability and permittivity can be regarded as gauge condition. With the substitution of this gauge condition, there is no change in the form of the Maxwell's equations or Maxwell's equation is invariant with respect to a set of negative values of permeability and permittivity. In a subsequent section, acoustical cloaking uses the concept of gauge invariance of the Maxwell's equation subjected to curvilinear coordinate transformations (used in general relativity) and metamaterial. This reconfirms that negative refraction and acoustical cloaking can be explained in terms of gauge invariance.

2.2 Limitation of Veselago's Theory

2.2.1 Introduction

Veselago [1] proposed in 1968 the concept of metamaterials for electromagnetic waves having simultaneous negative values of the permittivity and the permeability, or double negativity. In this section, we point out the limitation of Veselago's [1] theory. Veselago's [1] theory is based on the dispersion relation for isotropic solids. Our new approach or alternative approach is based on the gauge invariance approach to acoustic fields proposed by the author in 2007 [5]. We show that this approach can extend metamaterials from electromagnetic waves to acoustic waves from first principles without using analogy. Also it can remove the ambiguity of using the dispersion relation for the refractive index because both the positive and the negative signs for the refractive index simultaneously occur due to the square root sign and this has to be justified. In addition, it is applicable to acoustical cloaking using coordinates transformation, a form of gauge invariance. We also discover parity invariance in acoustic field equations although the Maxwell's equations are known to be parity invariant. Electromagnetic metamaterials are materials with artificial electromagnetic properties defined by their sub-wavelength structure rather than their chemical composition. The left-handed metamaterials are a special type of metamaterial with parity p equals -1 and having the properties of negative permittivity and negative permeability and with the Poynting vector for energy flow in the opposite direction to that of wave propagation.

2.2.2 Gauge Invariance of Homogeneous Electromagnetic Wave Equation

Veselago [1] started with the dispersion relation for the propagation of electromagnetic wave in isotropic material. He considered the dispersion relation

$$k^2 = \frac{\omega^2}{c^2} n^2 \tag{2.1}$$

and

$$n^2 = \varepsilon\mu \tag{2.2}$$

where k = wave number, ω = frequency, c = wave velocity, n = index of refraction of the medium, ε = permittivity and μ = permeability.

Neglecting losses and regarding n, ε and μ as real numbers, it can be seen from (2.1) and (2.2) that a simultaneous change of the signs of ε and μ has no effect on these relations. That is, (2.1) and (2.2) are also valid for $-\mu$ and $-\varepsilon$. He then shows that for $\varepsilon > 0$ and $\mu > 0$ then $\vec{E}, \vec{H}$ and k form a right-handed triplet of vectors and if $\varepsilon < 0$ and $\mu < 0$ they form a left-handed set where $\vec{E}$ = electric field and $\vec{H}$ = magnetic field. He then introduced direction cosines for the vectors $\vec{E}, \vec{H}$ and $\overrightarrow{k}$ and denote them by α_i, β_i, and γ_i respectively, to characterize wave propagation in a medium:

$$G = \begin{pmatrix} \alpha_1 & \alpha_2 & \alpha_3 \\ \beta_1 & \beta_2 & \beta_3 \\ \gamma_1 & \gamma_2 & \gamma_3 \end{pmatrix} \tag{2.3}$$

The determinant of this matrix is equal to +1 if the vectors $\vec{E}, \vec{H}$ and $\overrightarrow{k}$ are a right-handed set and −1 if this set is left-handed. He then denoted this determinant by p and said that p characterized the "rightness" of the given medium. That is, the medium is "right-handed" if $p = +1$ and "left-handed" if $p = -1$.

In this section, I replace "rightness" by parity and parity = −1 is for left-handed set and parity = +1 is for right-handed set. Parity is the language of gauge invariance. All physics laws obey parity invariance except the *β decay in weak interaction*.

Also Poynting vector $\vec{S}$ which denotes energy flow and the parameter of highest interest in electromagnetic wave is given by

$$\vec{S} = \frac{c}{4\pi} \left[\vec{E} \wedge \vec{H}\right] \tag{2.4}$$

From (2.4), the vector $\vec{S}$ always forms a right-handed set with the vectors $\vec{E}$ and $\vec{H}$. Accordingly, for right-handed substances $\vec{S}$ and k are in the same direction and for left-handed substances, they are in opposite directions [1]. Since the vector k is in the direction of the phase velocity, it is clear that left-handed substances with a so-called negative group velocity, which occurs in particular in anisotropic substances or when there is spatial dispersion. That is for left-handed substance or parity = −1, the Poynting vector is of opposite direction to the phase velocity or the direction of wave propagation. For right-handed substance or parity = +1, the Poynting vector is of same direction as the phase velocity.

In this section, we build left-handed metamaterial on the framework of gauge invariance as it covers the both characteristics of left-handed material: negative permeability and negative permittivity and the Poynting vector pointing in the opposite direction to the phase velocity direction.

Next, we will show that the homogeneous electromagnetic wave equation is gauge invariant to negative permeability and negative permittivity.

For homogeneous medium, the electromagnetic wave equations can be given as:

$$\nabla^2\vec{E} - \frac{\varepsilon\mu}{c^2}\ddot{\vec{E}} = 0, \quad \nabla^2\vec{H} - \frac{\varepsilon\mu}{c^2}\ddot{\vec{H}} = 0 \tag{2.5}$$

We find that there is no change in the form of Eq. (2.5) if ε and μ are to be replaced by $-\varepsilon$ and $-\mu$. This shows the gauge invariance of Eq. (2.5) to negative values of permittivity and permeability.

2.2.3 Gauge Invariance of Acoustic Field Equations

The Helmholtz homogeneous acoustic wave equation is given by

$$\nabla^2 P + \frac{\omega^2}{\rho\kappa}p = 0 \tag{2.6}$$

where p = acoustic pressure, ρ = mass density and κ = bulk modulus.

Again we find that there is no change in the form of Eq. (2.6) if ρ and κ are replaced by $-\rho$ and $-\kappa$. This shows that the Helmholtz wave equation is gauge invariant to the negative values of ρ and κ.

Here, we have extended the left-handed media to acoustics using gauge invariance formulation. We also discover the parity invariance of acoustic field equation instead of using the Veselago's theory. Left-handed media has parity equals −1.

2.2.4 Acoustical Cloaking

Acoustical cloaking is the first introduction of acoustics to curvilinear space-time. Previously, all associations of acoustics with curvilinear space-time are only to describe the geometrical shape of certain structure. They are not dealing with the propagation or bending of sound wave in curvilinear space-time.

Acoustical cloaking deals with the deflection of bending of sound wave and the control of the propagation and direction of sound wave according to our specified direction.

Again Veselago [1]'s theory of using dispersion relation is not relevant here. We use coordinate transformations, a form of gauge invariance. That is, there is no change in the form of the acoustic field equation after the coordinate transformations or the acoustic field equation is gauge invariant subjected to coordinate transformations.

As an illustration, we quoted the results from Cummer [6].

Cummer [6] illustrated coordinate transformations for acoustics by using the linear acoustic equation for inviscid fluid:

$$j\omega p = -\kappa \nabla \cdot \vec{v}, \quad j\omega p\vec{v} = -\nabla p \tag{2.7}$$

where ω = angular frequency, v = sound velocity.

Next, he imposed a new set of curvilinear coordinates x', y′ and z' on these equations. Using A as the Jacobian matrix of coordinate transformations from (x, y, z) to (x', y', z'), he expressed the gradient operation in the new primed coordinates as:

$$\nabla p = A^T \nabla' p = A^T \nabla' p' \tag{2.8}$$

and the divergence operation can be expressed as

$$\nabla \cdot \vec{v} = \det(A) \nabla' \cdot \frac{A}{\det(A)} \vec{v} = \det(A) \nabla' \cdot \overrightarrow{v'} \tag{2.9}$$

With these expressions, the original Eq. (2.7) can be written in the new coordinates as

$$j\omega p' = -\kappa \det(A) \nabla' \cdot \overrightarrow{v'}$$

$$j\omega \det(A) \left(A^T\right)^{-1} \rho \left(A^{-1}\right) \overrightarrow{v'} = -\nabla' p' \tag{2.10}$$

which is in the same form as the original Eq. (2.7) but with the new medium parameters:

$$\kappa' = \det(A)\kappa, \quad \overline{\overline{\rho}} = \det(A) \left(A^T\right)^{-1} \rho \left(A^{-1}\right) \tag{2.11}$$

Physically, this means that if one applies a coordinate transformations to a solution to Eq. (2.7) and changes the medium properties according to Eq. (2.11), the transformed fields are a solution to the acoustic equations in the new medium.

2.2.5 *Gauge Invariance of Nonlinear Homogeneous Acoustic Wave Equation*

The nonlinear homogeneous acoustic wave equation up to the second order can be given as:

$$\kappa_1 \nabla^2 p + \kappa_2 \nabla^2 p \left(\frac{\partial p}{\partial x}\right) + \frac{\omega^2 p}{\rho} = 0$$

or

$$\rho\kappa_1 \nabla^2 p + \rho\kappa_2 \nabla^2 p \left(\frac{\partial p}{\partial x}\right) + \omega^2 p = 0 \tag{2.12}$$

where κ_1 = second-order bulk modulus and κ_2 = third-order bulk modulus.

Again if we replace ρ and κ_1, and κ_2 by $-\rho$, $-\kappa_1$ and $-\kappa_2$, there is no change in the form of Eq. (2.12). In another word, the nonlinear acoustic wave equation is gauge invariant to negative values of ρ, κ_1, and κ_2.

2.2.6 *My Important Discovery of Negative Refraction Is a Special Case of Coordinate Transformations or a Unified Theory for Negative Refraction and Cloaking*

Here, we are considering both cloaking and negative refraction under the umbrella theory of coordinate transformations or gauge invariance of the form of equations under coordinates transformation. This is a pattern of nature and is applicable to all equations of physics covering both Maxwell's equations and the acoustic equation of motion. When the determinant of the direction cosines matrix (or transformation matrix) equals −1, one will have negative refraction or parity equals −1. Also when multiplying the original permittivity and the original permeability by the determinant value of −1 will produce negative values of the permittivity and the permeability. This shows that negative refraction is a special case of coordinate transformations used in cloaking problem when the determinant of the transformation matrix equals −1. This can be illustrated as follows:

$$\begin{pmatrix} v_x' \\ v_y' \\ v_z' \end{pmatrix} = \begin{pmatrix} \propto_1 & \propto_2 & \propto_3 \\ \beta_1 & \beta_2 & \beta_3 \\ \gamma_1 & \gamma_2 & \gamma_3 \end{pmatrix} \begin{pmatrix} v_x \\ v_y \\ v_z \end{pmatrix} \tag{2.13}$$

When the determinant of the direction cosines matrix on the right-hand side of (2.13) equals −1, we have

$$\overrightarrow{v'} = -\vec{v} \tag{2.14}$$

Replacing the vectors by the examples of permeability and permittivity, we will have

$$\overrightarrow{\mu_{ij}'} = -\overrightarrow{\mu_{ij}} \quad \text{and} \quad \overrightarrow{\varepsilon_{il}'} = -\overrightarrow{\varepsilon_{il}} \tag{2.15}$$

This shows that negative refraction also produces negative permeability and negative permittivity.

Since this gauge invariance of the form of equation is a pattern of nature of all physics equations, it is also applicable to the acoustic case where the equivalence of the permittivity and permeability is the mass density and the bulk modulus or compressibility.

This also shows that cloaking material or component will become the lens in the special case of negative refraction, and refraction is a special case of cloaking or the bending of light wave or sound wave when the path of wave propagation becomes linear from nonlinearity.

This shows that gauge invariance has a broader coverage and applications than Veselago [1]'s dispersion relation.

Also reflection invariance (or right-left symmetry) can be introduced to explain negative refraction. In fact, $-\mu$ and $-\varepsilon$ can be considered as the mirror image of μ and ε and $-\rho$ and $-\kappa$ can be considered as the mirror image of ρ and κ. Again here the concept of coordinate transformations is used.

Of course, it should be also mentioned here that gauge invariance approach to negative refraction removes the ambiguity caused by using the dispersion relation. There are both positive and negative signs occur simultaneously due to the square root sign of the dispersion relation and this has to be justified.

2.2.7 *Conclusions*

The above evidence shows that Veselago's [1] theory is applicable only to electromagnetic waves and for isotropic materials and for the special case of double negativity and for linear case. Gauge invariance approach on the other hand has broader applications even to acoustic waves, to anisotropic materials, to cloaking problems, to negative refraction and to nonlinear acoustics. It also has the important

contribution of removing the ambiguity occurred of whether to use the positive or the negative sign of the dispersion relation.

In fact after Smith's [4] and Pendry's [3] accomplishments with metamaterials, Veselago realized that the most important contribution of his original 1968 paper is not that a composite material can be designed to produce a negative refraction, but that a composite material can be designed to produce any value for permittivity and permeability. This reconfirms my important discovery that negative refraction or double negativity in permittivity and permeability is only a special case of the general case of cloaking using coordinate transformations where a composite material can be designed to produce any value for permittivity and permeability.

2.3 Multiple Scattering Approach to Perfect Acoustic Lens

The multiple scattering theory (MST) usually known as the KKR (Korringa, Kohn and Rostoker) approach [7, 8] was developed mainly for the calculation of electronic band structures although it originated from the study of classical waves including acoustic waves used by Liu et al. [9] to calculate the propagation of sound waves in periodic structures such as phononic crystals. The phononic crystals in this case are stainless steel balls immersed in water. They found theoretically and experimental agreement using ultrasound experiment of the observation of a sizable directional stopband in the transmission along (001) centred at about 0.65 units, coincides with unexpectedly directional gap along the $\Gamma - x$ direction in the band structure. In the transmission along (111) they observed a narrow stopband at about 0.65 units, corresponding to the small gap at the L point in the band structure at the same frequency.

Other works on the studies on the existence and properties of phonon band gap are [10–13]. These are due to Bragg scattering when the sound wavelength is comparable with the lattice constants. This leads to frequency bands where wave propagation is forbidden. This enables the understanding of how to achieve large complete band gaps in physically realizable materials and the mechanism of wave transport at band frequencies due to tunnelling [14]. Also there has been relatively less attention paid to investigate how periodicity affects wave propagations over a wide range of frequencies outside the band gaps where novel refraction, diffraction and focusing effects may be possible.

At low sound frequencies, an effective continuum or medium approximation can be used to study the wave properties and accurately predict the wave speed. In this frequency range, there is much in common with the properties of low-frequency phonons in atomic crystals, where phonon focusing phenomena have been systematically studied [15]. However, at higher frequencies, much less is known about the behaviour in pass bands where the wavelengths can be much less than the lattice constant. Suxia Yang et al. [14] have addressed this problem by theoretically and experimentally investigating the character of wave pattern and propagation in a 3D phonon crystal at frequency above the first complete band gap. They showed how a

dramatic variations in wave propagation with both frequency and propagation direction can lead to novel focusing phenomena associated with large negative refraction. This is a different approach to negative refraction from that of Veselago's work for the electromagnetic wave based on negative values of permittivity and permeability. They demonstrated the effect of negative refraction experimentally by using ultrasound technique to image the transmitted wave field and show that a flat crystal can focus a diverging incident beam into a sharp focal spot that can be seen remarkably far from the crystal.

They also calculated the field pattern theoretically using a Fourier imaging technique in which wave propagation through the crystal is accurately described by the 3D equifrequency surfaces predicted from the multiple scattering theory (MST) [16]. Their theoretical results also give an excellent explanation of the experimental data, showing how wave physics in the regime can be accurately modelled and how the theoretical structures on the equifrequency surfaces of phonon crystal can give rise to potential applications.

Zhang and Liu [17] first discussed the issue of negative refraction for acoustic waves in phononic crystals. They also repeated the observation of the negative refraction of acoustic wave in phononic crystals, occurring at the frequencies with $\vec{S} \cdot \vec{k} > 0$ where $\vec{S}$ represents the Poynting vector. They considered a 2D phononic crystal consisting of infinite-length "rigid" or liquid cylinders embedded in a background which have been studied extensively in Refs. [18–20]. Two types of phononic crystals were used by them. One is steel cylinders in air background, and the other is water cylinders in mercury background. The band structures of these two types of phononic crystals were plotted in Fig. 2.1a, b, respectively. Both of them were calculated by the MST (or Korringa-Kohn-Rostoker method given in Ref. [21]).

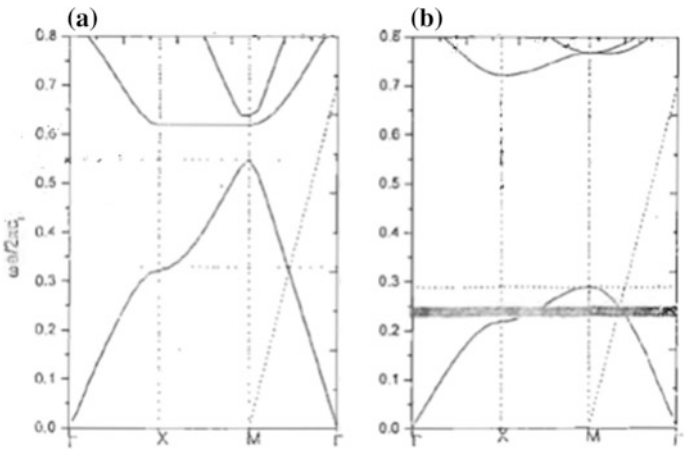

Fig. 2.1 **a** The acoustic band structures for a square lattice of steel cylinders in air background, with cylinder radius $R = 0.36a$. **b** The acoustic band structures for a square lattice of water cylinders in mercury background with cylinder radius $R = 0.4a$. The light line shifted to M is shown in dashed line. Dot-dashed lines mark the region for negative refraction and the shadow represent the AANR region. From Zhang and Liu [17]

To visualize and analyse refractive effects of the acoustic wave when it hits the above phononic crystal interfaces, Zhang et al. [17] investigated the equifrequency surfaces (EFS) of the band structures just like the case for the electromagnetic waves in the photonic crystals because the gradient vector of constant-frequency contours ink-space give the group velocities of the phononic modes. Hence, the propagation direction of energy velocity of acoustic wave can be reduced from them. The EFS can also be calculated using the MST or the Korringa-Kohn-Rostoker method. The features of the EFS for these two kinds of system within the first band are similar. Thus, only the results of water-mercury system with $R = 0.4a$ in given in Fig. 2.2. The equifrequency surface contours at several relevant frequencies such as 0.05, 0.1, 0.2, 0.235 and 0.27 are demonstrated. It is clear that the lowest band has $\vec{S} \cdot \vec{k} > 0$ everywhere within the first Brillouin zone, meaning that the group velocity is never opposite to the phase velocity. The 0.05 and 0.1 contours are very close to a perfect circle, and the group velocity at any point of the contour is collimated with the k vector, indicating that the crystal behaves like an effective homogeneous medium at these two long wavelengths.

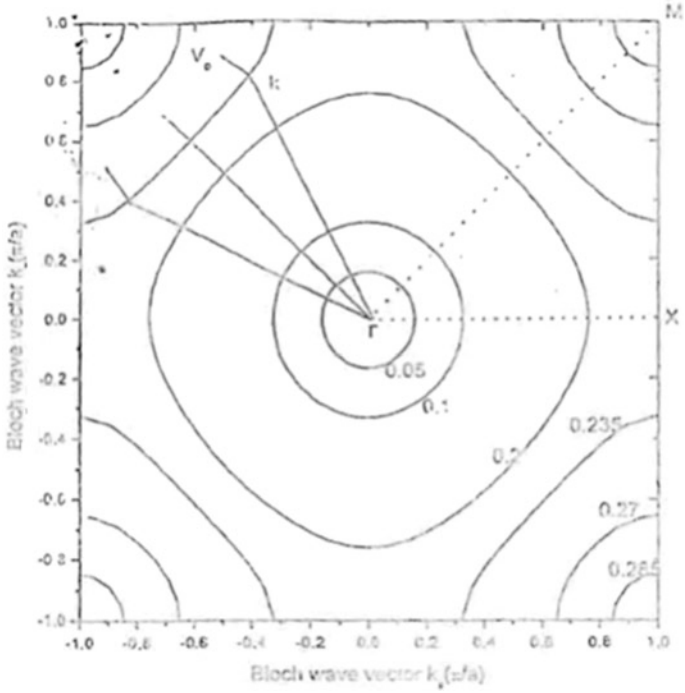

Fig. 2.2 Several constant-frequency contours of the first band of the 2D phononic crystal, which is composed of a square lattice of water cylinders in mercury background with $R = 0.4a$. The numbers in the figure mark the frequencies in unit of $2\pi c_l/a$

The 0.2 contour is a little bit distorted from a circle, and the 0.235 contour is convex around the M point due to a negative phononic "effective band". The conservations of the component along the surface of refraction would result in the negative refractions effect in some frequency region, marked as dotted lines in Fig. 2.1.

Furthermore, according to the analysis approach of [18, 22], the required condition for all-angle negative refraction (AANR) effect in some cases can be observed. Under these conditions, an acoustic beam incident on the ΓM surface with various incident angles will couple to a single Bloch mode that propagates into this crystal on the negative side of the boundary normal. Therefore, we can define a frequency region for the AANR by using these criteria.

From Fig. 2.1a, we noted that the AANR region is absent in the steel-air system, although the negative refractive region is very large. However, in the water-mercury system, the AANR region exists within the range of about 63 near $\omega = 0.24(2\pi c_l/a)$ (shadow region in Fig. 2.1b). This point differs from the two kinds of system. This difference is very important for the superlensing and focusing of acoustic waves in phononic crystals.

In order to test this theoretical analysis, Zhang et al. [17] performed a numerical simulation to the two phononic crystals system based on the MST [19]. They used a 30° wedged sample which consisted of 238 water cylinders of $R = 0.4a$ in the mercury background with a square array. The shape of the sample and an illustration of the refraction process are shown on the top of Fig. 2.3. The black frame marked the boundaries and the size of the sample. The wedged surface was the (11) surface when a slit beam of frequency $\omega = 0.235(2\pi c_l/a)$ with a half-width $wl = 2a$ incident normal to the left surface of the sample, it transports along the direction of incidence wave until it meets the wedge (11) interface of the sample, and then a part of it will refract outside of the sample and the other reflect inside. There are two possibilities for the refracted wave. It may travel on the right side (positive refraction) or left side (negative refraction) of the surface normal. The simulation results are plotted in Fig. 2.3. The field energy pattern of the incidence and refraction is shown in the figure. The arrows and text illustrate the various beam directions. It can be clearly seen that the density flux of the refractive wave outside of the sample travels on the negative refraction side of the surface normal. The refraction angle is consistent with the estimation from the wave vector space in Fig. 2.2. The simulation results show clearly that the negative refraction of the acoustic wave exists in the first band for the case with $\vec{S} \cdot \vec{k} > 0$. Similar phenomena have also been demonstrated in the steel-air system.

The concept of perfect lens or microsuperlens has been designed using the concept of negative refraction [1, 20] and fabricated with 2D photonic crystals [18].

Such a superlens can focus a point source on one side of the lens into a real point image on the other side even for the case of a parallel sided slab of material. The advantage of the superlens or perfect lens is the capability to defeat the diffraction limit or Rayleigh resolution criterion of wavelength divided by two. Such an image

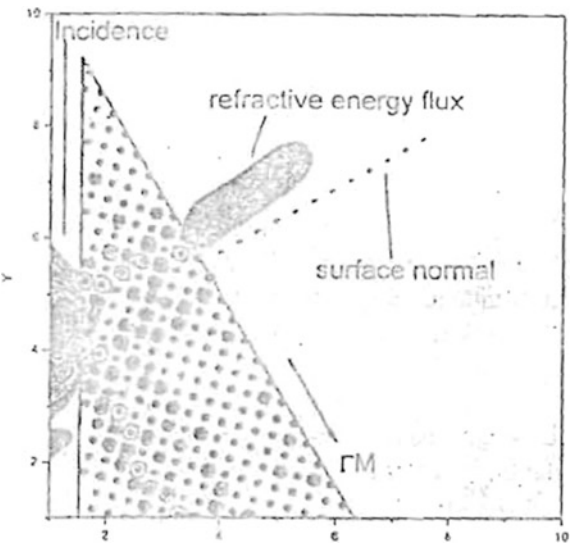

Fig. 2.3 Simulation of negative refraction. The boundaries of the sample are marked with black frame. The intensity of pressure field for incidence and refraction are shown in different shadows. A wedged sample considered here consists of water cylinders in mercury background with $R = 0.4a$ as shown on top of the figure. The frequency of incident wave is $\omega = 0.235(2\pi c_l/a)$

can be realized by flat slab instead of curved shapes and thus fabrications can be easier in principle. Zhang and Liu [17] demonstrated the design of such a perfect lens for sound waves which possess the same advantage as that of optical system. They used a slab of the sample with $40a$ width and six layers thick. A continuous wave point source is placed at a distance $1.0a$ from the left surface of the slab. The frequency of the incident wave emitting from such a point source is $\omega = 0.24(2\pi c_l/a)$, chosen to be within the region where all-angle negative refractions may occur (Fig. 2.1b).

The MST method is used to calculate the propagation of an acoustic wave in such a system. The typical results of field pattern of pressure wave and their images across the slab sample are given in Fig. 2.4. The geometry of the phononic crystal slab is also displayed. One can find quite a high-quality image formed in the opposite side of the slab. A closer look at the data reveals a transverse size (full size at half-maximum) of the image spot as $0.6a$ (or 0.14λ) at a distance of $1.0a$ from the right surface of the slab. The focusing size of the image depends on certain parameters such as the thickness of the slab and the distance between the source and the slab which is similar to the case for the optical system. The tuning of these parameters will produce a clearer acoustic image.

They also studied the effect on the image quality when the frequency of the sound wave is outside of the AANR region and system without the AANR region such as steel-air system. For these cases, the focusing phenomena are degraded. These show that the AANR is very important for the image formations.

This shows that negative refraction for acoustic wave in the 2D phonons crystal exists in a manner similar to that of optics.

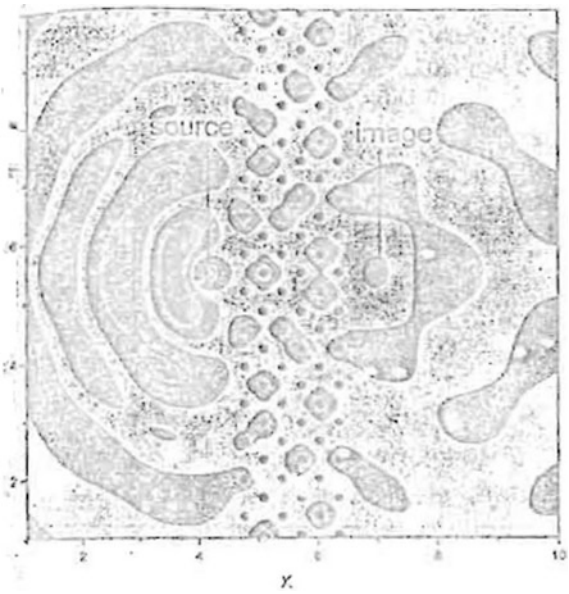

Fig. 2.4 Field pattern of pressure wave of a point source and its image across a six-layer slab at frequency $\omega = 0.24(2\pi c_l/a)$. The system considered here consists of some water cylinders in mercury background with $R = 0.4a$. Dark and bright regions correspond to negative and positive values, respectively

2.4 Acoustical Cloaking

2.4.1 Introduction

Acoustical cloaking can be classified as a form of acoustical imaging because by placing a metamaterial acoustical cloak on the object to be cloaked it will render its disappearance from one sight. The concept of acoustical cloaking also extended from electromagnetic cloaking [21, 23]. Electromagnetic cloaking uses concepts of gauge invariance from general relativity that is the form of the Maxwell's equations remain unchanged under arbitrary coordinate transformations with transformed permittivity and permeability values which are scaled by a common factor. Because of the nature of negative refraction of metamaterial, by cloaking the object with a metamaterial, the light rays will be deflected, stretched and bended and guided around the object and returned to their original trajectory.

However, due to the dispersion nature of the light, the cloaking effect is specific only to a single frequency and not broadband.

The concept of acoustical cloaking was extended to acoustics by Milton et al. in 2006 [24] and by Cummer and Schurig in 2007 [6]. The analysis by Milton et al. [24] indicated that the coordinate transformations approach cannot be extended to elastodynamic waves in solids in the fully general case or even for the special case of compressional waves in a fluid. However, a scattering theory analysis has shown that the cloaking solution exists for acoustic waves in fluids as three dimensions [25–27] and by analogies with electromagnetics. It has been shown that 2D acoustic waves [6] and 3D acoustic waves [28] can be made transformation invariant.

The material parameters required to implement acoustic coordinate changes have also been obtained by Greenleaf et al. [29].

It has to be noted that the phenomenon of acoustical cloaking cannot be transplanted blindly from electromagnetic cloaking using analogy. As shown in Sect. 2.2, Veselago's [1] theory is not applicable to acoustic waves and even for electromagnetic waves is valid only to isotropic case and not for anisotropic cloaking material which most cloaking materials are made of. Also the acoustic metamaterial has to be derived using the theory of elasticity and not from dispersion relation as what used to derive the Veselago [1]'s negative permeability and negative permittivity. Our gauge invariance approach can provide better physical understanding of negative refraction and cloaking. We also noted that acoustic negative refraction can be obtained from multiple scattering theory (MST) besides the approach of negative mass density and negative bulk modulus. This also confirms negative refraction is a form of multiple scattering. The above analysis is also given in Sect. 2.2.

Our idea of objection to use analogy between acoustic wave and electromagnetic wave is supported by Cummer et al. [25]. They pointed out that demonstrating the invariance through analogy of acoustic wave with electromagnetic wave masks some of the physics of the transformations approach particularly how vectors such as particle velocity and the pressure gradient change under transformation. Through an analysis of how power flow and constant phase surfaces must transform for completely general waves, they show that the velocity vector in acoustics must transform in a different way than the $\vec{E}$ and $\vec{H}$ *vectors* in electromagnetics. This explains why Milton et al.'s [24] elastodynamics analysis which assumed that the acoustic velocity transforms like $\overrightarrow{E}$ and $\overrightarrow{H}$ did not result in acoustic equation transformation invariance. We feel that this further shows the intrinsic elastic properties of acoustic wave as different from the electromagnetics. The treatment of negative refraction using theory of elasticity approach by Lee et al. [30] and Gan's analysis on the gauge invariance of acoustic fields [5] further confirm this. An example of the fabricating of acoustical cloak is given by Cheng et al. [31].

2.4.2 *Derivation of Transformation Acoustics*

Here, we follow approach of Cummer et al. [26]. The fluids version of the linear acoustic field equations will be used:

$$\nabla p = i\omega\rho(\vec{r})\rho_0\vec{v} \tag{2.16}$$

$$i\omega p = \kappa(\vec{r})\kappa_0\nabla\cdot\vec{v} \tag{2.17}$$

where $\rho(\vec{r})$ and $\kappa(\vec{r})$ are the normalized density and bulk modulus, respectively, of the medium and are coordinate transform invariant. We will demonstrate how the

acoustic velocity vector $\vec{v}$ must transform by considering $\vec{v}$ in a nonorthogonal coordinate system described by coordinate q_1, q_2 and q_3 with unit vectors $\hat{u}_1$,$\hat{u}_2$ and $\hat{u}_3$, respectively. Following Pendry et al. [23] and letting $i = 1, 2, 3$

$$Q_i^2 = \left(\frac{\partial x}{\partial q_i}\right)^2 + \left(\frac{\partial y}{\partial q_i}\right)^2 + \left(\frac{\partial z}{\partial q_i}\right)^2 \tag{2.18}$$

$$\hat{n} = (\widehat{u_1} \times \widehat{u_2})/(/\widehat{u_1} \times \widehat{u_2}/)$$

$$\text{Area} = Q_1 \mathrm{d}q_1 Q_2 \mathrm{d}q_2 |\hat{u}_1 \times \hat{u}_2|$$

Figure 2.5 shows what happens when we apply the divergence theorem to an infinitesimal volume in this nonorthogonal coordinate system.

Deriving the net outward flux of $\vec{v}$ from this volume and setting it equal to the divergence of $\vec{v}$ times the infinitesimal volume, it can be shown that

$$(\nabla \cdot \vec{v}) Q_1 Q_2 Q_3 |\hat{u}_1 \cdot (\hat{u}_2 \times \hat{u}_3)| = \frac{\partial}{\partial q_1}[Q_2 Q_3 \vec{v} \cdot (\hat{u}_2 \times \hat{u}_3)] + \frac{\partial}{\partial q_2}[Q_1 Q_3 \vec{v} \cdot (\hat{u}_1 \times \hat{u}_3)] + \frac{\partial}{\partial q_3}[Q_1 Q_2 \vec{v} \cdot (\hat{u}_1 \times \hat{u}_2)] \tag{2.19}$$

Let $V_{\text{frac}} = |\hat{u}_1 \cdot (\hat{u}_2 \times \hat{u}_3)|$ because this is the fraction by which a unit volume is compressed by the coordinate nonorthogonality and we use the conventional superscript (subscript) notation for contravariant (covariant) vector components using

$$\vec{v} \cdot (\hat{u}_2 \times \hat{u}_3) = v^1 \hat{u}_1 \times (\hat{u}_2 \times \hat{u}_3) \tag{2.20}$$

Equation (2.19) can be rewritten as

$$(\nabla \times \vec{v}) Q_1 Q_2 Q_3 V_{\text{frac}} = \frac{\partial}{\partial q_1}\left(Q_2 Q_3 V_{\text{frac}} v^1\right) + \frac{\partial}{\partial q_2}\left(Q_1 Q_3 V_{\text{frac}} v^2\right) + \frac{\partial}{\partial q_3}\left(Q_1 Q_2 V_{\text{frac}} v^3\right) \tag{2.21}$$

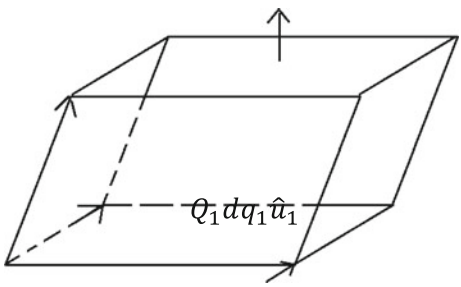

Fig. 2.5 Parallel piped that defines an infinitesimal volume in the transformed coordinates. The area and unit normal of each face enter in the calculation of the net flux of a vector out of this volume. From Cummer et al. [26]

Noting that the divergence in the transformed coordinates is defined by $\nabla_q \cdot \vec{v} = \frac{\partial v^1}{\partial q_1} + \frac{\partial v^2}{\partial q_2} + \frac{\partial v^3}{\partial q_3}$, we can write

$$(\nabla \cdot \vec{v}) Q_1 Q_2 Q_3 V_{\text{frac}} = \nabla_q \cdot (V_{\text{frac}} \overline{\overline{Q}}_{\text{per}} \left[v^1 v^2 v^3\right]^T = \nabla_q \cdot \tilde{v} \tag{2.22}$$

where

$$\overline{\overline{Q}}_{\text{per}} = \begin{bmatrix} Q_2 Q_3 & 0 & 0 \\ 0 & Q_1 Q_3 & 0 \\ 0 & 0 & Q_1 Q_2 \end{bmatrix} \tag{2.23}$$

and the transformed velocity vector $\tilde{v}$ is given by

$$\tilde{v} = V_{\text{frac}} \overline{\overline{Q}}_{\text{per}} \left[v^1 v^2 v^3\right]^T \tag{2.24}$$

The per subscript on the tensor $\overline{\overline{Q}}_{\text{per}}$ is to denote that the diagonal elements transform each vector component by the product of the coordinate scaling factors perpendicular (more general, not parallel, for the case of nonorthogonal coordinates) to the direction of the vector component. Recall that our qualitative discussion above, summarized in Fig. 2.6, showed that this is precisely how the velocity vector must transform in a compressed wave in order for transformation acoustics to work. Note that the elements of the volume vector $\left[v^1 v^2 v^3\right]^T$ are the contravariant components of $\vec{v}$ in the nonorthogonal coordinate system while the element of the vector $\vec{v}$ is the component in the original orthogonal coordinate system.

Multiplying (2.17) (with $\lambda(\vec{r}) = 1$) by $Q_1 Q_2 Q_3 V_{\text{frac}}$ and using (2.24) results in the equation in the transformed coordinates,

$$i\omega p = \kappa(\vec{q}) \kappa \nabla_q \cdot \tilde{\vec{v}} \tag{2.25}$$

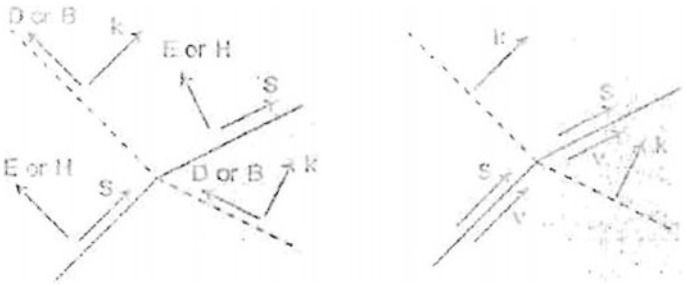

Fig. 2.6 Transformation of vectors in electromagnetic (left) and acoustic or compressional elastodynamic (right). The white converging arrows denote which component of each vector is compressed by the coordinate transformations. From Cummer et al. [26]

with

$$\kappa(\overline{q}) = (Q_1 Q_2 Q_3 V_{\text{frac}})^{-1} \tag{2.26}$$

This demonstrates the coordinate to function invariant of (2.17) provided that the bulk modulus is modified according to (2.26) and the velocity vector is transformed according to (2.25). More generally, this also shows how a vector must transform in order for the gradient operator to maintain its basis form.

Cummer et al. [26] derived how (2.16) and therefore the gradient operator transforms under a coordinate change using the gradient theorem and integrating ∇p along a short length in the q_1 coordinate directions, they find that

$$\nabla p \cdot Q_1 \hat{u}_1 = \frac{\partial p}{\partial q_1} = \left(\nabla_q p\right)^1 \tag{2.27}$$

The left-hand side contains the scaled covariant components of ∇p which must be converted to covariant components before it can be equated component-wise to $\nabla_q p$, the gradient in the transformed coordinates. They find that

$$\nabla_q p = \overline{\overline{Q}}_{\text{par}} \overline{\overline{h}}^{-1} (\nabla p) \tag{2.28}$$

where $\overline{\overline{Q}}_{\text{par}}$ is the diagonal tensor containing coordinate scaling factors parallel to the direction of the vector component or

$$\overline{\overline{Q}}_{\text{par}} = \begin{bmatrix} Q_1 & 0 & 0 \\ 0 & Q_2 & 0 \\ 0 & 0 & Q_3 \end{bmatrix} \tag{2.29}$$

and

$$\overline{\overline{h}}^{-1} = \begin{bmatrix} \hat{u}_1 \cdot \hat{u}_1 & \hat{u}_1 \cdot \hat{u}_2 & \hat{u}_1 \cdot \hat{u}_3 \\ \hat{u}_2 \cdot \hat{u}_1 & \hat{u}_2 \cdot \hat{u}_2 & \hat{u}_2 \cdot \hat{u}_3 \\ \hat{u}_3 \cdot \hat{u}_1 & \hat{u}_3 \cdot \hat{u}_2 & \hat{u}_3 \cdot \hat{u}_3 \end{bmatrix} \tag{2.30}$$

Note that this $\overline{\overline{h}}^{-1}$ is the same as $\overline{\overline{g}}^{-1}$ defined by Pendry et al. [23]. They rename this tensor because they will use $\overline{\overline{g}}$ later to denote the metric tensor which is not quite the same as this $\overline{\overline{h}}$.

Finally multiplying (1) (with $\rho(\vec{r}) = 1$) by $\overline{\overline{Q}}_{\text{par}}$, they find

$$p_q p = i\omega \overline{\overline{Q}}_{\text{par}} \overline{\overline{h}}^{-1} \rho_0 \vec{v} = i\omega \overline{\overline{Q}}_{\text{par}} \overline{\overline{h}}^{-1} \overline{\overline{Q}}_{\text{par}}^{-1} V_{\text{frac}}^{-1} \rho_0 \vec{v} \tag{2.31}$$

leaving us with the equivalent of (12.16) in fully transformed coordinates:

$$\nabla_q p = i\omega\overline{\overline{\rho}}\rho_0\vec{v} \tag{2.32}$$

with

$$\overline{\overline{p}} = \overline{\overline{Q}}_{\text{par}}\overline{\overline{h}}^{-1}\overline{\overline{Q}}_{\text{par}}^{-1}\overline{\overline{V}}_{\text{frac}}^{-1} \tag{2.33}$$

Equations (2.25) and (2.32) show that the acoustic equations are fully transformation invariant with the modified material parameters in (2.26) and (2.33).

They further show that these experiments are equivalent to those shown by Chen and Chan [24] purely by analogy with electromagnetics through the electric conductivity equation [32] and those derived by Greenleaf et al. [29] for the general scale Helmholtz equation. Consequently, cloaking shell, concentrator and other devices that have been designed theoretically by electromagnetics can also be realized for acoustics provided that the bulk modulus and anisotropic effective mass density tensor can be realized in practice as specified by (2.26) and (2.33). This first principles derivation without using analogy shows explicitly in (2.24) how the acoustic velocity vector must transform under coordinate change, which as noted above is different from how the $\vec{E}$ and $\vec{H}$ field, transform in electromagnetics. The scalar pressure is, however, not changed by the coordinate transformations and thus like phase fronts and power flow lines is simply deformed by any coordinate transformations.

2.4.3 Application to a Specific Example

We consider the spherical cloaking transformation [6] as illustrated in Fig. 2.7 and specified by $r' = a + r(b-a)/b$ where a and b are constants and $b > a$. This coordinate transformations is orthogonal and then $\overline{\overline{h}} = 1$ and $V_{\text{frac}} = 1$ which are good simplification. The Q_i length scaling factors are straightforward to calculate provided one realizes that the azimuthal and polar angles and not length, as in Cartesian coordinates and (2.18) must be modified slightly. The Q_i is defined by the ratio of infinitesimal lengths in the transformed and untransformed coordinates and thus,

$$Q_r = \frac{\mathrm{d}r}{\mathrm{d}r'} = \frac{b}{b-a}, \quad Q_\phi = \frac{r\mathrm{d}\phi}{r'\mathrm{d}\phi'} = \frac{b}{b-a}\frac{r'-a}{r'} \tag{2.34}$$

$$Q_\Theta = \frac{r\,\sin\,\theta}{r'\,\sin\,\theta'}\frac{\mathrm{d}\theta}{\mathrm{d}\theta'} = \theta_\varphi \tag{2.35}$$

in agreement with the parameter found through other approaches by Chen and Chan [28], Greenleaf et al. [29] and Cummer et al. [27].

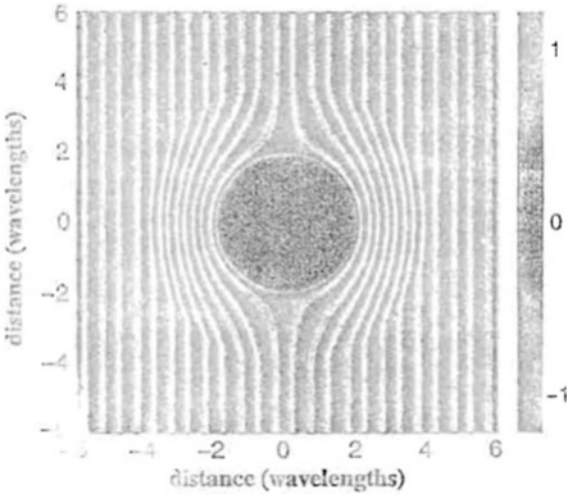

Fig. 2.7 The real part of the pressure field in the $r-\theta$ plane of the problem domain computed from the series solution. The plane wave is incident from the left

Thus, Cummer et al. [26] showed $\vec{E}$ and $\vec{H}$ of electromagnetics transform differently from $\vec{v}$ of acoustic waves under coordinate transformations. It shows that a first principle analysis of the acoustic equation under arbitrary coordinate transformations confirms that the divergence operator is preserved only if velocity transforms in this physically correct way.

2.5 Acoustic Metamaterial with Simultaneous Negative Mass Density and Negative Bulk Modulus

This is a different approach from that of using multiple scattering theory(MST) to produce acoustic negative refraction using phonons crystals [17, 33] (of Sect. 2.3 of MST) and also different from that of the fabrication of acoustical metamaterials for acoustical cloaking based on the invariance of the acoustic field equations under coordinate transformations. The concept is based on the gauge invariance of the acoustic field equations [5]. That is, there is no change in the form of the acoustic field equation with the replacement of the density and bulk modulus by negative density and negative bulk modulus. We have shown in Sect. 2.2 that the concept of negative permittivity and negative permeability giving rise to negative refraction ([1] of Section one) can also be explained by the gauge invariance of the Maxwell's equation with the replacement of the positive permeability and positive permittivity by negative permeability and negative permittivity. In fact, gauge invariance is more appropriate than the approach of Veselago [1] using the dispersive relation as the starting point to introduce negative permeability and negative permittivity as this will give rise to the restriction that only single frequency electromagnetic

cloaking is allowed and also the Veselago [1]'s dispersion relation is used only to the isotropic case whereby most acoustic cloaking materials are anisotropic.

Applying gauge invariance of acoustic fields [34] to negative refraction, broadband double negative spectral range in the structure can be obtained [30]. This is also an experimental verification of my hypothesis on the gauge invariance of acoustic fields [5]. Lee et al. [30] fabricated an acoustic double negativity (DNG) acoustic metamaterial with both membranes and side holes (Fig. 2.8). Here, the acoustic waves are governed by Eqs. (2.36) and (2.37)

$$-\nabla p = \left[\rho - \frac{\kappa}{\omega^2}\right]\frac{\partial \vec{u}}{\partial A} \tag{2.36}$$

and

$$\nabla \cdot \vec{u} = -\left[\frac{1}{B} - \frac{\sigma_{\mathrm{SH}}^2}{\rho_{\mathrm{SH}} A \omega^2}\right]\frac{\partial p}{\partial A} \tag{2.37}$$

where κ = new elastic modulus, $\vec{u}$ = velocity of the fluid (air in this case), ρ = dynamic mass density, B = bulk modulus, A = cross section of the tube, σ_{SH} = SH-cross sectional-density, ρ_{SH} = SH-mass-density.

The existence of the side holes (SH) does not modify Eq. (2.36). Likewise, because the membranes do not sink any fluid, Eq. (2.37) is still valid. Then, the system is described by the dynamic and continuity equations

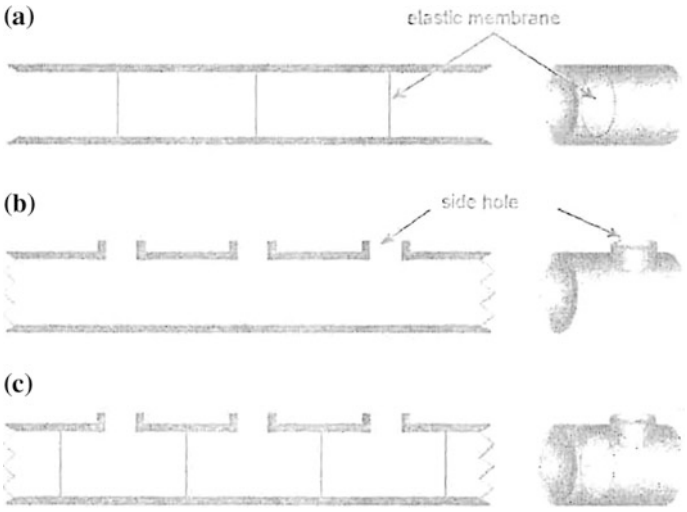

Fig. 2.8 **a** One dimensional SAE structure consisting of thin tensioned elastic membranes in a tube. Negative effective density is observed in this system. **b** A tube with an array of side holes that exhibits negative effective modulus. **c** An acoustic DNG structure with both membranes and side holes. From Lee et al. [30]

$$-\nabla p = \rho_{\text{eff}}\left(\frac{\partial y}{\partial A}\right)\nabla \cdot \vec{u} = -\left(\frac{1}{B_{\text{eff}}}\right)\left(\frac{\partial p}{\partial A}\right)$$

with the effective density and modulus are given by (2.36) and (2.37)

$$P_{\text{eff}} = \rho' - \frac{\kappa}{\omega^2} = \rho'\left[1 - \frac{\omega_{\text{SAE}}^2}{\omega^2}\right] \tag{2.38}$$

$$B_{\text{eff}} = \left[\frac{1}{B} - \frac{\sigma_{\text{SH}}^2}{\rho_{\text{SH}} A\omega^2}\right]^{-1} = B\left[1 - \frac{\omega_{\text{SH}}^2}{\omega^2}\right]^{-1} \tag{2.39}$$

where ω_{SAE} = critical frequency = $\sqrt{\frac{\kappa}{\rho'}}$

The resulting wave equation gives the phase velocity,

$$v_{\text{ph}} = \pm\sqrt{\frac{B_{\text{eff}}}{\rho_{\text{eff}}}} = \pm\sqrt{\frac{B}{\rho'\left(1 - \omega_{\text{SAE}}^2/\omega^2\right)\left(1 - \omega_{\text{SH}}^2/\omega^2\right)}} \tag{2.40}$$

where $\omega_{\text{SH}} = \left(B\sigma_{\text{SH}}^2/A\rho_{\text{SH}}\right)^{1/2}$

The experimental set-up is given in Fig. 2.9a.

It consists of a nonmetal tube on the left and the DNG metamaterial on the right. The absorbers at both ends completely absorb the acoustic energy, preventing any reflection so the system behaves as if it extends to infinity. This eliminates concerns about the effect of the finite number of cells used in the experiment, as well as the interference effect from the reflected waves. The sound source rejects acoustic energy into the tube through a small hole, generating incident waves propagating to the right. At the boundary, a position of the incident energy is reflected and the rest is transmitted into the metamaterial regions. On the metamaterial side, the transmitted acoustic energy flow steadily to the right until it hits the absorber.

Pressure was measured as a function of time and position on both the normal tube side and the metamaterial side. It can be seen that on the normal tube side, the wave proceeds forward, but on the metamaterial side, the wave propagated as indicated by the arrows. Clearly, the wave on the metamaterial propagated in a direction antiparallel to the energy flow. This confirms the theoretical prediction of negative phase velocity. It was noted that the amplitudes and the apparent phase velocity in the normal tube deviated from the actual values of the incident wave because of the interference of the reflected wave from the boundary. In the metamaterial, there is no such interference effect because there is no reflected wave.

The comparison between the theory and experiment is shown in Fig. 2.10.

Theoretically, expected single negative gap is experimentally confirmed by the transmission data (inset). In the DNG and DPS (double positions) pass bands, the phase velocities experimentally determined agree well with the theoretical values. The calculations are given as accurate description of the behaviour of the phase

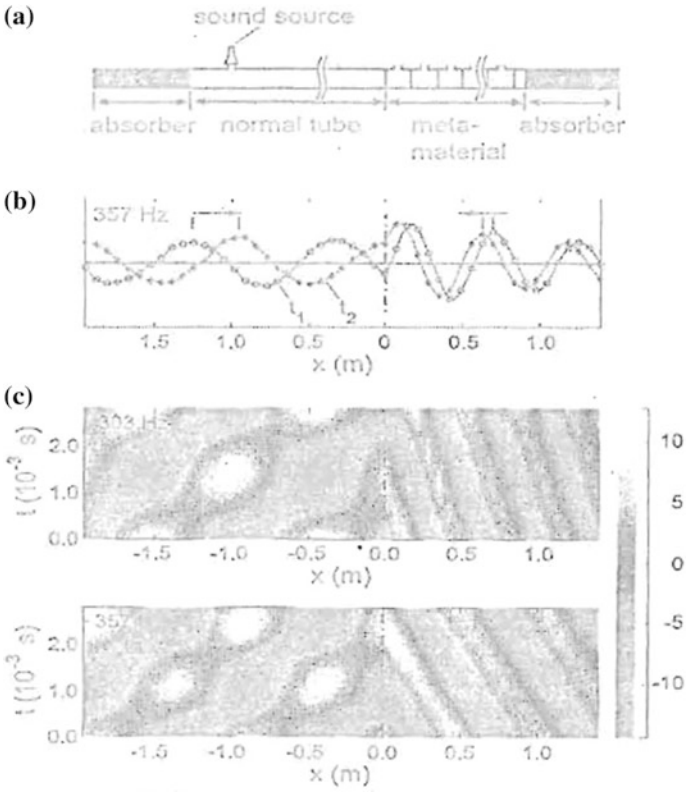

Fig. 2.9 **a** Experimental set-up for the transmission and phase velocity measurements. **b** 'Snapshots' of measured pressure distribution showing backward wave propagation in the metamaterial ($x > 0$). **c** Characteristic diagrams of pressure measurements for the frequencies 303 and 357 Hz. Negative slopes of the wave-paths in the metamaterial sides ($x > 0$) indicate negative phase velocities. From Lee et al. [30]

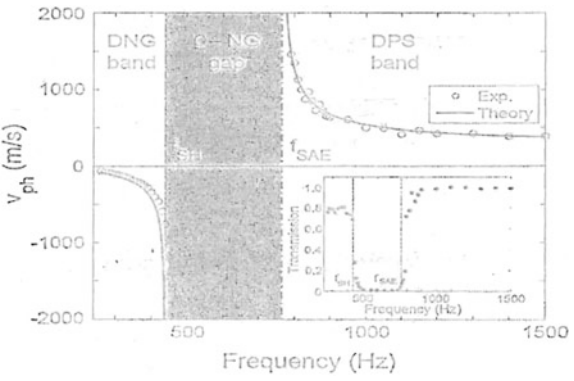

Fig. 2.10 Transmission (inset) and phase velocities of the present acoustic DNG medium. From Lee et al. [30]

velocity in the frequency range from 250 to 1500 Hz. Which is broadband? Because the experiment confirms the theoretical prediction of negative phase velocity, it can be concluded that the density and the bulk modulus actually becomes simultaneously negative in the frequency range below 440 Hz.

We would like to point out the novel concept of spatially anchored elasticity [16] was used. This uses a homogenized structure of membranes to produce negative effective density. This is termed spatially anchored elasticity (SAE) because the fluid is elastically anchored in space by the membranes. The new elasticity can be regarded as an intrinsic variables that characterizing the behaviour of the metamaterial according to Eq. (2.41)

$$\nabla p = -\kappa \vec{\xi} \tag{2.41}$$

where κ = new elastic modulus, ξ = displacement of the fluid, p = pressure of the fluid.

Furthermore, by making additional side holes along the tube wall, acoustic DNG materials were obtained and backward-wave propagation was observed. The constructed structure exhibited DNG characteristic in the spectral range from 240 to 440 Hz which is broadband unlike the electromagnetic case which is limited only to a single frequency due to dispersion. The phase velocity in this band was negative and highly dispersive.

Again this proves that acoustic metamaterial cannot be just transplanted by analogy from the electromagnetic case. It has to be based on the theory of elasticity unlike for the electromagnetic which is based on the dispersion relation of Veselago [1].

2.6 Acoustical Cloaking based on Nonlinear Coordinate Transformations

So far the coordinates transformations used in acoustical cloaking are based on linear coordinate transformations [6]. Akl et al. [35] extended to nonlinear transformation using

$$r^1 = a + (b - a)\left(\frac{r}{b}\right)^n \tag{2.42}$$

where n = an arbitrary transformation exponent that accounts for the degree of nonlinearity in the transformation and can be used as an additional degree of freedom in designing and controlling the bending of the acoustic wave inside the cloak. For unity value of n, the transformation returns back to the linear transformation proposed by Cummer and Schurig [6].

Linear transformation is effective for the case of rigid objects. However, the cloaking becomes less perfect and dependent on the selection domain when flexible

objects are considered where its permeable nature might induce considerable absorption of sound wave which would bring less perfection to the cloak. Akl et al. [35] have presented acoustic cloaking based on different nonlinear coordinate transformations. They developed a finite element model developed through time-harmonic analysis to study the preserve field distribution using different nonlinear coordinate transformations. Such transformations have shown considerable improvements to the cloak performance when applied to flexible objects allowing for wider applicability bandwidth (broadband) as well as for providing additional control of the shape of acoustic wave bending inside the cloak region.

For a metamaterial anisotropic acoustic cloak of a flexible object, the cloak works in a limited frequency range around its resonant frequency. In order to show this fact, a quantifiable measure for the cloak's performance has been developed. They proposed a new performance indicator of the cloak's quality using the acoustic pressure value at a preselected set of points downstream of the cloak. The set of points selected for pressure measurements were distributed along the fluid in such a way to accurately predict the calculation from ideal cloak. The proposed indicator is based on the fact that for ideal cloak, the r.m.s. of the difference between the acoustic pressure values along the wave front downstream of the cloak and a reference value measured along the same wavefront at a reference wave propagation line tend to be zero. A reference wave propagation line located at the middle of the domain is quite a good unbiased choice. This process is repeated with as many planes in the axial direction (along wave propagation lines) and lateral directions as needed to scan the entire fluid domain, where the sum of all the calculated values is divided by the number of measurement points as given in Eq. (2.43)

$$\text{P.I.} = \sum_{j=1}^{j_{\max}} \sqrt{\sum_{i=1}^{i_{\max}} \left(P_{i,j} - P_{i,\text{ref}}\right)^2} \tag{2.43}$$

to yield the targeted performance indicator (P.I.). The measurement grid points are as illustrated in Fig. 2.11.

In this case, any determination of the cloak performance would result in a positive r.m.s. value of the proposed pressure difference. The number of points selected was large enough to capture even the smallest deviation from the ideal cloak performance.

In Eq. (2.43) i is the measurement point index along the wave propagation line (axial direction), which j represents the point index in the lateral directions. Based on this indicator the performance of an anisotropic acoustic cloak surrounding a flexible object is quantified at different excitation frequency values such that the larger the indicator values, the more deterioration in the cloak performance is.

The proposed nonlinear transformations of Akl et al. [35] have proven to improve the way in which the acoustic metamaterial anisotropic cloak works away from the limited frequency values. This is shown in Fig. 2.12 by plotting the performance indicator of the linear cloak and one of the nonlinear cloaking over the

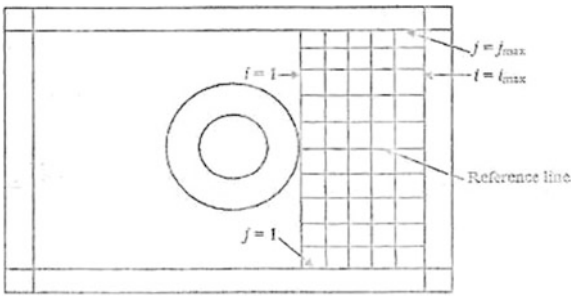

Fig. 2.11 Schematic of the measurement grid points required revaluation the performance indicator. From Akl et al. [35]

frequency range under study. It is clear that the nonlinear cloak performance at frequency ranges away from these domain resonant frequencies is much better. The same conclusion is drawn from Fig. 2.13 where the acoustic pressure field for both the linear and nonlinear transformation for frequency values away from the domain resonance frequency is plotted. In order to show the degree by which the nonlinear transformation has improved the cloaking performance, the difference between the performance indicator values for nonlinear transformation with minimum PI value and those for linear transformation at each frequency is calculated and plotted against the excitation frequency as shown in Fig. 2.14. In this figure, the higher the positive difference, the more improvement of the acoustic cloak performance is achieved. Once more, it is evident that a perfect linear acoustic cloak is achievable only at the same specific frequency values and the proposed nonlinear transformation has improved significantly the way in which the acoustic metamaterial anisotropic cloak works away from the limited frequency values. Although the simulations of the acoustic metamaterial anisotropic cloak around flexible objects encounter some sort of numerical error, the proposed nonlinear transformations open the door for searching for different coordinate transformations function that would lead to simulation results insensitive to the solution domain dimensions.

2.7 Acoustical Cloaking of Underwater Objects

A group at the Mechanical Engineering Department of the University of Illinois led by Nicholas Fang have created a numerical model to build a metamaterial cloak that guides sound waves around objects in water. The model is based on the acoustic lumped circuit network. The unit cell of the network is so small compared to the wavelength of the sound that it becomes and effective anisotropic medium that guides sound flow around the cloaked object. Computer simulations demonstrated that the numerical model successfully achieved a cloaking effect. The next step is to construct and test an actual physical version of the cloak based on that numerical model. If the metamaterial cloak also works, considerably more work needs to be done before the cloak could be scaled up to hide a ship or a submarine. Their mesh

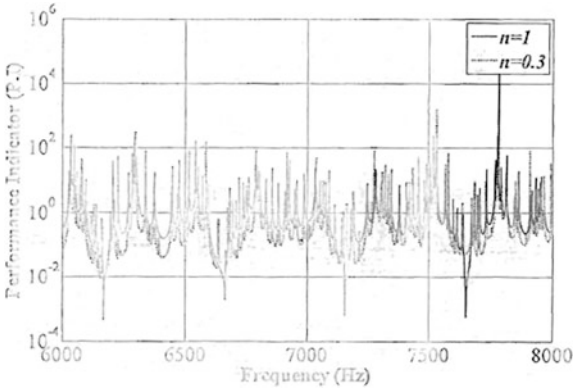

Fig. 2.12 Nonlinear ($n = 0.3$) acoustic cloak performance against the linear cloak when surrounding the host medium at different frequency values. From Akl et al. [35]

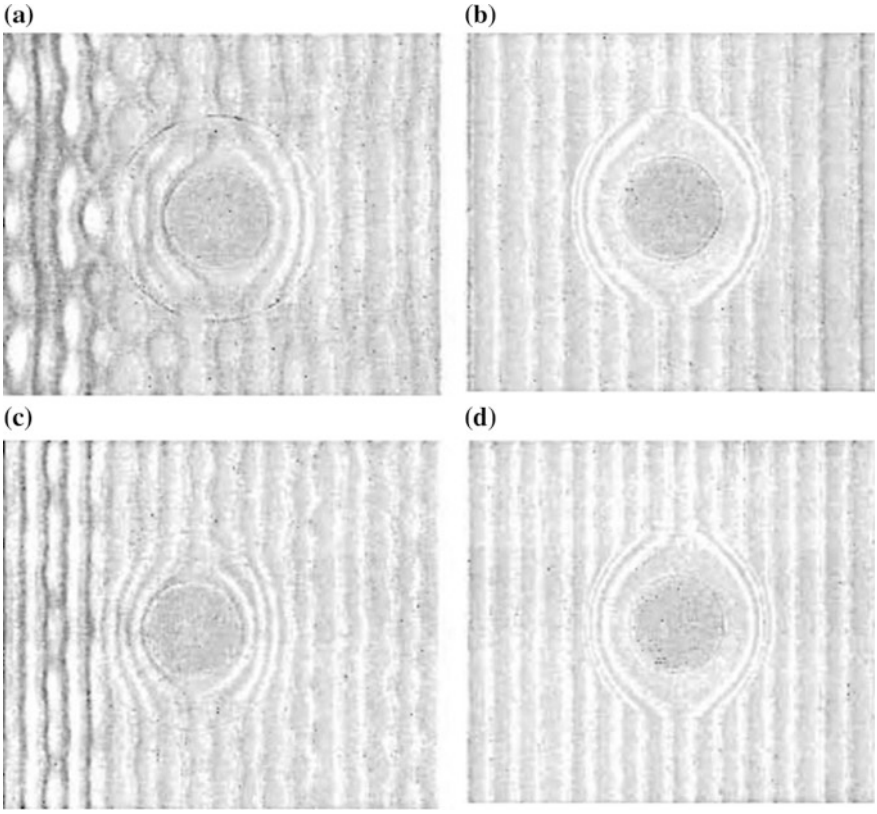

Fig. 2.13 Full wave time-harmonic acoustic pressure field plot of the analyzed ideal cloak with water as base medium: **a** linear at 6000 Hz, **b** nonlinear ($n = 0.3$) at 6000 Hz, **c** linear at 7000 Hz and **d** nonlinear ($n = 0.3$) at 7000 Hz. From Akl et al. [35]

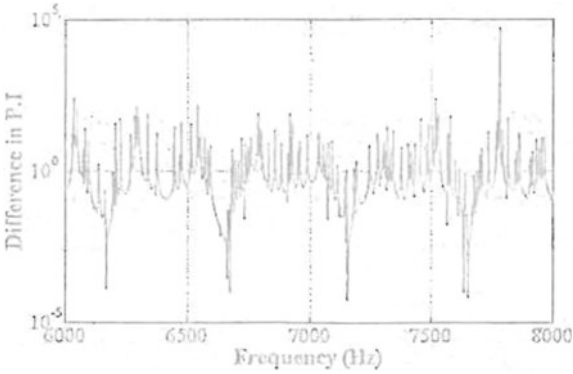

Fig. 2.14 Performance indicator difference between linear and nonlinear cloaks at different frequency values. From Akl et al. [35]

model is based on cloaking an object with a diameter of about 0.67 times the wavelength of light a far cry from the 50-foot beam of a nuclear submarine. Their work is published in the 15 May 2009 issue of the Physical Review Letters [36].

2.8 Extension of Double Negativity to Nonlinear Acoustics

The lossless form of nonlinear acoustic wave equation up to the third-order elastic coefficient can be given by Thurstone and Shapiro [37] as

$$\ddot{u} = \frac{M_2}{\rho_0}\frac{\partial^2 u}{\partial x^2} + \frac{M_3}{\rho_0}\left(\frac{\partial^2 u}{\partial x^2}\right)\left(\frac{\partial u}{\partial x}\right) \tag{2.44}$$

where u = displacement, x = Lagrange coordinate in the direction of motion of a particle and anisotropic solid is used.

Where M_2 is a linear combination of second-order elastic coefficients and M_3 is a linear combination of second- and third-order elastic coefficients.

To allow for energy dissipation, Eq. (2.44) is modified by adding a term to include the frequency dependent attenuation coefficient $\alpha = \alpha(\omega)$, to the right hand side

$$\ddot{u} = \frac{M_2}{\rho}\frac{\partial^2 u}{\partial x^2} + \frac{M_3}{\rho}\left(\frac{\partial^2 u}{\partial x^2}\right)\left(\frac{\partial u}{\partial x}\right) + \frac{2\alpha}{\omega^2}C^3\frac{\partial^2 u}{\partial x^2 \partial t} \tag{2.45}$$

where $C^2 = M_2/\rho$ = speed of propagation of an infinitesimal amplitude sound wave and ρ = mass density of medium.

By replacing ρ by $-\rho$ and M_2 and M_3 by $-M_2$ and $-M_3$. There is no change in the form of equation. Hence, the nonlinear acoustic new equation is also gauged invariant in the mass density and the elastic coefficient.

References

1. Veselago, V.G.: The electrodynamics of substances with simultaneous negative values of ε and μ. Sov. Phys. Usp. **10**(4), 509 (1968)
2. Mandel'stam, L.I.: JETP **15**, 475 (1945)
3. Pendry, J.B., Holden, A.J., Robbins, D.J., Stewart, W.J.: Magnetism from conductors and enhanced non-linear phenomena. IEEE Trans. Microw. Theory Techn. **47**(11), 2075–2984 (1999)
4. Shelby, R.A., Smith, D.R., Schultz, S.: Experimental evidence of a negative index of refraction. Science **292**(5514), 77 (2001)
5. Gan, W.S.: Gauge invariance approach to acoustic fields. In: Akiyama, I. (ed.) Acoustical Imaging, vol. 29, pp. 389–394. Springer, Dordrecht (2007)
6. Cummer, S.A., Schurig, D.: One path to acoustic cloaking. New J. Phys. **9**, 45 (2007)
7. Korringa, J.: Physica (Amsterdam) **XIII**, 392 (1947)
8. Kohn, W., Rostoker, N.: Phys. Rev. **94**, 1111 (1951)
9. Liu, Z., Chan, C.T., Sheng, P., Goertzen, A.L., Page, J.H.: Elastic wave scattering by periodic structures of spherical objects: theory and experiment. Phys. Rev. B **62**(4), 2446–2457 (2000)
10. Sigalas, M.M., Economou, E.N.: J. Sound Vib. **158**, 377 (1992)
11. Kushwaha, M.S., Halevi, P., Dobrzynski, L., Djafrari-Rouhani, B.: Phys. Rev. Lett. **71**, 2022 (1993)
12. Sanchez-Perez, J.V., Caballero, D., Martinez-Sala, R., Rubio, C., Sanchez-Dehesa, J., Meseguer, F.: Phys. Rev. Lett. **80**, 5325 (1998)
13. Kafesaki, M., Economou, E.N.: Phys. Rev. B **52**, 13317 (1995)
14. Yang, S., et al.: Phys. Rev. Lett. **88**, 104301 (2002)
15. Wolfe, J.P.: Imaging Phonons: Acoustic Wave Propagation in Solids. Cambridge University Press, Cambridge, England (1998)
16. Liu, Z., et al.: Phys. Rev. B **62**, 2446 (2000)
17. Zhang, X., Liu, Z.: Negative refraction of acoustic waves in two-dimensional phononic crystals. Appl. Phys. Lett. **85**(2), 341–343 (2004)
18. Luo, C., Johnson, S.G., Joannopoulos, J.D.: Appl. Phys. Lett. **83**, 2352 (2002)
19. Lai, Y., Zhang, X., Zhang, Z.Q.: Appl. Phys. Lett. **79**, 3224 (2001)
20. Pendry, J.B.: Phys. Rev. Lett. **85**, 3966 (2000)
21. Schurig, D., Mock, J.J., Justice, B.J., Cummer, S.A., Pendry, J.B., Starr, A.F., Smith, D.R.: Metamaterial electromagnetic cloak at microwave frequencies. Science **314**, 977–980 (2006)
22. Luo, C., Johnson, S.G., Joannopuolos, J.D., Pendry, J.B.: Phys. Rev. B **65**, 201104 (2002)
23. Pendry, J.B., Schurig, D., Smith, D.R.: Controlling electromagnetic fields. Science **312**, 1780–1782 (2006)
24. Milton, G.W., Briane, M., Willis, J.R.: On cloaking for elasticity and physical equations with a transformation invariant form. New J. Phys. **8**, 248 (2006)
25. Cummer, S.A., Raleigh, M., Schurig, D.: New J. Phys. **10**, 115025–115034 (2008)
26. Cummer, S.A., Rahm, M., Schurig, D.: Material parameters and vector scaling in transformation acoustics. New J. Phys. **10**, 115025 (2008)
27. Cummer, S.A., et al.: Scattering theory derivation of a 3D acoustic cloaking shell. Phys. Rev. Lett. **100**, 024301 (2008)
28. Chen, H., Chan, C.T.: Acoustic cloaking in three dimensions using acoustic metamaterials. Appl. Phys. Lett. **91**, 183518 (2007)
29. Greenleaf, A., Kurylev, Y., Lassas, M., Uhlmann, G.: Comment on "Scattering derivation of a 3D acoustic cloaking shell" (2008)
30. Lee, S.H., Kim, C.K., Park, C.M., Seo, Y.M., Wang, Z.G.: Composite acoustic medium with simultaneously negative density and modulus. In: Proceedings of ICSV17 (2010)
31. Cheng, Y., Xu, J.Y., Liu, X.J.: One-dimensional structured ultrasonic metamaterials with simultaneously negative dynamic density and modulus. Phys. Rev. B **77**, 045134 (2008)

32. Greenleaf, A., et al.: Anistropic conductivities that cannot be detected by EIT. Physiol. Meas. **24**, 413–419 (2003)
33. Yang, S., Page, J.H., Liu, Z., Cowan, M.L., Chan, C.T., Sheng, P.: Focusing of Sound in a 3D Phononic Crystal. Phys. Rev. Lett. **93**(2), 024301-1–024301-4 (2004)
34. Hu, J., Zhou, X., Hu, G.: A numerical method for designing acoustic cloak with arbitrary shapes, Comput. Mater. Sci. **46**, 708–712 (2009)
35. Akl, W. Elnady, T., Elsabbagh, A.: Improving acoustic cloak bandwidth using nonlinear coordinate transformations. In: Proceedings of ICSV17 (2010)
36. Fang, N., Zhang, S.: Phys. Rev. Lett. (2009)
37. Thurston, R.N., Shapiro, M.J.: J. Acoust. Soc. Am. **41**, 1112 (1967)

Chapter 3
Basic Mechanisms of Sound Propagation in Solids for Negative Materials

Abstract The three basic forms of sound propagation in solids are diffraction, refraction and scattering. Acoustical metamaterials will enable the control and manipulation of these three mechanisms and hence the manipulation of the direction of sound propagation in solids. A detailed description of this three mechanisms for the case of negative mass density and negative bulk modulus enabling negative acoustical metamaterial are given.

3.1 Methods to Treat Multiple Scattering in Conventional Solids

The basic mechanisms of sound propagation in solids and fluids are scattering, diffraction and refraction. For natural, conventional positive materials with parity = +1, the usual treatment of multiple scattering is by Rytov approximation, Born approximation, statistical treatment and *T*-matrix. For negative material, with parity = −1 and negative bulk modulus and mass density, the above methods can still be used. However, in this book, only the *T*-matrix method will be used.

3.2 *T*-Matrix of Multiple Scattering

T-matrix of multiple scattering was first used in quantum scattering since the 1930 s. *T*-matrix stands for transition matrix. It is used frequently together with *S*-matrix or scattering matrix. In 1965, Peter Waterman introduced this method of multiple scattering into classical electromagnetic scattering [1] and acoustic scattering [2]. The acoustic scattering properties of an obstacle are completely described by its infinite acoustic *T*-matrix. The *T*-matrix is particularly useful when one is interested in analysing changes in sound wave propagation with respect to various changes in orientation or configuration of single or multiple scatterings. This is because the *T*-matrix is independent of the incoming wave directions and hence can

W.S. Gan, *New Acoustics Based on Metamaterials*, Engineering Materials,
https://doi.org/10.1007/978-981-10-6376-3_3

be used to easily simulate the scattered sound waves without the need to fully set up and solve each reconfigured system. However, in practice, one must use the truncated finite-dimensional *T*-matrix which is usually computed using the null field method. For acoustically large obstacles or highly nonspherical particles, the null field method is numerically unstable.

Acoustic scattering simulation using the *T*-matrix method exterior to a ball circumscribing and centred inside the nonspherical scattering object is based on series expansion of the incident and scattered fields using spherical wave functions. In sound wave propagation simulation, the coefficients in the expansion of the input data(incident field) and the coefficients in the expansion of the output data (the scattered far field) processed through the Helmholtz operator are connected by an infinite matrix, because the Helmholtz equation is linear. This transition matrix is called the *T*-matrix [3, 4, 5, 6]. The acoustic scattering properties of an obstacle are completely described by its infinite acoustic *T*-matrix.

The *T*-matrix is a powerful tool when one is interested in scattering properties averaged over a range of incident directions because such information is readily obtained directly from the *T*-matrix. The *T*-matrix is also very useful for simulation of multiple scattering by ensembles of obstacles because the individual *T*-matrix of each scatterer can be combined using the translation addition theorem [3, 4]. Waterman [1] initially developed the *T*-matrix for electromagnetic scattering by a single scatterer. It was extended to multiple scatterers by Peterson and Ström [5]. The truncated *T*-matrix is usually computed using the null field also known as the extended boundary condition method [1, 3, 6–8].

For medium- to high-frequency problem or highly nonspherical obstacles, the null field method is numerically unstable. This is usually due to fast growth of the spherical Hankel function used in expansion of the surface field in the null field method [3]. For acoustically large or highly nonspherical obstacles, the *T*-matrix computation can become divergent [7, p. 543]. There are several approaches to tackle this problem [3, 4, 7] such as using expansions based on spheroidal or ellipsoidal functions for high-aspect ratio convex obstacles, and using slow extended precision arithmetic to minimize the effect to round off errors.

The *T*-matrix method could be computed using far field simulation based on surface integral equation for incident spherical waves, but to date, no algorithm of this type has been developed for acoustic scattering in three dimensions [3]. Many good algorithms exist for far field computations, and such details are described by Ganesh and Graham [5].

The fundamental computational difficulty in computing the *T*-matrix using a stable far field surface integral method is that this approach requires solving a large number of complex dense linear systems with a fixed scattering matrix (obtained by discretizing the associated surface integral operator) but thousands of right-hand sides(corresponding to each wave function used in expanding the incident field). Consequently, using a computational scattering algorithm that allows set-up, storage and LU-factorization of the numerical scattering matrix is crucial. LU-factorization is not practically possible for three-dimensional scattering problem using low-order schemes such as the standard boundary element methods that

usually require hundreds of thousands to millions of unknowns for low- to medium-frequency scattering for each incident direction. Such large systems require iterative solvers to avoid setting up and storing the scattering matrix, and hence, thousands of acoustic scattering problems are to be set up and solved for each term in the incident wave expansions separately. Ganesh and Graham [5] give computational complexity and CPU time requirements to three-dimensional scattering problems. They describe a spectrally accurate three-dimensional scattering algorithm that requires less than 10% of the unknown than several established algorithms and hence is ideal for acoustic *T*-matrix computation, solving for thousands of terms in the incident field expansion using simple back and forward substitution technique after the storage of the LU-factorization of the numerical scattering matrix which is only computed once.

3.3 Application of *T*-Matrix to Multiple Scattering in Acoustical Metamaterials

The existence of frequency ranges where the effective medium presents negative constitutive parameters is related to sub-wavelength resonances of the individual scatterers that constitute the metamaterial. These resonances can be, for example, due to soft-resonances or to Helmholtz-like resonances. The same phenomenon is found in EM waves under the name of Mie resonances, and they present an alternative way of designing EM metamaterials to that offered by split-ring resonators or metal-lodielectric composites which have been the dominant structures so far. Therefore, metamaterials based on local resonances are important not only for acoustic but also for EM metamaterials. It is known that the monopolar resonances in the individual scatterers are responsible for negative bulk modulus and that the dipolar ones are responsible for negative mass density [9, 10]. However, the behaviour of aggregates of scatterers in the homogenization limit has been partially explained since multiple scattering effects or anisotropic lattices have not been studied in depth.

Torrent and Sanchez-Dehesa [11] applied *T*-matrix method to multiple scattering in acoustic metamaterials. The description of acoustic metamaterials was given by using a multiple scattering approach under the assumption that the wavelength in the background is asymptotically large, whereas inside the scatterer, it remains finite. It is based on their theory which is already applied to the homogenization of sonic crystals [12–14]. They consider in the long wavelength limit an ensemble of ordered or disordered scatterers as an effective medium with acoustic parameters that are frequency dependent and can take negative values in certain frequency regions. The frequency-dependent parameters are given in terms of the lattice symmetry, the multiple scattering interactions and the fields at the scatterers' surface. This formulation covers all the previous results regarding single negative metamaterials (SNM) and double negative metamaterials (DNM) and, moreover, can be applied to any type of radially symmetric scatterer, to nonsymmetric lattices and even to any filling fraction.

3.4 Low-Frequency Resonances Giving Rise to Locally Negative Parameters

Low-frequency resonances will lead to locally negative parameters in acoustic metamaterials. The homogenization theories for aggregates of scatterers will be used here. These theories are based on small-wave number (long wavelength) expansions of the fields in both the background and the scatterers. When working with metamaterials, it is assumed that the wave number in the background is asymptotically small although the wave number inside the scatterer still be finite. Physically, it means that outside the scatterers, the wave field propagates through an effective medium, but the scatterers are still allowed to have complex scattering processes. The complexity leads to negative parameters in a narrow frequency region, as will be explained below.

A simple example of this type of scatterer A is a homogeneous fluid-like scatterer. If the sound speed inside this scatterer is much smaller than that of the background, $ca \ll cb$, then for a given frequency ω, the wavelength inside the scatterer, λa, is also much smaller than that in the background, i.e. $\lambda a \ll \lambda b$. Thus, outside the scatterer, the field will be a function of $kb = \omega/cb$, which is a slowly oscillating function, while inside the scatterer, the field will be a rapidly oscillating function of $ka = \omega/ca$. Since the low-frequency limit is considered, in principle, the medium to behave as an effective homogeneous medium with constant parameters, but in fact, due to the fields inside the scatterer, the resulting effective medium has parameters that are frequency dependent.

3.5 Acoustic Scatterers with Locally Negative Parameters

The wave equation for a pressure field in an inhomogeneous fluid is given as [15]

$$\nabla\left[\rho^{-1}(\boldsymbol{r})\nabla P(\boldsymbol{r})\right] + \frac{\omega^2}{\kappa(\boldsymbol{r})}p_{\boldsymbol{r}} = 0, \tag{3.1}$$

where $\rho(\boldsymbol{r})$ and $\kappa(\boldsymbol{r})$ are the fluid mass density and bulk modulus, respectively, and $\boldsymbol{r} = (r, \theta)$ defines an arbitrary point in the x–y-plane in polar coordinates. Here, the scatterer has radius Ra and is radially symmetric with parameters $\rho(r)$ and $\kappa(r)$, and embedded into a fluid background with acoustic parameters ρ_b and κ_b.

This is a canonical problem whose solution outside the scatterer is given in terms of the Bessel and Hankel functions [15]:

$$P(r, \theta; \omega) = \sum_{q=-\infty}^{\infty} A_q^0\left[J_q(k_b r) + T_q H_q(k_b r)\right]\mathrm{e}^{iq\theta}, \quad r > R_a \tag{3.2}$$

with $k_b^2 = \omega^2\rho/\kappa_b$. The coefficients A_q^0 are determined by the incident field, and the scatterer response is described by the matrix elements T_q. This matrix is diagonal for the case considered due to axial symmetry of the scatterer, and it can be obtained by solving the wave Eq. (3.1) inside the scatterer and applying boundary conditions at the scatterer surface, $r = R_a$. The conditions are the continuity of the pressure field and the normal component of the velocity:

$$P(R_a^+) = P(R_a^-), \tag{3.3a}$$

$$\frac{1}{\rho_b}\partial_r P(R_a^+) = \frac{1}{\rho(R_a^-)}\partial_r P(R_a^-). \tag{3.3b}$$

Since the scatterer is radially symmetric and parameters ρ and κ depend only on the radial coordinate, the field inside the scatterer can be expressed as a Fourier series of the form

$$P(r,\theta;\omega) = \sum_{q=-\infty}^{\infty} \kappa_q(\omega)\psi_q(r;\omega)\mathrm{e}^{iq\theta}, \tag{3.4}$$

where the eigenfunctions ψ_q(r; ω) are the solutions of the radial part of Eq. (3.1) in cylindrical coordinates,

$$\frac{\rho(r)}{r}\partial_r\left(\frac{r}{\rho(r)}\partial_r\psi_q(r;\omega)\right) + \left(\omega^2\frac{\rho(r)}{\kappa(r)} - \frac{q^2}{r^2}\right)\psi_q(r;\omega) = 0. \tag{3.5}$$

From this equation, after applying the boundary conditions, the general expression for the diagonal components of the T-matrix is easily obtained:

$$T_q = -\frac{\chi_q J_q'(k_bR_a) - J_q(k_bR_a)}{\chi_q H_q'(k_bR_a) - H_q(k_bR_a)}, \quad \chi_q = \frac{\rho(R_a)}{\rho_b}\frac{\psi_q(R_a;\omega)}{\partial_r\psi_q(R_a;\omega)}k_b. \tag{3.6}$$

This matrix contains two contributions: the background contribution is described by the Bessel and Hankel functions, while the scatterer contribution is described by the function χ_q. In general, Eq. (3.5) must be solved in order to obtain the χ_q functions; for example, for a homogeneous and isotropic cylinder of mass density ρ_a and speed of sound c_a, the solutions to Eq. (3.5) are Bessel functions; thus,

$$\chi_q = \frac{\rho_a c_a}{\rho_b c_b}\frac{J_q(k_aR_a)}{J_q'(k_aR_a)}. \tag{3.7}$$

Standard homogenization theory based on multiple scattering uses the asymptotic form of these expressions to derive the effective medium properties. In particular, the monopolar and dipolar terms ($q = 0$ and $q = 1$) are used to obtain the effective modulus and mass density, respectively, both being positive [13, 16].

However, it is shown below that metamaterial behaviour (i.e. effective parameters with negative values) appears in the regime where only the Bessel and Hankel functions of the background are replaced by their asymptotic forms at low frequencies. In other words, when the wavelength in the background is large, the wavelength in the scatterer is comparable in size.

So the arguments of the Bessel and Hankel functions are considered to be small, $k_bR_a \ll 1$, and use their asymptotic forms [17]. Then, the monopolar component of the T-matrix becomes

$$T_0 \approx \frac{\mathrm{i}\pi R_a^2 k_b^2}{4} \frac{1 + \frac{1}{2} k_b R_a \chi_0}{\frac{k_b^2 R_a^2}{2} \ln k_b R_a - \frac{1}{2} k_b R_a \chi_0}, \tag{3.8}$$

where the logarithmic term in the denominator is negligible in comparison with the linear term in kb in the low-frequency limit but cannot be neglected when dealing with metamaterials. This term, which has been omitted in many preceding studies about acoustic and EM metamaterials, is of paramount importance to determine the metamaterial effective parameters.

Equivalently, the dipolar component of the T-matrix is

$$T_1 \approx \frac{\mathrm{i}\pi R_a^2 k_b^2}{4} \frac{\chi_1 / k_b R_a - 1}{\chi_1 / k_b R_a + 1}. \tag{3.9}$$

Since behaviour is expected to that of a homogeneous scatterer with effective acoustic parameters ρ_a and κ_a, the matrix elements should have the standard form

$$T_0 \approx \frac{\mathrm{i}\pi R_a^2 k_b^2}{4} \left[\frac{\kappa_b}{\kappa_a} - 1 \right], \tag{3.10a}$$

$$T_1 \approx \frac{\mathrm{i}\pi R_a^2}{4} \left[\frac{\rho_a - \rho_b}{\rho_a + \rho_b} \right] k_b^2. \tag{3.10b}$$

Now, comparing Eqs. (3.8) and (3.9) with Eqs. (3.10a) and (3.10b), one can introduce frequency-dependent bulk modulus and mass density functions as follows:

$$\kappa_a(\omega)/\kappa_b = \frac{k_b^2 R_a^2}{2} \ln k_b R_a - \frac{1}{2} k_b R_a \chi_0 \tag{3.11a}$$

$$\rho_a(\omega)/\rho_b = \chi_1 / k_b R_a. \tag{3.11b}$$

These functions depend on the mass density at the scatterer surface, $\rho(r = R_a)$, and also depend on the field and its derivative at the surface: that is, $\psi_q(r = R_a; \omega)$ and $\partial_r \psi_q$ $(r = R_a; \omega)$, respectively. These quantities are frequency dependent and are responsible for the frequency dependence of the parameters $\kappa_a(\omega)$ and $\rho_a(\omega)$. It is worthwhile to show that $\kappa_a(\omega) \equiv \kappa_b$ and $\rho_a(\omega) \equiv \rho_b$ for a homogeneous

scatterer. This is done in Appendix (http://iopscience.iop.org/article/10.1088/1367-2630/13/9/093018/meta;jsessionid=7CB9A734A04B2E377A0FBBEED20097D3.c3#nj381920s6).

The derivation described above is similar to that in [9, 10] where the authors employed the coherent potential approximation method and seek the self-consistent solution to ensure that the inhomogeneous system embedded within an effective medium generates no scattering in the lowest order of frequency. However, in [9, 10], the expressions are left as functions of the so-called scattering coefficients, and therefore, they are very general and valid for any type of isotropic scatterer. Here, a further step is given and analyse the low-frequency limit of the scattering coefficients under the assumption that only the wave number in the background is asymptotically large, which allows us to understand metamaterial phenomena.

3.6 Multiple Scattering of Acoustic Waves in the Low-Frequency Limit

A cluster of cylindrical scatterers defined by their homogeneous parameters ρ_a and κ_a will behave in the low-frequency limit (i.e. for wavelengths larger than the typical separation between scatterers) as a homogeneous medium with effective parameters ρ^* and κ^*. These parameters were obtained by Berryman [18] in 1980 by making a comparison of the scattering properties of the cluster and the effective scatterer. The resulting estimate was not exact because multiple scattering effects were neglected. This approach was recently generalized by including all the multiple scattering interactions between scatterers, and very general expressions were obtained in [13, 14, 16].

The following subsections present a generalization of the results of previous studies to the case of metamaterials in which effective parameters are frequency dependent. It will be considered that parameters ρ_a and κ_a can be replaced by their corresponding frequency-dependent values $\rho_a(\omega)$ and $\kappa_a(\omega)$. It is demonstrated that this procedure is self-consistent and therefore gives a correct method for the extraction of the effective parameters of acoustic metamaterials.

3.7 Multiple Scattering Effects: The Δ Factor

A cluster of scatterers periodically distributed in a fluid background is considered. In the low-frequency limit, the cluster behaves like an effective fluid-like medium with the parameters given as [18]

$$\frac{1}{\kappa^*(\omega)} = \frac{1-f}{\kappa_b} + \frac{f}{\kappa_a(\omega)}, \tag{3.12a}$$

$$\rho*(\omega) = \frac{\rho_a(\omega)(1+f) + \rho_b(1-f)}{\rho_a(\omega)(1-f) + \rho_b(1+f)}\rho_b, \tag{3.12b}$$

where the frequency dependence of scatterer parameters (see Eqs. 3.11a and 3.11b) has been included.

While Eq. (3.12a) is valid for all filling fractions, Eq. (3.12b) is valid for diluted clusters only (i.e. low filling fractions). In [13] and [14], the expressions for the effective density were generalized to the case of high filling fractions, and all the multiple scattering terms were introduced in Eq. (3.12b) by means of the so-called Δ factor, leading to

$$\rho*(\omega) = \frac{\rho_a(\omega)(\Delta+f) + \rho_b(\Delta-f)}{\rho_a(\omega)(\Delta-f) + \rho_b(\Delta+f)}\rho_b. \tag{3.13}$$

The factor Δ represents a correction to the effective density and takes into account all the multiple scattering interactions between the cylinders in a cluster or in an infinite lattice. Technical details of its derivation are given in Appendix (http://iopscience.iop.org/article/10.1088/1367-2630/13/9/093018/meta;jsessionid=A9746E63EF7AAEE3334FA959047513E6.c3#nj381920s7). Δ also contains information on the mass density of the cylinders forming the cluster, and hence, if we want to introduce a frequency-dependent factor $\Delta(\omega)$, the frequency-dependent mass density must also be considered.

It has been shown that the contribution of the scatterers' density to the Δ factor is made through the factor η defined as [13, 14]

$$\eta = \frac{\rho_a - \rho_b}{\rho_a + \rho_b}. \tag{3.14}$$

It is tempting to replace $\rho_a \rightarrow \rho_a(\omega)$ in order to define the frequency-dependent $\Delta(\omega)$. However, it must be remembered that the η factor appears in the power expansion of the q-component of the T-matrix as follows:

$$\lim_{k_b \to 0} \frac{T_q}{k_b^{2|q|}} = \frac{\mathrm{i}\pi R_a^{2q}}{q!(q-1)!2^{2q}} \frac{\rho_a - \rho_b}{\rho_a + \rho_b}. \tag{3.15}$$

Then, for the Δ factor to be consistent with our theory, we must compute Tq given by Eq. (3.6) taking into account that the wavelength inside the scatterer is still finite. This leads to the following equation that replaces Eq. (3.15):

$$\frac{T_q}{k_b^{2|q|}} \approx \frac{\mathrm{i}\pi R_a^{2q}}{q!(q-1)!2^{2q}} \frac{q\chi_q/k_bR_a - \rho_b}{q\chi_q/k_bR_a + \rho_b}. \tag{3.16}$$

This equation shows that we can generalize the Δ factor as long as one makes the substitution

$$\eta \rightarrow \eta(\omega) = \frac{q\chi_q/k_bR_a - \rho_b}{q\chi_q/k_bR_a + \rho_b} \tag{3.17}$$

in the corresponding multipolar components in [13, 14].

The Δ factor was studied in the quasi-static limit (i.e. for $\lambda \rightarrow \infty$), and it was demonstrated that its contribution is important only for high filling fractions and for strong scatterers [13, 14]. This is because the coupling to higher multipolar components is always weaker. Similar behaviour is expected for the frequency-dependent factor, $\Delta(\omega)$, although we would expect in this case the presence of resonances different from monopolar or dipolar. However, it was shown in [14] that the multipolar contributions to the Δ factor are proportional to a set of lattice sums Sq, whose values depend on the lattice symmetry. Thus, for the square or hexagonal lattices, only the sums such that $q = 4n$ or $q = 6n$, respectively, for $n = 1, 2, \ldots$, are different from zero. Thus, the first multipolar term appearing in the Δ factor is that with $q = 4$ for a square lattice and with $q = 6$ for a hexagonal one. The resonances of these modes for a lattice of homogeneous cylinders occur at frequencies higher than those for $q = 0$ and $q = 1$. Thus, they cannot be observed in the low-frequency limit. It does not mean, however, that the Δ factor is not relevant, as will be discussed in the following example, but rather that the higher-order resonances do not contribute to the effective parameters.

The contribution of the Δ factor to the effective parameters is better understood for strong scatterers. For the case of almost rigid scatterers (i.e. cylinders made of heavy solid materials embedded in air), this factor contributes considerably to the calculation of the effective parameters, but since these cylinders do not possess low-frequency internal resonances, they are of no interest to this study. In contrast, the case of soft scatterers like air cylinders embedded in water represents the opposite system and is discussed below.

Figure 3.1 shows the bulk modulus of a hexagonal lattice of air cylinders in a water background ($\kappa_a = 5.14 \times 10^{-5}\kappa_b$), $\rho_a = 10^3$ kg m^{-3} and $\rho_b = 1.24$ kg m^{-3}) for several filling fractions. It has been pointed out that the effective bulk modulus does not need a multiple scattering correction. However, this example demonstrates that the homogenization limit can be defined here only from a frequency-dependent theory since the modulus is negative in a wide frequency range. The expression for the frequency-dependent bulk modulus is given by Equation (http://iopscience.iop.org/article/10.1088/1367-2630/13/9/093018/meta;jsessionid=A9746E63EF7AAEE3334FA959047513E6.c3#nj381920eqnA.1a), where we observe that, since $B_a/B_b \approx 5\times10^{-5}$, the dominant contribution comes from the logarithmic term. The second term contributes to a weak resonance near the reduced frequency of 0.3, as can be

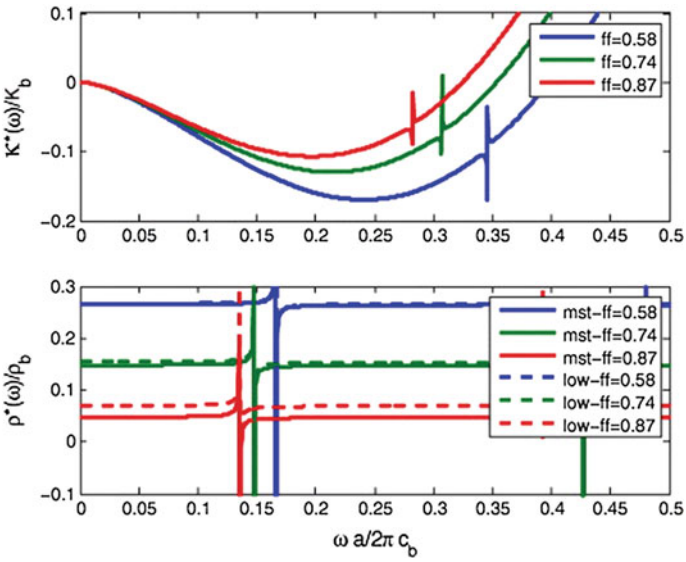

Fig. 3.1 Upper panel effective bulk modulus of a composite medium made of air cylinders distributed in a hexagonal lattice and embedded in water. The results are shown for three filling fractions *ff*. The effective bulk modulus is negative in the whole frequency region considered as homogenization. Only in a very narrow region corresponding to infinite wavelength is the effective bulk modulus positive. Lower panel the corresponding effective mass densities. The dashed lines correspond to the dilute approximation (low-*ff*), and the continuous lines represent calculations where the multiple scattering terms are considered (mst-*ff*) (After Daniel and Jose Sanchez-Dehesa)

observed in the figure. On the one hand, this resonance is too sharp to be measured in a real system; on the other, it occurs beyond what one could consider the homogenization limit, which is found to be at $a/\lambda \approx 0.25$.

The lower panel of Fig. 3.1 shows the frequency-dependent mass density for three different filling fractions. The continuous line corresponds to the calculation considering the $\Delta(\omega)$ factor as explained above; the dashed line corresponds to the low filling fraction approximation. It is shown how the multiple scattering correction is important for high filling fractions only, as expected, and also, one can see that the resonant frequency is almost the same in both situations, showing that the Δ factor is relevant mainly in the quasi-static limit.

Finally, Fig. 3.2 shows the imaginary part of the effective speed of sound. As the effective bulk modulus is negative for the whole range of frequencies considered as the homogenization limit, the effective speed of sound is always purely imaginary. It becomes real only in the narrow region where the effective mass density is also negative, due to the local resonance. This sharp resonance can be observed numerically; however, it is hard to believe that this could be observed experimentally. Thus, one can conclude that the system of air cylinders in a water background will always be a nonpropagating medium in the low-frequency limit.

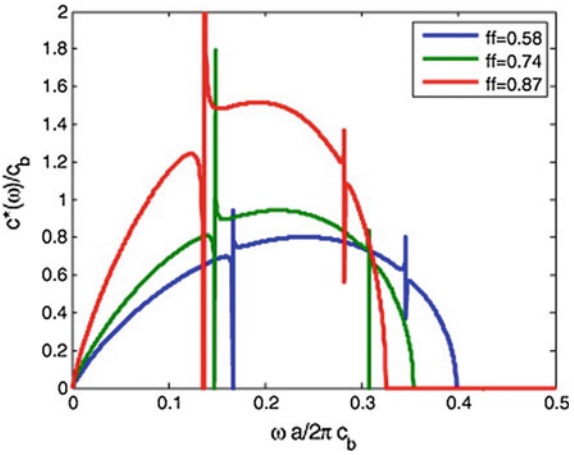

Fig. 3.2 Imaginary part of the effective sound speed for a medium consisting of a hexagonal lattice of air cylinders in a water background. The lattice constant is a

Zoom In Zoom Out Reset image size

3.8 Suitability of the *T*-Matrix Method to Multiple Scattering in Acoustic Metamaterials

There are several methods for dealing with multiple scattering in solids. They should not be used blindly. Acoustic metamaterials are artificial composites/crystals with periodic structures enabling negative material parameters such as negative mass density and negative bulk modulus. This is due to local resonances due to propagating sound waves with restriction to certain frequencies range. This will enable the control of multiple scattering by the choice of uniting cells of the metamaterial to produce negative mass density and negative bulk modulus. The *T*-matrix method of multiple scattering is introduced from quantum field theory of multiple scattering, although there are other methods of multiple scattering. But they are for treating scattering in random media. *T*-matrix is a symmetry transformation. Hence, it is suitable for treating a medium with symmetry property such as metamaterial.

3.9 Diffraction

Diffraction refers to various phenomena which occur when a wave encounters an obstacle or a slit. It is defined as the bending of wave around the corners of an obstacle or aperture into the region of geometrical shadow of the obstacle. In classical physics, the diffraction phenomena are described as the interference of waves according to the Huygens–Fresnel principle. These characteristic behaviours are exhibited when a wave encounters an obstacle or a slit that is comparable to its

wavelength. Similar effects occur when wave travels through a medium with a varying refractive index or when a sound wave travels through a medium with varying acoustic impedance. If the obstructing object provides multiple, closely spaced openings, a complex pattern of varying intensity can result. This is due to the addition, or interference, of different parts of a wave interference that travels to the observer by different parts, where different path lengths result in different phases.

Diffraction arises because of the way in which waves propagate. This is described by the Huygens–Fresnel principle and the principle of superposition of waves. The propagation of a wave can be visualized by considering every particle of the transmitted medium on a wavefront as a point source for a secondary spherical wave. The wave displacement at any subsequent point is the sum of these secondary waves. When waves are added together, their sum is determined by the relative phases as well as the amplitudes of the individual waves so that the summed amplitude of the waves can have any value between zero and the sum of the individual amplitudes. Hence, diffraction patterns usually have a series of maxima and minima. There are various analytical models which allow the diffracted field to be calculated, including the Kirchhoff–Fresnel diffraction equation, which is derived from wave equation, the Fraunhofer diffraction approximation of the Kirchhoff equation which applied to the far field and the Fresnel diffraction approximation which applied to the near field. Most configurations cannot be solved analytically, but can yield numerical solutions through finite element and boundary element methods.

It is possible to obtain a qualitative understanding of many diffraction phenomena by considering how the relative phases of the individual secondary wave sources vary, and in particular, the conditions in which the phase difference equals half a cycle in which case waves will cancel one another out.

The simplest descriptions of diffraction are those in which the situation can be reduced to a two-dimensional problem. For water waves, this is already the case; water waves propagate only on the surface of the water. For light, we can often neglect one direction if the diffracting object extends in that direction over a distance far greater than the wavelength. In the case of light shining through small circular holes, we will have to take into account the full three-dimensional nature of the problem.

3.10 Diffraction by Negative Inclusion

In acoustic metamaterial, the diffraction will take place in a negative material with negative mass density and negative bulk modulus.

3.11 Theory of Diffraction by Negative Inclusion

3.11.1 Formulation of Forward Problem of Diffraction Tomography

The diffraction in a double negative medium (DNG) can be studied following the formulation of diffraction tomography. The ability to control and manipulate diffraction will give rise to a new form of diffraction and a new theory of diffraction. We will consider the diffraction by negative inclusion which described a double negative medium compared with the conventional diffraction tomography which deals with positive medium with parity equals +1. We shall follow the approach of Burov et al. [19] who use the linearized hydrodynamic equation as the starting point instead of the Helmholtz wave equation to derive the Lippmann–Schwinger equation used in diffraction tomography. The reason is the Helmholtz wave equation involves the refractive index squared. This is not quite consistent and requires additional justifications concerning the sign of n in a left-handed medium that is associated with the necessity of doing a positive work by the source, with the direction of the vector of the energy flux away from the source, with the causality principle, etc. We have to resort to the causality principle to justify the negative sign of the refractive index for a negative medium [16]. The linearized hydrodynamic equation, on the other hand, does not involve inconsistency, arises in choosing the sign of n, the refractive index.

The linearized hydrodynamic equation (for acoustics) is:

$$\begin{aligned} \frac{\delta}{\delta t}(\hat{\kappa} p) + \nabla \vec{V} &= \varphi \\ \frac{\delta}{\delta t}(\hat{\rho} p) + \nabla \vec{p} &= \vec{f} \end{aligned} \tag{3.18}$$

where φ and $\vec{f}$ are the scalar and vector primary sources of the acoustic field, respectively. For media without dispersion, $\vec{p}$ and $\hat{\kappa}$ are scalars. When dispersion is present, they are convolution-type operators over the time variable.

A four-dimensional representation of the field variables (pressure p and three components of velocity $\vec{V}$) is used in (3.18). The resonator response function $Q(\tau)$ which characterizes the appearance of a secondary source in response to the incident field is then a 4×4 matrix at each fixed τ. The properly transformed Krämers–Krönig relations also acquire a matrix form.

Since ρ and κ can be negative only in a narrow frequency band, whose width is determined by the resonator Q-factor, Burov et al. [19] discuss only stationary monochromatic fields at this stage. As a result, they can abstract from the specific resonator design and disregard the explicit form of the response function $Q(\tau)$, reasoning in the language of effective functional parameters ρ and κ, which depend

only on the coordinates at a fixed frequency. It should be noted that the monochromatic case cannot give an answer to the question about the relationship between the real and imaginary parts of each functional parameters characterizing the medium since this relationship follows precisely from the Krämers–Krönig relations. However, this relationship should also be taken into account when working with monochromatic fields.

An ordinary (positive) medium is considered as a background with parameters ρ_o and κ_o, while a negative medium is obtained from it by adding corrections $\rho'(\vec{r})$ and $\kappa'(\vec{r})$ (which are not small): $\rho(\vec{r}) \equiv \rho_o + \rho'(\vec{r})$, $\kappa(\vec{r}) \equiv \kappa_o + \kappa'(\vec{r})$. This approach allows the propagation of waves in media with arbitrary (in magnitude and sign) ρ and κ distributions to be calculated using the well-known methods of the scattering theory that are not based on the Born approximation or similar assumptions.

In the monochromatic case, the system of Eqs. (3.18) for time dependence —$\exp(-i\omega t)$ transforms to

$$\nabla\vec{V} - i\omega qp = \varphi; \nabla p - i\omega\rho\vec{V} = \vec{f} \tag{3.19}$$

Burov et al. [19] introduce column vectors $\check{U} \equiv \begin{bmatrix} \vec{V} \\ P \end{bmatrix}$, $\check{F} \equiv \begin{bmatrix} \vec{f} \\ \varphi \end{bmatrix}$ and an operator $\hat{A}$ in the form of a matrix acting both in the coordinate space and in the space of field variables $\begin{bmatrix} \vec{V} \\ P \end{bmatrix}$:

$$\hat{A} \equiv \begin{bmatrix} -i\omega\rho(\vec{r}) & \nabla \\ \nabla & i\omega\kappa(\vec{r}) \end{bmatrix} = \hat{A}_o - \hat{A},$$

where $\hat{A}_o \equiv \begin{bmatrix} -i\omega\rho_o & \nabla \\ \nabla & i\omega\kappa_o \end{bmatrix}$ and $\hat{A}_1 \equiv \begin{bmatrix} i\omega\rho'(\vec{r}) & 0 \\ 0 & i\omega\kappa'(\vec{r}) \end{bmatrix}$ are the operators that characterize the homogeneous medium of a positive background and its perturbation, respectively. It should be noted that the introduced quantities are a combination of both scalar and vector field components in the region under study. In matrix form, system (3.19) is $\hat{A}\check{U} = \check{F}$. At $\hat{A}_1 = 0$, implying the absence of corrections $\rho'(\vec{r})$ and $\kappa'_o(\vec{r})$, the sources $\check{F}$ produce the incident field $\check{U}_o \equiv \begin{bmatrix} V_o \\ P_o \end{bmatrix}$, in the region under consideration, and the system is

$$\hat{A}_0\check{U}_o = \check{F} \tag{3.20}$$

hence

$$\check{U}_o = \hat{A}_o^{-1}\check{F} \tag{3.21}$$

Let $\hat{G}$ be the retarded Green function of a homogeneous medium for the system of (3.20), i.e. a system of type (3.19),

$$\hat{A}_o^{-1}(\cdot) = \int \hat{G}(\vec{r} - \vec{r}')(\cdot)d\vec{r}'$$

In the presence of corrections ρ' and κ', the following relation holds for the $\check{U}$:

$$\begin{aligned}\check{U} &= \hat{A}^{-1}\check{F} = \hat{A}^{-1}\hat{A}_0\hat{A}_o^{-1}\check{F} = \left[\hat{A}^{-1}\hat{A}_0\right]\check{U}_o \\ &= \left[\hat{A}^{-1}\hat{A}\right]^{-1}\check{U}_o = \left[\hat{A}_o^{-1}\left(\hat{A}_0 - \hat{A}_1\right)\right]^{-1}\check{U}_o = \left[\check{U} - \hat{A}_{o1}^{-1}\right]^{-1}\check{U}_o\end{aligned}$$

Hence

$$\check{U} = \left[\hat{E} - \hat{G} * \hat{A}_1\right]^{-1}\check{U}_o \tag{3.22}$$

where $\hat{E}$ = unit operator and $*$ denote the convolution operation in the coordinate space.

Equation (3.22) is an operator form of the solution to the Lippmann–Schwinger equation for the field $\check{U}$:

$$\check{U}(\vec{r}) = \check{U}_o(\vec{r}) + \int_R \hat{G}(\vec{r} - \vec{r}')\left[\hat{A}_1(\vec{r}')\check{U}(\vec{r}')\right]d\vec{r}' \tag{3.23}$$

where R is the localization region of the ρ' and κ' inhomogeneities.

Here, the operator $\hat{A}_1(\vec{r}')$ acts in the space of wave variables $\left[\vec{\vec{P}}\right]$, while in the coordinate space, it is a local multiplication operator at each point $\vec{r}$. The inverse operator in (3.22) exists since all its eigenvalues are complex for passive media, to which the media under consideration belongs [20] and imposes no constraints on the scatterer strength.

An explicit expression for the matrix form of the retarded Green function $\hat{G}$ can be derived [21] by passing the space of wave vector $\vec{\kappa}$, i.e. by decomposing the fields using a set of plane harmonic waves for which the pressure and oscillation velocity varies as—$\exp(-i\omega t + i\vec{\kappa}\vec{r})$. In this space, the operator $\hat{A}_o$ takes the form of an ordinary matrix $\begin{bmatrix} -i\omega\rho_o & i\vec{\kappa} \\ i\vec{\kappa} & -i\omega\kappa_o \end{bmatrix}$, whose inversion gives $\begin{bmatrix} -i\omega\rho_o & i\vec{\kappa} \\ i\vec{\kappa} & -i\omega\kappa_o \end{bmatrix}^{-1} = \frac{1}{\kappa_o^2 - \vec{\kappa}^2}\begin{bmatrix} -i\omega\kappa_o & i\vec{\kappa} \\ i\vec{\kappa} & -i\omega\rho_o \end{bmatrix}$, where $k_o = \omega\sqrt{\rho_o\kappa_o}$ is the wave number in the background medium. To obtain the Green function $\vec{G}$ in coordinate representation, we must perform the inverse Fourier transform (the transition from $\vec{\kappa}$ to $\vec{r}$) of this expression. In this case, a pole appears in the denominator going around which requires introducing an infinitesimal imaginary part $\pm\xi$ for the wave number: $k_o = \omega\sqrt{\rho_o\kappa_o} \pm i\xi$, where $\xi \to +0$. The "+" or "−" sign in front of the

infinitesimal but positive ξ defines whether the Green function will be retarded or advanced one. As a result, for the retarded Green function, we derive the expression $\hat{G}(\vec{r}-\vec{r}\,') \equiv \begin{bmatrix} -i\omega\rho_o & \nabla \\ \nabla & i\omega\kappa_o \end{bmatrix} G(\vec{r}-\vec{r}\,')$, where $G(\vec{r}-\vec{r}\,')$ is the retarded Green function of the Helmholtz equation for a homogeneous space of the corresponding dimension with parameters ρ_o and κ_o, whose analytical form is well known. The operator $\nabla \equiv \nabla_r$ acts on the argument $\vec{r}$ of the function $G(\vec{r}-\vec{r}\,')$: in the one-dimensional (D = 1) and two-dimensional (D = 2) cases, the Green function for the system of Eq. (3.19) is then

$$\hat{G}_{D=1}(x-x') = \frac{\exp(ik_o|x-x'|)}{2} \begin{bmatrix} \sqrt{\frac{k_o}{\rho_o}} & sgn(x-x') \\ sgn(x-x') & \sqrt{\frac{\rho_o}{k_o}} \end{bmatrix} \tag{3.24}$$

$$\hat{G}_{D=2}(\vec{r}-\vec{r}\,') = \frac{i}{4} \begin{bmatrix} -i\omega\kappa_0 H_0^{(1)}(\kappa_0|\vec{r}-\vec{r}\,'|) & \frac{\vec{r}-\vec{r}\,'}{|\vec{r}-\vec{r}\,'|}\kappa_0 H_1^{(1)}(\kappa_0|\vec{r}-\vec{r}\,'|) \\ \frac{\vec{r}-\vec{r}\,'}{|\vec{r}-\vec{r}\,'|}\kappa_0 H_1^{(1)}(\kappa_0|\vec{r}-\vec{r}\,'|) & -i\omega\rho_0 H_0^{(1)}(\kappa_0|\vec{r}-\vec{r}\,'|) \end{bmatrix} \tag{3.25}$$

Equations (3.22) and (3.23) are written for the system of hydrodynamic Eq. (3.19) and not for the Helmholtz wave equation.

Since the background medium in Eqs. (3.22) and (3.23) is positive, there is no need to use the advanced Green function to calculate the field in a negative medium. These relations allow the field to be reproduced for any configuration of a finite (in size) scatterer that consists of a positive or negative material for an arbitrary incident field $\breve{u}_0$.

One has to discretize Eq. (3.23). The region under consideration is sampled by dividing it into areas δS_n, characterized by the radius vectors of their centres $\vec{r}_n$. The area size is chosen to be much smaller than the wavelength, in such a way that the parameters of the medium ρ and κ, within each area as well as the incident field $\breve{u}_0$ and the diffracted field $\breve{u}$, may be considered constant. The integration on the right-hand side of Eq. (3.23) is reduced to the summation over the area δS_n, in each of which $\hat{A}_1$ and $\breve{u}$ are assumed to be constants determined only by the area number n. For the field inside area m, the sampled form of the Lippmann–Schwinger equation becomes:

$$\begin{aligned} \breve{u}_m &= \breve{u}_{om} + \sum \left[\int\limits_{\delta S_n} \hat{G}(\vec{r}_m - \vec{r}\,')\hat{A}_1(\vec{r}\,')\breve{u}(\vec{r}\,')d\vec{r}\,' \right] \\ &\approx \breve{u}_{om} + \sum_n \left[\int\limits_{\delta S_n} \hat{G}(\vec{r}_m - \vec{r}\,')d\vec{r}\,' \right] \left[\hat{A}_1\breve{u}\right]_n \end{aligned} \tag{3.26}$$

From Eqs. (3.24) and (3.25), the Green function is smooth everywhere in the one-dimensional case and at $\vec{r} \neq \vec{r}'$ in the two-dimensional case. The amount of calculations can then be reduced significantly when calculating the elements of the matrix $\hat{G}_{mn} \approx \int_{\delta S_n} \hat{G}(\vec{r}_m - \vec{r}')d\vec{r}'$, by assuming it to be constant within the area and equal to its value at the area's centre in these cases:

$$\hat{G}_{mn} \approx \hat{G}(\vec{r}_m - \vec{r}_n)\delta S_n \tag{3.27}$$

Equation (3.27) cannot be used to calculate the matrix elements $\hat{G}_{mn}$ in the two-dimensional and three-dimensional case at $m = n$ and must perform the integration over the area $\delta S_n = m$. In this case, the singularity of the function $\hat{G}$, that arises when its argument tends to zero (in the two-dimensional case, the Hankel functions $H_0^{(1)}$ and $H_1^{(1)}$ have a singularity) is integrable.

As a result of the estimation of all matrix elements $\hat{G}_{mn}$, Eq. (3.26) takes the form

$$\breve{u}_m = \breve{u}_{om} + \sum_n \hat{G}_{mn}\left[\hat{A}_1\breve{u}\right]_n \tag{3.28}$$

The following is the sampled analogue of Eq. (3.22):

$$\breve{u}_m = \left[E_{nm} - \left[\hat{G}\hat{A}_1\right]_{nm}\right]^{-1}\breve{u}_{on} \tag{3.29}$$

In Eq. (3.29), the matrix elements $\left[\hat{G}\hat{A}_1\right]_{nm}$ are formed by the products of the matrices $\hat{G}_{mn}$ and $\left[\hat{A}_1\right]_m$ at fixed m. All quantities in Eqs. (3.22) and (3.23) and (3.16–3.29) are defined on the direct product of the space of field variables and the coordinate space of vector $\vec{r}$ sampled in terms of the indices m and n. Hence, it is appropriate to use Eq. (3.29) to find the field inside the scatterer localization region R and in its neighbourhood with minimum sizes required by the problem, and since in the case of an unjustifiable increase in the sizes of the region being analysed, the matrix inversion operation requires a very large amount of a computer's random access memory.

It has to be noted that during the inversion of the nonsampled operator in Eq. (3.22), the width of its spatial spectrum increases, since the inversion procedure reflects the entire set of rescattering process [22]. Therefore, even at the formation stage of the direct matrix $E_{nm} - \left[\hat{G}\hat{A}_1\right]_{nm}$, one has to significantly reduce the spatial sampling step for the inversion of the matrix in Eq. (3.29) to lead to the correct values of $\breve{u}_m$. The optimal choice of the sampling step will be considered during the process of numerical simulation. Once the internal field $\breve{u}_n$ and consequently the secondary sources of the scattered field have been found at all points of region R, the total field $\breve{u}_m$ out of any point $\vec{r}_m \notin R$ can be found as the sum of the incident field from the primary sources and the scattered field from the sampled secondary

sources $\left[\hat{A}_1\check{u}\right]_n$ from Eq. (3.23), which after the sampling taken a form similar to Eq. (3.26):

$$\check{u}_m^{out} = \check{u}_{om}^{out} + \sum_n \hat{G}_{mn}\left[\hat{A}_1\check{u}\right]_n \tag{3.30}$$

Hence, Burov et al. [19] have constructed a mathematical framework suitable for modelling the wave processes in both positive and negative media.

3.11.2 *Modelling Diffraction Procedure in a Negative Medium*

In diffraction to tomography, one is concerned with the propagation of sound wave in an inhomogeneous medium which in this case is the composite double negative material (DNG). This will involve refraction, reflection, transmission and multiple scattering processes at the boundaries. Bliokh and Bliokh [23] argued that a two-dimensional medium with negative refraction of a wave at a boundary can be considered as a left-handed medium. However, there exist several more effects that allow one to talk about a negative medium even in the one-dimensional case. First, these include the wave reflection and transmission coefficients in pressure and oscillation velocity in combination with information about the sign of the effective density of the medium. Thus, for example, in the special case of a perfect match between the bordering positive (with density ρ_0 and phase velocity c_0) and negative (ρ and c) acoustic media, when their densities and compressibilities relations $\rho = \rho_0$ and $\kappa = -\kappa_0$ hold, the impedances $\rho c = \rho_0 c_0$ and the absolute values of the phase velocities of these media coincide. Owing to the coincidence of the impedances, there is no wave reflected from the boundary. Thus, while talking about a one-dimensional negative medium, the phase velocity c in it may be considered from the absence of a reflected wave and a priori knowledge about the negativity of the effective density $\rho < 0$ to be also negative. Secondly, the conclusion about whether the directions of the energy propagation and the phase velocity are the same or opposite can be drawn directly from the following effect.

For a plane monochromatic acoustic wave with a wave vector $\vec{k}_0$, propagating along the Z axis (pressure and velocity $P_0, v_0 \sim e^{i\vec{k}_0\vec{r}} = e^{\pm ik_0 z}$), the three-dimensional plot with the imaginary and real part of the pressure or oscillation velocity along the X and Y axis, respectively, and with the only spatial coordinate along the z axis is a left-handed or right-handed helix, depending on whether the wave vector and, hence, the phase velocity are oriented in the negative (Fig. 3.5; $P_0 v_0 \sim \mathrm{e}^{-ik_0 z}$) or positive direction of the Z axis. In other words, for a fixed time dependence $\sim \mathrm{e}^{-i\omega t}$, there is a unique relationship between the orientation of vector $\vec{k}_0$ and the sign of helicity, i.e. the sign of HELICX is determined by the direction of $\vec{k}_0$ in a given medium, positive or negative. If two waves propagate in opposite

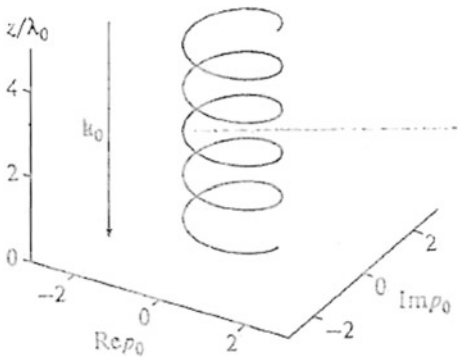

Fig. 3.3 Graphic representation of the incident monochromatic wave. The arrow indicates the direction of the wave vector $\vec{k}_0$ (From [19])

directions in a positive or negative medium, then the circular helix becomes an elliptical one or even concentrates in the form of oscillations on a plane if the amplitudes of both waves are equal. Since the direction of rotation of the circular helix is uniquely related to the direction of the phase velocity in the medium, the change of the sign of helicity at the boundary between two media is a criterion that one of them is negative.

Since Eqs. (3.29) and (3.30) suggest the field construction simultaneously in the entire scattering region R, scatterers with finite sizes are considered in numerical simulations. A background medium with $\rho_0 \equiv 1$ and $\kappa_0 \equiv 1$ is assumed to be unbounded, and the incident field $\breve{u}_0$ is defined analytically everywhere. In the numerical simulations of Burov et al. [24], they considered a layer of the background medium with a thickness of $5\lambda_0$ where λ_0 is the wavelength in the background medium. In turn, a thinner layer of a positive ($\rho \equiv 2$ and $\kappa \equiv 5$) or perfectly matched (with the background medium) negative ($\rho \equiv -1$ and $\kappa \equiv -1$) material with a thickness of $2\lambda_0/3$ was placed in the middle part of this layer. The sampling step was $\lambda_0/100$. The acoustic pressure field of the incident plane wave P_0 which is described by one component in the one-dimensional case of normal incidence on the layer here is shown in Fig. 3.3.

3.11.3 Results of Numerical Simulation

The total pressure P and the scattered field $P_{SC} \equiv P - P_0$ calculated when a layer of a positive material was included in the background medium are presented in Fig. 3.6.

The helix corresponding to the total pressure field P (Fig. 3.4a) changes its shape (but not the sign of helicity) at the boundaries of the layer, because the waves reflected from the boundary appear. Figure 3.4b shows the field scattered by the layer. It shows that the helix corresponding to the wave reflected from the layer has an inverse helicity with respect to the incident field (Fig. 3.3), since the wave vectors of the incident and reflected waves are directed oppositely. The radius of

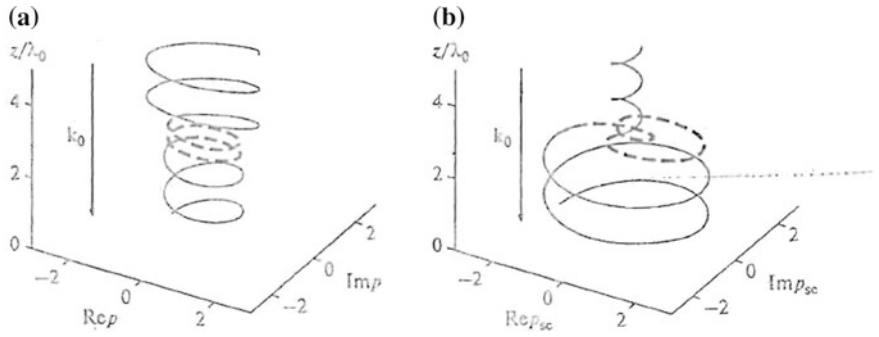

Fig. 3.4 Calculated total acoustic pressure field P (**a**) and scattered field P_{SC} (**b**) in a layer of a positive material. The solid and dashed lines indicate the fields in the background positive medium and in the layer placed in it, respectively. The arrow indicates the direction of the wave vector $\vec{k}_0$ of the incident wave

this helix, which is equal to the amplitude of the reflected wave $|R_p P_0|$ (here $|P_0| = 1$), shows the magnitude of the reflection coefficient from the layer in pressure $|R_p|$ to be estimated. This coefficient can be compared with its theoretical value calculated from the formula [22, p. 40]

$$|R_p| = \frac{|s^{-1} - s|}{\sqrt{(s^{-1} - s)^2 + 4\cot^2(kd)}} \tag{3.31}$$

where $S \equiv \frac{\rho_0 c_0}{\rho c}$, k and c are the wave number and the speed of sound in the medium, k_0 and c_0 are those in the background medium, and d is the layer thickness. For $\rho \equiv 2$ and $\kappa \equiv 5$, $|R_p|$ can be analytically obtained as approximately 0.3588. The magnitude of the reflection coefficient calculated using the data from Fig. 3.4b $|R_p| = 0.3576$, corresponding to its theoretical value within the limits of the errors caused by sampling. This is indicative of an adequate qualitative and quantitative description of the fields with Eqs. (3.22) and (3.23).

Figure 3.5 presents similar plots for an inclusion in the form of a layer of a negative material. Note that the sign of helicity of the total field changes (Fig. 3.5a) at the boundaries of the layer. This means that the phase velocity of sound in a negative medium is opposite in direction to that in positive one. It should also be noted that the radius of the helix of the scattered field (Fig. 3.5b) on the segment of the Z axis from $2.7\lambda_0$ to $5\lambda_0$ is 0, and hence, there is no reflection from the layer at $\rho \equiv 1$ and $\kappa \equiv 1$, as expected, owing to a perfect match between the background medium and the medium of a negative material with identical acoustic impedances. Since there is no reflected wave, the Poynting vector $\vec{S}$, along with the group velocity, is constant in the entire segment. Under consideration, it is directed along the Z axis. Thus, the wave vector $\vec{k}$ is directed along $\vec{S}$ in a positive medium and

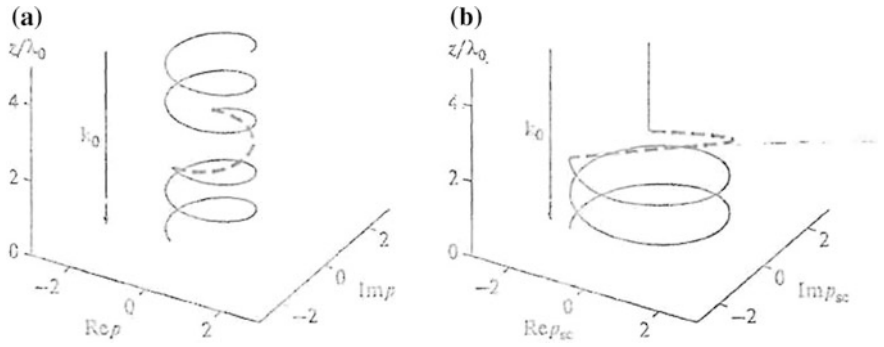

Fig. 3.5 Calculated total acoustic pressure field P (**a**) and scattered field P_{SC} (**b**) in a layer of a negative material. The solid and dashed lines indicate the fields in the background positive medium and in the layer placed in it, respectively. The arrow indicates the direction of the wave vector $\vec{k}_0$ of the incident wave (After [19])

opposite to it in a negative one. As a result, as the wave energy propagates along the vector $\vec{S}$, the coordinate phase shift of the wave has opposite signs in positive and negative media.

The numerical simulations above for the one-dimensional case show that the simultaneous negativity of the density and compressibility of the material is a sufficient condition that the medium has a number of properties usually attributed to negative refraction.

The next step is to consider two-dimensional model of a negative medium, which allows the effects of negative refraction to be observed. The following cases are considered: (a) scattering of plane waves by negative inclusions in the shape of a cylinder, (b) a plane parallel plate introduced in a positive background medium, (c) inclusions of a similar shape but composed of a positive material.

The problem about the scattering of a plane wave by a cylinder has an analytical solution. This problem was solved numerically using Eqs. (3.19) and (3.30). Subsequently, the field was calculated at a given distance from the cylinder centre at various angles with respect to the direction of the incident wave. The results of the calculations for an inclusion in the shape of a cylinder of radius $R = \lambda_0$ with parameters $\rho \equiv 1$ and $\kappa \equiv 5$ of the positive material are presented in Fig. 3.6

An angle of 0° corresponds to the direction of the incident plane wave in which the pressure amplitude was taken to be 1. The solid curve indicates the dependence of the pressure amplitude of the scattered field on the scattering angle at a distance of $4\lambda_0$ from the cylinder centre derived from the analytical solution, and the dotted line indicates the dependence calculated from Eqs. (3.29) and (3.30). The sampling step was $\lambda_0/10$. The deviation of the cylinder shape from a strictly cylindrical one caused by sampling in the calculation based on Eqs. (3.29) and (3.30) is responsible for the slight difference between the two curves. To within this error, a close

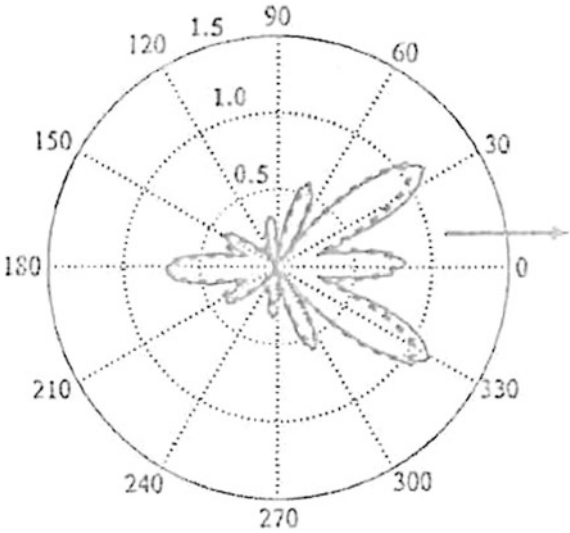

Fig. 3.6 Diagram of the acoustic pressure $|P_{SC}|$ of the field of a plane monochromatic wave with the unit's amplitude scattered by a cylinder of a positive material. The arrow indicates the direction of its propagation. The solid and dashed lines indicate the fields calculated using the exact formulae and Eqs. (3.29) and (3.30), respectively

coincidence is retained for various cylinder radii and contrasts. Thus, our comparison of the numerical simulations with the analytical solution indicates that the approach used is applicable.

In Fig. 3.7, the arrows indicate the path of the rays (corresponding to the pattern of energy propagation, i.e. the vector $\vec{S}$) calculated using the Snell's law and their focusing in a cylinder of radius composed of a negative medium. For example, at $\rho \equiv -1$ and $\kappa \equiv -1$, a plane wave in the paraxial approximation is focused by the

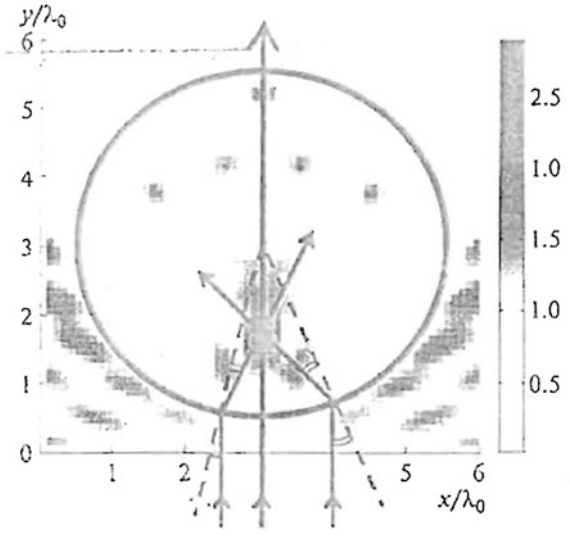

Fig. 3.7 Magnitude of the calculated acoustic pressure field $|P|$ of a plane wave refracted by a cylinder of a negative material. The arrows indicate the directions of the rays (After [19])

cylinder at a distance of r/z from its centre. The field for a cylinder with $r = 2.5\lambda_0$ is calculated numerically with a sampling step of $\lambda_0/10$. Although applying the geometric approximation for such small objects is not quite legitimate, the calculated total field in the cylinder also has a focus at this point, as can be clearly seen from Fig. 3.7.

To model the refraction of a wave on a plane parallel plate, a plane beam with a width of 5 λ_0 is used whose amplitude was taken to be 1. The plate has a thickness of 1.4 λ_0 and a length of 5 λ_0. It should be noted that since the method used does not allow scattering objects of infinitely large sizes or fragments of such objects to be modelled, this leads to an explicit or implicit appearance of boundary conditions and unavoidable undesirable consequences in the form of false reflection and the formation of standing waves. To reduce the edge effects caused by the finite plate and beam sizes, the beam edges were artificially smoothed. The beam fell at an angle of 18° to the normal to plate.

Figure 3.8a shows the result of the calculation for a plate of a positive material ($\rho \equiv 1$, $\kappa \equiv 4$). The wavelength in it and, hence, the speed of sound are approximately half those in the background medium, in agreement with the formula for the speed of sound $c = 1/\sqrt{\rho\kappa}$. The normals to fronts of the incident and refracted waves lie on opposite sides relative to the normal to plate, which corresponds to the case of classical wave refraction at a boundary. The angles of incidence and refraction obey the Snell's law. Since the impedances of the plate and the background medium do not match, there are waves reflected from the boundaries in the system that interfere and form a structure in the form of field minima and maxima along the front of the incident wave, as can be clearly seen from the figure.

When the beam falls on the plate of a negative material ($\rho \equiv -1$ and $\kappa \equiv -1$), the phenomenon of negative refraction is observed (Fig. 3.8b). The exact equality of the angles of incidence and refraction manifests itself in the symmetry of the

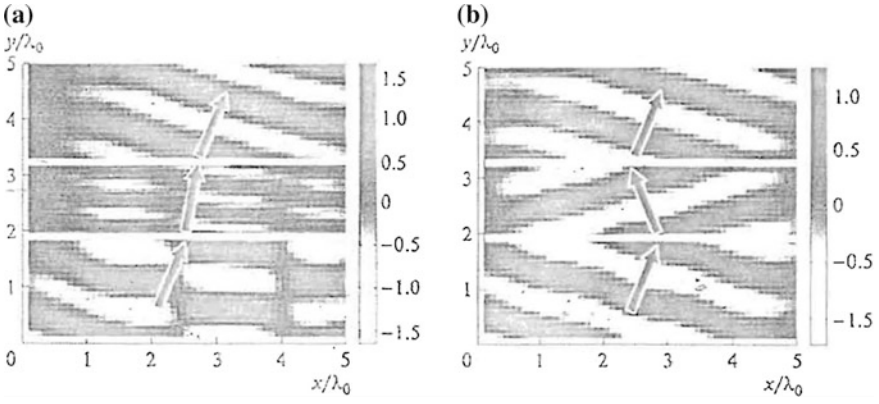

Fig. 3.8 Real part of the calculated acoustic pressure field $|P|$ for a plane wave incident on a plate of **a** positive and **b** negative materials. The arrows indicate the characteristic propagation directions of the wave energy; the white horizontal line represents the plate boundaries

picture of the wavefronts relative to the plate boundaries (the wavelength inside the plate remains equal to λ_0). The normal fronts of the incident and refracted waves directed along the vector $\vec{S}$ in the plate and the background medium are on the same side from the normal to plate. There is no reflected wave, since the impedances are equal. The vector $\vec{k}$ is directed along $\vec{S}$ in a positive medium and opposite to $\vec{S}$ in a negative one, and the Snell's law is satisfied: the wave vectors of the incident and refracted waves have identical (not only in magnitude but also in sign) projections onto the interface. Thus, we have shown that a set of phenomena similar to the phenomena in left-handed media in electrodynamics follows from the simultaneous negativity of ρ and κ in an acoustic medium.

Next, the case of a negative medium perfectly matched with the background is considered. This is a case of special interest because a plane parallel plate of such a material is a focusing one (Fig. 3.9)

It was noted in [22] that such a lens has a number of peculiarities. Firstly, as has already been illustrated, there are no losses by the reflection of the incident wave from it. Secondly, it has no focal plane. The image produced by it is a three-dimensional one, as in the case of a mirror, but, in contrast to the latter, it is real one. Thirdly, for each of rays emanated from one point, the length of the ray path is the same in negative and positive media. The coordinate phase shift in a negative medium is opposite in sign to that in a positive one and as a result, they cancel each other out. Therefore, the wave phase at the image point is exactly equal to the wave phase at the corresponding source point. In this sense, a plane parallel plate of a negative material is a perfect lens. The equality of the phases at the source and image points does not lead to any paradox and does not violate the causality principle, since it takes place only at one frequency at which the effective density and compressibility of negative medium satisfies the relations $\rho = -\rho_0$, $\kappa = -\kappa_0$. Strict satisfaction of this condition is not possible even in a narrow frequency band, and this is probably an important restriction in the application of such lenses. Another shortcoming of such a lens is that it produces real images of objects located only at a short distance $L < H$ from it, where H is the plate thickness.

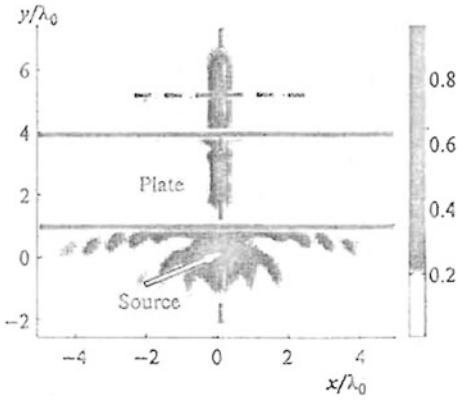

Fig. 3.9 Magnitude of the total calculated acoustic pressure field $|P|$, emerging when a point source is placed near a plane parallel plate of a negative material; the sampling step is $\lambda_0/10$. The dashes mark the lines along which the sections are considered; the solid horizontal lines represent the plate boundaries

Such a lens was proposed theoretically by Pendry [25] in 2000 showing that Rayleigh diffraction limit can be defeated. Information about the source's fine details is contained in its near field. It includes the inhomogeneous waves that are usually neglected, since it decays exponentially with distance from the source and are evanescent. However, the near field retains information about the initial phase and amplitude of the field near the source. Therefore, to reconstruct an ideal image, it will suffice to amplify it. A layer of a negative material can act as such an amplification. The fact that being a passive medium the hypothetical ideal negative material has no energy source to amplify the evanescent waves appears paradoxical. However, this is not required: the decay of the evanescent field in a positive medium with increasing the distance from its source does not lead to any energy loss or heat release. By analogy, the inverse process in a negative medium does not require any expenditure of energy either.

The refraction of the field of a point source illustrating the effect for plane parallel plates differs in length and parameters ρ, and κ. The thickness of all plates was the same, $3\lambda_0$. The scalar point source was located at the coordinate origin $(0, 0)$ at a distance of $1.5\lambda_0$ from the plate and was specified in the form $F(\vec{r}) = \begin{bmatrix} \vec{f} = 0 \\ \rho = \delta(\vec{r}) \end{bmatrix}$. Its field was calculated at each point as $\breve{u}_0 = \hat{\rho} * \breve{F}$ and was normalized in such a way that the magnitude of the acoustic pressure at the source point was equal to 1.

A plate of a negative material ($\rho \equiv -1$ and $\kappa \equiv -1$) with a length of $10\lambda_0$ is considered. The distribution of the magnitude of the calculated pressure field $|P|$ in the chosen region is shown in Fig. 3.9. Two focal spots are clearly seen: in the middle of and behind the plate. When the negative refractive index of the plate is taken into account, their locations correspond to the geometric construction and confirm the picture of operation of a negative material.

To determine and investigate the resolution of the plate used as a lens, Burov et al. [19] constructed two sections of the distribution of $|P|$: the longitudinal one (i.e. parallel to the normal to the plate) passing along the line connecting the centres of the source and the focal spots, and the transverse one (perpendicular to it) passing through the centre of the external focus (these sections are indicated in Fig. 3.9 by the dashes). The corresponding plots are presented in Fig. 3.10 (thick solid line). The values of $|P|$ in these sections were also calculated for a similar plate of negative material but with a length of $4\lambda_0$.

As the aperture of the lenses decreases, their resolution in both longitudinal and transverse directions is reduced (Fig. 3.10, thin solid line). For comparison, similar sections for a flat collecting lens with a length of $4\lambda_0$ are constructed. They are made in the shape of a plane parallel plate of a positive material with a variable (along the X axis) refractive index [20]. The focus produced by it is much more blurred than that for a plate of negative material, particularly in the longitudinal direction (Fig. 3.10, dashed line). The increase in the resolution of the lenses of a negative material is related to the amplification of the evanescent field component of the source in the negative medium.

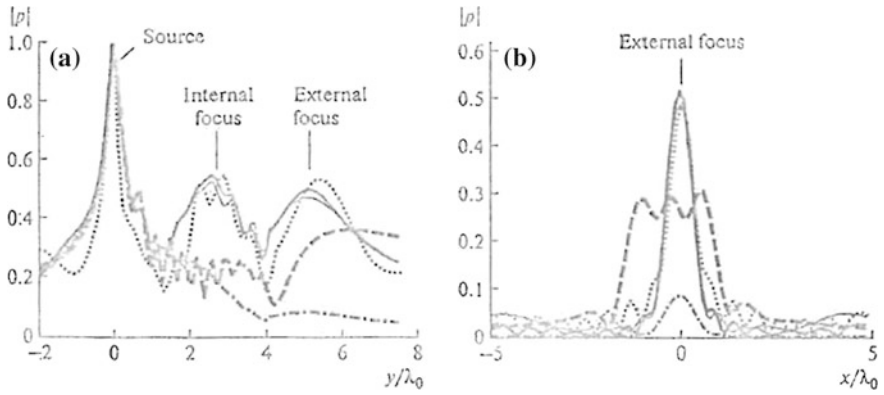

Fig. 3.10 Longitudinal (**a**) and transverse (**b**) sections of the acoustic pressure field passing through the external focus as shown in Fig. 3.11. The thick solid line corresponds to a lens of a negative material with a length of $10\lambda_0$, and the dash-dotted line corresponds to the same lens with absorption. The thin solid line corresponds to a lens of a negative material with a length of $4\lambda_0$; the dashed line corresponds to a lens of a positive material with a variable refractive index. In all these cases, the sampling step is $\lambda_0/10$. The dotted line corresponds to a lens of a negative material with a length of $10\lambda_0$ at a sampling step of $\lambda_0/7.5$

3.11.4 Points to Take Care of During Numerical Simulation

Choosing an optimal sampling step is important in a numerical analysis. Increasing the number of samples N per wavelength entails an increase in the sizes of the reversible matrices as $N^2 \times N^2$ (in the two-dimensional problem), increasing the amount of the random access memory used and the computational time. On the other hand, enlarging the resolution elements does not lead to any degradation of the quality of the field picture, possibly only to certain limits. In particular, as yet no increase in the sizes of the focal waist occurs (Fig. 3.10, dotted line). As the number of samples per wavelength decreases further, the field calculation procedure becomes unstable, causing the picture to be destroyed. The instability for plates of negative and positive materials arises at sampling steps of $\lambda_0/5$ or sparser and $\lambda_0/3$ or sparser, respectively. This is probably because when the evanescent field component is amplified, the errors caused by sparse sampling increases simultaneously. This is a manifestation of the fact that the problem here is an ill-posed one. The image quality can be slightly improved by applying regularization during the inversion of the operator in Eq. (3.22) similar to the least-square method:

$$\check{u} = \left[\hat{M}^{\dagger}\hat{M} + \chi\hat{E}\right]^{-1}\hat{M} + \check{u}_0 \tag{3.32}$$

where $\hat{M} \equiv \hat{E} - \hat{G} * \hat{A}_1$, $\chi > 0$ is a small regularization parameter. The results of the calculation for a coarse sampling step of $\lambda_0/5$ for the plate with regularization

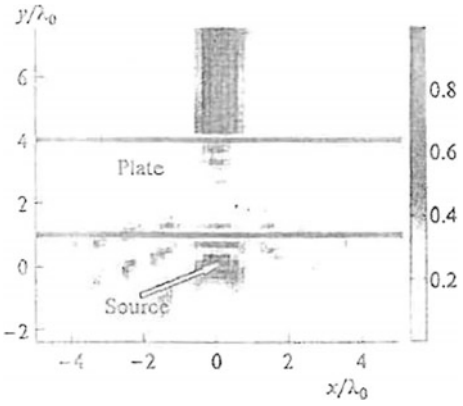

Fig. 3.11 Magnitude of the total acoustic pressure field $|P|$ emerging when a point source is placed near a plane parallel plate of a negative material and calculated using regularization. The sampling step is $\lambda_0/5$ (After [19])

are shown in Fig. 3.11. The image stability is restored as the focal spot broadens significantly. More surprisingly, the internal focus in the plate virtually disappeared, and it is so far difficult to explain this fact.

It should be noted that choosing a sampling step is important not only in computer simulations but also for the practical creation of negative metamedia, which are discrete in their nature. In particular, to achieve an acceptable lens resolution, there should be at least ten discrete elements of the metamedium per wavelength. This requirement is actually reduced to the fact that the speed of sound inside the element of the resonating inclusion should be at least an order of magnitude lower than that in the background medium, which is significantly difficult in creating such media.

3.12 Refraction

The third basic mechanism involved in sound propagation in solids and fluids is refraction. Refraction is the change in direction of propagation of a wave due to a change in its transmission medium. The phenomenon is explained by the conservation of energy and conservation of momentum. Due to change of medium, the phase velocity of the wave is changed but its frequency remains constant. This is most commonly observed when a wave passes from one medium to another at any angle other than 0° from the normal. Refraction of light is the most commonly observed phenomenon, but any type of wave can refract when it interacts with a medium, for example when sound waves pass from one medium into another or when water waves move into water of a different depth. Refraction is described by Snell's

law, which states that for a given pairs of media and a wave with a single frequency, the ratio of the sines of the angle of incidence θ_1 and angle of refraction θ_2 is equivalent to the ratio of phase velocities (v_1/v_2) in the two media, or equivalently, to the opposite ratio of the indices of refraction(n_2/n_1):

$$\frac{\sin\theta_1}{\sin\theta_2} = \frac{v_1}{v_2} = \frac{n_2}{n_1} \tag{3.33}$$

In general, the incident wave is partially refracted and partially reflected. The details of this behaviour are described by the Fresnel equations.

Refraction in acoustic metamaterials will be described in more details in Chap. 2 of this book.

References

1. Waterman, P.C.: Matrix formulation of electromagnetic scattering. Proc. IEEE **53**, 805–812 (1965)
2. Waterman, P.C.: New formulation of acoustic scattering. J. Acoust. Soc. Am. **45**, 1417–1429 (1969)
3. Martin, P.A.: Multiple Scattering: Interaction of Time-Harmonic Waves with N Obstacles. Cambridge University Press, Cambridge (2006)
4. Mishchenko, M.I., Trans, L.D., Lacis, A.A.: Multiple Scattering of Light by Particles: Radiative Transfer and Coherent Backscattering. Cambridge University Press, Cambridge (2006)
5. Ganesh, M., Graham, I.G.: A high-order algorithm for obstacle scattering in three-dimensions. J. Comput. Phys. **198**, 211–242 (2004)
6. Doicu, A., Wriedt, T., Eremin, Y.: Light Scattering by Systems of Particles, Null Field Method with Discrete Sources-theory and Programs. Springer, Berlin (2006)
7. Mishchenko, M.I., Trans, L.D., Mackowski, D.W.: T matrix computation of light scattering by non-spherical particles, a review. J. Quant. Spectros. Radiat. Trans. **55**, 535–575 (1996)
8. Kahnert, F.M.: Numerical methods in electromagnetic scattering theory. J. Quant. Spectros. Radiant Tran. **79–80**, 775–824 (2003)
9. Li, J., Chan, C.T.: Double-negative acoustical metamaterial. Phys. Rev. E **70**, 55602 (2004)
10. Wu, Y., Lai, Y., Zhang, Z.: Effective medium theory for elastic metamaterials in two dimensions. Phys. Rev. B **76**, 205313 (2007)
11. Torrent, D., Sanchez-Dehesa, J.: Multiple scattering formulation of two- dimensional acoustic and electromagnetic metamaterials. New J. Physics **13**, 093018 (2011)
12. Torrent, D., Hkansson, A., Cervera, F., Sánchez-Dehesa, J.: Homogenization of two-dimensional clusters of rigid rods in air. Phy. Rev. Lett. **96**, 204302 (2006)
13. Torrent, D., Sánchez-Dehesa, J.: Effective parameters of clusters of cylinders embedded in a nonviscous fluid or gas. Phys. Rev. B **74**, 224305 (2006)
14. Torrent, D., Sánchez-Dehesa, J.: Anisotropic mass density by two-dimensional acoustic metamaterials. New J. Phys. **10**, 023004 (2008)
15. Morse, P.M.C., Ingard, K.U.: Theoretical Acoustics. Princeton University Press, Princeton NJ (1986)
16. Torrent, D., Hkansson, A., Cervera, F., Sánchez-Dehesa, J.: Homogenization of two-dimensional clusters of rigid rods in air. Phys. Rev. Lett. **96**, 204302 (2006)

17. Abramowitz, M., Stegun, I.A.: Handbook of Mathematical Functions with Formulas, Graphs and Mathematical Tables. Dover, New York (1964)
18. Berryman, J.G.: Long-wavelength propagation in composite elastic media. I. Spherical inclusions. J. Acoust. Soc. Am. **68**, 1809 (1980)
19. Burov, B.A., Dmitriev, K.V., Sergeev, S.N.: Acoustic double-negative media. Acoust. Phys. **55**, 298–310 (2009)
20. Voitovich, N.N., Katsenelenbaum, B.Z., Nauka, A.N.: Generalized Method of Eigenoscillation in Diffraction Theory. Nauka, Moscow (1977). [in Russian]
21. Barkhatov, et al.: Acoustics in Problems, Nauka, Fizmatlit, Moscow (1996) [in Russian]
22. Burov, V.A., Vecherin, S.N., Rumyantseva, O.D.: Statistical estimation of the spatial spectrum of secondary sources. Akust. Zh. **50**, 14 (2004)
23. Bliokh, Y.K., Bliokh, Y.P.: Usp. Fiz. Nauk **174**, 439 (2004)
24. Burov, V.A., Dimitriev, K.V., Sergeev, S.N.: Wave effects in acoustic media with a negative refractive index. Izv. Ross. Akad. Nauk, Ser. Fiz. **72**, 1695 (2008)
25. Pendry, J.B.: Negative refraction makes a perfect lens. Phys. Rev. Lett. **85**, 3966 (2000)

Chapter 4
Artificial Elasticity

Abstract Acoustical metamaterials with negative mass density and negative bulk modulus enable negative elasticity and in turn artificial elasticity. This demonstrates the form invariance or symmetry of the acoustic field equation and in turn the symmetry properties of the acoustic fields. An example of an acoustical metamaterial demonstrating artificial elasticity is given.

4.1 Elastic Stiffness and Compliance

The basic theory of elasticity is given by Hooke's law which is valid only for the linear range. Hooke's law states that the strain is linearly proportional to the stress, or conversely, that the stress is linearly proportional to the strain. The second form can be written mathematically by writing each component of stress or elastic storing force as a general linear function of all the strain components. In general,

$$T_{ij} = c_{ijkl} S_{kl} \tag{4.1}$$

where summation over the repeated subscripts k and l. c_{ijkl} are known as the elastic stiffness constants. Like macroscopic spring constants, they have small values for easily deformed materials and large values for very rigid materials. Since (4.1) contains nine equations corresponding to all possible combinations of the subscripts ij, and each equation contains nine strain variables, there are 81 elastic stiffness constants.

However, these are not all independent. In fact:

$$c_{ijkl} = c_{jikl} = c_{ijlk} = c_{jilk}$$

which reduces the number of independent constants to 36. Further, it can be shown that $c_{ijkl} = c_{klij}$ and this means that the constants are further reduced to 21. This is the maximum number of constants for any medium. Usually, the number is much less than this, because of additional restrictions imposed by the microscopic nature of the medium.

W.S. Gan, *New Acoustics Based on Metamaterials*, Engineering Materials,
https://doi.org/10.1007/978-981-10-6376-3_4

Alternatively, the strains may be expressed as general linear functions of all the stresses:

$$S_{ij} = s_{ijkl} T_{kl} \tag{4.2}$$

$$i, j, k\, l = x, y, z$$

Here, the constants s_{ijkl} known as compliance constants are measures of the deformability of the medium and have large values for easily deformed materials and small values for rigid materials.

Equation (4.2) and its converse are called the elastic constitutive relations. The compliance constants s_{ijkl} describe the elastic properties of a medium in a manner analogous to the description of its electrical properties by the permittivity matrix elements ε_{ij}, where the electrical constitutive relation corresponding to (4.2) is:

$$D_i = \varepsilon_{ij} E_j \tag{4.3}$$

$$I, j = x, y, z$$

4.2 Symmetry Properties of Stress Field and Particle Velocity Field

It is known that the acoustic equation of motion has symmetry properties. It has invariance under gauge transformation. The symmetry will be in the form of rotational invariance in the phase factor of the solution of the equation and the form invariance of the equation. The acoustic fields here will be the particle velocity field and the stress field. This is analogous to the gauge invariance introduced by Hermann Weyl to Maxwell's equations in 1929. There are two forms of symmetry in the propagation of the sound wave in solids and in fluids. One is the rotational symmetry of the solution and the other is translational symmetry of the solution for a continuum but broken translational symmetry for a discrete media such as crystals giving rise to the phonons which are broken translational symmetry mode and a Goldstone mode. There are two aspects of symmetry to be considered during sound propagation in solids and fluids. One is symmetry of the medium, and the other is symmetry property of the propagating sound wave. This is analogous to the two forms of nonlinearity when finite amplitude wave propagating in solids and fluids. One is the nonlinearity of the medium, and the other is nonlinearity of the propagating sound wave.

The rotational invariance of the solution of the acoustic equation of motion can be demonstrated in the symmetry of the particle velocity field and the stress field. Usually, the acoustic equation of motion is expressed in terms of the particle velocity and not in the stress. This is because particle velocity is a vector quantity with three components and whereas stress is a tensor quantity with nine components and more complicated to deal with. However, it can be shown that there is a high

degree of symmetry between the particle velocity field and the stress field analogous to the high degree of symmetry between the electric field and the magnetic field. This can be illustrated as follows, by deriving the acoustic equation of motion for infinitesimal amplitude sound waves in solids. There are two basic field equations: the first is obtained from Newton's laws of motion in mechanics, and the second from Hooke's law in the theory of elasticity. The first field equation expresses Newton's laws of motion, written as

$$\nabla \cdot \mathbf{T} = \rho \frac{\partial^2 \mathbf{u}}{\partial t^2} - \mathbf{F} \tag{4.4}$$

The second field equation is the strain-displacement relation related to Hooke's law given as

$$\mathbf{S} = \nabla_s u \tag{4.5}$$

where **T** = stress, u = displacement, **F** = body force, **S** = strain and ρ = density of medium.

In order to solve the two variables: u and **T**, a second equation is necessary and this is given by Hooke's law from the theory of elasticity states that the strain is linearly proportional to the stress. That is

$$T_{ij} = c_{ijkl} S_{kl} \tag{4.6}$$

$$i, j, k, l = x, y, z$$

with summation over the repeated subscripts k and l. The microscopic spring constants c_{ijkl} in (4.6) are called elastic stiffness constants.

We consider source-free region, so **F** = 0. The next step is to eliminate **T** from (4.4) to (4.6). From (4.5) to (4.6), $\mathbf{T} = c_{ijkl} \nabla_s \mathbf{u} = c_{ijkl} \frac{\partial u}{\partial x}$, if only one dimension, x-direction is chosen. Substituting in (4.4), we obtain

$$c_{ijkl} \frac{\partial^2 u}{\partial x^2} = \rho \frac{\partial^2 u}{\partial t^2} \tag{4.7}$$

The above equation is also known as the Christoffel equation.

Equation (4.7) is the equation of a travelling wave and the solution can be given as

$$u = u_0 e^{i(\omega t \pm kx)} \tag{4.8}$$

which gives

$$\rho \omega^2 = c_{ijkl} k^2 \tag{4.9}$$

Phase velocity is given by $v = \omega/k$. Thus for transverse (or shear) waves, the velocity is

$$v_s = \sqrt{\frac{c_{ijkl}}{\rho}} \tag{4.10}$$

4.2.1 Symmetries between the Particle Velocity Field Acoustic Equation of Motion and the Stress Field Acoustic Equation of Motion

Equation (4.5) can be written in terms of the particle velocity and compliance as

$$\nabla_s \mathbf{v} = s : \frac{\partial \boldsymbol{T}}{\partial t} \tag{4.11}$$

where s = compliance.

Acoustic wave equations can be obtained by eliminating either T or v from the acoustic field equations. Usually, the stress field is eliminated since it is a tensor quantity and consists of nine field components rather than three like a vector field.

For infinitesimal amplitude sound waves, the lossless acoustic field equations are given by (4.4) and (4.5). We will now eliminate the velocity field from (4.4) to (4.11).

Differentiating (4.11) with respect to t:

$$\nabla_s \frac{\partial v}{\partial t} = s : \frac{\partial^2}{\partial t^2}\mathbf{T} \tag{4.12}$$

With F = 0 for source-free region, and taking the divergence of both sides of (4.4)

$$\nabla_s(\nabla \cdot \mathbf{T}) = \rho \nabla_s \frac{\partial \boldsymbol{v}}{\partial \boldsymbol{t}} \tag{4.13}$$

Substituting (4.12) into (4.13) we have

$$\nabla_s(\nabla \cdot \mathbf{T}) = \rho s : \frac{\partial^2}{\partial t^2}\mathbf{T}$$

or

$$c\nabla_s(\nabla \cdot \mathbf{T}) = \rho \frac{\partial^2}{\partial t^2}\mathbf{T} \tag{4.14}$$

This is a new stress equation. The potential and the applications of this equation have yet to be explored.

We also discover an important property. That is the acoustic wave Eqs. (4.7) and (4.14) are symmetrical in u and T. This symmetrical property can give rise to several simplications in the solving of acoustic wave equations.

4.3 Rotation Invariance of the Stress Field and Particle Velocity Field for an Isotropic Solid

In an isotropic solid, there is rotational invariance in the stress field and particle velocity field which are the principal acoustic fields. Rotational invariance means invariance of the stress field and the particle velocity field with respect to rotation. The type of rotation is U(1) rotation or U(1) symmetry. Also in an isotropic solid, there is global U(1) rotation symmetry for the whole object and also there is local U(1) rotation symmetry at every point in space-time in unison with the whole object. The consequence is the particle velocity and the stress field is the same in all directions in an isotropic solids.

4.4 Reflection Symmetry as a Special Case of Rotational Symmetry

Here, both the particle velocity field and the stress field are under a clockwise rotation of the coordinate axes through an angle 180° about the z axis. The consequence is negative values of the particle velocity field and stress field are obtained, or there is a reflection image of the velocity field and the stress field. This is known as reflection symmetry. The coordinate transformation matrix for this case is:

$$\begin{bmatrix} a_{xx} & a_{xy} & a_{xz} \\ a_{yx} & a_{yy} & a_{yz} \\ a_{zx} & a_{zy} & a_{zz} \end{bmatrix} = \begin{bmatrix} \cos\xi & \sin\xi & 0 \\ -\sin\xi & \cos\xi & 0 \\ 0 & 0 & -1 \end{bmatrix} = -1 \tag{4.15}$$

Transformation of a particle velocity field v to the rotated coordinate system is performed with the matrix equation

$$\begin{bmatrix} v'_x \\ v'_y \\ v'_z \end{bmatrix} = \begin{bmatrix} \cos\xi & \sin\xi & 0 \\ -\sin\xi & \cos\xi & 0 \\ 0 & 0 & -1 \end{bmatrix} \begin{bmatrix} v_x \\ v_y \\ v_z \end{bmatrix} = - \begin{bmatrix} v_x \\ v_y \\ v_z \end{bmatrix} \tag{4.16}$$

or

$$v' = -v \tag{4.17}$$

Transformation of a stress field T to the rotated coordinate system is performed with the matrix equation

$$\begin{bmatrix} T'_{xx} & T'_{xy} & T'_{xz} \\ T'_{yx} & T'_{yy} & T'_{yz} \\ T'_{zx} & T'_{zy} & T'_{zz} \end{bmatrix} = \begin{bmatrix} \cos\xi & \sin\xi & 0 \\ -\sin\xi & \cos\xi & 0 \\ 0 & 0 & -1 \end{bmatrix} \begin{bmatrix} T_{xx} & T_{xy} & T_{xz} \\ T_{yx} & T_{yy} & T_{yz} \\ T_{zx} & T_{zy} & T_{zz} \end{bmatrix}$$
$$= -\begin{bmatrix} T_{xx} & T_{xy} & T_{xz} \\ T_{yx} & T_{yy} & T_{yz} \\ T_{zx} & T_{zy} & T_{zz} \end{bmatrix} \tag{4.18}$$

Or

$$T' = T \tag{4.19}$$

4.5 Form Invariance of the Particle Velocity Field Acoustic Equation of Motion

The Helmholtz homogeneous acoustic wave equation is given by

$$\nabla^2 P + \frac{\omega^2}{\rho\kappa} p = 0 \tag{4.20}$$

where p = acoustic pressure, ρ = mass density and κ = bulk modulus.

Again, we find that there is no change in the form of Eq. (4.20) if ρ and κ are replaced by $-\rho$ and $-\kappa$. This shows that the Helmholtz wave equation is gauge invariant to the negative values of ρ and κ.

Here, we have extended the left-handed media to acoustics using gauge invariance formulation. Another demonstration of the form invariance of the acoustic equation of motion is acoustical cloaking.

Acoustical cloaking deals with the deflection of bending of the sound wave and the control of the propagation and direction of sound wave according to our specified direction.

We use coordinate transformations, a form of gauge invariance. That is there is no change in the form of the acoustic field equation after the coordinate transformations, or the acoustic field equation is gauge invariant subjected to coordinate transformations.

As an illustration, we quoted the results from Cummer [1]

Cummer [1] illustrated coordinate transformations for acoustics by using the linear acoustic equation for inviscid fluid

$$j\omega p = -\kappa \nabla \cdot \boldsymbol{v}, \quad j\omega p\boldsymbol{v} = -\nabla p \tag{4.21}$$

where ω = angular frequency, $\boldsymbol{v}$ = sound velocity.

Next a new set of curvilinear coordinates x', y' and z' are imposed on these equations. Using A as the Jacobian matrix of coordinate transformations from (x, y, z) to (x', y', z'), he expressed the gradient operation in the new primed coordinates as:

$$\nabla p = A^T \nabla' p = A^T \nabla' p' \tag{4.22}$$

and the divergence operation can be expressed as

$$\nabla \cdot \boldsymbol{v} = \det(A) \nabla' \cdot \boldsymbol{v}' \frac{A}{\det(A)} \boldsymbol{v} = \det(A) \nabla' \cdot \boldsymbol{v}' \tag{4.23}$$

With these expressions the original Eq. (4.21) can be written in the new coordinates as

$$j\omega p' = -\kappa \det(A) \nabla' \cdot \boldsymbol{v}'$$

$$j\omega \det(A) \left(A^T\right)^{-1} \rho \left(A^{-1}\right) \boldsymbol{v}' = -\nabla' p' \tag{4.24}$$

which is in the same form as the original Eq. (4.21) but with the new medium parameters:

$$\kappa' = \det(A)\kappa, \overline{\overline{p}} = \det(A) \left(A^T\right)^{-1} \rho \left(A^{-1}\right) \tag{4.25}$$

Physically, this means that if one applies a coordinates transformation to a solution to Eq. (4.21) and changes the medium properties according to Eq. (4.25), the transformed fields are a solution to the acoustic equations in the new medium.

4.6 Gauge Invariance of Nonlinear Homogeneous Acoustic Wave Equation

The nonlinear homogeneous acoustic wave equation up to the second order can be given as

$$\kappa_1 \nabla^2 p + \kappa_2 \nabla^2 p \left(\frac{\partial p}{\partial x}\right) + \frac{\omega^2 p}{\rho} = 0$$

or

$$\rho\kappa_1\nabla^2 p + \rho\kappa_2\nabla^2 p\left(\frac{\partial p}{\partial x}\right) + \omega^2 p = 0 \tag{4.26}$$

where κ_1 = second-order bulk modulus and κ_2 = third order bulk modulus.

Again, if we replace ρ and κ_1, and κ_2 by $-\rho$, $-\kappa_1$, and $-\kappa_2$, there is no change in the form of Eq. (4.26). In another words, the nonlinear acoustic wave equation is gauge invariant to negative values of ρ, κ_1, and κ_2.

4.7 Acoustic Metamaterial with Simultaneous Negative Mass Density and Negative Bulk Modulus-Demonstration of Artificial Elasticity

The concept is based on the gauge invariance of the acoustic field equations. That is, there is no change in the form of the acoustic field equation with the replacement of the density and bulk modulus by negative density and negative bulk modulus.

Applying gauge invariance of acoustic fields to negative refraction, broadband double negative spectral range in the structure can be obtained. [2] This is also an experimental verification of my proposal on the gauge invariance of acoustic fields [3]. Lee et al. 2010 [2] fabricated an acoustic double negativity (DNG) acoustic metamaterial with both membranes and side holes (Fig. 4.1). Here, the acoustic waves are governed by Eqs. (4.27) and (4.28)

$$-\nabla p = \left[\rho - \frac{\kappa}{\omega^2}\right]\frac{\partial v}{\partial A} \tag{4.27}$$

and

$$\nabla \cdot \boldsymbol{v} = -\left[\frac{1}{B} - \frac{\sigma_{\mathrm{SH}}^2}{\rho_{\mathrm{SH}} A\omega^2}\right]\frac{\partial p}{\partial A} \tag{4.28}$$

where κ = new elastic modulus, $\boldsymbol{v}$ = velocity of the fluid (air in this case), ρ = dynamic mass density, B = bulk modulus, A = cross section of the tube, σ_{SH} = SH cross-sectional density, ρ_{SH} = SH mass density.

The existence of the side holes (SH) does not modify Eq. (4.27). Likewise, because the membranes do not sink any fluid, Eq. (4.28) is still valid. Then, the system is described by the dynamic and continuity equations

$$-\nabla p = \rho_{\mathrm{eff}}\left(\frac{\partial y}{\partial A}\right)\nabla \cdot \boldsymbol{v} = -\left(\frac{1}{B_{\mathrm{eff}}}\right)\left(\frac{\partial p}{\partial A}\right)$$

with the effective density and modulus given by (4.29) and (4.30)

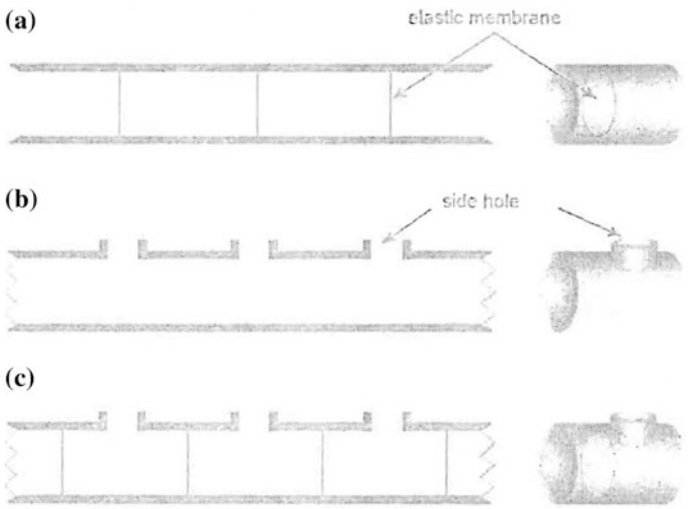

Fig. 4.1 **a** One-dimensional SAE structure consisting of thin tensioned elastic membranes in a tube. Negative effective density is observed in this system. **b** A tube with an array of side holes that exhibits negative effective modulus. **c** An acoustic DNG structure with both membranes and side holes. (From [2])

$$P_{\text{eff}} = \rho' - \frac{\kappa}{\omega^2} = \rho'\left[1 - \frac{\omega_{\text{SAE}}^2}{\omega^2}\right] \tag{4.29}$$

$$B_{\text{eff}} = \left[\frac{1}{B} - \frac{\sigma_{\text{SH}}^2}{\rho_{\text{SH}} A\omega^2}\right]^{-1} = B\left[1 - \frac{\omega_{\text{SH}}^2}{\omega^2}\right]^{-1}$$

where

$$\omega_{\text{SAE}} = \text{critical frequency} = \sqrt{\frac{\kappa}{\rho'}} \tag{4.30}$$

The resulting wave equation gives the phase velocity,

$$v_{\text{ph}} = \pm\sqrt{\frac{B_{\text{eff}}}{\rho_{\text{eff}}}} = \pm\sqrt{\frac{B}{\rho'\left(1 - \omega_{\text{SAE}}^2/\omega^2\right)\left(1 - \omega_{\text{SH}}^2/\omega^2\right)}}$$

where

$$\omega_{\text{SH}} = \left(B\sigma_{\text{SH}}^2/A\rho_{\text{SH}}\right)^{1/2} \tag{4.31}$$

The experimental set-up is given in Fig. 4.2a.

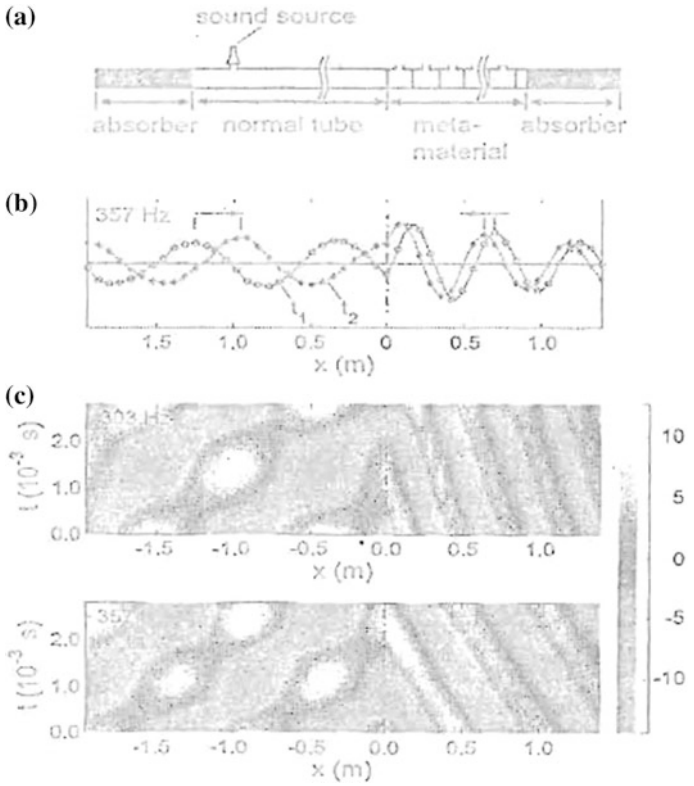

Fig. 4.2 **a** Experimental set-up for the transmission and phase velocity measurements, **b** "Snapshots" of measured pressure distribution showing backward-wave propagation in the metamaterial ($x > 0$). **c** Characteristic diagrams of pressure measurements for the frequencies 303 and 357 Hz. Negative slopes of the wave paths in the metamaterial sides ($x > 0$) indicate negative phase velocities. (From [2])

It consists of a nonmetal tube on the left and the DNG metamaterial on the right. The absorbers at both ends completely absorb the acoustic energy, preventing any reflection so the system behaves as if it extends to infinity. This eliminates concerning about the effect of the finite number of cells used in the experiment, as well as the interference effect from the reflected waves. The sound source rejects acoustic energy into the tube through a small hole, generating incident waves propagating to the right. At the boundary, a position of the incident energy is reflected and the rest is transmitted through the metamaterial regions. On the metamaterial side, the transmitted acoustic energy flows steadily to the right until it hits the absorber.

Pressure was measured as a function of time and position on both the normal tube side and the metamaterial side. It can be seen that on the normal tube side, the wave proceeds forward, but on the metamaterial side, the wave propagated as indicated by the arrows. Clearly, the wave on the metamaterial propagated in a

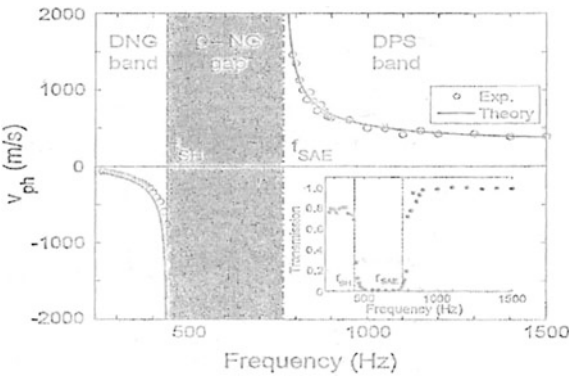

Fig. 4.3 Transmission (inset) and phase velocities of the present acoustic DNG medium. (From [2])

direction antiparallel to the energy flow. This confirms the theoretical prediction of negative phase velocity. It was noted that the amplitudes and the apparent phase velocity in the normal tube deviated from the actual values of the incident wave because of the interference of the reflected wave from the boundary. In the metamaterial, there is no such interference effect because there is no reflected wave.

The comparison between the theory and experiment are shown in Fig. 4.3.

Theoretically expected single negative gap is experimentally confirmed by the transmission data (inset). In the DNG and DPS (double positive) pass bands, the phase velocities experimentally determined agree well with the theoretical values. The calculations are given as an accurate description of the behaviour of the phase velocity in the frequency range from 250 to 1500 Hz, which is broadband. Because the experiment confirms the theoretical prediction of negative phase velocity, it can be concluded that the density and the bulk modulus actually become simultaneously negative in the frequency range below 440 Hz.

We would like to point out the novel concept of spatially anchored elasticity [2] was used. This uses a homogenized structure of membranes to produce negative effective density. This is termed spatially anchored elasticity (SAE) because the fluid is elastically anchored in space by the membranes. The new elasticity can be regarded as an intrinsic variable that characterizes the behaviour of the metamaterial according to Eq. (4.32)

$$\nabla p = -\kappa \vec{\xi} \tag{4.32}$$

where $\kappa =$ new elastic modulus, $\xi =$ displacement of the fluid, $p =$ pressure of the fluid.

Furthermore, by making additional side holes along the tube wall, acoustic DNG materials were obtained and backward-wave propagation was observed. The constructed structure exhibited DNG characteristic in the spectral range from 240 to 440 Hz which is broadband unlike the electromagnetic case which is limited only to a single frequency due to dispersion. The phase velocity in this band was negative and highly dispersive.

4.8 The New Field of Artificial Elasticity

The successful fabrication of material with negative bulk modulus as shown above confirms the symmetry property of the acoustic equation of motion and the symmetry property of the acoustic fields: particle velocity field and the stress field. This enables the control of the key parameter if elasticity: bulk modulus and hence the elastic constant:

$$\text{bulk modulus} = \kappa = C_{44}, \text{a Lam}\acute{e} \text{ constant} \tag{4.33}$$

This paves the path towards artificial elasticity.

References

1. Cümmer, S.A., Schürig, D.: One path to acoustic cloaking. New J. Phys. **9**, 45 (2007)
2. Lee, S.H., Kim, C.K., Park, C.M., Seo, Y.M., Wang, Z.G.: Composite acoustic medium with simultaneously negative density and modulus, In: Proceedings of ICSV17, Cairo, Egypt (2010)
3. Gan, W.S.: Gauge invariance approach to acoustic fields. In: Akiyama, I. (ed.) Acoustical Imaging, vol. 29, pp. 389–394. Springer, The Netherlands (2007)

Chapter 5
Artificial Piezoelectricity

Abstract First, piezoelectricity is explained as an example of second-order phase transition with the spontaneous symmetry electrical polarization and spontaneous symmetry breaking. Artificial piezoelectricity with negative permittivity, negative piezoelectric strain constant and negative piezoelectric stress constant is described. The stiffened Christoffel equation for artificial piezoelectricity is given. Artificial piezoelectricity opens the way for artificial second-order phase transition and control and manipulation of artificial second-order phase transition.

5.1 What Is Piezoelectricity?

The Hooke's Law equation does not fully describe the response of a solid to acoustic strain. Certain materials become electrically polarized when they are strained. This effect, known as the direct piezoelectric effect, manifests itself experimentally by the appearance of bound electrical charges at the surfaces of a strained medium. It is a linear phenomenon and the polarization changes sign when the sign of the strain is reversed. Piezoelectricity is intimately related to the microscopic structure of solids and although a complex subject, can be explained qualitatively in terms of a rather simple atomic model. Briefly, the atoms of a solid and also the electrons within the atoms themselves are displaced when the material is deformed. The displacement produces microscopic electrical dipoles with the medium, and in certain crystal structures these dipole moments combine to give an average macroscopic moment or electrical polarization.

The direct piezoelectric effect is always accompanied by the converse piezoelectric effect, whereby a solid becomes strained when placed in an electric field. Like the direct effect, this is also linear and the piezoelectric strain reverses sign with reversal of the applied electric field. Since the piezoelectric strain produced by an electric field will always generate internal stresses, the converse piezoelectric effect must be included in the Hooke's Law equation by adding a stress term that is linearly proportional to the electric field. This linear electrically induced stress will be present only in materials with microscopic structures appropriate to the existence

W.S. Gan, *New Acoustics Based on Metamaterials*, Engineering Materials,
https://doi.org/10.1007/978-981-10-6376-3_5

of piezoelectricity. There is, however, another kind of electrically induced stress that occurs in all materials. This stress, called electrostrictive stress, is a quadratic function of the electric field. It is produced by the same microscopic mechanism that causes the converse piezoelectric effect, namely by electrical forces acting on the ionized atoms that form the crystal lattice, but, by contrast with the piezoelectric stress, it produces a macroscopic effect in all materials.

Since electrostriction is a second-order phenomenon, its role will be negligible in the small signal approximation of a linear theory. Piezoelectricity, on the other hand, introduces linear coupling between the acoustic field equations and Maxwell's electromagnetic field equations. In magnetic materials, two analogous effects are observed. Magnetostriction is quadratic magnetically induced stress present in materials of all symmetry classes, and piezomagnetism is a linear magnetoacoustic coupling that occurs only when certain lattice symmetry conditions are satisfied. Intrinsic piezomagnetic effects are not, at the present time, of any practical significance. Technologically useful linear magnetoacoustic coupling can, however, be realized by applying both a dc bias field $(H)_{\mathrm{dc}}$ and a time-varying signal field $(H)_{\mathrm{signal}}$ to certain kinds of magnetic materials. In this case, the quadratic or magnetostrictive effect produces stress terms, proportional to terms such as $(H)_{i_{\mathrm{dc}}}(H_j)_{\mathrm{signal}}$ that are linearly dependent upon the applied signal field. This biased piezomagnetism is a strong effect and has many important engineering applications.

In one way or another, piezoelectricity and biased piezomagnetism provide the physical basis for almost all practical applications of acoustic fields. This is because they provide an effective means for electrically generating and detecting acoustic vibrations. In order to design the electroacoustic converters or transducers used for this purpose, it is necessary to establish a mathematical formalism relating the coupled electromagnetic and acoustic fields. It would hardly seem necessary to consider at this point the familiar equations governing uncoupled electromagnetic fields in nonpiezoelectric media. There is, however, an important benefit to be gained from doing so. By making some very simple notational changes, one may cast the acoustic field equations into a form that very closely parallel Maxwell's equations of electromagnetism. This procedure provides much more than a satisfying mathematical symmetry. The field problems of greatest interest in acoustics are of the same general nature as problems, such as uniform plane wave propagation, guided waves, periodic waveguides, coupled modes, resonators and filters, that have received much attention in electromagnetism, particularly in the area of microwave theory. Presentation of the acoustic field equations in a form analogous to Maxwell's equations simplifies the task of transferring to acoustics, the analytical methodology and techniques that have been applied to problems of this kind in electromagnetism. In this chapter, the electromagnetic–acoustic analogy is first established and then illustrated by comparing the basic characteristics of electromagnetic and acoustic uniform plane waves. Then, the concept of negative materials is introduced in the equations, and how it modifies the equations are shown. Then, this is applied to the vibration problem, to the transmission line method, the resonance theory and the stiffened Christoffel equation.

5.2 Piezoelectric Constitutive Relations

Within a solid medium, mechanical forces are described by the stress field components T_{ij} and mechanical deformations by the strain field components S_{ij}. If the equilibrium state of all field variables is defined to be zero, one can write the field equations as:

$$\begin{aligned} D_i &= \varepsilon_{ij}^{T} E_j + d_{ijk} T_{jk} \\ S_{ij} &= d_{ijk} E_k + s_{ijkl}^{\mathrm{E}} T_{kl} \end{aligned} \tag{5.1}$$

where D = electrical displacement, d = piezoelectric strain constant, ε = dielectric constant, d = piezoelectric strain coefficient, e = piezoelectric stress coefficient. Superscripts T and E have been added to ε and s to show that these constants describe dielectric and elastic properties measured under conditions of constant stress and constant electric field, respectively. Because of the coupling between electric and acoustic fields in a piezoelectric solid, measurements of the electrical properties depend upon the mechanical constraints imposed on the medium and vice versa.

For a negative piezoelectric medium, the dielectric constant ε will be replaced by $-\varepsilon$.

5.3 Coupled Acoustic Field Equations and Maxwell's Equations

The electromagnetic field equations are given by:

$$\nabla \times E = \frac{\partial B}{\partial t} \tag{5.2}$$

$$\nabla \times H = \frac{\partial D}{\partial t} + J_c + J_s \tag{5.3}$$

were shown to have a strong analogy with the acoustic field equations:

$$\nabla \cdot T = \frac{\partial p}{\partial t} - F \tag{5.4}$$

$$\nabla_s v = \frac{\partial S}{\partial t} \tag{5.5}$$

And for nonpiezoelectric media, plane wave solutions to these two sets of equations were found to have many characteristics in common. The most striking difference is that the electromagnetic equations have two plane wave solutions

while the acoustic equations have three. In a nonpiezoelectric medium, the electromagnetic and acoustic solutions are completely independent of each other. But in the piezoelectric case, they are coupled together through the piezoelectric strain equations:

$$D = \varepsilon^T \cdot E + D : T \tag{5.6}$$

$$S = d \cdot E + s^E : T \tag{5.7}$$

or the piezoelectric stress equations:

$$D = \varepsilon^S \cdot E + e : S \tag{5.8}$$

$$T = -e. + c^E : S \tag{5.9}$$

Plane wave solutions in a piezoelectric solid are therefore coupled electromagnetic–acoustic waves. Since there were five plane wave solutions (two electromagnetic and three acoustics) to the uncoupled equations, there must also be five-coupled-wave solutions. For a negative piezoelectric medium, the ε will be replaced by $-\varepsilon$. The negative piezoelectric medium can be achieved by using acoustic metamaterial. This gives rise to artificial piezoelectricity.

5.4 The Stiffened Christoffel Equation for Piezoelectricity

It was noted that the effects of piezoelectric coupling between electromagnetic and acoustic uniform plane waves in unbounded media are completely negligible in comparison with the influence of the quasi-static electric field. Consequently, insignificant errors are introduced if the rotational or electromagnetic part of E is neglected in the coupled acoustic and electromagnetic equations. This is known as the quasi-static approximation, and it leads to a very great simplification of the analysis. Removal of all terms in $E^{(r)}$ from those equations reduces the set of equations to two:

$$\nabla \cdot c^{\mathrm{E}} : \nabla_s v - \rho \frac{\partial^2}{\partial t^2} v = -\nabla \cdot \left(e \cdot \frac{\partial \nabla \Phi}{\partial t} \right) \tag{5.10}$$

$$0 = -\mu_0 \nabla \cdot (\varepsilon^S \cdot \frac{\partial^2}{\partial t^2} \nabla \phi) + \mu_0 \nabla \cdot \left(e : \nabla_s \frac{\partial v}{\partial t} \right) \tag{5.11}$$

These equations govern plane wave solutions that travel at velocities comparable to acoustic velocities. In the quasi-static approximation, quasi-electromagnetic waves are regarded as purely electromagnetic. The conversion of (5.10) and (5.11) to matrix form is carried out in the following way:

$$\nabla_{iK} c^E_{KL} \nabla_{Lj} v_j - \rho \frac{\partial^2}{\partial t^2} v_i = -\nabla_{iK} e_{Kj} \nabla_j \frac{\partial \Phi}{\partial t} \tag{5.12}$$

These equations are not restricted to uniform plane waves and will be applied to more general problems. For plane wave solutions proportional to the complex wave function $(\omega t - k\hat{I} \cdot r)$ where $\hat{I}$ is a unit vector in the propagation direction, they may be reduced still further. First, one may write

$$-k^2 (l_{iK} c^E_{KL} l_{Lj}) v_j + \rho \omega^2 v_i = i\omega k^2 (l_{iK} e_{Kj} l_j) \Phi \tag{5.13}$$

$$\omega^2 k^2 (l_i \varepsilon^S_{ij} l_j) \Phi = -i\omega k^2 (l_i e_{iL} l_{Lj}) v_j \tag{5.14}$$

The factor multiplying Φ on the left-hand side of (5.14) is a scalar and may be divided out, giving the potential in terms of the particle velocity. That is

$$\Phi = \frac{1}{i\omega} \left(\frac{l_i}{l_{i\varepsilon^S_{ij}} l_j} e_{iL} l_{Lj} \right) v_j \tag{5.15}$$

After substitution into (5.13) and some rearrangement of terms, one has

$$k^2 \left(l_{iK} \left\{ c^E_{KL} + \frac{[e_{Kjl_j}][l_i e_{iL}]}{l_i \varepsilon^S_{ij} l_j} \right\} l_{Lj} \right) v_j = \rho \omega^2 v_i \tag{5.16}$$

This has exactly the same form as the Christoffel equation but with c_{KL} replaced by the expression in curly brackets, $\left\{ c^E_{KL} + \frac{[e_{Kjl_j}][l_i e_{iL}]}{l_i \varepsilon^S_{ij} l_j} \right\}$ which is called a piezoelectrically stiffened elastic constant.

It is worth noting that for negative piezoelectricity, the piezoelectrically stiffened elastic constant will be of negative value after the substitution of negative values for c^E_{KL}, e_{Kj}, e_{iL} and $\varepsilon^S_{ij.}$

5.5 Application of Metamaterial to Acoustic Resonator

Practical acoustic resonators take many forms, differing from the basic thin-plate geometry of the plane wave transducer. Here, a variety of the basic types will be considered, with emphasis on methods of analysing the natural frequencies of the free resonant modes and the equivalent circuits for electrical input impedances or admittance of a forced resonance. Modal analysis will be used. For a resonator with no losses, the free modes are undamped free oscillations. These are characterised by a set of natural frequencies ω_v and the distribution elastic displacement u_v. As in the

forced waveguide problem, the forced response of a resonator is represented by the sum of the individual mode responses.

The transmission line model will be used to illustrate the general principles of resonator analysis. This model represents plane acoustic wave propagation in isotropic medium. It is also an analogue for wave propagation on a stretched string. The resonator analysis begins with the derivation of a mode orthogonality relation and a mode excitation formula. First, the transmission line equations are reduced to a pair of wave equations for I and V:

$$\frac{\partial^2}{\partial z^2} I = -\omega^2 LCI \tag{5.17}$$

$$\frac{\partial^2}{\partial z^2} V = -\omega^2 LCV \tag{5.18}$$

A reciprocity relation for the wave equation (5.17) is obtained by assuming two solutions "1" and "2" with frequencies ω_1 and ω_2 Solution one is first written into the equation, which is multiplied by solution two. A corresponding expression, with subscripts one and two interchanged, is then formed and subtracted from the first

$$I_2\left(\frac{\partial^2}{\partial z^2} I_1 + LC\omega_1^2 I_1\right) - \left(\frac{\partial^2}{\partial z^2} I_2 + LC\omega_2^2 I_2\right) = 0 \tag{5.19}$$

Using the derivative identity

$$\frac{\partial}{\partial z}\left(A\frac{\partial}{\partial z}B\right) = A\frac{\partial^2}{\partial z^2}B = A\frac{\partial^2}{\partial z^2}B + \frac{\partial A}{\partial z}\frac{\partial B}{\partial z} \tag{5.20}$$

Equation (5.19) can be reduced and rearranged into the form

$$\frac{\partial}{\partial z}\left(I_2\frac{\partial I_1}{\partial z} - I_1\frac{\partial I_2}{\partial z}\right) = LC(\omega_2^2 - \omega_1^2) I_1 I_2 \tag{5.21}$$

This is the real reciprocity relation for the current wave equation. A corresponding expression can be derived from (5.18).

A mode orthogonality relation for the transmission line resonator is obtained by integrating (5.21) over the resonator length, with subscripts one and two now changed to mode subscripts μ and ν. The left side is zero because of the open circuit boundary conditions and from the right side

$$\int_0^l I_\mu I_\nu \, \mathrm{d}z = 0, \quad \omega_\mu^2 \neq \omega_\nu^2 \tag{5.22}$$

An analogous voltage orthogonality relation is obtained from the voltage version of (5.21).

A mode excitation formula and an expression for the input impedance can also be obtained (5.21). Solution "1" is now the forced solution at frequency ω expressed as a sum over the open circuit modes,

$$I_1 \equiv I(z) = \sum_{\mu} a_\mu I_\mu(z) \tag{5.23}$$

with

$$I_\mu = \sin\frac{\pi\mu}{l}z$$

Solution "2" is the th free mode at frequency ω_μ. Substituting into (5.21) and integrating over the resonator length now gives

$$I_s\frac{\pi v}{l} = LC(\omega_v^2 - \omega^2)\sum_{\mu} a_\mu \int_0^l I_\mu I_v \mathrm{d}z$$

where I_s is the drive current. From (5.22), only the vth term in the summation is nonzero. The amplitude of the vth mode is then

$a_v = \frac{K_v I_s}{w_v^2 - w^2}$ with

$K_v = \frac{1}{LC}\frac{\pi v}{l}\frac{2}{l}$ and v arbitrary. Substitution into (5.23) gives

$$I(z) = I_s\sum_{\mu} K_\mu[\sin(\pi\mu/l)z]/(\omega_\mu^2 - \omega^2) \tag{5.24}$$

To find the resonator input Z_r impedance, the voltage at the resonator input is derived from (5.24) and the transmission line equation

$$\frac{\partial I}{\partial z} = -iwCCV$$

The impedance is then obtained as $V(0)$ over I_s,

$$Z_\mathrm{r} = -\frac{1}{i\omega C}\sum_{\mu} K_\mu(\pi\mu/l)/(\omega_\mu^2 - \omega^2) \tag{5.25}$$

To model more realistically, the response of an acoustic resonator, the transmission line resonator is excited through a series capacitor. The input impedance is then

$$\begin{aligned} Z_{\mathrm{IN}} &= \frac{1}{i\omega C_s} + Z_r \\ &= \frac{1}{i\omega C_s} + \frac{2}{i\omega Cl}\sum_{\mu} \omega_{\mu}^2(\omega^2 - \omega_{\mu}^2) \end{aligned} \tag{5.26}$$

An equivalent circuit representation can be constructed by noting that the impedance of a simple parallel LC resonant circuit can be reduced to the form

$$Z_{LC} = \frac{1}{i\omega C_p}\omega^2/(\omega^2 - \omega_r^2) \tag{5.27}$$

With

$$\omega_{\mathrm{r}} = (L_P C_P)^{-1/2} \tag{5.28}$$

Equation (5.28) gives the resonance frequency of the acoustic resonator. Using the analogue between the acoustic field equation and the electrical transmission line equations, the L is equivalent to the mass density, and the C is equivalent to the inverse stiffness constant. Hence, the resonance frequency of the acoustic resonator should be given by

$$\omega_{\mathrm{r}} = (\rho/c_{JJ})^{-1/2} \tag{5.29}$$

For an acoustic resonator made from metamaterial with negative mass density and negative stiffness, there is no change in the form of (5.29) or there is form invariance in (5.29), and the same formula for the resonance frequency can be used.

5.6 Application of Metamaterial to Acoustic Waveguide

The ability to use double-negative material (DNG) to control and manipulate scattering will give rise to a new form of scattering and a new theory of scattering. The use of double-negative material (DNG) as substrate of acoustic waveguide can improve the directivity and optimize the far field radiation. Wu et al. [1] studied the use of metamaterial as antenna substrate to enhance gain for electromagnetic waves. Their idea can be extended to acoustic waves. They studied the radiation set-up and simulated the far field radiation and calculated the electric fields and radiated power. They manipulated ε and μ through the specific inclusion of metal in dielectrics to achieve substrate properties in order to yield optimum radiation characteristics. For calculation of scattering in acoustical waveguides, the following procedure has to be taken [2].

To calculate the scattering of quasi-longitudinal plane sound wave at a boundary between two anisotropic media of different parities, one with parity equals to $+1$, a

normal double-positive material (DPS) and a left-handed material (DNG) with parity equals to -1. Auld [2] has obtained results for two media of same parity $+1$. It would be of great interest to extend this calculation to two media of different parities. These will produce equations for new reflection coefficient, refraction coefficient, transmission coefficient and scattering coefficient for both SV wave and P wave for different polarizations. Fresnel equations for anisotropic solids for the two media of different parities will have to be derived. This will study the scattering at the boundary between the two media. It would be of great interest to study the behaviour of reflected evanescent wave and transmitted evanescent wave at the boundary of two media of different parities.

The new phenomena of scattering in DNG material can be manifested in the salient and conventional features of acoustic cavity resonators, acoustic waveguides, scatterers and antennas loaded or covered with double-negative and/or double-positive (DNG, DPS) metamaterials. The unconventional acoustical characteristics of metamaterials are exhibited when these materials are paired with other materials with at least one oppositely signed constitutive parameters, In other words, when we pair a DNG material with a DPS layer, we may obtain interesting wave propagation properties that may be absent if we paired one DNG layer with another one.

It is of great interest to notice that the interface between two media with at least one pair of oppositely signed parameters can play a major role in offering anomalous behaviours for the combined structure. At the boundary between such two media, using the acoustic field equation one can write the continuity of the tangential stress field and particle velocity field components. It is clear that the normal derivatives of these tangential components are not necessarily continuous and furthermore, if ρ_1 and ρ_2 and/or κ_1 and κ_2 have opposite signs, then the derivatives of the tangential fields on both sides of the interface will have opposite signs. The discontinuity for the tangential components of fields at the interface between such media may imply a concentrated resonant phenomenon at that interface similar to the current and voltage distributions at the junction between an inductor and a capacitor at the resonance of an L-C circuit. This feature can lead to interesting characteristics for wave interaction in devices and components containing metamaterials.

It is also worth noticing that this interface resonance is independent of the total thickness of the paired layers, since it arises along the discontinuity between two such conjugate materials. The mechanism behind this resonance can be described by the equivalent circuit approach. These resonant characteristics, which may occur in sub-wavelength structures formed by pairing such media, have provided us with ideas for acoustic cavities, acoustic waveguides, scatterers, acoustic antennas and acoustic lenses that may operate with dimensions below the conventional diffraction limits.

This concentrated resonant phenomenon can be used to design, thin, sub-wavelength acoustic cavity resonators and parallel-plate acoustic waveguides in which a layer of DNG material is paired with a layer of DPS material. By exploiting the antiparallel nature of the phase velocity and acoustic Poynting

vector in a DNG slab, we found the possibility of resonant modes in electrically thin-parallel-plate structures containing such bi-layered structures. This is an outcome of parity equals -1.

5.7 Piezoelectricity as Second Order Phase Transition

Piezoelectricity is the conversion of mechanical energy phase to electrical energy phase and involves spontaneous electrical polarization. Also there is lining in parallel of the dipole moments, with the system becomes more orderly as it cools through the transition temperature and spontaneous symmetry breaking takes place. These are the basic ingredients of a second-order phase transition. Some of the examples of second-order phase transition are superconductivity, superfluid, magnetization, turbulence and sonoluminescence.

The following description will give a more detailed explanation of what is meant by second-order phase transition by giving the illustration of turbulence as an example of second-order phase transition.

In 2009, Gan [3] proposed the transition of laminar flow to turbulence flow as a second-order phase transition with spontaneous symmetry breaking. The examples of second-order phase transition with spontaneous symmetry breaking are magnetization, superconductivity and superfluids. This hypothesis has been subsequently supported by the experimental work of Goldenfeld's [4] group which showed that turbulence has the same behaviour as magnetization. In his paper, he presented experimental evidence that turbulent flows are closely analogous to critical phenomena from a reanalysis of friction factor measurements in rough pipes. He found experimentally two aspects that confirm that turbulence is similar to second-order phase transition such as magnetization in a ferromagnet. These are experimentally verified power-law scaling of correlation functions which is reminiscent of the power-law fluctuations on many length scales that accompany critical phenomena for example in a ferromagnet near its critical point which is second-order phase transition. Another aspect is the phenomena of data collapse or Widom scaling [5]. For example, in a ferromagnet, the equation of state, nominally a function of two variables, is expressible in terms of a single reduced variable which depends on a combination of external field and temperature. This has been confirmed by the experiments of Nikuradze [6] in 1932 and 1933 which showed data collapse. Goldenfeld's [4] work proposed that the features of the turbulence can be understood as arising from a singularity at infinite Reynolds number and zero roughness. Such singularities are known to arise in second-order phase transition such as that occurs when iron is cooled down below the Curie temperature and becomes magnetic. The theory predicts that the small-scale fluctuations in the fluid speed, a characteristic of turbulence, are connected to the friction, and this can be demonstrated by plotting the data in a special way that causes all of the Nikuradze [6] curves at different roughness to collapse into a single curve. According to Goldenfeld's [4] study, the formation of eddies in turbulence might be

a similar phenomenon to the lining of spins in magnetization. The rise of temperature in case of magnets is similar to the increase in velocity in case of the fluid passing through a pipe. Eddies are thus similar to the clusters of atoms. Goldenfeld [4] hope that as a result of these discoveries, the approaches that solved the problem of phase transitions will now find a new and unexpected application in providing a fundamental understanding of turbulence. On the other hand, it seems that turbulence offers us at macroscopic level, a view of what happens during other phase transitions at microscopic level. Thus, when we are looking at eddies in a river, at turbulence, at a cascade or at cigarette smoke, we can also imagine that we are actually watching what happens to molecules during a melting process, or how magnetism gradually vanishes when a magnet is melted. With the mature status of statistical physics and the gauge theory in today's scientific world, these two available disciplines are used to solve turbulence. Statistical physics was first used by Landau [7] in 1937 in the phenomenology of describing the second-order phase transition, with the use of order parameter and spontaneous symmetry breaking (SSB). Examples of gauge theory are the standard model of particle physics, Yang Mills theory, quantum chromodynamics and general relativity. Maxwell's equations are the oldest gauge theory, and SSB is a property of gauge theory. The gauge theory is a more sophisticated theory than the chaos theory which is sometimes used in describing turbulence. The beauty of gauge theory is that it can be applied to both the classical regime and the quantum regime.

Landau's [7] theory of second-order phase transition which is phenomenology can be extended to a more rigorous approach by using statistical physics and gauge theory. The Gross-Pitaevskii equation or nonlinear Schrodinger equation (NLSE) will be used. Turbulence is proposed as a condensate with pairing of molecules which is a property of condensate. The proposal that turbulence is a condensate is supported by Prof. Gregory Falkovitch's group's work [8] with the following quotes from his paper: "In fluids, condensates are system sized vortices or zonal flows. Turbulence with the condensate shares many properties with quantum systems displaying both fluctuations and coherences". This closeness is shown perhaps most vividly within the framework of the nonlinear Schrodinger (Gross-Pitaevskill) equation (NSE). In their paper [6], turbulence is considered with a Gross-Pitaevskii model and the creation of a coherent condensate via an inverse cascade originating at small scales. The growth of the condensate leads to a spontaneous breaking of statistical symmetries of over condensate fluctuations. They describe a phenomenon of spontaneous symmetry changes in the turbulent state by the change in a single parameter, the condensate level. We call this the condensate wave function. The results of their paper are supported by computer simulations. Here, turbulence is proposed as a classical analogue of the Bose Einstein condensate as the Gross-Pitaevskii equation is also used in the description of Bose Einstein condensate. Pumping to increase the condensate level is also used in Bose Einstein condensate. It has to be noted that Bose Einstein condensate such as superfluids is second-order phase transition. This in turn supports that turbulence as condensate is second-phase transition. Landau's [7] theory of second-order phase transition using order parameter is a phenomenology and a mean field theory. It has these

conditions: (1) the free energy must be analytical; (2) it must be independent of the detailed mechanism that causes symmetry in the Hamiltonian. The order parameter was introduced by Landau [7] to describe spontaneous symmetry breaking. The weakness of the theory lies in its assumption of the coefficients of the order parameter and its inability to describe the fluctuations in the critical point over a range of temperatures since it is a mean field theory. Landau [7] first showed the general relation between phase transition of the second kind and the change in the symmetry of the body. Landau's [7] theory of second-order phase transition states the thermodynamic potential or Landau free energy Φ in the format of a power series in the order parameter η:

$$\Phi(p, T, \eta) = +\alpha(p, T)\eta + A(p, T)\eta^2 + B(p, T)\eta^3 + C(p, T)\eta^4 + \cdots \tag{5.30}$$

The Landau free energy is equivalent to the Hamiltonian for the gauge invariance of the system at temperature above the critical temperature and no condensation takes place. For temperature at and below the critical temperature and condensation takes place and causes degeneracy in the ground state of the Landau free energy and spontaneous symmetry breaking takes place. Landau [7] observes that during a phase transition, the system becomes more orderly as it cools through the transition temperature. He proposed to measure the orderliness by a field parameter called the order parameter.

There are currently two research groups in the world whose works confirmed the hypothesis that turbulence is a second-order phase transition. The first is Nigel Goldenfeld's group [4] at the University of Illinois. Prof. Goldenfeld showed that the turbulent state is indeed not random but contains subtle statistical coordinations similar to those known to exist at second-order phase transition such as the onset of magnetism in crystals. A metal becomes magnetic when clusters of atoms feel one another's magnetic forces and align, their magnetic moments in the same direction, like a collection of tiny arrows all adding up to one big arrow. If one heats them up, the arrows jiggle more and more and at very high temperatures, they all point in random directions. However, there is an intermediate Curie temperature, where atoms can still feel one another's magnetism and form aligned clusters, although each cluster points in a random direction. According to Goldenfeld's [4] studies, the formation of eddies might be a similar phenomenon. The rise of temperature in case of magnets is similar to the increase in velocity in case of the fluid passing through a pipe. Eddies are thus similar to the cluster of atoms. The second confirmation came from the works of the research group of Prof. Gregory Falkovitch [8] from Weizmann Institute of Science. They consider turbulence within the Gross-Pitaevskii mode and the use of this equation and look into the creation of a coherent condensate via an inverse cascade originating at small scales. The growth of the condensate leads to a spontaneous breaking of statistical symmetry of over condensate fluctuation. This shares many properties with second order phase transition such as superconductivity.

The phenomenon and the meaning of condensation in two-dimensional turbulence [4] are a very striking example of the self-organization of large scale

coherence from small-scale fluctuations. The process works via the so-called inverse cascade mechanism whereby energy injected into a two-dimensional fluid by a small scale stochastic force is transformed to large scales by nonlinear coupling between different scales of motion in the Navier Stokes equations. When this inverse cascade reaches the size of the system, the energy carried by the inverse cascade accumulates at the largest scales and subsequently self-organizes to form large-scale coherent vortices. Condensation is self-organization. Self-organization is a process where some form of global order or coordination arises out of the local interactions between the components of an initially disordered system. This process is spontaneous, and it is not directed or controlled by any agent or subsystem inside or outside of the system. However, the laws followed by the process, and its initial condition may have been chosen or caused by an agent. It is often triggered by random fluctuations that are amplified by positive feedback. The resulting organization is wholly decentralized or distributed over all the components of the system. Examples of self-organization are crystallization, magnetization and superconductivity, where spontaneous symmetry breaking takes place. In analogous to the role of electrons pairing in superconductor, which is responsible for superconductivity, the molecule interaction is responsible for turbulence. There are two reasons to support the hypothesis of the pairing of water molecules: one is that the Gross–Pitaevskii equation for the purpose of simplification assumes that the interactions between condensate particles are of the contact two-body type. The second reason is that to exhibit Bose Einstein condensation, the fermions must pair up to form compound particles (e.g. molecules or Cooper pairs) that are bosons. To understand turbulence, one needs to understand the detailed pairing mechanism. In turbulence, the fluid condenses and forms an ordered line up in pairs of molecules. The mechanism of pairing is a special form of nonlinear interaction analogous to the mechanism of Cooper pairing which is a special form of electron–electron interaction. Due to the attractive force of pairing, the condensation free energy will go downwards to the ground state and condense and cause spontaneous symmetry breaking of the ground state of the Hamiltonian. Hence, the pairing potential is the force needed to pull the pair of molecules apart. The pumping technique can be used to increase the condensate level to achieve turbulence at critical point. As condensate grows, there is symmetry breaking. The more one pumps the system the more ordered the system becomes. The pairing of molecules is a special form of molecules alignment. Pairing points towards an ordered system, and the degree of pairing can be expressed in terms of entropy which can be calculated. The nonlinear interaction between molecules is responsible for pairing. The control parameter is the condensate level. The condensates are system sized vortices. An inverse cascade culminates in the creation of a spectral condensate mode that is spatially coherent, and one can use the same condensate wave function throughout the space. We expect the molecules pair to condensate until an equilibrium point is reached. As condensate grows, it leads to a spontaneous breaking of statistical symmetry. There is change in the pattern of distribution of the molecules from laminar flow to turbulence causing spontaneous symmetry breaking. Pairing is a form of molecular distribution. The condensate wave function is Landau order parameter here. These

are huge number of distribution of molecular pairs, and their distribution will be described by the Boltzmann distribution. The hypothesis that turbulence is a second-order phase transition has now been confirmed by Goldenfeld [4] and Falkovitch's [8] research groups. Landau's [7] theory of second-order phase transition is phenomenology and a mean field theory. Now a microscopic theory is built up for turbulence. The understanding of superconductivity is that it is a Bose Einstein condensate with the mechanism which is the interaction of the electrons, the Cooper pairing of the electrons. The classical analogue for the understanding of turbulence is that it is a coherent condensate with pairing of water molecules which is the mechanism of molecular interaction. The condensation free energy will be derived for turbulence. It will be shown that there is spontaneous symmetry breaking at the ground state of the condensate free energy, and the fluctuations in the critical point over a range of temperatures are explained. Turbulence is well understood to be a condensate [8] and Vladimirova et al.'s [8] work also confirmed that turbulence is condensate. The Gross-Pitaevskii equation is used in their treatment as what is used for the treatment of Bose Einstein condensate.

Following the above procedure for treatment of second-order phase transition, the critical temperature for piezoelectricity when the spontaneous parallel lining of dipole moments and spontaneous electrical polarization can be obtained.

5.8 Artificial Piezoelectricity

Metamaterial with negative piezoelectric strain constant and negative permittivity constant can be used as artificial piezoelectric material. This will enable the manipulation and control of piezoelectricity.

5.9 Fabrication of Artificial Piezoelectricity

This will be done by extending the method used for fabricating negative elastic material by replacing the material used for the unit cell of the resonator with piezoelectric material.

First, we will start with the split-ring resonator. Figure 5.1 shows an example of a split-ring resonator.

In 2004 split-ring resonators (SRR) became the object of acoustic metamaterial research [7]. Prior research with SRRs fabricated as negative index *electromagnetic* metamaterials was referenced as the progenitor of further research in acoustic metamaterial [7]. An analysis of the frequency band gap characteristics, derived from the inherent limiting properties of artificially created SRRs, paralleled an analysis of sonic crystals. The band gap properties of SRRs were related to sonic crystal band gap properties [7]. Inherent in this inquiry is a description of

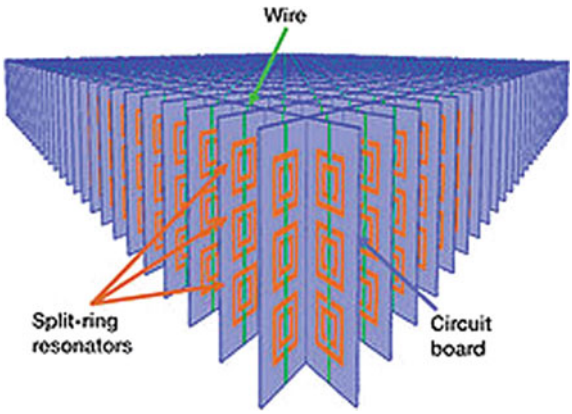

Fig. 5.1 Copper split-ring resonators and wires mounted on interlocking sheets of fiberglass circuit board. A split-ring resonator consists of an inner square with a split on one side embedded in an outer square with a split on the other side. The split-ring resonators are on the front and right surfaces of the square grid, and the single vertical wires are on the back and left surfaces [10]

mechanical properties and problems of continuum mechanics for sonic crystals, as a macroscopically homogeneous substance [7].

The correlation in band gap capabilities includes locally resonant elements and elastic moduli which operate in a certain frequency range. Elements which interact and resonate in their respective localized area are embedded throughout the material. In acoustic metamaterials, locally resonant elements would be the interaction of a single 1-cm rubber sphere with the surrounding liquid. The values of the stopband and band gap frequencies can be controlled by choosing the size, types of materials and the integration of microscopic structures which control the modulation of the frequencies. These materials are then able to shield acoustic signals and attenuate the effects of anti-plane shear waves. By extrapolating these properties to larger scales, it could be possible to create seismic wave filters (see Seismic metamaterials) [7]. According to research prior to this analysis, arrayed metamaterials can create filters or polarizers of either electromagnetic or elastic waves [7]. Here, a method is shown which can be applied to two-dimensional stopband and band gap control with either photonic or sonic structures [7]. Similar to photonic and electromagnetic metamaterial fabrication, a sonic metamaterial is embedded with localized sources of mass density ρ and the (elastic) bulk modulus κ parameters, which are analogous to permittivity and permeability, respectively. The sonic (or phononic) metamaterials are sonic crystals. These crystals have a solid lead core and a softer, more elastic silicone coating [8]. The sonic crystals have built-in localized resonances due to the coated spheres which resulted in almost flat dispersion curves. Low-frequency band gaps and localized wave interactions of the coated spheres were analyzed and presented in [7]. Similar method can be used to tune band gaps inherent in the material and, also, create new low-frequency band

gaps. It is also applicable for designing low-frequency phononic crystal waveguides (radio frequency). Doubly periodic square array of SRRs is used to illustrate the methodology [7].

The concept of split-ring resonator used in acoustics is an extension of the invention of Movchan and Guenneau [9]. They used split-ring resonator for electromagnetic waves. In their split-ring resonator, due to local resonance effect, it is possible to produce negative magnetic permeability. In addition, they have shown that microstructures built from nonmagnetic conducting sheets exhibit an effective magnetic permeability which can be tuned to values not accessible in naturally occurring materials, including large imaginary components of the magnetic permeability. The microstructure is on a scale much less than the wavelength of radiation, is not resolved by incident microwaves, and uses a very low density of metal so that structures can be extremely lightweight. Most of the structures are resonant due to internal capacitance and inductance, and resonant enhancement combined with compression of electrical energy into a very small volume greatly enhances the energy density at critical locations in the structure, easily by factors of a million and possibly by much more. Weakly nonlinear materials placed at these critical locations will show greatly enhanced effects raising the possibility of manufacturing active structures whose properties can be switched at will between many states and the production of negative magnetic permeability. By extending their split-ring resonator concept to acoustic waves, it is possible to produce negative bulk modulus and negative mass density due to local resonance effect.

Here, split-ring resonator concept is further extended to piezoelectricity with the replacement of copper in the unit cell of the resonator by piezoelectric material. The local resonance effect will produce negative electrical permittivity and negative piezoelectric strain constant.

References

1. Wu, B.I., Wang, W., Pacheco, J., Chen, X., Grzegorczyk, T., Kong, J.A.: A study of using metamaterial as antenna substrate to enhance gain. In: Progress in Electromagnetics Research, PIER**51**, 295–328, (2005)
2. Auld, B.A.: Acoustic Fields and Waves in Solids, vol. I and II, pp. 1–220. Robert E. Drieger Publishing Company, Malabar, Florida, USA (1990)
3. Gan, W.S.: Application of spontaneous symmetry breaking to turbulence. In: Proceedings of ICSV16, Krakow, Poland, 5–9 July 2009
4. Goldenfeld, N.: Roughness-induced critical phenomena in a turbulent flow. Phys. Rev. Lett. **96**, 04450 (2006)
5. Widom, B.: Equation of state in the neighborhood of the critical point. J. Chem. Phys. **43**, 3898 (1965)
6. Nikuradze, J.: VDI Forschungsheft (Springer-VD), Verlag, Berlin (1933), vol. 361; English translation available as National Advisory Committee for Aeronautics Report No. 1292, 1950 (unpublished); online at http://hdlhandlenet/2060/19930093938
7. Landau, L.D.: Phys. Z. Sowjetunion. **11**(26), pp. 545 (1937), in German; English translation in Collected Papers on Landau, L.D., ter Haar, D. (ed.), pp. 193 (1967)

8. Vladimirova, N., Derevyanko, S., Falkovich, G.: Phase transitions in wave turbulence. Phys. Rev. E **85**, 010101–010104 (2012)
9. Movchan, A.B., Guenneau, S.: Split-ring resonators and localized modes. Phys. Rev. B **70** (12), 125116 (2004)
10. Smith, D.R., Padilla, W.J., Vier, D.C., Nemat-Nasser, S.C., Schultz, S.: Composite medium with simultaneously negative permeability and permittivity. Phys. Rev. Lett. **84**(18), 4184–4187 (2000)

Chapter 6
Acoustic Diode

Abstract The acoustic diode is an application of metamaterial in the nonlinear acoustics regime. Here, the broken time reversal symmetry is achieved by introducing a nonlinear medium made of nonlinear phononic crystal. The acoustic diode has potential application in acoustical imaging such as medical imaging with the elimination of acoustic disturbances caused by sound waves going in two directions at the same time and interfering with each other. The propagation direction of output wave can be controlled freely and precisely. This enables clearer images.

6.1 Nonlinear Acoustics based on the Metamaterial

6.1.1 Principles

This is an introduction of nonlinear acoustics-based on metamaterial. The metamaterial chosen here is the nonlinear phononic crystal, a form of band gap metamaterial. The wave dynamics in strongly nonlinear phononic crystals based on granular chains in a Silicone elastometer or Teflon matrix will be considered. The wave equation for strongly nonlinear solitary wave has to be used [1]. This is more general than the weakly nonlinear KdV equation:

$$u_{tt} = -c^2 \left\{ (-u_x)^{3/2} + \frac{a^2}{10} \left[(-u_x)^{1/4} \left((-u_x)^{\frac{5}{4}} \right)_{xx} \right] \right\} \tag{6.1}$$

where $-u_x > 0,\ c^2 = \frac{2E}{\pi\rho_0(1-\nu^2)},\ c_0 = \left[\frac{3}{2}\right]^{1/2} c\xi_0^{1/4}$.

Here, c is not a sound speed, instead c_0 is a sound speed corresponding to initial strain ξ_0. This equation has no characteristic wave speed independent on amplitude. Despite its complex nature, it has simple stationary solutions with unique properties. In a system moving with a speed v_p, its periodic solution is represented by a sequence of humps ($\xi_0 = 0$) [2]:

W.S. Gan, *New Acoustics Based on Metamaterials*, Engineering Materials,
https://doi.org/10.1007/978-981-10-6376-3_6

$$\xi = \left[\frac{5v_p^2}{4c^2}\right]^2 \cos^4\left[\frac{\sqrt{10}}{5a}x\right] \tag{6.2}$$

Solitary shape can be taken as one hump of periodic solution (with only two harmonics) with finite length equal five particle diameters. This unique wave was observed in numerical calculations and detected in experiments [3]. Solitary wave can be considered as a quasiparticle with mass equals about 1.4 mass of grain in the chain, and its speed V_s has a nonlinear dependence on maximum strain ξ_m or particle velocity v_m:

$$v_s = \frac{4^{1/2}}{5} c\, \xi_m^{1/4} = \left[\frac{16}{25}\right]^{1/5} c^{4/5} v_m^{1/5} \tag{6.3}$$

Equation (6.3) shows that the speed of this wave can be infinitely small if the amplitude is small. This means that using this material as a matrix in Nonlinear Tunable Phononic Crystals (NTPC) one can ensure infinite elastic contrast of components, important for monitoring of band gaps. At the same time, the speed of solitary waves can be considered as constant at any relatively narrow interval of amplitudes due to power law dependence with small exponent. These properties enable NTPC to be used as effective delay lines with exceptionally low speed of signal.

Also when one-dimensional testing was performed by Daraio et al. [1] using chains of stainless steel spheres placed in Teflon or Silicone elastomer matrixes, a remarkable feature of "sonic vacuum" is observed, meaning a very rapid decomposition of initial impulse on the distances comparable with the soliton width. This example also demonstrates that short-duration impact on highly nonlinear ordered periodic systems (lattices) with weak dissipation may result in a chain of solitary waves instead of intuitively expected shock wave. This property of strongly nonlinear phononic crystal can be used for controlled impulse transformation in relatively short transmission lines. If chains of grains are placed into a polymer matrix, the nonlinear elastic behaviour is accompanied by strong dependence of electrical resistivity on local pressure [3]. Nesterenko et al. [4] also performed testing of the heavy light interface of the two strongly nonlinear granular media under the magnetically induced precompression resulted in a dramatic change of reflectivity. Anomalous reflected compression waves and transmitted rarefaction waves were detected in experiments and numerical calculations. They name this phenomenon the "acoustic diode" effect because of the dramatic change of the reflectivity triggered by the precompression. The nonlinear phenomenon described here can be used as tunable controllers of information flow through interfaces and in the design of novel types of tunable shock protection layers. The precompression can be employed for designing tunable information transportation lines with the unique possibility of manipulating the signal's delay, reflection and decompositions at will for security-related information.

It also has to be noted that the tunability of strongly nonlinear system with the variation of the elastic modulus of the stainless steel beads can be used for the design of tunable acoustic focusing lenses.

6.1.2 Nonlinear Acoustic Metamaterials for Sound Attenuation Applications

The previous section shows that an acoustic crystal composed of tightly packed spherical particles can exhibit a wide spectrum of acoustic properties with responses varying from linear to highly nonlinear regimes. The physical attractiveness of these crystals resides in the controllability of such acoustic responses by simple manipulation of static precompression applied to the material. Jinkyu and Chiara Daraio [5] showed that from the fundamental understanding of the energy transmission through these crystals in relation to the tunable acoustic nonlinearity, one can control the degree of nonlinearity. To do this, three parameters have to be varied: precompression, striker velocity and striker mass, maintaining an identical configuration of one-dimensional granular structures. The transmission gain in the stop/pass frequency band of the granular chain was evaluated as a function of the nonlinearity. The evolution of the frequency band structure was studied as the degree of nonlinearity was changed. The transmission gain of the granular structure showed a remarkable dependence on the structural linearity level.

To combine the frequency filtering response governed by the discrete particles with an amplitude filtering response, they assembled a system composed of a highly nonlinear granular chain and a deformable linear medium. Acoustic wave propagation can then be efficiently manipulated and redirected with such added degree of freedom.

In the second part of the study, they build a hybrid linear/nonlinear metamaterial to allow high-energy transmission only in a selected range of external impact amplitude. In this hybrid structure, the nonlinear granular chain takes the role of transmitting energy when the system is excited with low-amplitude impacts, controlled by structural deflections. A strong correlation of transmission gain with external impact amplitudes was verified, showing an order of magnitude reduction of transmission gain for large-amplitude impacts compared to that of low-amplitude impacts. The wave propagation and impact mitigation were evaluated in the nonlinear acoustic metamaterial using a combined discrete particle model and a finite element method. Finally, it was verified that the numerical results are in excellent agreement with the experimental results.

The proposed metamaterials are fundamentally different from any other approach to vibration isolation. They do not use active modulation to suppress vibration/impacts, but rely on passive insulation. Furthermore, they are stiff and load-bearing, present large recovery to external deformation, and do not develop permanent damage in the ranges of excitations studied. The proposed systems are designed to forbid the propagation of waves in selected frequency ranges (also

known as band gaps or stop bands). Incident waves in these forbidden frequency ranges experience an exponential decay of their amplitudes (i.e. they are evanescent waves), and they are fully reflected. The presence of nonlinearity in the structure may allow the redirection of part of the incoming energy into allowed modes. This type of acoustic filter system could be useful in protecting soldiers against hearing damage from weapons fire, while largely retaining their situational awareness.

6.2 Acoustic Diode Enabling One-Way Sound Transmission

An acoustic diode was introduced in August 2009 [6]. An electrical diode allows current to flow in only one direction in a wire; it is an essential electronic device which had no analogues for sound waves. However, the reported design partially fills this role by converting sound to a new frequency and blocking any backwards flow of the original frequency. In practice, it could give designers new flexibility in making ultrasonic sources like those used in medical imaging. The proposed structure combines two components: The first is a sheet of nonlinear acoustic material—one whose sound speed varies with air pressure. An example of such a material is a collection of grains or beads, which becomes stiffer as it is squeezed. The second component is a filter that allows the doubled frequency to pass through but reflects the original. The acoustic diode is like a one-way mirror for sound waves.

A diode allows electric current to flow in only one direction in a wire and is essential in electronics, but no such one-way device exists for sound waves. Bin Liang et al. [6] describe a design that partially fills this role by converting sound to a new frequency and blocking any backwards flow of the original frequency. If the technique is practical, it could give designers new flexibility in making ultrasonic sources like those used in medical imaging.

Usually, waves can travel just as easily in either direction along a given path. So lasers, for example, are sometimes protected from their own reflections by shining them through clear magnetic materials that sidetrack any reflected light. But there is no analogous trick to deflect backtracking sound waves that might disturb the operation of an ultrasound source.

In related work, however, researchers have recently proposed “thermal diodes” [7]—layered structures that let heat flow one way but not the other. Inspired by these results, Jian-chun Cheng and his colleagues at Nanjing University in China designed a device, which they call an acoustic diode that passes some sound energy in only one direction [6].

Their proposed structure combines two components. The first is a sheet of “nonlinear” acoustic material–one whose sound speed varies with air pressure. An example of such a material is a collection of grains or beads, which becomes stiffer as it is squeezed, says Vitali Nesterenko of the University of California in San Diego. A sound wave passing through such a nonlinear material creates additional sound waves at other frequencies—including some with twice the original

frequency—much as an over-amplified sound system adds extra noise to the music. Cheng and colleagues calculated the effect of putting this doubling material face to face with a second component: a filter that allows the doubled frequency to pass through but reflects the original.

If the sound comes from the right, it hits the nonlinear material first, creating doubled-frequency sound that passes through the filter. But any sound coming from the left at the original frequency is blocked before it reaches the doubling layer. Choosing a set of specific material parameters, the researchers calculate that about 100,000 times less energy can pass left-to-right than right-to-left.

This acoustic diode differs from its counterpart used in electronic circuits because it only works for sound waves in a narrow range of frequencies. In addition, the transmitted sound has twice the frequency, so it can pass back through the filter, even though the original frequency cannot. Nonetheless, Cheng is hopeful that the device may be useful in "a variety of significant situations where the acoustic waves need to be specially controlled or modified", such as the use of focused ultrasound to break up kidney stones.

Nesterenko says that the numbers used in the paper may not be representative of real materials, and "a lot of work remains to be done, especially experimentally". But he still thinks the structure is innovative and opens new design possibilities. Nicholas Fang of the University of Illinois in Urbana-Champaign finds the "almost completely one-way transmission" to be impressive.

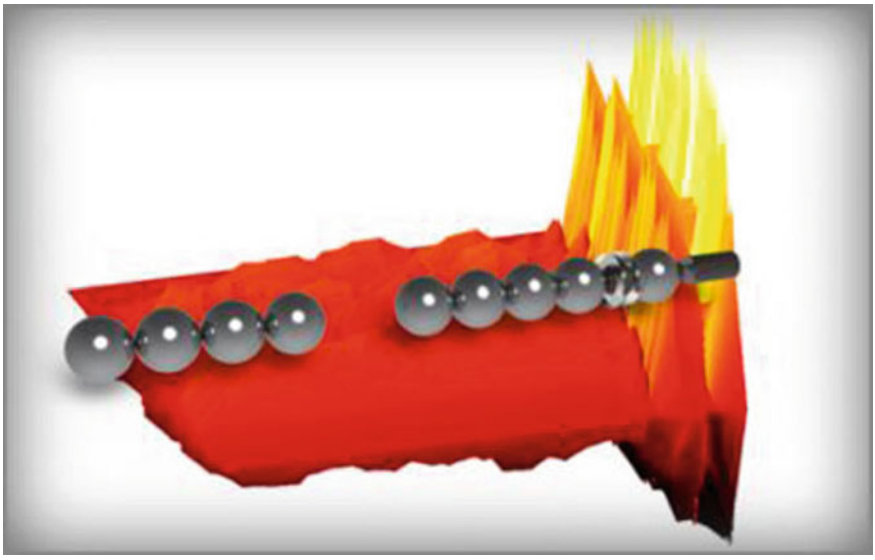

(Chiara Daraio/Caltech)

The Acoustic Diode. By tuning the elastic spheres in certain ways—by changing their sizes and shapes from one end of the chain to the other, for instance—it's possible to manipulate a sound wave as it travels down the chain, downshifting the frequency or making it possible for sounds to travel in one direction but not the other

We have few mature technologies that enable us to control and manipulate the way sound travels. But Caltech researchers are working to change that via the first tunable, acoustic diode that can be used to let sound flow in one direction only.

The acoustic diode works much like the electrical component of the same name, letting current (or, in this case, sound waves) to pass in one direction but blocking it in the other. Composed of a structured arrangement of elastic spheres that ferry the sound through the material, the diode can be tuned to work only at certain frequencies or to downshift the frequencies moving through the material to lower frequencies as needed.

That opens the technology up to several potential applications. In the case of soundproofing, the technology could enable true one-way transmission of sound (rather than the simple dispersion and muting performed by "soundproofing" foams). But perhaps more interestingly, the material could be used to harvest energy from sound waves.

For instance, the tunable diode could scavenge energy from noisy machinery and channel it back into a transducer that converts those sound vibrations into electricity that could be fed back to the machine, reducing net energy consumption. It could also downshift sound frequencies to ranges that are optimal for energy conversion.

All that's a long way off, but the notion is pretty intriguing. In the meantime, the Caltech team is also exploring a range of other technological applications for their wave-manipulating technology, including medical uses (ultrasound), architectural acoustics and insulating materials that regulate temperature.

Based on a simple assembly of granular crystals that transmit sound vibrations, Caltech researchers have created the first tunable acoustic diode that allows sound to travel only in one direction.

"We exploited a physical mechanism that causes a sharp transition between transmitting and non-transmitting states of the diode," explained Chiara Daraio, lead author of the new study. "Using experiments, simulations, and analytical predictions, we demonstrated the one-way transmission of sound in an audible frequency range for the first time."

The system, described in *Nature Materials*, is based on a simple assembly of elastic spheres—granular crystals that transmit the sound vibrations—that could be easily used in multiple settings, can be tuned easily, and can potentially be scaled to operate within a wide range of frequencies, meaning its application could reach far beyond soundproofing.

Similar systems have been demonstrated previously, but they all featured smooth transitions between transmitting and non-transmitting states instead of the sharp transitions needed to be more effective at controlling the flow of sound waves. To obtain the sharp transition, the team created a periodic system with a small defect that supports this kind of quick change from an "on" to an "off" transmission state.

According to Daraio, this means the system is very sensitive to small variations of operational conditions, like pressure and movement, making it useful in the development of ultrasensitive acoustic sensors to detect sound waves.

The system can also operate at different frequencies of sound and is capable of downshifting, or reducing the frequency of the travelling signals, as needed. "We propose to use these effects to improve energy-harvesting technologies", she added. "For example, we may be able to scavenge sound energy from undesired structural

vibrations in machinery by controlling the flow of sound waves away from the machinery and into a transducer. The transducer would then convert the sound waves into electricity".

- The new mechanism may have applications beyond soundproofing and energy harvesting. "Because the concepts governing wave propagation are universal to many systems, we envision that the use of this novel way to control energy might enable the design of many advanced thermal abstract".

6.3 Application of Acoustic Diode to Acoustical Imaging

An acoustic diode, enabling the one-way transmission of sound waves, could dramatically improve the quality of medical ultrasound imaging and lead to better sound dampening materials. Such a device has now been created by researchers at China's Nanjing University led by Professor Jian-chun Cheng [6].

Acoustic diodes are analogous to the electric diodes that produce unidirectional flow of current through electronic devices, protecting them from sudden and damaging reversals of flow. Electric diodes, which are akin to the check valves in car engines, work by providing nearly zero resistance to current flow in one direction and very high resistance in another. However, says associate professor and team member Bin Liang, "there is no analogous method to protect ultrasound sources from the disturbance of backtracking acoustic waves. Indeed, such unidirectional flow is far tougher to achieve with acoustic waves than with electric current because sound waves travel just as easily in both directions along any given path".

The acoustic diode consists of two parts. The first is an ultrasound contrast agent (UCA), made from a suspension of microbubbles. The UCA has a strong acoustic nonlinearity, which means it converts the acoustic energy of an incident wave into a wave with twice as many pulsations per second. Therefore, Liang says, "sound waves enter such a material at a particular frequency and leave with a frequency twice as great". The UCA microbubbles come in a broad range of sizes, so they can produce acoustic nonlinearity over a broad frequency range.

The second part of the acoustic diode is a superlattice consisting of thin alternating sandwich-like layers of water and glass. The superlattice acts like a filter that allows the sound waves with the doubled frequency to pass through the material but not the original sound waves.

"Hence," Liang says, "if the sound comes from the side of the nonlinear material, it will hit that material first, creating doubled frequency sound that passes through the filter, while any sound coming from the other side at the original frequency is blocked before it reaches the doubling layer."

In clinical medical imaging using ultrasound, acoustic waves are sent into the body, and the reflected waves are received by the scanning instrument and the surrounding sensors to form the ultrasound images of the internal organs. "However, some of the reflecting waves interfere with the ingoing waves, which

may lower the brightness and the resolution of the image. Therefore, preventing waves from coming back toward the ultrasound source would help to improve the quality of the ultrasound image", Liang says.

"In general," he adds, "we hope that the acoustic diode could apply to diverse situations where a special control of acoustic energy flux is required, for example, to improve the quality and effect of medical ultrasound diagnosis and therapy, or the design of unidirectional sound barriers."

Another group with Chang Liu et al. [8] also proposed alternative acoustic diode (AD) mode for acoustical imaging. The acoustic diode (AD) can provide brighter and clearer ultrasound images by eliminating acoustic disturbances caused by sound waves travelling in two directions at the same time and interfering with each other. Such an AD could give designers new flexibility in making ultrasonic sources like those used in medical imaging or nondestructive testing. However, current AD designs, based on nonlinear effects, only partially fill this role by converting sound to a new frequency and blocking any backward flow of the original frequency. In this work, an AD model that preserves the frequencies of acoustic waves and has a relatively high forward-power-transmission rate is proposed. Theoretical analysis indicates that the proposed AD has forward, reverse and breakdown characteristics very similar to electrical diodes. The significant rectifying effect of the proposed AD is verified numerically through a one-dimensional example. Possible schemes for experimental realization of this model as well as more complex and efficient AD designs are also discussed.

One-way flow of sound would create brighter and clearer ultrasound images by eliminating acoustic disturbances caused by sound waves going in two directions at the same time and interfering with each other, says Prof Jian-chun Cheng. Propagation direction of the output wave would be controlled freely and precisely.

The research team developed its theoretical diode model based on a material not found in nature—a near-zero index metamaterial (ZIM)—and an asymmetric prism to create high-transmission-efficacy acoustic waves that strike a reflective boundary from two opposite sides. According to Cheng, this would produce a unique tunnelling effect and an unprecedented property that the output waveform is kept consistent with those of the waves travelling towards a boundary.

6.4 Theoretical Framework of the Acoustic Diode [9]

6.4.1 Introduction

Realizations of one-way manipulations in various kinds of energy flux are always highly desirable. The most famous example should be the invention of electric diodes which marked the emergence of modern electronics and resulted in worldwide technology revolutions. Acoustic wave, albeit a classical wave with much longer research history in comparison with the electricity, has long been

thought to propagate easily along two opposite directions in any path. Hence, it should be intriguing to realize the one-way transmission of acoustic waves by designing the acoustical analogy of electric diodes, which would have deep implications in all the acoustics-based applications and the field of acoustics in general. Acoustic one-way manipulation has become a new frontier of science and is of remarkable significance in both the physics and engineering communities. The emergence of the first "acoustic diode", formed by coupling a phononic crystal (PC) with a nonlinear medium, offers the possibility of rectifying acoustic energy flux by breaking through the barrier of reciprocity principle via the introduction of nonlinearity. Despite of the efforts in enhancing the performances of nonlinear acoustic diodes by updating their structures, the inherent shortcomings in nonlinear systems such as low efficiency and narrow bandwidth still attract considerable attentions on the potential of linear structures, aiming at constructing a one-way manipulation on particular modes of an acoustic wave without breaking the reciprocity principle. A series of linear acoustic one-way devices have already been designed and fabricated with significantly improved performances. On the basis of asymmetric mode conversion, a linear one-way plate for Lamb waves is designed. High efficient one-way transmission for plane waves propagating along two opposite directions is realized by coupling a PC and a diffraction structure. Unidirectional waveguide is designed and fabricated which only allows for a plane wave incident from one of the two openings to pass. A unidirectional structure with a total thickness as thin as the wavelength is realized by reconstructing the otherwise plane wavefront with acoustic gratings. An acoustic gradient-index structure is proposed that can directly manipulate the wave trajectory asymmetrically and then yield asymmetric acoustic transmission within a considerably broad band. Acoustic metamaterials with near-zero indexes have also been employed to realize unidirectional transmission with a controllable transmitting angle and consistent wavefront. These advances are important steps toward the practical applications which generally require integration and minimization of devices having high efficiency and broad bandwidth. The recently emerged "acoustic transistor" can be regarded as the acoustical counterpart of an electric transistor and enables the amplification and switch of acoustic waves by an acoustic wave, or by exploiting the three-wave mixing effect. The usage of acoustic one-way devices in controlling acoustic waves has both challenge and promise. The realizations of one-way manipulations in various kinds of energy flux are always highly desirable. The most famous example should be the invention of electric diodes which marked the emergence of electronics.

6.4.2 Physics of Acoustic Diode

Electrical diodes, due to their capability of rectification of current flux, have significantly revolutionized fundamental science and advanced technology in various aspects of our routine life. Motivated by this one-way effect of electric currents,

considerable effort has been dedicated to the study of the unidirectional nonreciprocal transmission of electromagnetic waves, showing important promise in optical and rf communications [10–15]. The realization of such nonreciprocal and unidirectional propagation requires either a broken time reversal symmetry [10–13] or a broken spatial inversion symmetry [14, 15] in the artificial photonic structures (e.g., photonic crystals).

Sonic crystals (SCs), in an analogy with the electronic and photonic band structures of semiconductors and photonic crystals, have shown promising impacts in acoustic devices and applications that can efficiently trap, guide and manipulate sound [16–24]. In the past two decades, with rapid developments in SCs ranging from engineering of band structure for bulk acoustic waves to design of acoustic grating for surface waves, a series of fascinating acoustic effects are consequently demonstrated, such as acoustic band gaps [24, 25], negative refractions [10] and extraordinary transmission [24]. It is therefore expected, with a sophisticated SC design, that the exotic properties of SCs can lead to more counterintuitive sound manipulation, for example, the realization of acoustic diodes that can break down the conventional transmission reciprocity [25–27]. Similar to electromagnetic wave, sound usually propagates reciprocally back and forth along a given path. Unidirectional flux transmission requires considering the breaking of parity and time reversal symmetry simultaneously in uniform media [28] that do not typically exist in nature. Therefore, SCs are currently considered good candidates to implement nonreciprocal and unidirectional sound propagation. Previous studies proposed the utilization of acoustic nonlinear effects combined with SCs to implement the broken time reversal symmetry as shown in the upper panel of Fig. 6.1a [25, 26]. The nonlinear medium induces the frequency conversion as the solid red line in Fig. 6.1b indicates, and the adjacent SC acts as a frequency filter to block the incidence from the right since only the fundamental frequency locates within the band gap. However, the unidirectional transmission from left to right is quite low due to the inherent low conversion efficiency in acoustic nonlinear activities.

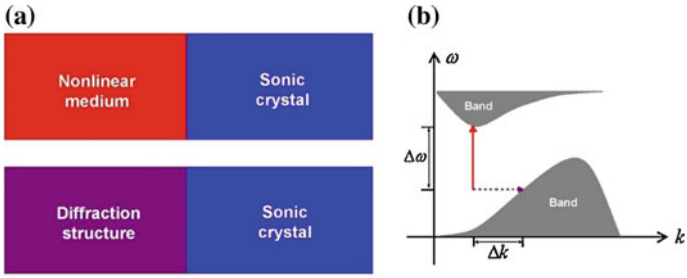

Fig. 6.1 **a** Illustration for two diode models, with the top one coupling nonlinear medium to SC and the bottom one using diffraction structure. **b** Schematic for transitions between different modes: the solid red line represents the transition with frequency change and the dashed purple line represents the transition between different spatial modes. (Li et al. [9]) colour figure online

Here, a more sophisticated design approach is used by Li et al. [9] to break the spatial inversion symmetry in the constructed SCs, and both experimentally and numerically demonstrate unidirectional transmission in such SCs. The constructed SC-based acoustic diodes can be further controlled by simply mechanically manipulating the unit cell of SCs [23] to support either reciprocal or nonreciprocal sound transmission. The SC-based acoustic diode here is a completely linear system without any acoustic nonlinearity. The acoustic diode is designed with an asymmetric periodic corrugated SC as shown in the lower panel of Fig. 6.1a that consists of a diffraction structure and a regular SC. The diffraction structure causes the transition between two spatial modes with different spatial frequencies as indicated by the dashed purple line in Fig. 6.1b. The adjacent SC thus behaves as a spatial filter due to its intrinsic anisotropy of acoustic band structures, such that different spatial modes, especially high-order diffraction modes with different parallel wave vectors, can be either transferred or prohibited in the designed SC.

The concrete design of the acoustic diode by Li et al. [9] as shown in Fig. 6.2a, consisted of a two-dimensional (2D) SC arranged in a square mesh with a lattice constant of $a = 7$ mm and a corrugated diffraction structure with a modulation period of $L = 6a$ in the y direction to the left of the SC. Both the SC and the diffraction structure were composed of square steel rods with the width of $d = 4$ mm in an air background. Finite element simulation was implemented to evaluate the unidirectional transmission property of the acoustic diode, as shown in Fig. 6.2d, where the transmission spectra clearly demonstrates nonreciprocal transmission efficiencies for the left incidence (LI) and the right incidence (RI) with a normally incident plane wave. The unidirectional frequency band is indicated by the blue-shaded region in Fig. 6.2d. In the experiment, the manufactured acoustic diode had seven corrugation periods in the y direction, and acoustic field scanning measurement was carried out in two ranges of frequencies from 15.0 to 25.0 and from 35.0 to 50.0 kHz, due to the limited response range of transducers. In spite of limitations of the finite size in the transverse direction and slight imperfection of the plane wave source in the experiment, the measurement results shown in Fig. 6.2e still agreed with the simulation. Especially within 17.5–19.5 and 38.7–47.5 kHz, LI was associated with high transmission efficiency, but transmission was not allowed for RI, showing a relatively broadband unidirectional transmission only for LI as indicated by the blue shaded region in Fig. 6.2e. In order to illustrate this unidirectional transmission more clearly, spatial intensity distributions of the acoustic pressure field are mapped out both numerically and experimentally as shown in Figs. 6.2b and 6.2c at two frequencies of 18.0 and 47.0 kHz, respectively. Because of the SC's directional band gap in the x direction (Γ−X), RI was almost completely reflected without any transmission. In the case of LI, however, strong acoustic field can be observed in the output area; for example, the transmission at 18.0 kHz was about 69%. But since the outgoing waves are not parallel to the incident waves, it is evident that energy in the normal incidence was converted, through high-order diffractions, to other spatial modes that have different spatial frequencies to overcome the barrier imposed by the −X directional band gap. The

unidirectional transmission was therefore established, and the output field was actually the interference of outgoing beams from different diffraction orders.

To clearly quantify the performance of the acoustic diode, the contrast ratio (R_c) is defined by Li et al. [9] as

$$R_c = (T_L - T_R)/(T_L + T_R) \tag{6.4}$$

where T_L and T_R are the transmissions for L_I and R_I respectively. The absolute value of R_C represents the relative transmission weight between these two incident cases. R_c was also evaluated as a function of frequency as shown in Fig. 6.2f. Within the specific frequency ranges where unidirectional transmission was clearly observed, R_c reaches 1 with a good agreement with experiments and simulations.

In addition to the broken spatial symmetry resulting from the diffraction structure, the building block of the SC, the steel square rod also introduces a broken rotational symmetry to the unit cell itself [29]. The introduced broken rotational symmetry can cause the change of the SC's band dispersion by simply mechanically rotating all the square rods with the same lattice configuration, as different rotations affect the effective scattering section for acoustic waves significantly. It is therefore expected to effectively control the sound rectification (i.e., efficiently tune the relative transmission weight between LI and RI) with the acoustic diode by rotating the rods. In the experiment, we rotated all the square rods 45 degrees with keeping other parameters the same in the diode configuration, as shown in Fig. 6.3a. Intrinsic characteristics of multiple scatterings in the SC were consequently dramatically changed, leading to a broader first band gap of SC as shown in Fig. 6.3d due to the increase of the effective scattering section. The unidirectional transmission could still be observed from 16.2 to 22.3 kHz. But from 40.0 to 50.0 kHz, transmission was allowed for both LI and RI, and the one-way phenomenon was deactivated. Therefore, it is evident that the sound rectification effect could be effectively turned on or off in the acoustic diode by rotating the square rods of the SC. This tunable acoustic diode was further confirmed with mappings of spatial intensity distribution of the acoustic pressure field at 17.25 and 47.0 kHz, as shown in Figs. 6.3b and c, respectively. Consistent with transmission spectra in Figs. 6.3d and e, pronounced unidirectional transmission can be seen at 17.25 kHz, but equivalent transmission was obtained in both directions at 47.0 kHz. The contrast ratio in Fig. 6.3f also confirmed that the relative transmission weight is 1 from 16.5 to 22.5 kHz, and the unidirectional character thus remains the same (compared to Fig. 6.2), while the weight was around 0 from 35.0 to 50.0 kHz, showing the change from unidirectional to bidirectional transmission. In addition, this tunable unidirectional transmission effect could also be influenced by different rotation angles and filling fractions (see Fig. S4 in [29]). In principle, with a more systematic design of the square-rod-based SC, this tunable acoustic diode could be constructed either in the first or the second band (as demonstrated above), or both. And the frequency range of unidirectional transmission might be anticipated to be effectively controlled with different rotational angles of these square rods.

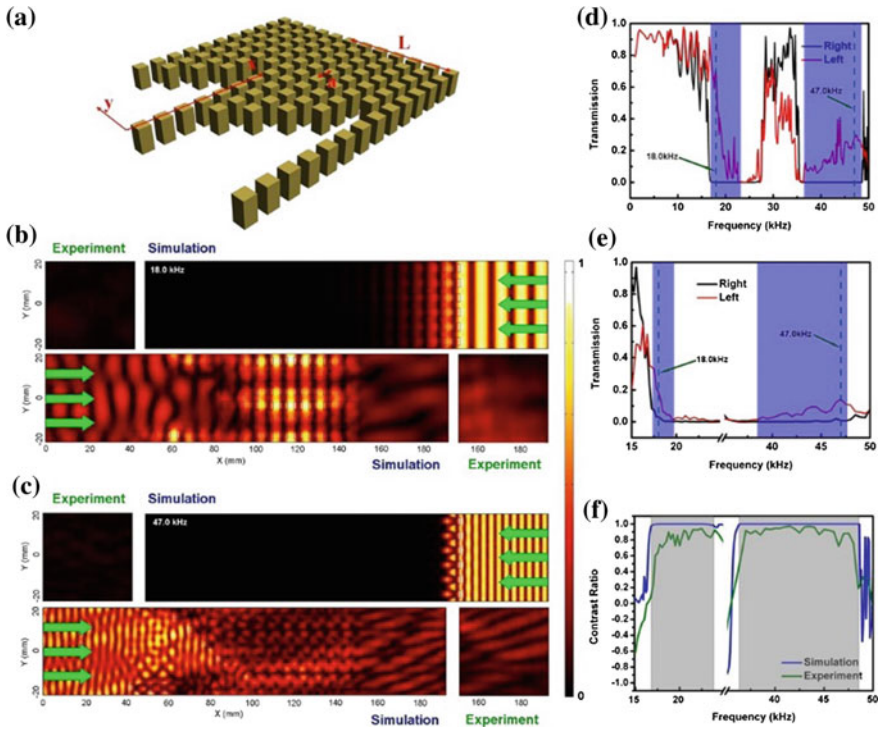

Fig. 6.2 **a** Schematic diagram of the SC-based acoustic diode which is periodic in y direction. **b**, **c** Simulated and experimental field distribution mappings with the incident wave frequency at 18.0 and 47.0 kHz, respectively. Green arrows indicate the propagation directions. **d**, **e** Numerically calculated and experimentally measured transmission spectra of LI and RI, respectively. Green arrows indicate the frequency at which field distribution is mapped. **f** Contrast transmission ratio of the acoustic diode. (Li et al. [9]) colour figure online

To gain deeper insight, the mechanism underlying this unidirectional transmission phenomenon was analytically investigated by Li et al. [9] as follows.

With a plane wave incidence the acoustic pressure field in the input and output half-spaces can be Fourier expanded as

$$P(x,y) = \exp(jk_0x) + \sum_{n=-\infty}^{\infty} \rho_n \exp(j \propto_n y + j\beta_n x) \tag{6.5}$$

$$P(x,y) = \sum_{n=-\infty}^{\infty} \tau_n \exp(j \propto_n y + j\beta_n x) \tag{6.6}$$

where $\beta_n = \left(k_0^2 - \propto_n^2\right)^{1/2}$, $\propto_n = 2n\pi/L$ (n is the diffraction order), k_0 is the free-space wave number, and $\propto_n$ and β_n are amplitudes of the nth order diffraction beams in reflection and transmission, respectively. The mechanism of the acoustic diode is closely relevant to these two diffraction terms. These diffraction terms represent the energy conversion among different diffraction orders. The difference of structure geometries on two sides resulted in different diffraction orders, and only the orders locating within the propagating band of the SC could transmit the energy from one side to the other. Notice that, however, the diode in this study cannot be completely analytically described by Eqs. (6.5) and (6.6), due to its complex diffraction construction. Therefore simplified diode geometry was studied and compared to them.

As shown in Figs. S2(b) and S2(d) of [28], tunable unidirectional transmission effect is also realized with a much weaker diode behaviour. The optimized complex geometry here has advantages over this simplified diode in two aspects. (1) With the adiabatic change in the complex asymmetric corrugation, the reflection of the acoustic wave incident from the left side could be efficiently reduced. (2) Compared to diffractions through the simpler corrugation, it is more efficient to generate higher order diffraction modes through the complex asymmetric corrugation due to the large slope angle.

In order to illustrate nonreciprocal sound propagation in the acoustic diode, Li et al. [9] further analyse the equifrequency surfaces (EFSs) at different frequencies of the SC as shown in Fig. 6.4. For the case of RI in Figs. 6.4a and 6.4b, high diffraction orders completely fell in the evanescent regime ($\propto_n$ and β_n are 0) in the interested frequency ranges, and thus all the energy was still conserved in the zero order, i.e., normal incidence to the SC, which was located within the directional band gap of the SC. Therefore, sound transmission for RI was prohibited by the SC. However, for the case of LI, the existence of the diffraction structure before the SC converted the normal incidence mode to high-order diffraction modes. This can be more clearly visualized in Fig. S3 of [29] where an incident beam with a finite width was considered. The transmitted beams propagated along different directions, corresponding to different positive and negative diffraction orders due to the complex diffraction structure. Consistent with EFSs in Figs. 6.4a and 6.4b, 1 and 2 modes significantly contributed to transmission through the SC and resulted in unidirectional sound transmission. After the rotation of the square rods, EFS from 17 to 19 kHz remained almost the same as shown in Fig. 6.4c, demonstrating a nonreciprocal feature as all the diffracted beams easily transmits through the SC for LI as shown in Fig. S3(f) of [29]. But from 45 to 49 kHz, EFS was drastically changed as shown in Fig. 6.4d, and the original directional band gap in Fig. 6.4b disappeared. Therefore, sound transmission was also allowed for RI, and the nonreciprocal sound propagation is thus expected to be simply mechanically controlled by rotating the rods of the acoustic diode.

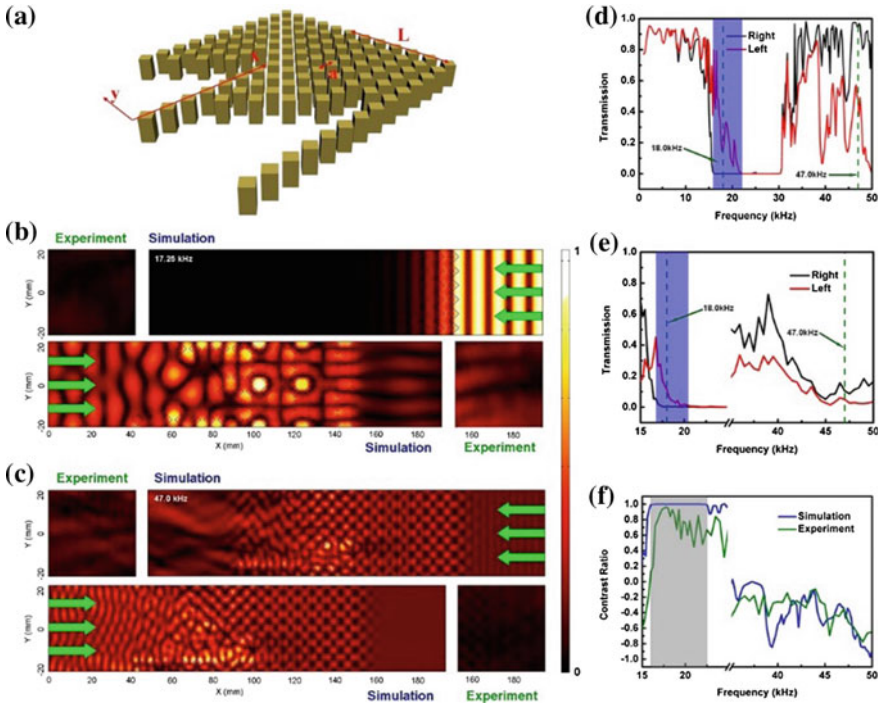

Fig. 6.3 **a** Schematic diagram of the SC-based acoustic diode after rotating the square rods. **b**, **c** Simulated and experimental field distribution mappings with the incident wave frequency at 17.25 and 47.0 kHz, respectively. Green arrows indicate the propagation directions. **d**, **e** Numerically calculated and experimentally measured transmission spectra of LI and RI, respectively. Green arrows indicate the frequency at which field distribution is mapped. **f** Contrast transmission ratio of the acoustic diode. (Li et al. [9]) colour figure online

The above description showed the theory proposed by Li et al. [9] and experimentally demonstrated by constructing a sonic-crystal-based acoustic diode with a broken spatial inversion symmetry in which nonreciprocal propagation and unidirectional transmission of sound were clearly observed. Furthermore, the introduced broken rotational symmetry of the unit cell of the sonic crystal results in a sophisticated mechanical manipulation of the observed nonreciprocal sound transmission. Compared to previously proposed acoustic diodes using nonlinearities, the system described is a completely linear system, showing advantages such as broadband operation, high conversion efficiency and much less power consumption. The same concept is also expected to implement an on-chip isolator for various types of acoustic waves, such as surface acoustic waves [30] and Lamb waves [31].

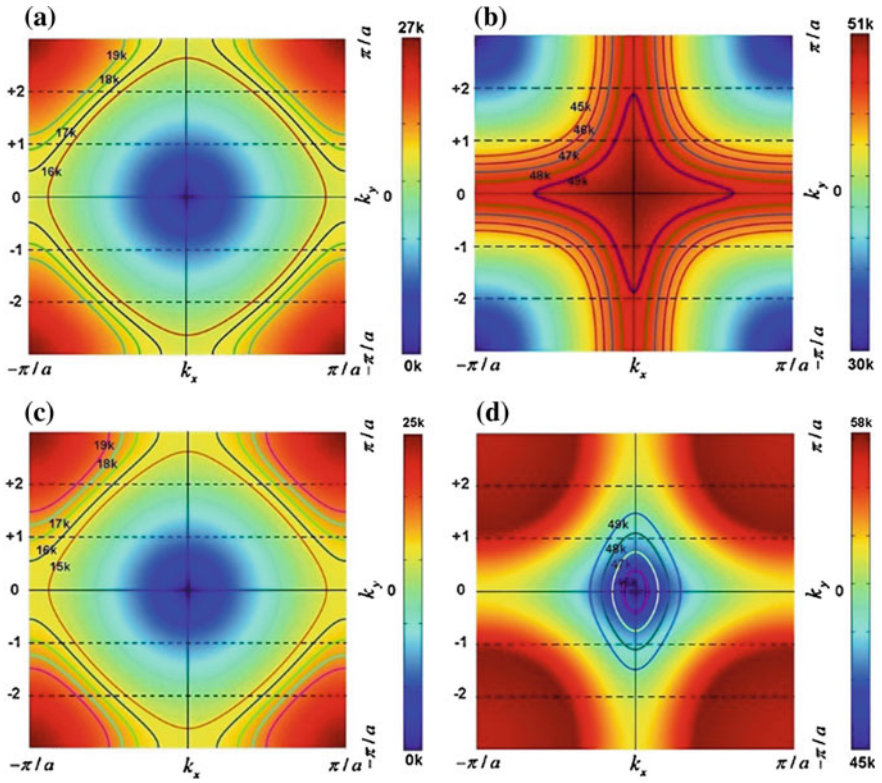

Fig. 6.4 **a**, **b** EFSs of the SC in first Brillouin zone from 16 to 19 and from 45 to 49 kHz, respectively. The numbers (2, 1, 0, þ1, þ2) on left and right sides correspond to the diffraction orders. **c**, **d** EFSs of the SC after the rotation of rods in two frequency ranges. (Li et al. [9]) colour figure online

References

1. Daraio, C.,Nesterenko, Jin, V.S.: Strongly nonlinear waves in 3D phononic crystals, Shock Compresson of Condensed Matter. In: Furnish, M.D., Gupta, Y.M., Forbes, J.W. (eds.) American Institue of Physics, pp. 197–200 (2003)
2. Nesterenko, V.F.: Dynamics of Heterogeneous Materials. Springer-Verlag, New York (2001)
3. Jin, S., Tiefel, T., Wolfe, R., Sherwood, R., Mottine, J.: Optically transparent, electrically conductive composite medium. Science **255**, 446 (1992)
4. Nesterenko, V.F., Daraio, C., Herbold, E.B., Jin, S.: Anomalous wave reflection from the interface of two stongly nonlinear granular media. Phys. Rev. Lett. **95**, 158702 (2005)
5. Yang, J., Daraio, C.: http://www.embeddedtechmag.com/component/content/article/12254
6. Liang, B., Yuan, B., Cheng, J.C.: Acoustic diode: rectification of acoustic energy flux in one-dimensional system. Phy. Rev, Letts (2009)
7. Li, B., Wang, L., Casati, G.: Thermal diode: rectification of heat flux. Phy. Rev. Letts. **93**, 184301 (2004)
8. Liu, C., Du, Z., Sun, Z., Guo, X.: Phys. Rev. Applied **3**, 064014 (2015)

9. Li, X.F., Ni, X., Feng, L., Lu, M.H., He, C., Chen, Y.F.: Tunable unidirectional sound propagation through a sonic-crystal based acoustic diode. Phy. Rev. Lett. **106**, 084301–084304 (2011)
10. Wang, Z., et al.: Phys. Rev. Lett. **100**, 013905 (2008)
11. Haldane, F.D.M., Raghu, S.: Phys. Rev. Lett. **100**, 013904 (2008)
12. He, C., et al.: Appl. Phys. Lett. **96**, 111111 (2010)
13. Yu, Z., Fan, S.: Nat. Photon. **3**, 91 (2009)
14. Serebryannikov, A.E.: Phys. Rev. B **80**, 155117 (2009)
15. Serebryannikov, A.E., Ozbay, E.: Opt. Express **17**, 13335 (2009)
16. Lu, M.H., Feng, L., Chen, Y.F.: Mater. Today **12**, 34 (2009)
17. Kushwaha et al. M.S.: Phys. Rev. Lett. **71**, 2022 (1993)
18. Martı´nez-Sala et al. R.: Nature (London) **378**, 241 (1995)
19. Lu, M.H., et al.: Nat. Mater. **6**, 744 (2007)
20. Feng, L., et al.: Phys. Rev. Lett. **96**, 014301 (2006)
21. Feng, L., et al.: Phy. Rev. **B72**, 033108 (2005)
22. Zhang, X.D., Liu, Z.Y.: Appl. Phys. Lett. **85**, 341 (2004)
23. Feng, L., et al.: Phys. Rev. B **73**, 193101 (2006)
24. Zhou, Y., et al.: Phys. Rev. Lett. **104**, 164301 (2010)
25. Liang, B., Yuan, B., Cheng, J.C.: Phys. Rev. Lett. **103**, 104301 (2009)
26. Liang, B., et al.: Nature Mater. **9**, 989 (2010)
27. Nesterenko, V.F., et al.: Phys. Rev. Lett. **95**, 158702 (2005)
28. Ruter, C.E., et al.: Nature Phys. **6**, 192 (2010)
29. See supplemental material at http://link.aps.org/supplemental/10.1103/PhysRevLett.106.084301 for detailed elucidation of the contribution of different diffraction modes to the one-way effect and influence of rotation angles and filling fraction on the tunability
30. Sun, J.H., Wu, T.T.: Phys. Rev. B **74**, 174305 (2006)
31. Huang, C.Y., Sun, J.H., Wu, T.T.: Appl. Phys. Lett. **97**, 031913 (2010)

Chapter 7
Energy Harvesting and Phononics

Abstract Energy can be harvested from the heat energy produced by phonon–phonon interaction. Acoustical metamaterial in the form of phononic crystal will be used in the structure of the system for energy harvesting. Here, one needs to design the phononic crystal structure. To enable this, one needs to design the phononic crystal system's dispersion relation and phonon–phonon interaction in the structure. A classical treatment using continuum medium is used. The thermoelectric efficiency is defined and its relation to the phononic crystal structure is described.

7.1 Introduction—Technological Application of Phononic Networks

The pursuit of a universal design framework to control the flow of phonons, photons and other vector/scalar waves through rational design of artificial structures affords an extremely interesting way to greatly further the reach of materials science and engineering. Phononic crystals and metamaterials have contributed greatly to the development of classes of interesting devices, such as super-resolution negative refractive lenses, broadband filters, supercouplers and even acoustical cloaks and sound insulation materials. The approach to the science of manipulating phonons should avoid potential pitfalls of adopting empirical design rules often arising from engineering constraints and instead concentrated on the fundamental symmetry principles to control phonon propagation behaviour. In this chapter, descriptions are made on the technological applications of phononics and energy harvesting. Here, we demonstrated the possibility of creating artificial structures with various unique band diagrams, from those having extremely large single complete spectral gaps, to those having multiple complete in-plane spectral gaps. Such structures offer unique opportunities for exploring the control of nonlinear wave propagation and wave interactions. In the dispersion relations in the linear phonon regime, it was noted the ability to create multiple frequency spectral gaps which also implied the ability to control the interactions between phonons of different frequencies, i.e. phonon–phonon interactions. While the phonon–phonon scattering process is inelastic and

W.S. Gan, *New Acoustics Based on Metamaterials*, Engineering Materials,
https://doi.org/10.1007/978-981-10-6376-3_7

often times nonlinear, the intrinsic material nonlinearities, which govern the phonon–phonon scattering processes, are embodied in the material constitutive relations and hence do not alter the fundamental continuity and flux equation starting points. Hence, even in the linear regime, the designed phononic structures offer a valid starting point as well as a framework on which to build on the development and understanding of these nonlinear processes. Some of the most promising applications that come to mind include (i) improving the ZT of thermoelectric materials by engineering the thermal conductivity to (ii) phononic crystals for breaking up the propagation of high-energy nonlinear pulses, such as shock waves and solitons. Here, some speculation and possible future directions for technological considerations for phononic structures are given.

Before embarking on the technology of energy harvesting, the following steps have to be studied:

1. Elastodynamics of Artificial Structure
2. Classification of Lattices: Physical Topology of Phononic Structures
3. Designing Dispersion Relation in Phononic Crystals, I. Avoid Crossings
4. Designing Dispersion Relation in Phononic Crystals, II. A Polychromatic Nonsymmorphic Phononic Crystals.

7.2 What Is Phononic Crystal?

The control and manipulation of acoustic/elastic waves is a fundamental problem with many potential applications, especially in the field of information and communication technologies. For instance, confinement, guiding and filtering phenomena at the scale of the wavelength are useful for signal processing, advanced nanoscale sensors and acousto-optic on-chip devices; acoustic metamaterials, working in particular in the sub-wavelength regime, can be used for efficient and broadband sound isolation as well as for imaging and super-resolution.

Phononic crystals, which are artificial materials constituted by a periodic repetition of inclusions in a matrix, are proposed to achieve these objectives via the possibility of engineering their band structures. The elastic properties, shape and arrangement of the scatterers modify strongly the propagation of the acoustic/elastic waves in the structure. The phononic band structure and dispersion curves can then be tailored with appropriate choices of materials, crystal lattices and topology of inclusions.

Similarly to any periodic structure, the propagation of acoustic waves in a phononic crystal is governed by the Bloch [1] or Floquet theorem from which one can derive the band structure in the corresponding Brillouin zone. The periodicity of the structures, which defines the Brillouin zone, may be in one (1D), two (2D) or three dimensions (3D). The propagation of acoustic waves in layered periodic materials or superlattices which are now being considered as 1D phononic crystals has been extensively studied [2] since the early paper of Rytov [3]. However, the

concept of phononic crystal was introduced only two decades ago in relation to 2D [4–6] and 3D [7] periodic media, especially to seek for the possibility of the so-called absolute band gaps [8–10]. Indeed, the dispersion curves exhibit band gaps in which the propagation of waves is prohibited. Such gaps may occur for particular directions of the wave vector, but they can also span the whole 2D or 3D Brillouin zone where the propagation of elastic waves becomes forbidden for any polarization and any incident angle. Then, the structure behaves like a perfect mirror for any incidence angle, thus prohibiting the transmission of sound waves.

The concept of phononic crystal followed by a few years the analogous concept of photonic crystals [11, 12] for the propagation of electromagnetic waves. The existence of band gaps is especially well known in solid state physics in the field of electronic band structure of crystalline materials. In particular, the properties of semiconductors, such as electronic, conduction and optical properties, are dominated by the band gap separating the valence and conduction bands, and, moreover, these properties can be drastically modified and tailored by introducing defects into the semiconductor due to the emergence of new states inside the band gaps (the so-called localized modes associated with the defects which have a decaying wave function far from the defect position). Similarly, the introduction of defects such as waveguides and cavities in phononic or photonic crystals is at the origin of many of their potential applications for confinement, guiding, filtering and multiplexing of acoustic waves at the level of the wavelength [10] and paves the way for the realization of advanced sensors and acousto-optic devices.

The progress in the field of phononic crystals goes in parallel with their photonic counterpart, although they involve a larger variety of materials as concerns the possibility of high contrast among the elastic properties, large acoustic absorption and the solid or fluid nature of the constituents. Since the band structure is scalable with the dimensions of the structure (as far as the linear elasticity theory applies), a great deal of works has been devoted to macroscopic structures in the range of sonic (kHz) and ultrasonic (MHz) frequencies where the proof of concepts of band gaps and manipulation of sound (such as wave guiding, confinement and sharp bending) has been established with simple demonstrators. Yet, there is a continuous interest in the engineering of band structures with new structures and materials as well as the technological fabrication of sub-micron scale structures working in the hypersonic (GHz) regime.

The general mechanism for the opening of a gap is based on the destructive interference of the scattered waves by the inclusions and therefore requires a high contrast between the elastic properties of the materials. In periodic structures, this is called the Bragg mechanism and the first band gap generally occurs at a frequency which is about a fraction of c/a, where c is a typical velocity of sound and a the period of the structure. However, when the propagating waves in the embedding medium are strongly scattered by the internal resonances of the individual inclusions, one may obtain a so-called hybridization gap which results from the coupling between the propagating waves of the matrix and the localized mode of the scatterers [13, 14]. Such a gap is less sensitive to the periodicity and can persist even in presence of some disorder in the structure [15, 16]. For common materials, it may

happen that both types of gaps arise in the same frequency range since the internal resonances of the inclusions would be of the order of c/d where d is the typical diameter or size of the inclusion. In such cases, the combination of the two effects can widen the actual band gap. It is also worthwhile mentioning the concept of locally resonant sonic materials (LRSM) introduced by Sheng et al. [17] which later developed into the field of acoustic metamaterials. In the latter work, the coating of hard inclusions by a very soft rubber produced a very low-frequency resonance gap situated two orders of magnitude below the Bragg gap, thus allowing the sound isolation below kHz by a sample with a thickness of a few centimetres only.

Point or linear defects [18] such as cavities or waveguides [19] can be introduced into the phononic crystal by removing or modifying one, a few or a row of inclusions. Depending on their geometries and constitutions, such defects can give rise to new modes inside the band gap of the phononic crystal that correspond to localized or evanescent waves with a decaying displacement field far from the defect [20–22]. Therefore, they can be used for confinement and guiding [23, 24] of the acoustic waves, and the coupling between a waveguide and cavities provides the possibility of filtering devices [10, 25, 26].

7.3 Elastodynamics of Artificial Structure

7.3.1 Introductory Remarks

The control of phonon propagation in artificial structures (AS) hinges heavily on the ratio of the length scale of the inhomogeneity of the medium, normalized to the wavelength of the propagating phonon under consideration. In general, one also has to consider the specific displacement field pattern, i.e. the eigenmodes; this later fact stems from vector nature of the phonon, that is, the elastic fields are vector in nature. It is quite interesting how much of this fact, once we consider artificial structures, even though, one has no issues with this in considering anisotropic bulk crystals. In fact, recognizing that the distinction between artificial crystals and bulk atomic crystals lies in the length scale of the inhomogeneity is extremely pertinent towards the development of the universal framework. It allows us to renormalize and map the viewpoints between the traditional bulk atomic crystals and the artificial structures. Many of the apparent differences or anomalies demonstrated in AS stem from not being able to access length scales not previously obtainable experimentally. Indeed, it has only been with the advent of nanotechnology that we are able to characterize artificial structures (AS) where the measurement precision and access to length scales match the length scale of fabricated structures. Thankfully, this finally allows for the development of a toolset where we are able to truly test designed AS. The connection of phononics, and its relation to classical acoustics, elasticity and mechanics lies in the length scales. The classical field theory of mechanics is used for the description of phonons and their propagation behaviour, in the guise of elastic waves in a continuum. It turns out that the classical–quantum transition for

phonons in media is at a much smaller length scale than we were aware of [27]. One notes that it is quite remarkable, as well as quite reassuring, that in the age of advanced multiscale computational tools and techniques, one may verify that the classical limit still holds even at very small scales, (nanostructures $\sim$ 10–100 nm). Hence, one needs to recognize the critical length scales involved and adopt the correct computational tools most suited at those length scales. In all of these cases, the crucial point is to always recognize the issue of length. In fact, the timelessness of classical continuum mechanics has manifested itself interestingly in recent work on phonon transport at the nanoscale. Examples of these include the experimental discovery of the role of flexural and interface modes on supported graphene [28]. While the interactions themselves may sometimes breach the quantum regime (e.g. at extremely low temperatures), in many of these cases, it is collective mode at the longer length scales that are quite rigorously predicted and accounted for in the classical field theories, that one is interested in. Hence, it is stated here outright that one is working in the classical limit, i.e. the frequencies and wavelengths which one deals with are much lower than the actual atomic/intrinsic optical phonon limit. The latter point is the defining feature of the nonclassical limit of phonons in materials, contrary to common misuse in the literature [29], where the classically confined slab modes were regarded as exhibiting quantum effects. One focuses on ways of moulding the flow of phonons at the length scales where one can design and then successfully fabricate, in order to directly verify with experimental measurements the theoretical predictions. Hence, one is bounded below by the $\sim$10 nm regime, this being set by current state-of-the-art reproducible top down fabrication methods. This incidentally lies in the regime where the phonons are technologically relevant, e.g. ultrasonic (MHz) and hypersonic (GHz). It is also quite interesting that even the control of phonons in such structures and materials in the linear regime eludes our complete comprehension. Here, a universal framework is developed in order to both design and control the phonon propagation behaviour in AS materials. A subset of these AS materials is also conventionally known as phononic crystals (PnC) [30], or metamaterials (MM) [31], depending on the length scales of the phonons propagating through the medium. This will be systematically elaborated as we build up the framework. Hence, one utilizes the well-developed classical field theories in mechanics, within a mathematical framework that one shall use to develop this field theory which turns out to be extremely useful and suitable for designing structures to control the propagation behaviour of phonons. This universal design framework will be used for designing phononic structures.

7.3.2 Fundamental Equations and Governing Principles

While using classical field theory, one wishes to remark that while extremely complete in its exposition, the roots were more algebraic, rather than geometric in nature. Hence, the solutions of various mechanical problems arrived at by researchers were more microscopic and dynamic in nature, as opposed to the

geometrical approach, in which the observation of invariants and conserved quantities of the entire systems would be pursued. The former approach would solve the problem at the microscopic level and hence demonstrate its evolution along a path. The latter approach while not pinpointing the actual path that the solution evolves along would elucidate all the possible paths that were amenable, as well as impossible. One seeks to combine both approaches and reconcile them, enabling us to be able to shift one's viewpoint when it is more illuminating to the problem solution. Part of the reason this universal framework was not previously developed is simply a question of the disjoint timelines of the two viewpoints. To illustrate these two viewpoints, the fundamental equations of elastodynamics are developed from both approaches. First, the classical discrete harmonic crystal is reprised, and the continuum limit is taken to obtain the conventional linear acoustic dispersion curves for a homogeneous solid, highlighting the conversion from the discrete regime to the classical regime. This is the microscopic approach. This is also the only place where one is able to explicitly state the limits in which one is allowed to work within the continuum framework. This model is elaborated to show how a phononic structure is often regarded as a "larger-scale" atomic crystal through a renormalization of the length scale which is examined. Here, the concept of length scales involved is illustrated when visualizing the relevant length scales between a bulk crystal, and that of a phononic crystal. One notes that one may effectively "discretizes" the phononic crystal to the length scale of the building blocks, that is our discrete length scale is given by a, the size of the unit cell. This is equivalent to considering only the first two symmetric (bands 2 and 4 in solid black), or first two anti-symmetric branches, if one only allows one degree of freedom in comparing with the one-dimensional building block systems. One sees that these two branches are effectively analogous to the diatomic classical chain, with the two components of the phononic crystal being the two "atoms" in the chain. This is exactly the cut-off length scale which one is talking about! By taking this into account, it is shown that the models can be mapped onto one another. The distinctions that exist between the atomic and artificial that are often misunderstood are then highlighted, which can lead to erroneous conclusions in the literature. This treatment leads to the concept of quasi-statics, locality and nonlocality, and this turns out to be one of the central themes of the design framework given here. Then, a complimentary viewpoint is then approached, which is more mathematical but at the same time quite physical in nature. The premise for this is the validity of being able to describe the elastic displacements as a continuous field, and this allows us to use the tools of field theory, i.e. one may treat the medium as a continuum. One starts from the perspective of the conservation equations, namely of continuity of mass and momentum flow [32], in developing the general equations of classical waves. This is in contrast to the typical way of inducing an equation of motion (E.O.M) based solely on the stress–strain relation from the starting elastostatics equilibrium viewpoint. Since the equations of motion are microscopic in nature, i.e. the wave propagates and is subject to certain requirements of continuity in the medium but omits critical information about the system, which is actually derivable from the conservation equations. The implications of the equivalency of these two viewpoints are then discussed, noting that the

latter viewpoint will still be valid, for example in the event of shock wave propagation for example, because of the nature of the physical induction of the equations. Another reason for utilizing the conservation equations is the connection, often utilized in theoretical physics, to broken symmetries in the systems, and hence to the allowed symmetries of the phonon modes in the system. This serves to motivate the following work where, starting from the viewpoint of conservation and broken symmetries, elastodynamics is included into the mathematical framework.

7.3.3 The Discrete to the Continuum: Taking Limits

A regular lattice with a single atomic building block is considered, i.e. a mono-atomic lattice, in N dimensions. In the discrete approach, the many-body potential energy is represented, with the ionic coordinates $V(q1, q2, \ldots, qn)$. Within the harmonic approximation, one may represent the deformations in the potential energy to only second order in the displacements, $ua(r)$, where a represents the spatial component and r represents the position of the ion being considered. One may hence write this potential energy function under small perturbations as:

$$\mathrm{V} = V^0 + \frac{1}{2}\sum_{r_{\propto,r'_\beta}} \frac{\partial^2}{\partial q_{r,\propto}\partial q_{r',\beta}} \mathrm{V}\, u_\propto(\mathbf{r})u_\beta(\mathbf{r}') + \mathrm{O}(U^3) \tag{7.1}$$

where q is the generalized coordinate of the system, r is equilibrium positional coordinate of ion, and u is displacement variable from equilibrium position r.

The full Hamiltonian is given by $H = T + V$

where

$$T = \sum_{r,\propto} \frac{p_\propto}{2m}(\boldsymbol{r})^2 \tag{7.2}$$

$p_\propto(\mathbf{r})$ = momentum

Because we are working with a lattice, the discrete translation symmetry, which implies the lack of a unique origin, shows that the potential energy function should only depend on the difference between the position vectors r and r' and also that this translational symmetry allows us to diagonalize the Hamiltonian using the Fourier modes (the translational symmetry implies that we may use the wave vectors as conserved number and hence Fourier modes), i.e. we may express the displacement as:

$$U_\propto(r) = \sum_{\boldsymbol{k},1\mathrm{st\,BZ}} \frac{\mathrm{e}^{ik.r}}{\sqrt{N}} U_\propto(\mathbf{k}) \tag{7.3}$$

This sum is only restricted to lie within the first Brillouin zone (BZ); this is due to the intrinsic discrete length scale restriction of the minimum wavelength of a propagating phonon to the first BZ edge (shortest wavelength possible for discrete lattice). The final Hamiltonian, diagonalized in terms of the Fourier modes, is given by

$$H = V^0 + \frac{1}{2}\sum_{\boldsymbol{k},\propto,\beta} \frac{/p_{\propto}(\boldsymbol{k})/^2}{m} + K_{\propto,\beta}(\mathbf{k})u_{\propto}(\mathbf{k})u_{\beta}(\mathbf{k}) \tag{7.4}$$

This is the Hamiltonian that represents a lattice occupied by a discrete ionic basis. The discrete nature of the lattice is represented by the form of the Fourier mode decomposition, with the displacement at each ionic position given by:

$$u_n = \int_{-\pi}^{\pi/2} \frac{\mathrm{d}k}{2\pi} \mathrm{e}^{-kna} u(k) \tag{7.5}$$

where a is the equilibrium lattice spacing, and n is the nth ion in the entire lattice.

Hence, in this microscopic Hamiltonian, one essentially tracks the oscillating positions of all the ions in the lattice, and one describes, up to second order only, the harmonic displacement of the lattice about each equilibrium ionic position. Because of the (discrete) translation symmetry, one may perform a diagonalization and rewrite the equation in the Fourier basis with the wave vector k, which is constrained to lie only within the first BZ. Because translational symmetry implies that the system is invariant to translations operations of the entire lattice, the natural space for the displacement lies in the Fourier, or the reciprocal wave vector space, hence the diagonalization into k-space. However, one notes that this group of transformations is only distinguishable up to the unit lattice vector. Physically, this just tells us that the discrete nature of the lattice only allows a wave, to possess a minimum wavelength of 2 lattice translations, with the unit cell size being half a wavelength, represented by two adjacent ions being exactly out of phase in their motions. This is all of course done with a mono-atomic lattice. The discrete nature of the lattice is thus markedly manifested near values of the wave vector at the BZ edges, where strong interactions with wavelengths on the order of the unit cell size occur. When can one utilize the continuum approximation? Away from the BZ edge, the wave vectors and hence, the associated wavelength of the propagating phonons typically span numerous unit cells and hence, at each atomic position, the displacement caused by the wave is incremental, with individual displacements satisfying

$$u_{\propto}(\mathbf{r}) << /r_{\propto}^{n} - r_{\propto}^{n'}/ \tag{7.6}$$

In addition, if we consider long wavelength (small k numbers), the displacements take place at a length scales $l = \frac{a}{\varepsilon}$, $0 < \varepsilon \ll 1$. where a is the unit cell dimension. Hence, the wavelength is much longer than an individual unit cell.

Finally, provided that this lattice is approximately uniform (i.e. low defect, isotope densities, etc.) and considering processes that occur at longer time scales (i.e. the fast microscopic fluctuations die out quickly), one will hence be able to coarse-grain the system and apply the continuum approximation to the discrete lattice. The essence of this is that one is then able to replace the discrete displacements of the ions in the lattice with a continuous displacement field. One now develops the continuum approach inducing the equations of motion from the Hamiltonian. By taking $\frac{\partial \boldsymbol{p}}{\partial t} = \frac{\partial H}{\partial \boldsymbol{q}'}$ this gives us, in the original discrete form:

$$\frac{nd^2}{\mathrm{d}t^2} u_{\propto}^{n} = -\sum_{n'} K_{\propto,\beta}(n-n') u_{\beta}^{n'} \tag{7.7}$$

where n and n' represent different ionic positions.

The continuum approximation allows us essentially to treat the displacement as a continuous field; hence, we may carry out a Taylor expansion of the displacement:

$$u_{\beta}(\mathbf{r}') = u_{\beta}(\mathrm{r}) + \sum_{\propto}(r'_{\propto} - r_{\propto})\nabla_{\propto} u_{\beta}(\mathbf{r}) + \frac{1}{2}\sum_{\propto,\Upsilon}(r_{\propto'} - r_{\propto})(r'_{\Upsilon} - r_{\Upsilon})\nabla_{\Upsilon}\nabla_{\propto} u_{\beta}(\mathbf{r}) \tag{7.8}$$

u is displacement, r is the coordinate in space.

Due to stability requirements of the lattice near equilibrium, only the quadratic terms remain; hence, we obtain finally

$$m\frac{\mathrm{d}^2}{\mathrm{d}t^2} u_{\propto} = \sum_{\propto,\beta,\Upsilon,\eta} C_{\propto,\beta,\Upsilon,\eta}\nabla_{\Upsilon}\nabla_{\Upsilon} u_{\beta} \tag{7.9}$$

where m is the relevant mass, here we assumed point mass, u, is the displacement, C is the elasticity tensor which is exactly the linearized form of the elastodynamic E.O.M for a continuous medium. This shows explicitly where the continuum approximation of the original many-body problem is valid, i.e. whenever one is able to treat the displacements of a propagating wave as a continuous field. Physically, this implies that despite the intrinsic many-body nature in most systems, that the emergent collective modes of propagation dominate the behaviour of the entire system. In most situations, the classical discrete transition limit, i.e. the situations where the quantum behaviour is dominant should be considered properly and is different in considering different situations. For phonons, this crossover is somewhere in the sub-10 nm regime; in all cases, one needs to consider the ratio of the various length scales present in the system, the intrinsic atomic length scale, the length scale of the propagation mode/wave which one is interested in and hence the length scales of the inhomogeneity that exists in the system that the wave may and may not see. Now, one shall work with the displacement existing as a continuous field in the medium, which one may consider also as a continuum. We note here

that the condition of being able to take limits from the discrete into the continuum only lies in the validity of representing the displacement as a continuous field. Subsequently, even when one considers artificial structures (AS), which are inhomogeneous, this fact does not change, because the length scale of those inhomogeneities is "macroscopic", compared to the intrinsic unit cell size; hence, the medium is still continuing for our purposes. Now, one utilizes the two viewpoints of elastic wave propagation in the continuum limit, the first which is microscopic and hence is evolutionary (with time) in nature, while the second is based on conservation principles and hence is more variational in nature. That two viewpoints are needed is crucial because it is only through the second viewpoint that one is able to induce the concept of broken symmetries and generalize the concept of polarizations, allowing us to treat the vector nature of the phonon subsequently.

7.3.4 *Evolution versus Conservation: The Microscopic E.O.M. versus the Variational Principle*

We start first with the microscopic E.O.M. This is typically derived from the equilibrium conditions, or of force balance of an infinitesimal element, where equilibrium requires:

$$\nabla_j \sigma_{ji} + X_i = \rho \frac{\partial^2}{\partial t^2} u_i \tag{7.10}$$

where X_i = external body forces, σ_{ij} = stress tensor component u_i = particle displacement. Subsequently, depending on the exact solid, we have to include extra information on the elasticity tensor of the particular solid. In the case of an homogeneous isotropic, linearly elastic medium, this is reduced to the familiar form:

$$(\lambda + \mu)\nabla[\nabla \cdot \mathbf{u}(\mathbf{r})] + \mu \nabla^2 \mathbf{u}(\mathbf{r}) + X = \rho \frac{\partial^2}{\partial t^2} \mathbf{u}(r) \tag{7.11}$$

This is the common vector displacement E.O.M, or more commonly known as the elastic wave equation. In this microscopic approach, we only consider the conditions of equilibrium on an infinitesimal element in the body. Physically, this is equivalent to regarding a propagating elastic wave as a very small perturbation travelling through every microscopic element and the subsequent motion at each position acts to restore the slight perturbation from equilibrium. There is no external or additional knowledge about the nature, and form of the propagating wave through the medium, which is what one is actually interested in. The subsequent Ansatz on the solution form, namely $\mathbf{u}(\mathbf{r}) \bullet e[i(k \bullet \mathbf{r} - \mathrm{wt})]$, seems more of an exercise based on experience rather than one induced from the form of the phenomenon at hand. In fact, why does this Ansatz even work? One knows that this takes the form of a wave equation (although given the original vector form, it might

be hard to guess initially.), but why would one choose such a form of the solution? Given say a large disturbance, such as a shock wave that propagates through the body, the assumptions underlying this E.O.M undoubtedly break down and we seem to need to formulate a new, probably nonlinear E.O.M to describe now shock wave propagation. How would one does this? What does the k in the Ansatz imply? The answers to these fundamental questions lie in the second approach, which stems from conservation and will form the philosophical backbone behind the development of our framework. One now demonstrates this and reconciles this with the previous microscopic approaches. Initially, consider the medium to be a homogeneous continuum (later one relaxes this assumption); hence, we can represent the displacement as a continuous field. Since one is interested in the propagating wave, one focuses on the wave. In such a system, one knows that in the absence of dissipation, energy is conserved due to continuous symmetry in time. Because the system possess continuous spatial symmetry (at the length scales which we consider), linear momentum is conserved. If the system is not rotating, angular momentum is also conserved. These conservation principles allow us to define an equation of continuity of some conserved quantity, $M(t)$, in some region of space Ω, with a boundary $\mathrm{d}\Omega$, and boundary gradient normal n can be stated as:

$$\frac{\mathrm{d}M(t)}{\mathrm{d}t} = R(t) + S(t) \tag{7.12}$$

$$M(t) = \int_{\Omega} \rho(\boldsymbol{r}, t)\mathrm{d}V \tag{7.13}$$

$$R(t) = \int_{\Omega} F(\boldsymbol{r}, t) \cdot n \,\mathrm{d}S \tag{7.14}$$

$$S(t) = \int_{\Omega} s(\boldsymbol{r}, t)\mathrm{d}v \tag{7.15}$$

F (r, t) represents the corresponding flux of the quantity and s (r, t) represents any source and sink in the region. This continuity equation, which tracks all the processes that conserve the quantity M (r, t), is valid even in the presence of shock waves [32], as long as the medium doesn't tear and hence introduce new discontinuities via cracks, etc. For elastic waves (and avoiding dealing with shock waves), one may deal with the differential form of the conservation laws and now, recalling that the system conserves energy (mass) and linear momentum yields two such equations of continuity:

$$\frac{\partial(\rho \boldsymbol{v})}{\partial t} + \nabla \cdot \boldsymbol{T} = 0 \tag{7.16}$$

$$\frac{\partial \rho}{\partial t} + \nabla \cdot (\rho \mathbf{v}) = 0 \tag{7.17}$$

T is the momentum stress tensor, p is the mass density, v is the relevant flux velocity. Here, we input our constitutive equations, which represent the behaviour of the particular material we are interested in, e.g. linear elasticity and the anisotropy of the elasticity tensor. In this approach, it is only the constitutive relations which we input into our conservation equations that need to change when we are dealing with different systems. The modifications into the wave equation only occur as a result of the constitutive relations. We further assume a linearly elastic, isotropic medium, which allows us to approximate the form of the stress tensor T, and if we assume that the mass density varies on length scales (L) longer than that of the wavelength of the propagating wave (X) and hence the wave does not sample any mass density inhomogeneity, we recover the elastic wave equation:

$$(\lambda + \mu)\nabla[\nabla \cdot \mathbf{u}(\mathbf{r})] + \mu \nabla^2 \mathbf{u}(\mathbf{r}) + X = \rho \frac{\partial^2}{\partial t^2} \mathbf{u}(r)$$

X are all the relevant external body forces, if any. Once again, this time without considering small microscopic displacements from equilibrium as before. This second formulation, which one calls geometric, presents a slightly different viewpoint. By treating the wave initially as a propagation of an initial disturbance throughout the medium, one can regard this through any region in space as a flow of some quantity; in our case, this is linear momentum. In general, one may treat this propagation as a continuity equation for momentum. The constitutive relation, which in this case is the linear elastic response of an isotropic, linear elastic solid, inputs the phenomenological or material response of the material to the propagating wave. This is where the main piece of the appropriate material physical response comes into play for the system. This could include nonlinearity, viscosity and other nontrivial complexities in material response. Explicitly, these features enter through the stress tensor term, T, of the momentum continuity equation. After inputting this constitutive relation into the continuity equation, one recovers back the elastic wave equation, verifying that given the linear elastic response a general propagating disturbance will fulfil the following wave equation, as represented by the vector elastic wave equation. One notes here in passing that this method of derivation acknowledges fully the role of momentum conservation in deriving the resultant wave equation, whereas the microscopic method bypasses this knowledge. But what else does this geometrical approach offer us, in terms of insights? Because the wave equation is derived from the conservation of linear momentum, the system possesses continuous spatial symmetry (again, at these length scales); this immediately tells us that once again, the normal mode decompositions should be taken in Fourier space, $\mathbf{u}(\mathbf{r}) \cdot ei(k \cdot \mathbf{r} - \mathrm{wt})$, where the wave vector k represents the natural space in which the eigensolutions of this wave equation lie. This can be regarded as normal mode decomposition of the solutions in terms of Fourier modes; hence, one can choose solutions to be "carried" by the $ei(k * \mathbf{r})$ forms, which are the said

natural coordinates. This is precisely why the normal modes take the following form of $\mathbf{u(r)} \cdot e(k \cdot \mathrm{r} - \mathrm{wt})$, where k takes on either a discrete set or continuous spectrum of values that depends on the actual spatial symmetry. So now, we have utilized two countering viewpoints to derive the same elastodynamic wave equation, with the second geometrical approach giving an additional insight through correct identification of the processes that lead to the formation of the wave equation. The latter approach also identifies the significance of k as the normal mode index and explains the rationale behind the well-known plane wave type solutions to the wave equation. However, one needs to extend these principles further in order to be able to understand how to treat the vector nature of the elastodynamics. Right now, this equation does not possess any extra information about the vector nature of the elastic waves, or the number of polarization degrees of freedom. One needs to now introduce the concept of polarization, working from the concept of broken symmetries of a continuous system. This framework of viewing polarization and hence the vector nature of the phonon field will be crucial towards our universal framework, which enables us to treat vector fields as readily as scalar fields.

7.3.5 *Broken Symmetry and Polarizations of the Vector Phonon*

From the discrete viewpoint, the polarization of a phonon arises from the fact that it is connected to other material building blocks/atoms by virtue of the requirements of stability and the dimensionality of the space and material. From the continuum viewpoint, the polarization of a phonon arises also from the requirements of stability and dimensionality as well, albeit from considering the relevant potential "energy" and considering possible stable solutions. In this latter case, there is no assumption on the details of the internal structure of the medium except for the fact that it is a mechanically and energetically stable continuous medium. Yet the connectivity requirement is intimately connected to the stability of the medium. How then does the dimensionality of the medium lead to the induction of the allowable polarization degrees in a structure? This is exactly related to the conservation equations and to the concept of the broken symmetries and finally, the extension of length scales once inhomogeneities are introduced into the system. To get an insight into the polarization of the vector fields, one has to consider the existence of phonons from another perspective, that from broken symmetry [33] and Goldstone modes. The polarization degrees of freedom are constrained by both the dimensionality of the space with which we are considering the problem as well as the general rigidity of the system. The former is clearly shown by simply constricting the motion to occur in N dimensions and gives the maximum permitted degrees of freedom. The second condition of rigidity, however, gives the final allowed degrees of polarization freedom permitted by considering the physics of the problem. One example of this is exemplified by the difference between a fluid and a solid. A typical fluid supports a single "polarization" mode, a scalar acoustic wave

formed from mass density fluctuations. In contrast, an elastic solid, that resists both shear, torque and compression, possesses three polarization modes, in general, in any direction. One now elaborates somewhat on polarizations, since one has identified them as one major challenge towards the control of the designing the dispersion relations of different phononic structures. In a homogeneous three dimensional continuous medium, it has been taken for granted that one derives these solutions to be the two transverse (shear and rotational, no dilation) and the longitudinal modes (only dilatational/compressional, but not shear). Typically, this is derived from the fact that every possible vector displacement field takes the form [34]:

$$U(r) = \nabla\emptyset + \nabla x\psi \tag{7.18}$$

ϕ = scalar potential, ψ = vector potential. These two potentials yield the respective longitudinal and transverse modes but do not provide much intuition for understand the resultant mode. One may choose instead, to consider the Hamiltonian which is given by:

$$H = \frac{1}{2}\int d^d x\left[\sum_a\left(\rho\frac{\partial u_\propto}{\partial t}\frac{\partial u_\propto}{\partial t}\right) + \sum_{\propto,\beta}\left(2\mu u_{\propto\beta}u_{\propto\beta} + \lambda u_{\propto\propto}u_{\beta\beta}\right)\right] \tag{7.19}$$

μ, λ are the Lamé coefficients. It is clear from the repeated summation that the resultant Hamiltonian is rotationally invariant, and hence, in Fourier space, our Hamiltonian now should only contain rotationally invariant quantities and takes the form:

$$H = \frac{1}{2}\int \frac{d^d}{(2\pi)^d}\mathrm{k}\left[\frac{\rho}{2}/\frac{\partial \boldsymbol{u}(\boldsymbol{k})}{\partial t}/^2 + \frac{\mu}{2}\boldsymbol{k}^2/\boldsymbol{u}(\boldsymbol{k})/^2 + \frac{\mu+\lambda}{2}(\boldsymbol{k}\cdot\boldsymbol{u}(\boldsymbol{k}))^2\right] \tag{7.20}$$

By decomposing this Hamiltonian, one can group the modes into those that are transverse (k perpendicular to u) and longitudinal (k parallel to u), with the transverse modes having a degeneracy of $(d - 1)$, where d is the dimensionality. Now one considers what governs the available polarization modes in a medium. This has to be done in steps. First of all, phonons are a simple form of Goldstone modes, which derive from breaking the continuous symmetry of the medium. One notes that earlier, it is mentioned that the continuous symmetry is what gives rise to the phonon modes, so is there contradiction? The distinction here is precisely the question of the length scale of "continuous" which one is considering! First the Goldstone mode. In a solid, bonds are formed, with the formation of a crystalline lattice breaking the continuous translational symmetry at all scales, replacing the system with discrete translational symmetry instead. This broken continuous symmetry leads to the Goldstone modes which are our phonons (long wavelength). One characteristic of Goldstone modes is that their wavelength goes to infinity (frequency w goes to zero) at zero wave vector. Each such broken symmetry will give rise to a maximum of one new mode, hence giving rise to condition 1. This is

for the Goldstone modes. At the length scales where one considers the medium to be a continuum (much larger scales), however, one has continuous spatial symmetry (continuous and homogeneous) and one has not contradicted ourselves. This is why the recognition of the correct length scales is very important in general. Now, one needs to extend this concept of broken symmetry further. That the longitudinal and transverse modes are the only eigenmodes is derived from the symmetry of the system, in this case the isotropic solid. Such a crystal is still rather symmetric. Of course, actual structures are never elastically isotropic; even the highest symmetry cubic crystals have an extra rigidity constant. Excellent treatments for the correct classification of different crystal elasticity constants are given in Nye [35] and Landau. The pertinent point here is that the polarization eigenstates of an elastic wave that exists in a structure depends on its underlying symmetry. To give an example, if instead of an isotropic medium, we have a medium which possesses spherical symmetry, the polarization eigenstates naturally need to obey the spherical symmetry. One of the eigenstates will possess spherical symmetry (depends only on /**r**/), with the other possible eigenstates depending on their dependence on the angular coordinates (Φ, Θ). These are commonly recognized as the radial-like "breathing", dipolar-like, and quadrupolar-like modes, with the exact polarization of a propagating phonon depending on its propagation direction taken with respect to the crystal symmetry. In other words, it represents the eigenmodes present in the crystal along the direction which it is propagating in. This is geometrically often taken as a normal projection along the relevant quadric but clearly this is exactly equivalent to the projection into the relevant sub-space of the basis of eigenmodes of the relevant structure/medium, which we call the irreducible representations (Irreps). One recognizes that bulk crystals have lower symmetry than the isotropic system, and hence break the symmetry of the original higher symmetry system. This leads to the formation of different polarization eigenstates, with different propagation velocities along different directions, depending on the symmetry of the new system, much like how that of a spherical symmetric system differs from those in an isotropic system. Hence, the polarization eigenstates are not always purely transverse or longitudinal; they are fundamentally the polarization eigenstates of the elastic waves, which depend on the particular symmetry of the system. One can be easily misled by the conventional use in bulk crystals typically described using orthogonal coordinates. Let us now restate the crucial point about what polarization is and how one should treat polarization. The polarization degrees of freedom depend on the dimensionality of the medium and the conventionally known transverse and longitudinal modes in a system are but a subset of the larger class of possible modes, known more correctly as the polarization eigenstates. The nature and form of these polarization eigenstates depends on the underlying symmetry of the medium; this is the most general and correct classification of polarization eigenstates. These inhomogeneities further break the original symmetry of the homogeneous system at various length scales. In both the bulk crystal and this AS case, one breaks symmetry from an initially higher symmetry case, yet, the dispersion relations turns out to be clearly different, with the latter becoming visibly more complex. What is the origin of this behaviour? This is where once again the

length scale comes into play. In the artificial structure, the symmetry is broken above some length scale once the phonon can sense the inhomogeneity. This causes changes in the nature of the wave vector k, as well as its associated allowable spectrum of values; all of this represents the breaking of the spatial symmetry. However, in both cases, it remains true that polarization states are derived with the only difference in the length scales present in the latter, due to the artificial structuring, or the nonlocality present in the medium. Stated physically, the inhomogeneity present in the AS leads to changes in the wave propagation behaviour beyond certain length scales. This leads to spatial dispersion and is commonly known as the nonlocality of the structure. Mathematically, nonlocality in this context implies that the response of the medium to a propagating wave (its group velocity, etc.) depends on the wave vector k explicitly. One easy example would be a diatomic crystal; its first indication of the nonlocality is at the length scale of the sub-lattice separation and manifests itself as the optical phonon branch! This realization clarifies that the polarization of each eigenmode in the medium, whether bulk or artificially structured, stems from the proper diagonalization into the relevant sub-spaces, dictated by the symmetry of the crystal. The subsequent complexity from the polarization fields is due purely to the interactions from the nonlocality of the structure. The nature of these interactions may of course differ, depending once again on their length scales, ranging from scattering ($\lambda/a < 1$) to interference ($\lambda/a > 1$). But once again, the complexity is due to the mechanics of the interactions present, but they are governed still by the global invariants and the symmetry of the medium.

7.3.6 *Concluding Remarks on Elastodynamics from a Symmetry Breaking Perspective*

One utilized two viewpoints, one the more conventional microscopic method, and the second method, more geometric in nature and based on conservation and symmetry. By utilizing conservation principles and reconciling them with the more conventional microscopic method, one is able to develop more insight into the nature of elastic wave propagation and relate it with the conservation of linear momentum. One then showed that the polarization degrees of freedom actually derive from the broken symmetries at the atomic scale, leading to the formation of gapless Goldstone modes in homogeneous media. However, in contrast to convention, polarization eigenstates are not always decomposable into the common transverse and longitudinal modes. This decomposition is only true for systems with orthogonal symmetry, e.g. cubic, orthorhombic systems. In general, the existence of polarization stems from the broken symmetry from an initial continuous system (at all length scales). The exact form of the polarization eigenstates, however, respects the details of the symmetry which the structure possesses; hence, it may be arbitrarily complicated depending on the symmetry of the homogeneous

medium. This situation does not change in considering AS, where purposeful inhomogeneity occurs at various length scales as desired. The polarization state still follows the symmetry of the AS and while the dispersion relations may be much more complicated, the governing principle for the polarization eigenstates remains the same. What the inhomogeneity changes though, is that it changes the permissible values and actual physical meaning of the wave vector k. Now that we have shown that despite the apparent complexity of the polarization states, exemplified in a typical band diagram of a phononic structure, that their underlying 60 classification and nature is isomorphic to that of a bulk crystal. This points a way forward towards being able to identify and classify the polarization eigenstates in various AS. While one now can place the polarization eigenstates within our framework of broken symmetry and conservation laws, the question still remains now as to how to control the polarization states in these phononic structures, in order to control the dispersion relation of these structures in a rational way. It is shown that the polarizations obey the explicit symmetries which are bestowed upon the structure which it propagates. One also realizes that the restrictions/constraints which the explicit symmetry places on the structure is absolute and actually offers a way with which one can manipulate the polarizations, and hence the dispersion relations of phononic structures. The relation here is not so clear presently and requires a discussion of the effects of nonlocality in the structure. The remarks on the importance of understanding and controlling the polarization state of the phonon will become clear as one demonstrates unique phonon propagation behaviour as well as record performance metrics in the designs. These will be achieved simply by utilizing the notion of the length scales and polarization to develop a transparent design framework that can dramatically improve one's control over $w(k)$.

7.4 Development of a Universal Design Framework: Mathematical Structure

7.4.1 Introductory Remarks

The previous section highlighted the elastodynamic equations governing the propagation of classical phonon in general inhomogeneous media. The vector nature of a classical phonon, propagating in an inhomogeneous medium (waveguide, resonator, crystal or metamaterial) makes it rather difficult to track microscopically. From an applied perspective, it is desirable to be able to obtain rules for designing a particular inhomogeneous medium, in order to obtain a desired propagation behaviour of a phonon to be able to develop novel and useful applications for phononics. Hence, understanding and control over the vector nature of the phonons is both scientifically interesting and desirable from an engineering perspective. The question thus becomes is one able to find general governing relations in order to control the vector fields that propagate through the AS? When mapped

the polarization states of the phonons for an artificial structure and that of a bulk crystal onto the same network, it can be shown that the difference in the two stemmed from the relevant length scales of the inhomogeneity in the medium; this has direct implications to the nonlocality (dependence on the wave vector and the material wavelength) of the medium, which controls the type of interaction causing the dispersion of the propagating phonons. The interaction due to this nonlocality in turn, are bounded by global invariants, via the symmetry of the artificial structure, in terms of the possibility of an interaction occurring. Hence, the ability to develop control over this dispersion relation would extend the capabilities beyond just, e.g. creating complete spectral gaps; we will also be able to induce bands that effect negative refraction, generate double negative index bands, and even perform hyperlensing. In fact, one aims to control the curvature and the placement, i.e. frequencies of each individual band, in principle allowing unparalleled control over the propagation velocities and dispersion of the possible eigenmodes within a structure. Ideally, one would not want to be limited to a pedagogical infinite bulk system, but also to be able to incorporate the boundaries, interfaces between different media as part of our entire design framework; indeed, we would like our design framework to be as general, practical and as unrestrictive as possible. This implies that one would need to have control over the presence (or absence) of eigenstates as well as the curvature and dispersion of individual bands. How can this be done? It has been remarked in the previous section hat the projection into the correct sub-space of the degrees of polarization freedom allows one to extract the eigenmodes of the system. Naturally, these eigenmodes then form an irreducible basis of that invariant sub-space. The crucial question here is what governs these sub-space projections? Because each new mode originates from a broken symmetry of the original system, the polarization state of each mode is controlled by the global symmetry which the structure possesses. Group theory poses global invariants on the explicit spatial symmetries which a particular phonon eigenmode may possess; it has to be explicitly an irreducible representation of the isotropy group of the wave vector. While one refers to excellent texts for a detailed and clear exposition into groups and representations, one notes here that the representation theory is isomorphic to the sub-space projection of the phonon eigenmodes which one has been mentioning and have explicitly demonstrated in previous section. This will be the approach here, i.e. one will use the mathematical machinery to map explicitly to the physical process of designing different phononic AS for different applications. In this section, one endeavours to develop a general design framework, to mould the dispersion relations of phononic structures by casting the fundamental linear elastodynamics governing the phonon propagation within a concrete mathematical framework. This mathematical framework allows one to extract the global possibilities of the types of interactions that may occur, that may lead, for example to the formation of a spectral gap. This framework also allows us to treat the often complicated polarization fields of phonons with a surprising transparency that automatically accounts for the vector or scalar nature of the field which one is interested in. Finally, one is also able to directly control the size and extent of desired interactions present in the system; indeed one will be able to show,

quite clearly what kind of features are exactly needed in a phononic structure, in order to obtain a desired phonon mode. One claims that these are the main ingredients which one needs in order to achieve an unprecedented level of control in designing the dispersion relations of phonons in these structures. While one will develop all the pieces of the framework in detail here, one next concisely highlight the various aspects of the mathematical framework which allows us to treat the vector nature of these fields in a transparent manner that treats both infinite, finite and (non)-periodic systems with the same footing. This framework consists of the following main ingredients: (i) The general interaction process leading to the formation of the spectral gap is the avoided crossing between bands having the same symmetries, (ii) The nonlocality principle, which illustrates the importance of the lattice in controlling the dispersion and dynamics of phonon propagation, (iii) The local principle, which utilizes a variational perspective to tie together the microscopic physical details of the phonon propagation and controls the eigenfrequency spectra at several k positions, (iv) The global principle which ties together all the global invariants of a structure and the related phonon dispersion The combinations of these four aspects of our framework are instrumental in controlling and augmenting the position and size of complete spectral gap formation in phononic structures, both infinite as well as finite. To be clear, there is no actual restriction on the extent and presence/absence of boundaries of the structure. In fact, although seemingly purely mathematical and somewhat abstract in nature, it will turn out that the irreducible representations imparted by the group on the eigenmodes actually control the interactions due to the nonlocality which is present in the structure. A more accurate statement is that the irreducible representation provides the character, or signature of the eigenmodes and the possible interactions between the various bands. For now, let us keep in mind that this global principle enforces global constraints on the allowed behaviour of the eigenmodes of the phononic structure. Before we delve more deeply into the global principles, we first motivate the interaction process that allows us to design a fundamental spectral gap and now examine the conditions for the occurrence of an avoided crossing.

7.4.2 Generalization of Avoided Crossings and Perturbation Theory

The generality of a framework requires one to also be able to microscopically control the energetic, or in this case, the exact modes and their positions in the band dispersion relations. This is quite important as while global constraints allow us to limit the possibilities that the phonon propagation may have, it does not allow us to create a particular functionality. In order to do this, one needs to deal with the microscopic, or the dynamics involved in designing the dispersion relation. In general, a phonon propagating through a structured medium involves encounters with various interfaces and subsequent multiple scattering events. In classical

systems, one envisions that this phonon remains a coherent wave (with no dissipation) at least to first order. In the previous section, one mentioned briefly that the polarization and hence, the eigenmodes of the phonons in an AS or bulk medium, depends on its underlying symmetries. One also showed, in the case of a one-dimensional phononic crystal, examples of eigenmodes and how they relate to the traditional concepts of transverse and longitudinal modes in bulk materials. Having established that the eigenmodes in an AS are determined by the underlying symmetries of the system, one now proceeds to examine the fundamental conditions that actually determine the formation of a spectral gap and hence the need for control of the eigenmodes. The phenomena of avoided crossings have been well known since the days of Zener and the early years of solid state physics with the theory of electrons and solid state band theory. However, the concept of an avoided crossing is quite general and can be traced back exactly to the study of the symmetry of the eigenmodes of the system and their behaviour in (w, k) space. One noted earlier that in a one-dimensional phononic crystal, the symmetries of the system resulted in the selection of two classes of eigenmodes which were (anti) symmetric with respect to the mirror plane along the direction of periodicity. One showed clearly that Bragg-type scattering at the BZ edges only occurred between pairs of modes which were (anti)symmetric, i.e. modes with the same symmetry. In fact, this Bragg-scattering mechanism, which is well known is precisely an example of an avoided crossing. Physically, this corresponds to the fact that degeneracy at the position where two eigenmodes meet or cross was not permitted by the symmetry of the system; hence, these bands interact and as a result form a spectral gap due to this interaction. An absolutely important point to note is that the underlying fundamental condition for the interaction to occur is that these two modes need to have the same behaviour with respect to the symmetry of the group which the AS possesses, i.e. they need to have the same irreducible representation. From a mathematical standpoint, the concept of avoided crossings and irreducible representations stem from the theory of representations as well as from group theory [36]. Here a physical intuition of an irreducible representation is developed. Let us consider now a system that has some symmetry in the two-dimensional X–Y plane and is invariant along the orthogonal Z-axis, i.e. the system possesses uniaxial symmetry. Hence, suppose one is describing say a general displacement in this system, we write it in the usual Cartesian coordinate as:

$$\mathrm{U} = \begin{bmatrix} u_x \\ u_y \\ u_z \end{bmatrix} = \begin{bmatrix} u_x \\ u_y \\ 0 \end{bmatrix} + \begin{bmatrix} 0 \\ 0 \\ u_z \end{bmatrix} = \mathrm{Irre}p_{xy} + \mathrm{Irre}p_z \tag{7.21}$$

We note that any symmetry operation of the group in the XY plane will only change $\mathrm{Irre}p_{xy}$, leaving $\mathrm{Irre}p_z$ invariant and likewise. For example, suppose we apply a rotation of 8 about the z-axis, in the XY plane, we get the following:

$$\hat{R}\mathrm{u} = \begin{bmatrix} \cos\theta & -\sin\theta & 0 \\ \sin\theta & \cos\theta & 0 \\ 0 & 0 & 1 \end{bmatrix} \begin{bmatrix} u_x \\ u_y \\ u_z \end{bmatrix} = \hat{R} \begin{bmatrix} u_x \\ u_y \\ 0 \end{bmatrix} + \begin{bmatrix} 0 \\ 0 \\ u_z \end{bmatrix} = \hat{R}\,\mathrm{Irre}\,P_{xy} + \mathrm{Irre}\,P_z \tag{7.22}$$

It is clear here that the rotation only affects Irrep_{xy} and the two sub-spaces as one has laid out here are orthogonal and do not interact with one another. This is a trivial example of the concept of an irreducible representation, i.e. it is basically the representation of a field variable, within the invariant sub-space it exists in. Hence, two eigenmodes which have the same irreducible representation exist in the same sub-space may interact, leading to the avoided crossings, whereas those with different irreducible representations simply cross each other in (w, k) space; this latter phenomenon is commonly denoted as an accidental degeneracy at the point of crossing. The whole point of identifying the symmetry of an AS lies exactly in retrieving the irreducible representations of each and every eigenmode of the band dispersion. This knowledge enables one then to predict and hence control where avoided crossings, and hence, spectral gap formation may occur. The physical problem can be viewed in a concrete mathematical framework where one may treat all physically distinct perturbations to the system, such as a change in the material components, the actual geometrical structure of the material, the inclusion of boundaries and interfaces with the exact same underlying mathematical framework.

Clearly, the exact polarization state of the eigenmodes is represented by their irreducible representations, which in turn depends on the symmetry of the system and very often, traditional concepts of longitudinal and transverse waves lose their exact meaning. One has to bear in mind that longitudinal and transverse modes originated from the original Lamé solution of elastic waves in an isotropic homogeneous medium; hence, they are eigenmodes of such a system, not of all systems.

By applying this concept of irreducible representations to such a classical problem, one finds that one is able to explain the behaviour of the band dispersions without tracing the k-evolution algebraically or microscopically. In fact, from an algebraic standpoint, the fact that this avoided crossing occurs may have itself been obscured. One chose to revisit this classical problem because of two factors, one that it has the simplest group, consisting of only the two element group $\{E, m\}$. Furthermore, it is a bounded system, i.e. has a finite dimension. These two factors help illustrate the generality of the approach of an avoided crossing, particularly in illustrating that one may treat the entire system, including both the bulk as well as the boundaries within the same system. At the same time, the low symmetry group of this particular system helps make the irreducible representations nearly trivial and tractable. One now wishes to do better and aim to induce multiple complete spectral gaps within this Lamb plate, not just a single spectral gap.

One recognizes here once again that the underlying principle behind the separation of the two sets of modes governing the dispersion in the original Lamb plate originated from the symmetry of the system. Hence, one physically enhances the interaction between bands by changing mathematically the character of the bands in

the dispersion, i.e. one is utilizing an underlying global principle of reducing all the irreducible representations to be only of the trivial identity representation. Physically, this amounts to controlling the interactions such that the only allowed eigenmodes obey the boundary conditions, which are anti-symmetric about the centre of the plate. We note there that while along *FX*, the only allowed irreducible representations are the trivial identity representations, this is not true at Γ.

One showed here, through the classical Lamb plate problem, that by correcting identifying the fundamental origins behind the eigenmodes of the system, that one is able to design quite novel changes to the system by altering the fundamental solutions themselves. In this particular instance, simply identifying the irreducible representations of the system and then subsequently reducing the symmetry of this system, one is able to create via anticrossings multiple spectral gaps into an otherwise homogeneous plate.

7.4.3 *Nonlocality: The Effect of the Lattice and its Interactions*

The eigenmodes of the AS, be it a phononic crystal or slab, must obey the discrete symmetries of the space/plane group of the crystal and only adopt the permitted irreducible representations which correspond to the isotropy group of the relevant wave vector [36]. This can be summarized as a consequence of the discrete symmetry invariance of the physical system and the adherence of the eigenmodes solutions to adopt the corresponding irreducible representations. From a less physical and more abstract perspective, the presence of a symmetry group that an AS possesses mathematically partitions, for a particular problem such as elastic wave, or electromagnetic wave propagation, the solutions into invariant and orthogonal sub-spaces; this is a consequence of Schur's second Lemma [38], which states that different irreducible representations are orthogonal. Avoided crossings may be said to be meso-scale as well as nonlocal. It occurs at all length scales, i.e. the process is meso-scale as we have made no approximations in the calculation of the spatial dispersion. Our pedagogical examples have demonstrated the same phenomenon from the simplest possible finite system, to an infinite lattice; in both cases, the avoided crossing was clearly identified to occur due to the irreducible representations. It is also nonlocal, i.e. its behaviour depends on the wave vector vis-a-vis the relevant isotropy groups and the formation of spectral gaps in finite plates and infinite phononic crystals are treated on the same footing. Hence, it automatically incorporates the nonlocality in the system, if present. It acknowledges all the forms of symmetries that will lead to interaction, regardless of the length scale, the specific type of symmetries, translational, point or time reversal, etc. Physically we understand that the strength of the spatial dispersion depends strongly on the nonlocality of the medium to the wave propagation; i.e. $E(k, w)$, where E is the response function of interest. This spatial dispersion is in turn

inherently linked to the interaction length scales between the wave, and the geometrical structures of the medium. For example, a linear dispersion relation implies that the medium is interacting with the wave independently of the length scales involved. At the other extreme, when the dispersion relation becomes independent of the wavelength, this implies that the wave is spatially localized, and has flat or zero dispersion. This is the extreme case of dispersion whereby any form of propagating extended state is not supported. Bands in the system typically lie between these two extremes and it seems an intractable task to be able to control how much dispersion occurs in a general system that has dimension $n > 1$. Analytically, one might apply perturbation theory to specific points where the interaction has occurred and hope to be able to capture the subsequent dispersion which occurs; this becomes a question of keeping the correct terms in the perturbation of the system [39]. The crucial question for one to actually ask is then, what is causing the perturbation in some general position in k-space? The answer to this lies in the symmetry of the bands because the symmetries must persist across multiple length scales (e.g. an entire band) and automatically keeps track of all the interactions, automatically manifesting itself through the final calculation. As we alluded to earlier, the occurrence of an interaction or avoided crossing depends on the irreducible representations.

By applying this concept of irreducible representations to such a classical problem, one finds that one is able to explain the behaviour of the band dispersions without tracing the k-evolution algebraically or microscopically. In fact, from an algebraic standpoint, the fact that this avoided crossing occurs may have itself been obscured. One chose to revisit this classical problem because of two factors, one that it has the simplest group, consisting of only the two element group $\{E, m\}$. Furthermore, it is a bounded system, i.e. it has a finite dimension. These two factors help illustrate the generality of the approach of an avoided crossing, particularly in illustrating that one may treat the entire system, including both the bulk as well as the boundaries within the same system. At the same time, the low symmetry group of this particular system helps make the irreducible representations nearly trivial and tractable. One now wishes to do better and aim to induce multiple complete spectral gaps within this Lamb plate, not just a single spectral gap. One notices that none of the bands in this structure ever cross, i.e. all the bands have undergone avoided crossings. This is incidentally the first demonstration of multiple spectral gaps in a structured slab, yet the underlying principle behind this design is exceedingly simple and quite amenable to fabrication. By recognizing that the original Lamb plate possessed two orthogonal sets of solutions, one now proceeds to reduce the irreducible representations to a single one along the—X direction, that of only the trivial identity, i.e. one removes the mirror plane in the original Lamb plate. This structuring of the two boundaries explicitly breaks the mirror symmetry, resulting in only one class of solutions remaining for the eigenmodes. Clearly, both these modes do not possess any mirror (anti)symmetry, both modes have the identity (trivial) irreducible representation hence avoided crossing occurs between them.

One recognizes here once again that the underlying principle behind the separation of the two sets of modes governing the dispersion in the original Lamb plate originated from the symmetry of the system. Hence, one physically enhances the interaction between bands by changing mathematically the character of the bands in the dispersion, i.e. one is utilizing an underlying global principle of reducing all the irreducible representations to be only of the trivial identity representation. Physically, this amounts to controlling the interactions such that the only allowed eigenmodes obey the boundary conditions, which are anti-symmetric about the centre of the plate. One notes there that while along *FX*, the only allowed irreducible representations are the trivial identity representations, this is not true at *r*. One showed here, through the classical Lamb plate problem, that by correctly identifying the fundamental origins behind the eigenmodes of the system, that one is able to design quite novel changes to the system by altering the fundamental solutions themselves. In this particular instance, simply identifying the irreducible representations of the system and then subsequently reducing the symmetry of this system, one was able to create via anticrossings multiple spectral gaps into an otherwise homogeneous plate.

7.4.4 Nonlocality: The Effect of the Lattice and its Interactions

The eigenmodes of the AS, be it a phononic crystal or slab, must obey the discrete symmetries of the space/plane group of the crystal and only adopt the permitted irreducible representations which correspond to the isotropy group of the relevant wave vector [37]. This can be summarized as a consequence of the discrete symmetry invariance of the physical system and the adherence of the eigenmodes solutions to adopt the corresponding irreducible representations. From a less physical and more abstract perspective, the presence of a symmetry group that an AS possesses mathematically partitions, for a particular problem such as elastic wave, or electromagnetic wave propagation, the solutions into invariant and orthogonal sub-spaces; this is a consequence of Schur's second Lemma [38], which states that different irreducible representations are orthogonal. Avoided crossings may be said to be meso-scale as well as nonlocal. It occurs at all length scales, i.e. the process is meso-scale as one has made no approximations in the calculation of the spatial dispersion. The pedagogical examples have demonstrated the same phenomenon from the simplest possible finite system, to an infinite lattice; in both cases, the avoided crossing was clearly identified to occur due to the irreducible representations. It is also nonlocal, i.e. its behaviour depends on the wave vector vis-a-vis the relevant isotropy groups and the formation of spectral gaps in finite plates and infinite phononic crystals are treated on the same footing. Hence, it automatically incorporates the nonlocality in the system, if present. It acknowledges all the forms of symmetries that will lead to interaction, regardless of the length

scale, the specific type of symmetries, translational, point or time reversal, etc. Physically one understands that the strength of the spatial dispersion depends strongly on the nonlocality of the medium to the wave propagation; i.e. $E(k, w)$, where E is the response function of interest. This spatial dispersion is in turn inherently linked to the interaction length scales between the wave, and the geometrical structures of the medium. For example, a linear dispersion relation implies that the medium is interacting with the wave independently of the length scales involved. At the other extreme, when the dispersion relation becomes independent of the wavelength, this implies that the wave is spatially localized, and has flat or zero dispersion. This is the extreme case of dispersion whereby any form of propagating extended state is not supported. Bands in the system typically lie between these two extremes and it seems an intractable task to be able to control how much dispersion occurs in a general system that has dimension $n > 1$. Analytically, one might apply perturbation theory to specific points where the interaction has occurred and hope to be able to capture the subsequent dispersion which occurs; this becomes a question of keeping the correct terms in the perturbation of the system [5]. The crucial question for one to actually ask is then, what is causing the perturbation in some general position in k-space? The answer to this lies in the symmetry of the bands because the symmetries must persist across multiple length scales (e.g. an entire band) and automatically keeps track of all the interactions, automatically manifesting itself through the final calculation.

As one alluded to earlier, the occurrence of an interaction or avoided crossing depends on the irreducible representations; this already implies the nonlocality of the propagation behaviour in the medium. In fact, it is actually the degree of nonlocality that is affected by the geometry and the contrast between the material constants of the different constituents. The nonlocality in the medium is extremely important because it influences the strength of the interactions between bands, and therefore naturally controls the group velocity along the bands, i.e. the curvature and dispersion of the bands. This latter fact has been often overlooked. Indeed, in the pioneering work of the locally resonant sonic (LSR) crystal [31], the nonlocality of the medium was not mentioned, primarily due to the focus by the authors on large elastic contrast between the constituents employed, which made the structure behave in the weakly nonlocal limit. In Liu's work, the originality arises from the "local" nature of the spectral gap opening mechanism, which was distinct from the common Bragg-type mechanism. However, in actuality, both mechanisms for gap formation are strictly avoided crossings, albeit at different k vectors and the presence of the lattice itself implied that the mechanism was not local, but only weakly nonlocal. The point which one wishes to emphasize here is that the mechanism of spectral gap opening is strictly nonlocal in the presence of the lattice. It is the degree of nonlocality which is affected by specific material choices. One next shows, through a series of very simple models, the clear influence of the lattice on the dispersion relations by utilizing the same building block and then introducing nonlocality via tuning of only one of the material phases. In all of these lattices, one retains the material choices of the solid scatterer ($E = 40$ GPa, $v = 0.3$, $p = 4000$ kg m^{-3}) and the matrix ($E = 4$ GPa, $v = 0.17$, $p = 1300$ kg m^{-3}), and

vary only the connecting—phase. One notes here that one has continuously tuned the LRS structure, from a classical phononic crystal into a resonant LRS by tuning only one of the material phases (i.e., 1). One minor point of note is that even in (d), our 1-phase is still three orders of magnitude stiffer than that in the original work [31], yet it has reproduced the same qualitative band structure. Hence, the perceived "local" mechanism was actually a result of the strength of a material perturbation on the nonlocality and not a distinct mechanism by itself. In fact, one may notice that the very statement of a local mechanism is wrong, since the avoided crossing has occurred at nonzero wave vector. Furthermore, by examining the eigenmodes, one recognizes that the irreducible representations of the bands are different, as the isotropy groups are also different. The irreducible representations of the eigenmodes once again emphasize the nonlocal nature of the spectral gap openings.

7.4.5 *Local Principles: The Variational Principle from a Geometric Viewpoint*

One has shown that one is able to control the extent of nonlocality both through a choice of materials, and the symmetries governing the system vis-a-vis avoided crossings. These principles have thus far been global in nature, i.e. they apply to all structures that fulfil a particular choice of space or plane group symmetry. One has utilized the materials choices to only tune the extent of the nonlocality, but not (i) the strength of the interactions in the spectral gap, (ii) the positions of the bands, i.e. their eigenfrequencies and (iii) the evolution of the bands across k-space. In the design of a phononic crystal, one usually considers the scattering strength of the scattering phase, the mechanical contrasts between the different material phases and the fill fraction. However, these design factors neither recognize the actual role of avoided crossings nor the lattice (nonlocality), which one has shown to be crucial for spectral gap formation. For example, while sub-wavelength and Bragg gaps are readily identified to originate from avoided crossings in our network, this underlying similarity is not so clear from the microscopic viewpoints of resonant tunnelling or Bragg scattering, respectively. Furthermore, these two microscopic mechanisms are strictly tractable only in isolated or simpler systems or lower dimensionality, i.e. structures with no long range order (resonant tunnelling) or simple one-dimensional lattices (Bragg scattering). There is a need as well for developing a general principle that governs the eigenfrequency distribution and hence the ability to treat the energetics involved in scattering and in tunnelling

equivalently. The variational perspective provides a natural approach with regard to the symmetries of the eigenmodes and their eigenfrequencies. In fact, most equations of motion can be converted into a variational form, in a method analogous to how we converted an E.O.M in a conservation equation in Sect. 7.3. The fundamental governing idea is that in the variational method, one formulates a relevant energy functional, $E\{u(r, t), u_t(r, t), u_r(r, t), r, t\}$, before projecting out each eigenmode, $/u_\lambda >$ and its eigenfrequency, λ. A simple example of this is to examine a freely vibrating acoustic sphere. The eigenmodes, in ascending order of eigenfrequencies, are the fully radial breathing mode, followed by an m-fold degenerate set of dipolar modes, etc. From a physical perspective, one may recognize that the eigenfrequencies increase with the number of nodes in the eigenmode profiles. This is linked to the exact form of the energy functional, which contains first-order spatial derivatives in the displacements; hence, the presence of increasing number of nodes increases the energies and hence the associated eigenfrequencies. While simplistic, this example of an acoustic sphere is actually quite representative of the variational method and the subsequent eigenmodes which it yields. One next illustrates this design principle and focuses on developing physical intuition. One first discusses the issue of design of the geometric structure in order to optimize a particular avoided crossing interaction.

By considering the problem from a variational perspective, one accounts simultaneously for all the microscopic processes that lead to the final evolution of the eigenfrequencies and all that one has to focus on is the eigenfrequency placement of each mode by considering the terms in the strain energy functional and the allowed irreducible representations in each k direction.

The above discussion demonstrated how one would apply variational principles based on the symmetry of the system; it turned out that this particular geometrical optimization process is equivalent to enhancing the Bragg-scattering process (in a phononic structure) to increase the size of the spectral gap. Our final principle is that of the global principle of utilizing group theory and the theory of representations [36]. While the concept of irreducible representations has been utilized in all our discussions and one did motivate the concept of irreducible representations from a simple uniaxial system, one did not address their relation to the entire band structure and dependence on the particular choice of the plane/space group. The choice of the global symmetry dictates the possibilities and bounds possible for a band structure; this will be the final development we shall undertake here The variational method, together with the avoided crossing, covers most possibilities for designing most of the major features in band structure, such as the formation of a spectral gap, one of the main interests in the phononics community. By complementing these local principles with the global symmetry principle, which governs the evolution of the dispersion bands in momentum space, one will be able to truly mould the dispersion relations to create the desired propagation behaviour, or spectral gap.

7.4.6 *Groups and Representations: Nonsymmorphicity and Wyckoff Positioning*

One now discusses the global design principle, which pertains to the group symmetry and its representations. Group symmetry is global because it controls the likelihood for interactions (avoided crossings) and determines the character of each eigenmode vis-a-vis their irreducible representations [36, 38]. Unfortunately, it has been used mainly as an analysis tool [36] and not so much as a design principle; in reality the two are equivalent, merely reversed in causality. It is no surprise then that group theory may be used as the underlying foundation as well as the language for our generalized design framework. In this section, we focus on two uncommon facts in group theory in its applications to solid state physics: (1) the concept of factor groups in plane groups, and specifically, the dressing of Wyckoff positions to modify the band structure of phononic metamaterials, and (2) the global properties of nonsymmorphic groups and specifically, the special property that they impart band sticking along certain directions along BZ boundaries/edges.

7.4.6.1 Translation Subgroups and Wyckoff Positions

It has been commonly conjectured that large optimal spectral gaps will be favoured in structures possessing the smallest irreducible Brillouin zones (IRBZ). The reasoning behind this was a direct extension of Bragg scattering from one dimension to greater than one dimension. This usually implied high symmetry plane groups, such as hexagonal plane groups (p6mm) as candidate space groups. However, this needs not be the case, and recent works have suggested that certain lower symmetry plane groups, such as a honeycomb-like lattice with a two-'atom' basis (p3m1) has a slightly larger spectral gap than the corresponding parent p6mm lattice. This discord originates from a lack of understanding of what the symmetries of a plane group actually impart upon an artificial structure (AS). The AS structures, chosen with a certain plane/space group may be regarded as having broken the symmetry from an initial structure which is isotropic at all length scales. Naturally, these eigenmodes, which reflect this broken symmetry, necessarily adopts the irreducible representations that result from this lower symmetry plane group. This is exactly analogous to how transverse and longitudinal modes are borne out of an elastically isotropic and homogeneous medium. Mathematically, when one says that an AS possesses a certain symmetry group, it implies that all functions (susceptibilities, fields such as displacements, etc.), have to conform to this set of symmetry operations. To summarize, the symmetry group which the AS possesses, be it spatial, spatiotemporal, or others, controls the nature of the eigenmodes, especially their vector polarization states vis-a-vis the irreducible representations. All forms of interactions, propagations and motions in the AS are governed by the symmetry group; the most classical examples of these include the selection rules in Raman and Brillouin inelastic scattering. Now one makes the explicit connection between

our earlier use of irreducible representations concretely from its induction from broken symmetry and an explicit space group. As the irreducible representations govern the vector polarization states of each eigenmodes, they also determine the absence/presence of avoided crossings which are crucial in spectral gap formation. Avoided crossings are only allowed between eigenmodes with identical irreducible representations. One also understands that along with a particular direction in k-space, the irreducible representations are determined by the isotropy group and not the entire point symmetry group. One now proceeds to develop the role of point group symmetry in controlling the band structure. One reminds that a plane or space group is actually an infinite (countable) group, because the translation operations are infinite. For symmorphic groups, i.e. groups that do not possess glide lines (in 2D) or glide planes or screw axes (in 3D) as primary group generators, the group of translations is actually a normal subgroup of the entire plane/space group. This implies that one only needs to deal with the relevant factor group, given by:

$$F = G/H \tag{7.23}$$

G is entire symmetry group, H is the translation subgroup, F is commonly known as the Factor Group/Quotient Group.

One outlined here the mathematical framework of group theory, which established the global principles governing the possibilities of the band dispersion relation. In addition, representation theory of the groups allowed the classification of eigenmodes into their irreducible representations. By identifying all spectral gap opening processes as avoided crossings and adopting a variational like approach, we are able to rationally control and design various features of the band structure. Most notably, one is able to augment spectral gaps and generalize various design principles within the same framework, utilizing the language of symmetry and conservation. One next discusses the actual dynamics of phonon propagation in these AS, which deals with the actual propagation behaviour of phonons in these AS. It will turn out that the dynamics of phonon propagation actually address the question of matching the optimal physical topology of a structure, as well as choice of materials, etc., for a particular phononic application.

7.4.7 Classifications of Lattices: Physical Topology of Phononic Structures

7.4.7.1 Introductory Remarks

We examine the unanswered question of the choice of the physical topology of a phononic structure to achieve desired phonon propagation properties. To date, there is no framework which is general, i.e. does not rely on some specific geometry of the scatterers within the artificial structure (AS), and is capable of treating different types of fields, both vector (electromagnetic, elastic, etc.) and scalar (acoustic) in a

coherent fashion. Current approaches suffer from their specificity to certain types of geometrical structures, either due to some particular choice of calculation methods [30], or utilizing physical models which are not transitive between fields possessing different polarization degrees of freedom. In general, one might consider the contrast in elastic constants, mass density, longitudinal and transverse velocities as possible parameters for controlling the size of the spectral gaps. However, there is neither a clear trend nor rational principle guiding the theoretical works, often leading to frustrations in attempting to elucidate a coherent principle to guide selection of the optimal topology for a particular structure for phononics, photonics or any wave in general. We argue here that this is due to several reasons. First of all, not all the above-mentioned parameters are independent; velocities are, strictly speaking, deduced values from the set of elastic constants and only hold for "homogeneous" media or for the inhomogeneous system in the geometric (short wavelength) limit. In isotropic media (at continuum length scales), the two independent elastic constants, along with the mass density determine the longitudinal and transverse velocities and this is only strictly true in the homogeneous limit or geometric limit for inhomogeneous systems (within each of the homogeneous component materials). In considering phonon propagation at length scales where the phonon wavelengths are on the order of the structure or the material inhomogeneity, one needs to recognize that wave velocities are highly dependent on the details of the AS. The homogeneous phonon velocities are physically meaningful only for two situations:(1) in the long wavelength limit ($X \gg a$) where the phonon samples no perturbation in the structure, or (2) in the geometrical limit ($X \ll a$) where the wavelength of the phonon is so short that one may physically consider it as a particle and hence one may associate a "particle" velocity with it within each homogeneous phase. At the intermediate length scales ($X \sim a$), commonly known as the scattering/diffraction regime, which is of primary interest, one needs to consider not just the velocity, elastic constants or mass densities separately, but instead the generalized energy flux at any interface, together with its physical wavelength, which depends on the local refractive index. In this situation, the detailed structure becomes crucial, due to proximity in the length scales between the phonon wavelength and the structure! Recalling that one may deduce the relevant wave equation from the original momentum continuity equation, the conservation of linear momentum is assured for all length scales. This is the motivation for insisting on utilizing the conservation as the starting point of our discussion and development of the design framework. One now shows that doing so makes the final developments to the framework totally transparent. In a linearly isotropic solid, the 3 elastic constants (two Lamé coefficients with twofold degeneracy in the shear component) lead in general to 3 Goldstone modes and hence three polarizational degrees of freedom. The flux of phonons through a region depends on their nature, i.e. the vector and scalar nature of the fields lead to disparate behaviour in their propagation and it is this distinction that holds the starting point for elucidating the underlying design principles governing the choice of the optimal physical topology for phononic and acoustic structures! It will turn out that by only considering the "dynamic impedance" at an interface between two media, one is able to develop a

concept of a "dynamical mechanical bond" to classify the nature of phonon propagation in various AS comprised of different materials in a general fashion. This leads to a classification scheme for phononic structures based on the spatial extent or degree of spatial (de)localization of the phonon eigenmodes. Structures are subsequently grouped between two bounding lattice classes, depending on the mechanical bond type. One will refer to these as the extended and tight-binding lattice (TBL) classes. This lattice class classification allows one to select target structure designs that achieve different phononic properties, from large spectral gaps, negative refraction bands with both isotropic and superprism type effects. In particular, we shall demonstrate large complete spectral gaps, indeed the largest ever reported in the literature, in both classes of structures as well as controllably induce negative refraction bands which are polarization specific. To be "complete", one examines the typical solid-solid AS lattice classes before one deals with the solid-air AS lattice class, which is advantageous due to fabrication considerations. Despite a critical difference between the two types of structures (solid–solid vs. solid–air/vacuum), the classification still holds true under an appropriate transformation. For the rest of the section, one develops some structures possessing various unique phononic properties. The necessary criteria for achieving various properties are discussed for various constraints on materials choice, and the particular type of application. Finally, one chooses to demonstrate this with two distinct phononic AS, belonging, approximately speaking, to the two ends of our lattice classification spectrum. One modifies these structures in an entirely coherent way, utilizing only the fundamental tools and framework which one has built up over the previous few sections to show that indeed, this method of classification and framework developed enables an entirely rational method of designing a phononic structure.

7.4.7.2 The Dynamical Mechanical Bond

One emphasized the role which the normalized wavelength ratio (X/a) plays in understanding phonon propagation. One has mentioned geometric and material inhomogeneity, the former deals with the situation that the structure plays a role vis-a-vis the boundaries; the latter is the more familiar case which we shall discuss shortly. The former, one has earlier mentioned is of second order importance as it deals with the exact geometry of scatterers in optimizing a specific functionality. There are, however, intrinsic characteristics inherited by the phonon transport with certain topological features of the phases. This naturally leads to the concept of the matrix and the scatterer phase. One differs here from the ad hoc usage of the network vs cermet topology for the following reasons. This analogy was borrowed from the earlier photonic crystals work where one phase is always air; hence, there is no ambiguity present in defining the nonair phase as either a disconnected (cermet) or connected (network) phase. In the case of phononic crystals though, there is no standard reference material phase, where the velocity is highest (as in light/vacuum–air); hence, the naming of a cermet or network phase is further convolved by assumptions about the "scattering" abilities of each material phase.

Using this new methodology of naming, the cermet and the network topology is classified according to the impedance contrast between the matrix and the disconnected phase, with the definition of the two components only dependent on the physical topography of the phases, and not their constituent material properties. This separates the actual physical network topography from the intrinsic material parameters, which is a crucial distinction because in this situation; we do not make any a priori distinction on the type of transport based on the intrinsic material parameters alone because the actual problem involves considering both the physical topography and the material impedance contrasts before the dominant mechanism of phonon transport can be deduced, vis-a-vis the mechanical bond. Hence, this method prevents one from making any invalid assumptions on phonon transport before trying to proceed to create optimal phononic structures for certain types of propagation behaviour. In fact, this methodology and approach greatly extends the framework for choosing an optimal physical topography for a particular phononic structure for desired transport properties and is not limited to just spectral gaps, but is appropriate more for properties such as negative refraction or slow modes, i.e. all aspects of phonon transport. The fundamental framework which one developed emphasized the need to recognize the correct length scales and the role of nonlocality of the eigenmodes that result from either the symmetry of the structural design and from material choices. Now we address the complementary problem, that is, how does the physical topography of the structure affect its dispersion relations? Previous works have focused attention onto the choice of topographies that favoured the appearance of complete spectral gaps [41]. However, from the concepts developed of avoided crossing as the primary underlying mechanism for creating spectral gaps, as well as the relations between the space/plane group symmetries and the probabilities of optimizing a complete gap, it suggests that one would be able to create complete spectral gaps in structures with different topographies, both cermet and network type While this is indeed the case, the physical topography choice for the structure possesses a tremendously more fundamental significance. It controls the dynamics of phonon propagation, i.e. the actual propagation and group velocities of the eigenmodes. This has tremendous importance in determining the optimal lattice classes for phonon propagation, such as negative refraction and slow modes.

In previous works, the physical topography of the structure was only considered in dealing with the possibilities of opening a complete spectral gap, i.e. only within a specific normalized frequency range, which one associates readily with either the Bragg-scattering regime or the resonant tunnelling regime. This viewpoint suffers from several drawbacks, including the (now clarified) point that observed gap sizes are not necessary correlated with the particular bands bounding them and indeed may have nothing very much to do with those hypothesized scattering mechanisms supposedly accounting for the presence of the gaps! Physical topography of the structure affects the propagation behaviour at all length scales. It is the length scale, i.e. the wavelength of the phonon with respect to the physical structure that determines the scattering (type), and hence propagation behaviour of the phonon in the different regimes. This implies that the eigenmodes of the phonon at some wave

vector k, takes on different displacement profiles with different frequencies. This displacement profile, or eigenvector, depends on the choice of the physical topography vis-a-vis the actual material constants and the physical geometrical interfaces and boundary/interface conditions, i.e. both the material and the geometrical structure. This eigenvector physically represents the trajectory of the phonon at some (w, k) within each unit cell; this is clear if we consider this from a variational viewpoint, where each eigenvector can be mapped to an irreducible representation that physically represents the trajectory of a phonon through each unit cell, showing how the energy propagates through the structure. The eigenvector represents the dynamics of the phonon propagation that is manifested through the slopes (linearized group velocity) and the curvature of the bands (group velocity dispersion). The variational viewpoint develops the physical concept of our dynamical mechanical bond, by considering the spatial (de)localization of the profile of the eigenmode. From a mathematical standpoint, a variational formulation [3] induces mathematically, for every eigenvalue problem corresponding pairs of eigenvalues and eigenvectors, from an energy minimizing perspective. Physically, each eigenvector corresponds to a normal mode, i.e. the displacement field profile of a phonon mode, at some (w, k) of the dispersion relation $w(k)$. In all of these cases, one defines the matrix phase as the connected phase, and the scatterers as the disconnected components. The displacement field provides information on the dynamics of phonon propagation at each (w, k): one sees the phonon propagating within the structured medium and taking on either a delocalized strain field spread throughout the matrix, or possessing a more localized strain field, for example being concentrated between scatterers along its trajectory. Of course, there can be some modes that are hybrid in between these two extreme regimes. These two situations are reminiscent of electronic structure and chemical bonding, with the delocalized, or "metallic-like" bond, and the localized, or directional "covalent-like" bond only now we are dealing with a dynamic situation where the nature of the bonds is reflected in the "dynamic" phonon eigenmodes which represent the dynamics of phonon energy propagation in the medium. Let us give a physical interpretation of the dynamic mechanical bond which links directly to the familiar scattering and hopping mechanisms. Each eigenmode determines the corresponding dynamics, or type of "mechanical bond "at each (w, k); the dynamics varies depending on the particular phonon wavelength versus the length scale of the structure. This length scale ratio affects the scattering cross section as the phonon propagates through the structure. While, the (an)isotropy of this scattering cross section certainly depends on the scattering resonance profiles of the scattering components and hence their actual geometric shape, this is of secondary importance compared to the dynamic impedance, which determines the nature of the mechanical bond. For phononic structures, the nature of the bond is exhibited most clearly by the dispersion of the particular band in question. An extended "metallic-like" bond exhibits a somewhat more linear dispersion, indicative of its spatially delocalized nature (this is distinct from the nonlocality discussed previously). Microscopically, this indicates that phonon energy transport is favoured primarily through the matrix, with appreciable strong perturbations occurring only at specific frequencies due to the resonant

scattering of the particular scatterers. This situation is what we classify as the extended lattices (EL). Subsequently, a typical characteristic of this class of lattice structure is that the dispersion of the bands is typically linear with only strong perturbations of the bands due to band–band interactions at certain positions; these are where the spectral gaps typically (but not always!) form. Next, the geometry of the scatterers comes into play. Their arrangements in the structure, and the resultant point group and little group symmetries determine the anisotropy of the spectral gaps, negative refractive bands, etc. At the other extreme, we have the localized, "directional" bond; we classify these structures as TBLs. The dispersion shapes of the bands in TBL structures are typically flatter, indicative that the transport of energy typically occurs along directed/localized trajectories between scatterers in direct contrast to energy transport in modes that are delocalized in the extended lattice. In TBL lattices, the strategy for designing optimal structures is somewhat different and more flexible, in the sense that the dispersion relations can be tuned more readily from local changes in the geometric structure. In TBL, the local point symmetries of the scatterers as well as their physical connectivity, either through the matrix or through connected architectures of the scatterers. These two considerations effectively control the dispersion of the band structure of the material, as we shall show later in the chapter. Viewed in this classification scheme, one may now understand that structures of different physical topology exhibit different types of dynamic phonon propagation behaviour; two of these examples include the EL case, where mostly extended wave propagation with resonant scatterings of the entire structure at certain spatial correlations, this is commonly associated with Bragg scattering. The second TBL case, involves mostly localized, hopping mode wave propagation among scatterers, i.e. resonant tunnelling mechanisms with individual resonant scattering. These regimes can be continuously spanned from one to the other by appropriate changes to the structure. For example, a periodic structure which has some spatial disorder, or as a trivial example, taking the wavelength asymptotically to infinity (all extended) for a system which is initially tight-binding. The question concerns what metric do we use as the measure for the dynamic mechanical bond? First, one notes that this description depends on the matching or not matching the number of polarizations between the two (or more phases) present. Thus for solid–solid structures, the dynamic mechanical bond can be defined generally regardless of the detail of the geometric structure, as long as the matrix and scatter phase has been defined. Solid–air structures provide a different situation for two reasons: (1) the number of polarizations differs across the solid–air boundary; hence, the definition of the dynamical mechanical bond is not as straightforward, and (2) the elastic contrasts of solid and air is so large that one may model the solid–air interface as a free surface [2, 4] for propagation in the solid. In this situation, the type of physical topology is transformed into the physical geometrical structure. However, this classification of the lattice type, now based on the actual geometric topography, is once again valid. This method of classification has been separately verified with Painter's work on opto-mechanical slabs, although it was not recognized that their studied structures were only one part of the larger classification scheme. We now return back to the issue at hand. The key need now

is to decide which metric to use. This choice is related to the contrast between the elastic constants and mass densities. The details of phonon propagation within an inhomogeneous medium depend on a multitude of factors, listed previously in the framework. However, in previous sections, one did not consider the dynamics of phonon transport nor how the choice of the component, i.e. and how the material choices affect the propagation behaviour. This is crucial as this offers us the ability and insight to guide phononic structural design. The metric in this case is the impedance contrast between the matrix and the scatterer phases; with the impedance is given by $Z' = pv'$, where i depends on the particular polarization being considered. The concept of the impedance turns out to be quite fundamental and together with the refractive index, forms an alternate set of dynamic variables, conjugate to that of the elastic constants and mass density [32, 40]. Hence, the choice of which pair of dynamic variables to use then depends on the particular problem one is concerned with. Recalling the equations of the conservation of linear momentum, as well as the values of the reflection and transmission coefficients at a flat interface between two media [34], one finds that the fundamental quantity of interest is that of the flux of a generalized linear momentum, expressed naively as pv. The dynamical bond concept applies equally well in structures consisting of two solid phases, solid–fluid phases as well as solid–air phases, with the proviso that we have to adjust the corresponding terms in the continuity equation to account for the changes in the polarization degrees of freedom. The utility of the concept of the dynamic mechanical bond lies in its general applicability. The reason is the following: the relevant phases (matrix and scatterers), and their roles are determined by the dynamic impedance, and hence, the dynamic impedance contrasts, which one defines as: $\Delta Z = Z_{\text{matrix}} - Z_{\text{scatterer}}$. The dynamic impedance contrast automatically determines the lattice class that the structure lies in. For solid–solid structures, one demonstrates explicitly now that by simply controlling the dynamic impedances that we may continuously tune the behaviour of a given structure from an extended lattice to a TBL.

It is clear that to develop a physically accurate framework of the dynamic mechanical bond, the classification scheme employed needs to be lucid and consistent. To verify that it is only the impedances and the associated refractive index which determine the dynamics of phonon propagation, we next take various combinations of "particle (geometric limit)" velocities, densities, parameters loosely associated with the scattering cross-sections, while maintaining the same overall impedances in each phase to show that ultimately, it is the impedances are the crucial parameters determining the classification.

In summary, one has shown here that it is the dynamic impedance, essentially the linear momentum, that is the physical parameter which determines, via the impedance contrast between the constituents, the dynamics of the phonon propagation. In order to be able to rationally design a phononic structure for a particular function, it is crucial to know the dynamics of the phonon transport partly because the type of scattering and interactions that lead to the desired properties depends on the very dynamics of the interactions. An important conclusion that can be drawn from this is that the spectral gap size is then not dependent on the scattering

mechanism directly, since the two bands bounding the gap sizes are not the two interacting bands.

In general, the actual mechanism of the linear phonon propagation through the medium depends on the wavelength of the phonon, the spatial correlation within the structure, the material components. These are all coupled into the variational formalism, which describes the trajectory of the flux of linear momentum within the domain, subject to all of the above constraints. The corresponding (λ, $|\lambda$)) pairs automatically set for each wavelength range (eigenvalue), the corresponding trajectory (eigenvector), based on the energy minimization. By deriving the elastic wave equation from the initial continuity equations, the problem is mapped to a variational problem. It is also this recognition that allowed us to recognize that the physical parameter or variable, which is governing the evolution of the eigenmodes, is actually the flux of linear momentum itself as modified by the impedance contrast of the structure. This is exactly why from just considering the intrinsic material parameters that one may deduce the nature of the trajectory of phonon transport and classify the lattice types based on that. Especially, key to one's distinction over prior work is that one recognizes the need to decouple the material contrast issue from the geometric structure issue; one's assignment of the matrix and scatterer phase is geometry dependent only, not material dependent. This assignment depends on the connectivity of the geometric structure, with the connected phase always being assigned as the matrix phase. Once these assignments have been made, one hence judges the dynamics of the phonon propagation, based on the materials parameters, which is reasonable, but only in the form of the linear momentum flow, or the impedance because based on the variational perspective, the momentum flux is actually the quantity being "diagonalized" or projected out into orthogonal modes to form all the eigenmodes of the system and build up the band structure. This is the rationale for the choice of impedance as the only physical parameter related to the material choice.

7.4.7.3 Specialization for Solid–Air/Vacuum Structures: An Exercise in Symmetry Breaking and the High Impedance Limit

One mentioned earlier that in the case for typical solid–air systems, that due to the extremely high impedance contrast, for the solid matrix case one may essentially ignore coupling to air (impedance contrast $\sim$99.994%! for silicon). In this situation, the solid matrix now forms the effective propagating medium which we are interested in; hence, the concept of the mechanical bond needs to be recast into the geometrical structure itself. The concept of the mechanical bond is actually more intuitive from the structure itself, because the bonds are now actually physically manifested through the structuring of the system.

In this series of structures, one retained the plane group symmetry but one varied the building blocks, such that one slowly increased the size of the building block at the (0, 0) and equivalent positions. One observes the evolution of the band structure from having a more extended lattice character in (a), to the gradual flattening of

bands which meet the length scales of the structures, in (b) and subsequently in the TBL (c). In all three cases, the avoided crossings result in the formation of the complete spectral gap from the 6th and 7th bands. What is perhaps more interesting of note though is that the avoided crossing takes place at different k values in (a) compared with (b) and (c), the latter pair of which take place at the Gamma point. Without the utilization of the avoided crossing framework, it could be falsely assumed that the gap formation is due to interactions between different pairs of bands. In this regime, the mechanical bonds are manifested through the connections between the building blocks geometrically, since the high impedance contrast between the constituents indicates that mode propagation will occur essentially only through the solid matrix phase.

From a fabrication and technological perspective, it is advantageous to be able to design and fabricate phononic structures which only require one material, i.e. solid–air systems. This is obviously due obviously to fabrication considerations if one has to scale the structures down to smaller scales and is the reason why most of the recent demonstrations of novel behaviour in phononic/acoustic crystals have been demonstrated at larger scales (mm scale or larger). To date, there is no procedure available to design targeted phonon transport, be it a simple acoustic wave or a mixed mode within the solid. Hence, it was unclear whether solid-solid systems are even necessary to obtain desired phonon propagation behaviour. Solving this puzzle is the rationale for seeking the governing rules for the dynamics of phonon propagation, as this complements our universal framework for the complete rational design of phononic structures. Based on the previous demonstrations, one has "abstractly" distilled our requirements for the phonon dynamics in terms of the lattice or topography class. This provides guiding principles for applications requiring considerations on the specific dynamic propagation of key modes, e.g. negative refraction, slow or fast modes of propagation. By showing that this classification can be renormalized with both the most generic solid-solid lattice structure as well as the solid–air/vacuum structures, one is able to reduce the dynamic requirements to a single material platform system, which is extremely favourable from technological considerations as well as scalability. Finally, with the correct renormalization of the lattice classes into the solid–air/vacuum cases, one is able now to design structures with desired dynamics based mainly on geometric considerations, not the particular choice of material combinations. This leads us to then implement the universal design framework which will enable rational design for almost all desired forms of phonon propagation behaviour. One now illustrates, using structures belonging to both the EL and the TBL classes (i) structures with polarization-specific negative refraction bands with low group velocity in a "fast" EL system, (ii) an anisotropic structure which has a higher transverse like velocity than longitudinal velocity and finally, (iii) a TBL structure which possesses the largest complete spectral gap known so far (by a factor of twofold).

7.4.7.4 Linking the Physical Topography to the Applications

The reasons for the concept of a dynamic mechanical bond are manifold. One is to search for a simple classification parameter that highlights the role of the material parameter, i.e. one that is physically relevant. Previous pioneering works overly relied on the identification of different terms of a similar equation (e.g. Schrödinger equation), resulting in inferences that are sometimes incomplete [41]. The second reason for this method of classification of the lattice via the strength of the bond, while borrowing from the foundations of the concepts of elementary solid state theory, is that it is physically intuitive in allowing the researcher to choose what kind of structures, and in which combination, to design and fabricate their structure for a particular application, this is especially true in solid–air systems. Different examples of desirable applications include, for example, the ability to achieve effective negative refraction, extremely large spectral gaps, as well as to provide a platform for studying nonlinear as well as defect interactions. One would prefer relatively linear dispersion with negative refraction and thus it becomes highly advantageous to have extended state like bonds, i.e. an EL structure to ensure efficient negative refraction behaviour. At the same time, in order to produce a large spectral gap, it is less clear which class of lattice would produce an outright superior candidate for the champion structure. In the next section, we obtain structures with large spectral gaps, utilizing both categories of lattices. The complete gaps we design are much bigger than what is currently demonstrated in the literature. In this situation, the TBL outperforms the extended lattice. However, we note there that the common physical mechanism underlying the large spectral gap is that the resonant mode of the geometric scatter lines up with the frequencies at which the Bloch symmetry (Bragg resonance) is in effect.

7.4.7.5 The Extended Lattice: Rational Design of Polarization-Specific Negative Refraction Bands

The nature of the bond between scatterers controls the character of phonon propagation behaviour ranging from a delocalized, extended bond type to the localized, tight-binding type bond, with an entire continuum of behaviour in between these limits. Mathematically, the bond nature determines the spatial dispersion of a band, i.e. its dependence on the wave vector; physically, this translates into the propagation velocity of the eigenmodes of the structure. This is an important factor to consider when designing a structure for a particular functionality. For example, to design a structure that possesses a large spectral gap within some frequency region, but otherwise quasi-linear dispersive behaviour for propagating modes, one would likely choose a structure that belongs to the extended lattice class. On the other hand, for a structure to possess multiple slow-group velocity modes, a TBL is preferred. To the best of our knowledge, this classification of different structures has not yet been recognized so the design of precious structures has not been guided nor optimized for the particular functionality. For example, in negative refraction, what

has been commonly done is to pick the second band which is related to the 2nd BZ as the negative refraction band. Depending on the band structure, one may or may not be able to have a complete region in the entire (w, k) space with only the desired negatively refracting bands, i.e. you might get undesired losses from mode mixing There is not much control over the design of this propagation behaviour in this sense. An additional complication arises from the fact that it is not always clear that a high order band immediately implies negative refractive behaviour; one needs to understand the details of the dynamic behaviour of the eigenmodes to be able to verify this behaviour. To demonstrate a rational way of designing specific functionality in certain dispersion bands, i.e. to truly mould phonon propagation behaviour, we need to demonstrate that one is able to specifically insert certain bands with characteristic propagation behaviour and to be able, as well, to control their vector polarization. We first demonstrate this control using a 2D extended lattice of solid/air. We opt to control the flow of phonons in their full vector nature through the solid as opposed to structures where the solid phase forms only discrete perturbing scatterers, and the scalar fluid is the main propagating medium. One will first create a structure that possesses a large complete in-plane spectral gap of $\sim 80\%$; it also possesses a complete spectral gap of 72%, which is larger than what has been obtained in the literature currently, to the best of one's knowledge. The EL design is implemented in a square lattice that possesses the maximal (for the square lattice) p4mm plane symmetry. By choosing to utilize only a single monolithic material, the designs are amenable to scaling and not reliant on specific material combinations and rely only on the specific material geometry and are thus materials property tolerant.

Hence, the choice of topography consisting of connected cylinders is to create the presence of multiple low group velocity modes, i.e. relatively flat bands. The reason for this occurrence stems once again due to our introduction of topographical cuts to link the cylinders with orthogonal channels, which allows for multiple localized modes which serve to localize the strain energies at the free surfaces, as shown earlier. One then chooses to geometrically induce a distortion by increasing the "connectivity" of the structure; this intuitively leads to an increase in group velocity in selected bands, forming our negative refracting bands; as previously shown, the mechanical connectivity is directly related to the resultant momentum flux and hence its spatial extent of (de)localization, which was discussed in some detail in the earlier sections; hence, one has induced locally in space, a reinstatement of the connectivity to 4 once again. These negative refracting bands are also polarization specific, i.e. these are negatively refracting polarization bands. This approach is different from current approaches of "producing" negatively refracting phononic crystals, in that one first creates a structure with a large complete spectral gap by utilizing an extended lattice structure. One then induces specific negative refractive bands into this spectral gap by geometrically increasing the connectivity of the structure. This maintains the size of the spectral gap while selectively modifying the behaviour of specific bands. To be precise, one controls their dispersion and hence makes them negatively refracting. This ensures the formation of a "clean" negative refracting region, since one has formed these bands in a spectral

gap. The ability to retain polarization persistence in the bands stems as well from the increase in connectivity of the structure while retaining specifically the point symmetry of the structure (4 mm); this ensures that the increase in connectivity does not lead to mode mixing, which would then destroy the polarization specificity. Intuitively, one notes that in structure (b), the transverse and longitudinal modes "see" the same structural rigidity and hence do not mix to form new eigenmodes.

One can visualize the physical process as follows. In (a), these flat bands were localized modes which effectively had zero group velocity and they are formally present due to the topology of the structure which induced the localized modes due to the presence of the extra boundaries. One notes that in (a), the three modes were respectively symmetric (a, c) an anti-symmetric (b) with respect to ox. However, one notes here that in (b), by increasing the connectivity of the structure, effectively will induce spatial dispersion to these very same modes (The interfaces for strong localization of energy cannot be sustained), one visualizes this connectivity increase as the inclusion of addition mechanical bonds, hence leading to coherent extended modes. Another interesting point of note is that this connectivity causes modes 4(c) and 6(a) to mix, forming the new modes (d) and (f) through bonding and anti-bonding combinations. This leads to the formation of polarization persistent negative refracting bands for transverse (anti-symmetric) and longitudinal(symmetric) polarization phonons. This tailored method of inducing negative refracting bands allows for efficient coupling of incident beams into negative refracting channels for solid elastic waves, which is something that is not trivially achieved in considering structures with full vectorial fields. To date, there has been no rational way of controlling the polarization persistence in solid phononic metamaterials, to our knowledge. In fact, due to the previous lack of knowledge as to how to actually deal with the vector phonon field that this control of polarization for individual bands has not been attempted or was not successful.

One demonstrated here a series of principles which one applied rationally in order to create a desired propagation behaviour. By choosing the initial topology of four connected cylinders, one created a structure with a large spectral gap to start. More importantly, the choice of the connected topography was to induce multiple localized flat modes, which we will subsequently tailor. This is done by changing the dynamics of the phonon propagation by utilizing an increase in their bond connectivity. We recall that in solid-air systems, this connectivity shapes the bond nature of the lattice and hence the associated propagation velocities. The net result of this is in the creation of three negative refracting bands, of which two are polarization-specific negative refracting bands. To date, this is the first known rational design of polarization refractive bands in a solid phononic metamaterial. One follows this by introducing the design of a nonresonant metamaterial which is anisotropic in its long wavelength properties. In particular, we seemingly defy the common knowledge of a homogeneous medium limits, by creating a structure which has a higher transverse than longitudinal velocity along one direction but behaves normally in the other principle direction.

The motivation in this section was to understand the relevant physical parameters involved in controlling the phonon dynamics in inhomogeneous media. The problem is interesting, in that one has to consider the physical topography of the structure, the elastic contrasts, as well as the frequency ranges of interest; hence, there are a lot of variables to consider. At the same time, because these variables are frequently coupled to, there is a lack of a sense of how to rationally treat combinations of these variables that makes the design transparent, and also physically accurate. One chooses to consider the fundamental process of phonon flux through a general structure and recognize that the linear momentum (in our system), or impedance, is the relevant quantity of interest. In other words, given a particular frequency, we are concerned with the resultant trajectory of a phonon flux through the entire structure. This is essentially a variational extremization of the continuity equation, with the momentum flux being the quantity of interest. One found that the linear momentum/impedance serves as the relevant parameter for determining the dynamics of the phonons, taking into account as well the physical wavelength of the phonon in the medium. This is in contrast to other previous works, which separately considered contrasts in elastic constants, mass density, etc., without being able to elucidate a general guiding principle that works in all cases. In contrast, the utilization of impedance contrast as the parameter holds valid, even under deliberately introduced conditions with different contrasts of the elastic constants and density. Hence, the impedance contrast is utilized as the first-order physical parameter that determines the phonon dynamics, giving us the concept of the mechanical bond. The assignment of a bond type to a particular structure depends on the impedance contrast, this is strictly dependent only on the materials involved, independent of the exact structure. The role of the physical topography comes in determining the matrix and the scatterer phase, from where we define the sign of the impedance contrast parameter value. In this sense, the assignment of the "matrix" or "scatterer" phase is only dependent on the geometric structure, not the particular set of materials. These two conditions then determine the dynamics of the phonons vis-a-vis the mechanical bond classification, hence giving a concrete grounding of types of material combinations and physical topography. We do not consider how these parameters affect the spectral gap opening tendencies because based on our general framework, this is not necessary. In a lot of the cases, the bounds of the gaps do not relate to the particular gap opening mechanism at work, as we have shown repeatedly throughout this and the previous sections. Instead, it is more important to understand the dynamics which the phonons inherit based on these parameters, hence the concept of the mechanical bond. The dynamics are more important in controlling the subsequent desired propagation behaviour and realistically speaking, we can create complete spectral gaps irrespectively of what lattice class we are in. One subsequently generalizes this approach also to solid-air structures and remapped the dynamical bond concept to rely on the geometry of the structure instead. One demonstrated full control by designing a structure with engineered polarization-specific negative refracting bands using a starting EL lattice type. One subsequently also created a phononic structure, based on a TBL concept, that possesses an in-plane spectral gap of 102% and a combined total spectral gap

of 88%. In the subsequent sections, one demonstrates further the combinations of the general design framework together with the phonon dynamics consideration to demonstrate a series of unique phononic metamaterials, utilizing only a single material platform, some with propagation behaviour that has not been demonstrated before nor thought possible in phononics.

7.5 Designing Dispersion Relation for Phononic Metamaterials I: Avoided Crossings

7.5.1 Introductory Remarks

The previous chapters sought to outline the governing physical principles of classical elastodynamics (Sect. 7.3), transitioning from discrete lattice dynamics into the continuum regime. This allowed one to view elastic waves as broken symmetry modes, both globally, which led to the formation of the transverse and longitudinal modes which we are familiar with, as well as the classical Rayleigh (edge) and Stoneley (interfacial) type modes, which is derived from symmetry breaking in a specific spatial region, analogous to surface plasmons. One took care to outline the different scenarios pertaining to bulk systems with induced discrete translational periodicities of different dimensionality as well as the connection of the bulk response of a medium and its interfaces in a general context of symmetry breaking and one was able to expound the role that group symmetry plays in tracking the actual eigenmodes of the phonons in a structure, which associated the entire details of each eigenmode's polarization field as having to conform to the symmetry representation of the mode, dictated by the little group of the respective k-vector. At the expense of being seemingly too general, the purpose was to highlight the most fundamental conserved quantities that are present in a dynamical process that takes place at a general interface. This is crucial to help distinguish the governing equations (which conserve the relevant system under which the evolution of the phonons occur) from the constitutive relations (elastic constants coefficients, mass density), which is somewhat more phenomenological and pertains directly to the material system being studied. This clear distinction is necessary in order to prevent one classification from being obfuscated with the other and subsequently, missing potential governing principles otherwise overlooked. As one seeks governing principles that are universal and hence are to a large extent, material system independent, this clear distinction and isolation is very important. This led to the development of a concrete mathematical structure (Sect. 7.4) that illustrated both the global as well as local principles of group theoretical and variational methods in order to control the band structure of a generic AS. It was also here where the concept of avoided crossings in the context of spectral gap formation was first outlined. In this section, one generalizes the requirements for the formation of spectral gaps in both phononic "metamaterials" and "crystals" by identifying what

are the irreducible requirements for the formation of the spectral gaps in all cases. We will show that the fundamental requirements here, are the (i) correct plane group symmetry, because they govern the allowed symmetry representations each dispersion bands can adopt, as well as (ii) controlling the avoided crossing, which leads to the spectral gap formation. One subsumes the current working knowledge tools by identifying their physical model as one of the possibilities in the generalized framework. One then illustrates how the generalized framework, by identifying the necessary and sufficient guiding principles, enable us to create both metamaterials and crystals (as defined in the current literature), using only a single elastic material. In fact, the design framework fully utilizes and accounts automatically the dispersion of the bands, i.e. their nonlocality; hence, the physical basis for the design principle for the band structure is assumption-free. This is in contrast to conventional working knowledge for phononic metamaterials, which is inherently quasi-static in nature, and hence ignores the effect of the lattice in a cavalier fashion. Through this process, we remove the artificial distinction between what constitutes a phononic metamaterial and what constitutes a crystal. This is demonstrated through two examples, the first being an AS which possess both a complete sub-wavelength gap and a crystalline like gap, hence straddling the metamaterial and crystal regime. Importantly, this structure was designed utilizing only a single material platform; hence, only explicit knowledge is made use of the plane group symmetry. The second example also builds on this theme, except that in this instance one creates a structure which possesses meso-scale gaps, specifically a sub-wavelength gap for transverse modes and a crystalline gap for longitudinal modes. We call this a meso-scale polarization-specific phononic metamaterial. To the best of the knowledge, these are the first demonstrations of such behaviour in phononic structures. More interestingly, these unique classes of behaviour are achievable using only a single monolithic material platform. In addition, these designs are largely material independent; hence, they are achievable using a significantly wide range of materials, ranging from polymer all the way to metals. This validates the value and utility of approaching the design of these structures from as global a perspective as possible. One now proceeds to demonstrate these different forms of phonon propagation behaviour, highlighting the governing principle in each demonstration.

7.5.2 From Crystals to "Resonant" Metamaterials

7.5.2.1 Untruths

As briefly mentioned, the conventional distinction between a resonant metamaterial and a crystal lies in the wavelength regime in which the spectral gap forms, together with their associated negative index bands. Another inherent assumption for metamaterials is the resonant response of the building blocks that determines the behaviour of the material, and hence the exact arrangement, i.e. lattice class doesn't

matter; this is somewhat linked to an erroneous interpretation of the effective medium approach [40], also commonly known as the locality approximation. The typical form of a metamaterial is strongly resembling a mechanical spring model. In these situations, typically three materials are needed, to take the role of the mechanical mass and springs. The associated signature is that of the typical dispersion relation, where the interaction occurs between the resonant mode and the "effective medium" mode, leading to the formation of a spectral gap, which is deeply sub-wavelength. The exact position of this gap depends on the material properties, which follows the model that the spring resonance scales inversely with the static mass. There are a few points of note here. First is that the formation of the spectral gap comes from the avoided crossing between the said two modes; hence, the uniqueness of the property is linked to the building blocks and not so much the lattice, or that is at least the conventional explanation. This is untrue and can be regarded as somewhat over misinterpreted due to the choice of the building blocks in this case. In the pioneering work of Liu et al. [31], their choice of the large contrast of the mechanical spring had a much larger impedance than the coupling rubber (the elastic constants have a ratio of $\sim 10^5$, and an incompressible rubber); hence, this leads to the fact that the resonances of the mechanical spring are only weakly coupled through the lattice; we gave a two-dimensional analogue of this system earlier where one discussed the role of nonlocality explicitly in the development of band structures. Hence, the response is very weakly nonlocal, i.e. the locality is a result of the material parameters choice and not a general mechanism, as it was purported to be. The second point is that the avoided crossing is occurring at a small, BUT still finite wave vector, which naturally implies nonlocality; this is further reinforced by the fact that by definition, the avoided occurs between two modes with like-symmetries, since we know that the eigenmodes can only adopt representations belonging to the isotropy group of the particular wave vector, this implies immediately that the eigenmodes encompass information about the lattice lies in. This implies that in resonant metamaterials, the dispersion is nonlocal in general [40]; any perceived locality is due to particular choices of the material components. One should not mistake the latter for the general case, as has been mistakenly done, for both electromagnetic and acoustic metamaterials [42]. This was illustrated very clearly in Sect. 3.4 where we took a common canonical structure of a 2D resonant metamaterial and plot the corresponding eigenmodes across the avoided crossing point, at various material parameters. One sees clearly that all the displacement fields maintain the symmetry of the isotropy group and not that of the isolated resonances. Hence, one now formally casts the necessary condition for opening a spectral gap, regardless of whether one is dealing with a metamaterial or a conventional crystal, as the respective avoided crossing with the correct symmetries. The perceived key distinction between a metamaterial and a crystal is then the wavelength at which this avoided crossing occurs. In contrast to conventional working knowledge, while this is common but not always so, we do not regard the spectral gap formation of crystal to be due to the discrete translational symmetry; there are numerous examples that show that many bounds of the spectral

gaps are not at the Brillouin zone boundaries [43]; hence, one subsumes the periodicity as translational Bloch symmetry and as but one of the possible symmetries that cause avoided crossings.

To summarize then, the present state-of-the-art suffers from several issues, mostly fundamental in nature (i) what are the usual and actual constraints when creating a spectral gap (ii) what is actually controlling the symmetry of the response functions and (iii), what are the true requirements for a dynamic negative susceptibility. Moreover, the problem of the choice of the optimal space and plane group symmetry and the subsequent symmetry of the response actually entail more than just the naive issue of reducing the size of the IRBZ, for both crystals The spatial nonlocality, or wave vector dependence of the AS response is inherently present and is meso-scale because it encompasses, in general, all the relevant length scales in the response through the irreducible representation of a particular band.

7.5.2.2 Truth: Avoided Crossings

To remove the artificial classifications of resonant type metamaterials and the classical phononic crystal, one recasts the concept of spectral gap formation into a framework which is scale-invariant, i.e. does not require an intrinsic length scale to interpret. In this sense, one may now identify phononic crystals as structures which possess spectral gaps primarily based on avoided crossings due to the Bloch symmetry, whereas for phononic metamaterials, spectral gaps occur due to avoided crossings between low-lying resonance modes and the longer nonlocal linearly dispersive bands of the medium. One thus removes the artificial distinction between what is a crystal and what is a metamaterial and classify them all within the same category of metamaterial from here on. Within this approach, one now identifies the requirement of the low-lying mechanical resonance as a geometrical structuring of the material to have low-lying resonant eigenmodes with the same irreducible representation as the long wavelength linear modes in order to create the sub-wavelength avoided crossing. The actual mimicking of a mechanical spring is no longer necessary. In addition, by controlling the types of these resonances, one can selectively induce different dynamic negative mass density, modulus, and even shear modulus. Recalling the previous discussion one notes that because in symmorphic symmetry groups, one may carry out the factor group decomposition on the infinite plane group, that for considerations of the dispersion relations, it suffices for one to consider only the relevant isotropy group of k being considered; this is the normal subgroup which one is interested in. Hence, reduction in point group symmetry is not as traumatizing as was originally purported to be.

One has created a metamaterial that has two-scale complete gaps, one sub-wavelength gap and one crystalline gap, using only a single monolithic elastic material with a geometric perturbation that changes the “connectivity” of the medium and lowers its symmetry utilizing the global and local variational principle outlined in Sect. 7.4. This completely generalizes requirements for generating sub-wavelength gaps which are “metamaterial”, and by creating both classes of

complete spectral in-plane gaps, one has hopefully established to the reader that a strict division between metamaterials and crystals is artificial, unnecessary and can be counterproductive for engineering the dispersion relations for devices and applications. It is also important to reiterate here that in the design of such a material, that we have shown that the process of generating these gaps depends strongly on nonlocality. In fact, in this demonstration, one utilizes the full extent of the nonlocality in the bands, clear from their dispersion to create the resultant band structure. This is distinct in execution from the classical method, which is based on a locality approximation, as discussed in Sect. 7.4. Finally, one notes that in order to create a negative index band, the initial motivation for metamaterial applications in order to achieve negative refraction, in an elastic material, is considerably more complicated than creating such a band in an acoustic medium; this is mathematically a classical analogue to what is known as a more general case of induced transparency, except here we are more interested in the induced dispersion relation than the phenomenon of tuning that transparency, i.e. we are more interested in the formation of the bands with desired dispersion rather than the dynamics of tuning this transparency.

7.5.3 Meso-scale Phononic Metacrystal: Polarization-Specific Spectral Gaps

In this section, we illustrate the design process using structures that specifically retain a square lattice and p4mm symmetry. This is complementary to Sect. 7.5.2 where one reduced the plane group symmetry in order to enforce avoided crossings. In this approach, one induces avoided crossings by utilizing the mechanical connectivity and hence variational principles to control the positions of the avoided crossings. The first part of the work involves choosing a structure which possesses a complete crystalline-scale spectral gap at the lattice scale, and by connecting sub-elements of the structure to induce the formation of a metamaterial which possesses polarization-specific spectral gaps at both the lattice scale and the sub-wavelength scale. This topographical change involves a simple change in the directions. which one would normally follow and hence, a reduction in the propensity that this change preserves the 4 mm point symmetry involves a volume fraction change from 39 to 51.5% in the connectivity of the structure along associate with increased channels for forming complete spectral gaps.

As noted, the original parent structure possesses a complete in-plane normalized gap width of approximately 80%. The origin of this quite large gap here can be traced to the condition where the building block dimension in this case optimizes the Bloch type avoided crossing process, similar to the situation described in Sect. 7.3.

One utilized here fully the nonlocality and the dispersion of the bands, through selective geometric perturbations, to control specifically the positioning of several

dispersion bands in order to enforce avoided crossings, resulting in the creation of spectral gaps in the frequency range that is desired. In the first example, we utilized symmetry reduction in order to enforce the avoided crossing and in this situation, we created two-scale complete spectral gaps in a deformed version of the honeycomb lattice. Crucial to this realization was that one introduced a geometric perturbation that interchanged the transverse-like and longitudinal-like mode, this was critical to enforce the avoided crossing in the desired frequency range. In the second example, we retained the plane and point symmetry of the system but this time one adopted the opposite approach and increased the connectivity to push the transverse-like mode to higher velocities, this allows the avoided crossings to occur at the sub-wavelength frequency range, in addition to the fundamental crystalline gap, enabling us to generate the meso-scale polarization-specific spectral gaps. One summarizes here that all these are based on the simple realization of what are the critical components for controlling the band structure of the structure and purely by utilizing geometric structuring; one is able to achieve quite a series of unique band structures without any reliance on specific material properties. This is to the best of the knowledge, the first demonstration of this general mechanism for controlling the band structures of any periodic structure, not just for phonons.

7.6 Designing Dispersion Relations Phononic Metamaterials II: A Polychromatic Nonsymmorphic Phononic Crystal

7.6.1 Introduction

In this second part to the design of dispersion relations in phononic metamaterials, one here utilizes a different approach, previously unemployed, in order to create a nonsymmorphic phononic crystal that possesses multiple complete spectral gaps. Instead of using avoided crossings which have been the default mechanism for creating spectral gaps and negative index bands, one utilizes a complementary approach from the variational perspective. In particular, one creates multiple complete in-plane high-frequency gaps, by not making use of any avoided crossings. In fact, here one makes use of both global and local principles to design such an AS. By recognizing that the relevant eigenmodes of the phonons obey the allowed Irreps corresponding to the isotropy group, one is able to control and treat the vector nature of the phonons as before by only considering the global plane group symmetry. However, instead of employing avoided crossings, here one utilizes the local variational principles by shaping of the building blocks of the AS structure; this allows one to control the eigenfrequencies at the r point. Together with the choice of the particular TBL lattice class, one controls the evolution of the bands in k-space, forcing them to be quasi-flat. This results in a natural two-scale splitting of eigenfrequencies at the r point, first due to the (anti)symmetry with

respect to a mirror plane parallel to the *k*-vector direction considered, and then the (anti)symmetry with respect to the primary C4 rotation operation. Together with the choice of the lattice class, which controls the transport dynamics, and the global plane group symmetry, one is able to control both the positions of the eigenfrequencies and their evolution in *k*-space. This entire suite of tools, developed in Sect. 7.4, allows one to design a phononic structure possessing multiple complete in-plane spectral gaps (6), spanning a total normalized gap width,

$$\Delta\omega = \sum_{n} \frac{\omega_{\text{upp}} - \omega_{\text{low}}}{\omega_{\text{mid}}} \tag{7.24}$$

of over 100. The creation of phononic metamaterials possessing multiple complete spectral gaps is very interesting, both from a fundamental and applications perspective, allowing for the study of nonlinear phonon–phonon interaction processes [44] to development as a structural material for shaping and moulding nonlinear waves such as solitons and shock waves [32].

7.6.2 *Global Symmetry: Nonsymmorphicity and Sticking Bands*

In addition to the previous illustrations on the utilization of the generalized avoided crossing, one hinted of the final governing principle which aids our universal framework by linking the global constraints with the local design principles highlighted in the previous two sections. Simply stated, it is an adiabatic perturbation theory in wave vector space which has its origins in the compatibility relations in group theory. Traditionally, this has been utilized for identifying the irreducible representations (Irreps) in the individual bands in electronic structure calculations. The perturbation can be fundamentally traced to a group-subgroup decomposition of the Irreps as one progresses along a particular trajectory in *k*-space, for example the Gamma Point to a generic position along the GX direction. One remarks that this entire band can be joined and treated in this manner is not obvious, or easily proved [45] but one is able to trace as a series of equivalence transformations as one adiabatically varies the wave vector along some direction in *k*-space. For the time being, we will accept that this procedure works well and is well verified. The elegance of this perturbation theory is that once again, it is scale-invariant, i.e. takes care intrinsically of the nonlocality of the bands and inherently conforms to the symmetry requirements along the trajectory in *k*-space. What one observes is the fact that this "analyticity" of the bands only sets together with the possible connections in *k*-space in terms of symmetry requirements, but it enables us still full freedom in choosing how and where in the reciprocal space do the bands choose to evolve across. This controls, to a very large extent, how the size of the gaps may evolve. In fact, this allows the possibility of a new paradigm in

designing spectral gaps, for example by controlling the position of eigenfrequencies at the Gamma point, which is local (k = O), and then controlling the evolution of the bands across the rest of reciprocal space such that, for example, to create polychromatic complete spectral gaps. To achieve this, one needs to control (i) the allowed dispersion of the bands as well as (ii) their allowed energies. This is because control over both these two features, in principle, allows us to have unprecedented freedom and control over where the dispersion bands exist in frequency, as well as their curvatures. Broadly speaking, in order to realize multiple complete gaps in a single structure, we want to reduce the dispersion of the bands as much as possible while at the same time create large spectral gaps, this requires control over both the curvature as well as the spectral positions of multiple bands as well as their evolution throughout the reciprocal space. A combination of a global constraint and local design principle is utilized to achieve this purpose. Broadly outlining the steps we shall undertake, the global constraint utilizes group theoretical principles [36] and casts the underlying mathematical structure onto the linearized elastic wave equation; this provides a framework within which to operate and engineer the band structure. The "local" design principle takes into account the propagation behaviour of the classical phonon and identifies the category of geometrical structure of the phononic crystal which we need in order to control the relative placement of energy eigenvalues of the dispersion bands. One chooses to do this, of course for the in-plane two-dimensional linearized elastic wave equation, given by:

$$\rho \frac{\partial^2}{\partial t^2} u_i = \frac{\partial}{\partial x_i}\left[\lambda\left(\frac{\partial u_l}{\partial x_l}\right)\right] + \frac{\partial}{\partial x_k}\left[\mu\left(\frac{\partial u_i}{\partial x_k} + \frac{\partial u_k}{\partial x_i}\right)\right] \tag{7.25}$$

ρ is the density λ, μ are the lâ me coefficients u_i are the displacement components.

The elastic wave, or phonon, possesses in general, three degrees of freedom; in two dimensions, the in-plane polarizations (two) are coupled with the final, out-of-plane polarization decoupled from the system, it is the former case which one is solving for now. Surprisingly, the nature of the field which one is trying to design, offers no more complication in the global constraint framework, once one has properly identified their rank (i.e. vector, scalar). In general, the definition of a transverse or longitudinal phonon loses meaning in an inhomogeneous medium and the phonon eigenmodes possess a nontrivial displacement field with mixed polarization, consisting of both transverse and longitudinal character. While the details of the displacement field may differ greatly, depending on the normalized length scale of the medium inhomogeneity (over the wavelength of the wave one is considering), a general rule remains: The eigenmodes will possess the relevant symmetries of the system [37]; whether the symmetries are dynamic, static or time-varying, this principle holds true. In phononic crystals, the eigenmodes hence must obey the discrete symmetries of the space (3D)/plane (2D) group of the system. Group theoretical principles have been utilized mainly as a powerful analysis tool [36]; one here applies it as a global constraint principle. While on its own, group theory

cannot be utilized to design a particular structure, its elegance and power lies in its ability to cast the governing equation of a physical problem into a concrete mathematical structure that states the possibilities the solutions may take, i.e. its invariants; in this case, group theory is able to dictate for us the allowed possibilities for the band structure, which is physically realized through our choice of the symmetry group of the phononic crystal. In the design of phononic crystals, one main challenge has been to control the dispersion of bands along general directions, i.e. low symmetry directions; this is especially important when one wishes to optimize complete spectral gaps. Hence, in order to create multiple complete spectral gaps, one needs to have a way of controlling or reducing band curvatures along these low symmetry directions. One chooses to employ band sticking, discussed earlier in Sect. 7.4, which enforces bands to exist at least as double degenerate pairs along entire Brillouin zone (BZ) faces (3D) and edges(2D) that typically have low symmetries. In particular, band sticking occurs in structures possessing nonsymmorphic plane/space groups, along with certain BZ faces/boundaries or edges.

One notes here that not all the nonsymmorphic plane groups will possess sticking bands; the strict requirement is that along the particular BZ boundary of interest, that there are two commuting symmetry elements with their invariant axes perpendicular to one another; for the p4mg plane group, these are the glide planes and twofold axes and happen to lie on the *XM BZ* face which we need to control. Although initially discussed for electronic systems, band sticking is rather general and exists for vector fields as well, since it relies only on the symmetry of the structure. The group theoretical principle is a powerful global constraint because it is valid regardless of the nature of the field or its dimensionality. The dispersion bands exist solely as degenerate pairs along the *XM BZ* boundary at all fill fractions, as they all maintain p4gm symmetry demonstrating that the sticking bands are a robust signature of the plane group symmetry. Hence, the global constraint has helped cast the wave equation with a concrete mathematical structure, bearing in mind that all of the allowed eigenmodes conform to the symmetries of the little group of the relevant wave vector.

It is important to note that the parameter of fill fraction is not so useful in the actual design of a phononic crystal, or any periodic structure for that matter although it is indeed useful from a fabrication standpoint as a practical tuning parameter. The issues lies in the fact that it is potentially misleading when utilized as an actual design parameter when exploring for ideal structures from a fundamental standpoint, i.e. what structures we should be looking at for the properties which one wants One shall end with the remark that the crucial design parameter is to identify the category of geometric lattice structure that is desired before considering the fill fraction of the building blocks within the correct category. This leads us now to the local design principles which one bases on variational arguments. As the purpose is to create structures with multiple complete spectral gaps, one wishes to reduce the curvature of our bands, indeed to flatten them as much as possible across the *XM BZ* boundary, if at all possible. In addition, one also needs to be able to control the band dispersions in order to maximize the complete spectral

gaps. This is achieved through the phononic analogue of the TBL class in the extreme sense. By choosing solid building blocks which have very specific anisotropic eigenmodes and then connecting them through weak "mechanical" bonds, one creates bands with very small curvatures, i.e. almost flat, across the *XM* boundary edges. Effectively, one has designed a lattice such that the eigenvalues are nearly degenerate at the *X* and *M* point, which belong to two different isotropy groups. The TBL enforces a series of constraints on the allowed frequencies and their subsequent evolution across k-space

The final design consideration is in controlling the positions of the energy bands. In order to achieve multiple sizeable spectral gaps requires us to control the evolution of the remaining bands from the r point to the respective sticking points at the *X* and *M* points such that the coalescing pairs of bands (from *F* to *X* or *M*) are separated by smaller spectral widths, preferably between adjacent bands. This is exactly where one is able to utilize the vector nature of the phonon to our advantage. The original two degrees of freedom (DOF) (two polarization modes) have hence been mapped into the irreducible representations of the isotropy group. From group compatibility relations in evolving from *r* to *X* or *M* (C4v to C2v), we know that the bands coalescing to the sticking point need to NOT both be either symmetric (A1, B1) or anti-symmetric (A2, B2) at the r point. This naturally establishes the desired criterion for how the symmetries of the eigenmodes should be arranged at each wave vector k. This is readily accomplished in the TBL through the choice of making the building blocks highly anisotropic, coupled with the fact that there are two DOF due to the vector nature, creates two orders of splitting in the energy eigenvalues at the r point. Hence this automatically groups (A1, B2) and (A2, B1) type bands adjacently, enabling us to finally arrive at the desired pairwise coalescing from *r* to *X* and *M*. Note that this two-energy scale splitting method is unique to our choice of geometrical structure in the TBL class, which is crucial to deriving the eventual band structure and is quickly lost once we move to structures that do not belong in this regime. Our final criterion is that one would require that the bands remain essentially flat across the *XM* face as part of the design criterion to maximize the sizes of the multiple spectral gaps; this is fulfilled with the combination of the choice of the global plane group symmetry (p4gm), the TBL lattice and most importantly, the building blocks. The choice of p4gm, the highest symmetry nonsymmorphic group ensures that one only needs to match the energy eigenvalues at the *X* and *M* points, since bands only exist pairwise degenerate along *XM*. In order to ensure the persistence of the gaps, one needs to ensure that the bands evolve from the *X* to the *M* point flat, i.e. they do not cross in the *XM* region. This is distinct from sticking bands, since nonsymmorphicity merely ensures that points at *X* and *M* are now double degenerate, it does not prevent the bands from crossing one another along *XM*. To do this, one has to design accidentally degenerate eigenmodes at the corresponding *X*, and *M* points. For the p4gm group, the isotropy groups at both the *X* and *M* points are C2v, hence by utilizing our TBL, the eigenfrequencies are determined strongly by the geometry of the unit cell, and hence the building blocks. One notes also the fact that the tight-binding nature of the lattice helps ensure the coalescence of the odd–even pairs of bands because of

the low energy requirement in switching the displacement fields between the two parities in the tight-binding regime.

By utilizing these two general design principles, one governing the global properties and one governing the local wave interactions of phonons within the structure, one demonstrates that it is indeed possible to impose controls over spectral gaps in a rational fashion and even control the band curvature. By first considering how the plane group symmetry of the crystal manifests itself in the global constraints placed on the dispersion relation of the crystal, one describes design principles for controlling the allowed evolution of the eigenmodes of the phononic crystal, this led one to choose a p4gm plane group for our starting structure, which ensures band sticking along low symmetry BZ edges. This global principle determines the Irreps of each eigenmode by defining specific site symmetry representations via the isotropy groups along various directions in k-space, giving a very useful and tractable handle towards controlling the eventual band dispersion. This directed the specific approach one should exploit in controlling the eigenfrequencies from a variational viewpoint, which was our local design principle. Finally, building on earlier work (Sect. 7.4), one recognizes that the actual dynamics, and hence dispersion and curvature of the bands hinges crucially on the lattice class of the structure, hence the final choice of a TBL class completed our design process, allow us to design a phononic crystal to have polychromatic spectral gaps utilizing a relatively simple geometric structure. Beyond its tremendous importance as an analysis tool in understanding certain selection rules in scattering processes and to examine spin-orbit coupling processes [36], the imprint of the symmetry of the system on the eigenmodes affords a powerful alternative to its usage as a tool to guide design of phononic crystals, cavities and waveguides, etc. Importantly, in this work, symmetry has allowed us to make sense of how to most completely deal with the vectorial nature of the in-plane elastic waves/phonons vis-a-vis our local design principles, to achieve our desired phononic structure. While the entire design principle might seem involved, one notes there that the salient point here is that the global symmetry principles determined the entire framework and language in an unambiguous manner, to allow us to "microscopically", or locally alter the dispersion relation in a coherent and controlled fashion. Symmetry has proven here, more than in the previous section, its power as an elegant language with which to design, not just analyse the dispersion relations because it laid the foundations with which to apply all the subsequent design principles which one has had to invoke to arrive the final design.

Here one developed a generalized framework for the design of Artificial Structures (AS) that control phonons, or elastic waves. The approach here differs from others because one focused on the fundamental physical limits of phonon propagation in structured materials, reducing the governing principles into an identifiable minimal set. One calls this the science of designing structures for manipulating phonons. By focusing on the own understanding of the propagation of phonons in structured materials, one believes that one will be able to develop a coherent understanding of phonon propagation that is valid across the meso-scales and is independent of the dimensionality and size of the structure. More

importantly, one believes that the current lack of a deterministic framework with which to guide the design of surfaces, waveguides and finite structures is due to the fact that technological concerns have been sometimes misinterpreted as scientific principles. One such instance is the reliance of fill fraction as a design parameter. Although a practical engineering parameter, fill fraction actually affects a multiplicity of issues in phonon propagation. These usually obscure the causal behaviour of $w(k)$ when fill fraction is viewed as a primary design parameter from the engineering perspective. Instead one takes inspiration instead from both a "more is different" [46] but at the same time, reductionist approach of paying care to the fundamental symmetries and develop the framework by building on symmetries and conservation principles. The framework utilizing group theory places the design of various phononic structures, crystals, metamaterials and plates on the same footing. Importantly, this point of view directly elucidates the vector nature of the phonon in a solid structure, an issue that has prevented the current scientific community from being able to identify the true underpinnings of the principles governing phonon propagation in Artificial Structures. The framework is surprisingly simple, in that it relies primarily only on two fundamental principles. One of these was the global group symmetry, which governs the allowed degeneracies of the eigenfrequencies at specific positions and along specific directions vis-a-vis the plane group and point group symmetry. The global symmetry imparts on the structure the second principle, namely the eigenmodes are classified by a set of irreducible representations. The irreducible representation confers significant physical insight: they are the actual classification of the polarization states of every eigenmode in any structure, just like the transverse and longitudinal modes, which one is familiar with, in bulk homogeneous systems. Moreover, the irreducible representations govern the possibility of interactions between different eigenmodes (scattering, resonant couplings, etc.), shaping the dispersion relations and forming the spectral gaps which result from avoided crossings of bands with the same irreducible representation. Furthermore, the irreducible representations, when viewed from a variational perspective, help interpret the relative positioning of the eigenfrequencies. For example, one utilized this to our advantage when designing the polychromatic phononic metamaterial, by controlling the positioning of eigenfrequencies in specific (anti)symmetric–symmetric pairs as a function of the energetics. This variational perspective of viewing the propagation of phonons is complimentary to the conventional microscopic method of tracing the time evolution of the equations of motion. It automatically incorporates all the interactions governing the final trajectory of the propagation into the set of possible $w(k)$ solutions for the structure. The two symmetry principles control the possibility of interactions and provide the framework and importantly, the language which one utilizes to design the dispersion relations. To realize the final design of a phononic structure, one further developed concepts, in our "symmetry" language, that govern the physical propagation of phonons within the structure. This is derived from conservation and continuity principles, enabling us to develop the concept of the dynamic mechanical bond and our lattice classification of the topology of the phononic structures. From the viewpoint of the continuity and flux equation

(Sect. 7.3), the variational perspective of flux flow in a inhomogeneous medium allowed us to uncover a simple material and geometric parameter in classifying the type of dynamics which the propagating phonons possess in artificial structures, leading to the concept of a dynamic mechanical bond and the classification of different structures, with different combinations (solid–solid, solid–air) into different lattice classes. This helped to reconcile a long-standing argument with regards to the optimal physical topography for a phononic crystal. Crucial to this was the recognition that one needs to separate the geometric definitions of the matrix and scattering phase from the material choices for each phase. This method of classification was able to identify and reconcile the observed phonon dynamics within these structures in a coherent fashion and properly subsumes previous results within this new lattice classification scheme. As a result, one is able to create phononic AS with a wide and even new set of properties, ranging from phononic materials with complete and polarization-specific meso-scale in plane gaps, to polychromatic gaps and to large single gaps that are a significant improvement over the current state of the art ($\sim$twofold to threefold), all by utilizing the same set of governing principles to deliberately design these properties. Many of these designs show a significant advancement over the current state of the art. Some of these, including the polychromatic band structure, have never been previously realized or thought possible and offer very interesting new routes towards the control of phonon–phonon interactions and even the moulding of nonlinear elastic waves. This new design paradigm for artificial structures allows new technologically useful properties via moulding phonon flow. The technological requirements and metrics become constraints and inputs for the realization of unique devices that exhibit novel behaviour enabled by the unique physics.

In this work, one developed a generalized framework for the design of Artificial Structures (AS) that control phonons, or elastic waves. The approach differs from others because we focused on the fundamental physical limits of phonon propagation in structured materials, reducing the governing principles into an identifiable minimal set. One calls this the science of designing structures for manipulating phonons. By focusing on the own understanding of the propagation of phonons in structured materials, one believes that one will be able to develop a coherent understanding of phonon propagation that is valid across the meso-scales and is independent of the dimensionality and size of the structure. More importantly, one believes that the current lack of a deterministic framework with which to guide the design of surfaces, waveguides and finite structures is due to the fact that technological concerns have been sometimes misinterpreted as scientific principles. One such instance is the reliance of fill fraction as a design parameter. Although a practical engineering parameter, fill fraction actually affects a multiplicity of issues in phonon propagation. These usually obscure the causal behaviour of $w(k)$ when fill fraction is viewed as a primary design parameter from the engineering perspective. Instead we take inspiration instead from both a “more is different” [46] but at the same time, reductionist approach of paying care to the fundamental symmetries and develop our framework by building on symmetries and conservation principles. The framework utilizing group theory places the design of various

phononic structures, crystals, metamaterials and plates on the same footing. Importantly, this point of view directly elucidates the vector nature of the phonon in a solid structure, an issue that has prevented the current scientific community from being able to identify the true underpinnings of the principles governing phonon propagation in Artificial Structures. The framework is surprisingly simple, in that it relies primarily only on two fundamental principles. One of these was the global group symmetry, which governs the allowed degeneracies of the eigenfrequencies at specific positions and along specific directions vis-a-vis the plane group and point group symmetry. The global symmetry imparts on the structure the second principle, namely the eigenmodes are classified by a set of irreducible representations. The irreducible representation confers significant physical insight: they are the actual classification of the polarization states of every eigenmode in any structure, just like the transverse and longitudinal modes, which we are familiar with, in bulk homogeneous systems. Moreover, the irreducible representations govern the possibility of interactions between different eigenmodes (scattering, resonant couplings, etc.), shaping the dispersion relations and forming the spectral gaps which result from avoided crossings of bands with the same irreducible representation. Furthermore, the irreducible representations, when viewed from a variational perspective, help interpret the relative positioning of the eigenfrequencies. For example, one utilized this to the advantage when designing the polychromatic phononic metamaterial, by controlling the positioning of eigenfrequencies in specific (anti)symmetric–symmetric pairs as a function of the energetics. This variational perspective of viewing the propagation of phonons is complimentary to the conventional microscopic method of tracing the time evolution of the equations of motion. It automatically incorporates all the interactions governing the final trajectory of the propagation into the set of possible $w(k)$ solutions for the structure. The two symmetry principles control the possibility of interactions and provide the framework and importantly, the language which one utilizes to design the dispersion relations. To realize the final design of a phononic structure, one further developed concepts, in our "symmetry" language, that govern the physical propagation of phonons within the structure. This is derived from conservation and continuity principles, enabling us to develop the concept of the dynamic mechanical bond and the lattice classification of the topology of the phononic structures. From the viewpoint of the continuity and flux equations (Sect. 7.3), the variational perspective of flux flow in a inhomogeneous medium allowed us to uncover a simple material and geometric parameter in classifying the type of dynamics which the propagating phonons possess in artificial structures, leading to the concept of a dynamic mechanical bond and the classification of different structures, with different combinations (solid–solid, solid–air) into different lattice classes. This helped to reconcile a long-standing argument with regards to the optimal physical topography for a phononic crystal. Crucial to this was the recognition that one needs to separate the geometric definitions of the matrix and scattering phase from the material choices for each phase. This method of classification was able to identify and reconcile the observed phonon dynamics within these structures in a coherent fashion and properly subsumes previous results within this new lattice

classification scheme. As a result, one is able to create phononic AS with a wide and even new set of properties, ranging from phononic materials with complete and polarization-specific meso-scale in plane gaps, to polychromatic gaps and to large single gaps that are a significant improvement over the current state of the art (∼twofold to threefold), all by utilizing the same set of governing principles to deliberately design these properties. Many of these designs show a significant advancement over the current state of the art. Some of these, including the polychromatic band structure have never been previously realized or thought possible and offer very interesting new routes towards the control of phonon-phonon interactions and even the moulding of nonlinear elastic waves. This new design paradigm for artificial structures allows new technologically useful properties via moulding phonon flow. The technological requirements and metrics become constraints and inputs for the realization of unique devices that exhibit novel behaviour enabled by the unique physics.

7.7 Thermoelectrics and Engineering Thermal Conductivity

Recent interest in the search for improved renewable and sustainable energy sources has highlighted the need for new technologies for harvesting energy; thermoelectric (TE) devices currently play a very minor role—mostly TE devices are employed in portable refrigeration units or as coolers for electronic equipment. However, with further research and exploitation, TE has a large future potential for major contribution to practical energy technologies since thermoelectrics can harvest energy from waste heat present in all technological processes. TEs thus provide the opportunity of an essentially "zero cost" source of either electrical power or cooling. At the same time, it is a well-known fact that controlling heat flow or phonon flow is a very challenging problem. The history of thermoelectric materials performance has exhibited essentially no change for nearly 40 years until the dramatic upswing in the figure of merit (ZT) in the past decade (Eq. 7.26). This sudden jump in progress can be attributed, in no small part, to the development of fabrication and characterization methods that allow manipulation of materials on the nanoscale. The efficiency of a thermoelectric device can be summarized in the following figure of merit (FOM):

$$\mathrm{ZT} = S(T)^2/\rho(\kappa_e + \kappa_l) \tag{7.26}$$

T = temperature, $S(T)$ = Seebeck Coefficient, ρ = electronic resistivity, κ_e = electronic thermal conductivity, κ_l = lattice thermal conductivity The efficiencies of both thermoelectric power generation as well as Peltier cooling depend on ZT. Hence, the higher the FOM, the more efficient a thermoelectric device and hence its potential to be an alternative energy source. The main strategy has been to

increase the Seebeck coefficient while at the same time reducing the electrical resistivity and thermal conductivity of the material system. The Seebeck coefficient, which corresponds to the voltage developed per unit temperature difference across the device, can be improved by controlling the electronic structure of the material, by engineering either the electronic density of states or the electronic transport properties of the material [39, 47]. At the same time the thermal conductivity (more specifically, the lattice contribution to the thermal conductivity) can be reduced by impeding phonon transport in the material. There have been many approaches for reducing the thermal conductivity, divided broadly into (1) bulk material composition approaches [47] and (2) artificial structuring of the material [48]. It is the latter approach that we focus on. Structuring of the thermoelectric material includes use of nanocomposites [5], superlattices [49] and nanowires. All these approaches aim to increase phonon scattering, by increasing the density of scattering surfaces/interfaces for the phonons by either geometrical confinement effects [nanowires, superlattices (in-plane propagation)] or introducing inhomogeneities in the structures [nanograin size composites, superlattice (out-plane)]. These approaches can be unified into the notion of fabricating materials with correct compositions and appropriate length scale structures, such that electrons and phonons will interact with the materials at their respective physical length scales, to produce the desired thermoelectric power generation or cooling effects. Appropriate length scales straddle the subnm to sub-micron regime and hence were not easily accessible until recently with the development of nanofabrication equipment—indeed, this explains the sudden jump in FOM via nanoscale breakthroughs over the past decade. Moreover, it appears that there has not yet been a clear focus towards a design strategy of an optimal thermoelectric material; theoretical approaches have explored only the available materials processing platforms or focused on computations for simple structures which have already been built. The structures considered have mostly been limited to superlattices; only recently have TE investigations been extended to nanostructures such as nanowires and nanocomposites. From a more fundamental perspective, current theoretical methods have not yet been able to make quantitative predictions on the thermal conductivity of nanostructured thermoelectric materials. Hence, while experimental capabilities have managed to allow access to these nanoscale dimensions, there are several fundamental notions on thermal transport and thermoelectric efficiency which have not been fully understood. It is important to note here that quantitative methods of predicting thermal conductivity would open the avenues not just to more efficient methods of designing optimal thermoelectrics, but also to the question of finally being able to control thermal management of structures and materials over the meso-scale, something that is crucial to device performance and reliability. For example, dielectric structures (films, multilayers) with high thermal conductivities are desired in order to rapidly dissipate heat on dense electronic device platforms, while structures with low thermal conductivities are required to enhance the efficiency of thermoelectrics. Theoretical methods that can quantitatively calculate and predict the conduction of heat at these small scales become crucial in the development of novel electronic and thermoelectric devices. While the strategies and routes towards

the nanoengineering of composite materials have been diverse, there remains a need for a series of rational design principles to help guide the realization of optimal structures for controlling thermal emission and thermal flow and phonon and photon propagation in general. A TE device that was structured as a phononic crystal would effectively reduce the thermal conductivity of the material while maintaining good electronic conductivity. This is possible because the physical de-Broglie wavelengths of phonons and electrons are very different, hence by structuring the materials at the correct length scales, one can selectively control the phonon behaviour and for example, increase the FOM by reducing thermal conductivity, while keeping the electron resistivity largely unaffected. For example, by adding inclusions(e.g. voids), one reduces both the electrical conductivity and the thermal conductivity by reducing the effective cross section (purely geometrical effect), but most importantly by designing the inclusion feature size and spacing to be on the order of the average phonon wavelength for the temperature of the material, we can greatly influence the phonon scattering by creating the set of interfaces between the two materials having quite different mechanical impedances and hence reduce the thermal conductance. Heat transport is nonlinear and is inherently coupled to the intrinsic material parameters of surface and interface roughness and compositional purity, which strongly impacts the mean free path and coherency of the phonons as well. The design framework allows us a coherent platform to probe the dynamics of phonon-phonon interaction because of our ability to correct classify the polarization states of the different phonon eigenmodes and hence the subsequent phonon–phonon interactions. This enables finding selection rules for the vector phonon-phonon interactions, something that has not been dealt with much so far [43]. From a scientific perspective, phonon–phonon interactions belong to the extremely rich realm of many-body physics. The control of the linear dispersion and most importantly, the polarization states, offer a promising route with which one may now design these AS to replicate many-body behaviour in a more-controlled manner, i.e. dealing with particular frequency regimes. While manipulating thermal conductivity points certainly to an immediate technological area of relevance, the possibilities of being able to rationally control the degree of (non)linearity in the interactions between phonons offers promise for the development of new thermal management materials.

7.8 Phononic Metamaterial Networks and Information Processing

The development of a complete theoretical tool-box operating with a universal set of design principles for the design of structures and devices with arbitrary application requirements would significantly open up technical applications and shorten the search for promising candidates for the desired device application before prototyping and subsequent experimental characterization. As previously mentioned, a

direct extension of this current work is the desire to enable wave propagation control using a structure with a form factor significantly more compact than that utilizing "scattering"; this was one of the touted considerations leading to the development of metamaterials, although this remains somewhat immature in its development. From a technological and device standpoint, it is important to be able to include form factor requirements in the development of devices that can exploit these unique phonon dynamics. Some of these questions include, how does one go about designing a finite device, based on the theoretical infinite systems in order to achieve the optimal level of performance possible in the required form factor? Producing entire classes of structures with unique opportunities for controlling the flow of photons and phonons within a wide window of frequencies/wavelengths, with the additional advantage of having a compact form factor (up to 1–2 orders of magnitude smaller compared to the wavelength of interest). Furthermore, by being able to create structures with different dispersion relations out of a single monolithic material, one will be able to design an entire network of structures that may almost arbitrarily mould, deflect and shape incident (non)linear elastic vector and acoustic scalar waves in a wide variety of applications, ranging from absorption to even information processing. To extend the work further, the generality of the framework is transitive from phonons to photons, spin waves as well as coupling interactions in inelastic processes. The proviso is to understand and classify the different waves into the correct lattice classes with respect to the structure we decide on.

7.9 Current and Future Work

The concepts of broken symmetry are general and can also apply to broken symmetries at an internal interface or free boundary. In bulk media, there are the well-known Stoneley modes and Rayleigh modes [4]. As the symmetry is broken along a free surface, in a semi-infinite medium, a new mode, the Rayleigh mode appears. This Rayleigh mode is an edge or surface mode, analogous to surface waves. In comparison, when we compare with a finite slab, as before in the classical Lamb plate the mirror symmetry and the presence of two symmetric boundaries, causes symmetry to be broken at two spatial locations, leading to two broken symmetry modes. In this case, the mirror plane forces the Rayleigh-like modes to be coupled at both boundaries, forming, symmetric and anti-symmetric irreducible representations with respect to the mirror plane.

This simple problem is exactly analogous to the situation of surface modes of phononic metamaterials. Current work in the community suffers from a lack of a governing principle with which to design a surface of an otherwise bulk volume phononic or photonic metamaterial. The design of the surface is extremely important for devices because the interface between the device and the external (interacting) environment governs the propagation and hence distribution of information within the metamaterial. Once again, the link between this demonstration of broken symmetry leading the presence of a surface, interface or edge

mode and that of surface, edge and interface modes lies once again in the length scale of the propagating waves and the artificial structure inhomogeneity. To reiterate, the eventual goal of this approach is, to borrow from PW Anderson's famous words, that "more is different", to understand complexity from a set of simple principles. In a somewhat analogous approach, we have focused on only utilizing the underlying symmetries of the system to deduce the possible eigenmodes of phonons. Moreover, the framework is not restricted to phonons, but works for all fields, vector or scalar, with the only proviso that one correctly identify the relevant length scales. This suggests that this approach would enable the design of efficient multifunctional phononic–photonic–magnonic networks that the different kinds of waves with one another at specific spatial locations because our design rules are not based on artificial requirements of infinite periodicity and may treat interfaces, boundaries and the bulk alike. It is interesting to contemplate Nature's various phononic networks, the auditory systems of all living organisms. From the complexity and meso-scale multiple sensing auditory system of insects to the compact yet broadband auditory systems of humans, it will be interesting to determine if nature exploits symmetries to develop an efficient auditory systems, subject to the needs of various situational awareness and of course, the constraint of the available constituent materials found in all living forms. A "complex" system can be described by a few "simple" fundamental principles, just like how a complicated phononic band structure can be described and dictated by a few governing rules. To truly realize a multifunctional phononic–photonic–magnonic metamaterial network, this same set of underlying simple principles will provide a tractable way for us to realize fully functional integrated material platforms and extend the materials design and performance paradigm and to be able to control complexity with simplicity.

References

1. Bloch, F.: Uber die Quantemechanikder Electroneninkristallgittern. Z. Phys. **52**, 555 (1928)
2. For a review, see El Boudouti, E.H., Djafari Rouhani, B., Akjouj, A., Dobrzynski, L.: Acoustic waves in solids and fluid layered materials. Surf. Sci. Rep. **64**, 471 (2009)
3. Rytov, S.M.: Acoustical properties of a thinly laminated medium. Sov. Phys. Acoust. **2**, 6880 (1956)
4. Sigalas, M.M., Economou, E.N.: Band structure of elastic waves in two dimensional systems. Solid State Commun. **86**, 141 (1993)
5. Kushwaha, M.S., Halevi, P., Dobrzynski, L., Djafari-Rouhani, B.: Acoustic band structure of periodic elastic composites. Phys. Rev. Lett. **71**, 2022 (1993)
6. Kushwaha, M.S., Halevi, P., Dobrzynski, L., Djafari-Rouhani, B.: Theory of acoustic band structure of periodic elastic composites. Phys. Rev. B **49**, 2313 (1994)
7. Sigalas, M.M., conomou, E.N.: Elastic and acoustic wave band structure. J. Sound Vib. **158**, 377 (1992)
8. Vasseur, J.O., Djafari-Rouhani, B., Dobrzynski, L., Kushwaha, M.S., Halevi,P.: Complete acoustic band gaps in periodic fibre reinforced composite materials: the carbon/epoxy and some metallic systems. J. Phys.: Condens. Matter **7**, 8759–8770 (1994)

9. For a review, see Sigalas, M.M., Kushwaha, M.S., Economou, E.N., Kafesaki, M., Psarobas, I.E., Steurer, W.: Classical vibrational modes in phononic lattices: theory and experiment. Z. Kristallogr. **220**, 765–809 (2005)
10. For a recent review, see Pennec, Y., Vasseur, J., Djafari Rouhani, B., Dobrzynski, L., Deymier, P.A.: Two-dimensional phononic crystals: examples and applications. Surf. Sci. Rep. **65**, 229 (2010)
11. Yablonovitch, E.: Inhibited spontaneous emission in solid-state physics and electronics. Phys. Rev. Lett. **58**, 2059–2062 (1987)
12. Joannopoulos, J.D., Meade, R.D., Winn, J.N.: Molding the Flow of Light, vol. 47. Princeton University Press, Princeton, 1995. 2 Fundamental Properties of Phononic Crystal
13. Psarobas, I.E., Modinos, A., Sainidou, R., Stefanou, N.: Acoustic properties of colloidal crystals. Phys. Rev. B **65**, 064307 (2002)
14. Sainidou, R., Stefanou, N., Modinos, A.: Formation of absolute frequency gaps in threedimensional solid phononic crystals. Phys. Rev. B **66**, 212301 (2002)
15. Still, T., Cheng, W., Retsch, M., Sainidou, R., Wang, J., Jonas, U., Fytas, G.: Simultaneous occurrence of structure-directed and particle-resonance-induced phononic gaps in colloidal films. Phys. Rev. Lett. **100**, 194301 (2008)
16. Croënne, C., Lee, E.J.S., Hu, H., Page, J.H.: Band gaps in phononic crystals: generation mechanisms and interaction effects. AIP Adv. **1**, 041401 (2011)
17. Liu, Z., Zhang, Y., Mao, Zhu, Y.Y., Yang, Z., Chan, C.T., Sheng, P.: Locally resonant sonic materials. Science **289**, 1734–1736 (2000)
18. Torres, M., Montero de Espinosa, F.R., Garcia-Pablos, D., Garcia, N.: Sonic band gaps in finite elastic media: surface states and localization phenomena in linear and point defects. Phys. Rev. Lett. **82**, 3054 (1999)
19. Kafesaki, M., Sigalas, M.M., Garcia, N.: Frequency modulation in the transmittivity of wave guides in elastic-wave band-gap materials. Phys. Rev. Lett. **85**, 4044 (2000)
20. Khelif, A., Djafari-Rouhani, B., VasseurJ. O., Deymier, P.A., Lambin, P., Dobrzynski, L.: Transmittivity through straight and stublike waveguides in a two-dimensional phononic crystal. Phys. Rev. B **65**, 174308 (2002)
21. Khelif, A., Djafari-Rouhani, B., Vasseur, J.O., Deymier, P.A.: Transmission and dispersion relations of perfect and defect-contained waveguide structures in phononic band gap materials. Phys. Rev. B **68**, 024302 (2003)
22. Khelif, A., Djafari-Rouhani, B., Laude, V., Solal, M.: Coupling characteristics of localized phonons in photonic crystal fibers. J. Appl. Phys. **94**, 7944–7946 (2003)
23. Khelif, A., Chouja, A., Djafari-Rouhani, B., Wilm, M., Ballandras, S., Laude, V.: Trapping and guiding of acoustic waves by defect modes in a full band-gap ultrasonic crystal. Phys. Rev. B **68**, 214301 (2003)
24. Khelif, A., Choujaa, A., Benchabane, S., Djafari-Rouhani, B., Laude, V.: Guiding and bending of acoustic waves in highly confined phononic crystal waveguides. Appl. Phys. Lett. **84**, 4400 (2004)
25. Benchabane, S., Khelif, A., Choujaa, A., Djafari-Rouhani, B., Laude, V.: Interaction of waveguide and localized modes in a phononic crystal. Europhys. Lett. **71**, 570 (2005)
26. Pennec, Y., Djafari-Rouhani, B., Vasseur, J.O., Larabi, H., Khelif, A., Choujaa, A., Benchabane, S., Laude, V.: Acoustic channel drop tunneling in a phononic crystal. Appl. Phys. Lett**. 87**, 261912 (2005)
27. Esposito, G., Marmo, G., Sudarshan, G.: From Classical to Quantum Mechanics: An Introduction to the Formalism Foundations and Applications. Cambridge University Press, UK (2010)
28. Seol, J.H., Jo, I., Moore, A.L.: Two dimensional phonon transport in supported graphene. Science **328**, 213–216 (2010)
29. Balandin, A., Wang, K.L.: Significant decrease of the lattice thermal conductivity due to phonon confinement in a free-standing semiconductor quantum well. Phys. Rev. B. **58**(3), 1544(1998)

30. Economou, E.N., Zdetsis, A.: Classical wave propagation in periodic structures. Phys. Rev. B **40**, 1334 (1989)
31. Liu, Z.Y., Zhang, X.X., Mao, Y.W., et al.: Locally resonant sonic materials. Science. **289**, (5485), 1734(2000)
32. Whitham, G.B.: Linear and Nonlinear Waves. Wiley-Interscience, USA (1970)
33. Goldstone, J., Salam, A., Weinberg, S.: Broken symmetries. Phys. Rev. **127**, 965 (1962)
34. Miklowitz, J.: The Theory of Elastic Waves and Waveguides. North Holland Publishing Company, Netherlands, p.215 (1978)
35. Nye, J.F.: Physical Properties of Crystals: Their Representations by Tensors and Matrices. Oxford University Press, UK (1957)
36. Lax, M.J.: Symmetry Principles in Solid State and Molecular Physics. Wiley, USA (1974)
37. Wigner, E.P.: The Theory of Groups and Quantum mechanics. Methuen and Company, London (1931)
38. Sternberg, S.: Group Theory and Physics. Cambridge University Press, UK (1995)
39. Poudel, B., Hao, Q., Ma, Y. et al.: High-thermoelectric performance of nanostructured bismuth antimony telluride bulk alloys. Science. **320**(5876), 634(2008)
40. Simovski, C.R.: Material parameters of metamaterials. Opt. Spectrosc. **107**, 726 (2009)
41. Kafesaki, M., Economou, E.N.: Intepretation of the band structure results for elastic and acousticwaves by analogy with the LCAO Approach. Phys. Rev. N. **52**(18), 13317 (1995)
42. Mei, J., Liu, Z., Wen, W., Sheng, P.: Effective dynamic mass density of composites. Phys. Rev. B. **76**, 134205 (2007)
43. Still, T., Cheng, W., Retsch, M., Sainidou, R., et al.: Simultaneous occurrence of structure-directed and particle-resonance-induced phononic gaps in colloid films. Phys. Rev. Lett. **100**, 194301 (2008)
44. Ziman, J.: Electrons and Phonons. Clarendon Press, UK (1962)
45. Cloizeaux, J.D.: Analytical properties of n-dimensional energy bands and Wannier functions. Phys. Rev. **129**, 554 (1963)
46. Anderson, P.W.: More Is different. Science **177**, 4047 (1972)
47. Nolas, G.S., Sharp, J., Goldsmid, H.J.: Thermoelectrics: Basic Principles and New Materials Development. Springer Press, Berlin (2001)
48. Harmann, T.C., et al.: Quantum dot superlattice thermoelectric materials and devices. Science **297**, 2229 (2002)
49. Venkatasubramaniam, R., Silvola, E., Colpitts, T., et al.: Thin-film thermoelectric devices with high room-termperature figures of merit. Nature **413**(6856), 597 (2001)

Chapter 8
Local Resonant Structures

Abstract The local resonance in the material was discovered in 2000. Since then, it has been developed as an acoustical metamaterial. The local resonance enables negative mass density and negative bulk modulus. A detailed description of the physics of local resonance is given. This is followed by several applications and even a list of potential areas under the early stage of development is given.

8.1 Introduction

The science of acoustic metamaterials begins with the study of phononic crystals around the early 1990s. Metamaterials are artificial materials capable of controlling and manipulating functionalities beyond the limits of natural materials. The concept of photonic crystals was proposed in late 1980s [1–4] and the concept of phononic crystal in early 1990s [1–4]. Both are realized experimentally [5–7]. Both concepts have involved with band gaps. The concept of band gap is the same as that of the band theory of solids in quantum mechanics. Here, electron waves interact with periodically structured atomic lattice to form energy bands separated by energy gaps. The formation of band gap will take place when the lattice constant has to be of the same order as the wavelength. Due to the long wavelength of sound wave in the audible range, phononic crystals are usually realized in the ultrasonic frequency regime. The arrival of acoustic metamaterial will resolve the sample size problem and introduce new functionalities.

To understand the origin of acoustic metamaterials, it would be useful to start with the phononic crystals.

W.S. Gan, *New Acoustics Based on Metamaterials*, Engineering Materials,
https://doi.org/10.1007/978-981-10-6376-3_8

8.2 Background of Phononic Crystals

Phononic crystals like photonic crystals belong to the class of metamaterials known as band gap metamaterials. This class of metamaterials is as important as double negative metamaterials (DNG).

The 1980s has seen a tremendous research interest in the physical properties of artificial structures comprised of two or more materials which differ in certain properties. The 1980s began with enthusiasm for microstructures of reduced dimensionality [8] such as quantum heterostructures, quantum wires and quantum dots. In the late 1980s, there has been ever increasing interest in macrostructures known as photonic crystals [1]. Typically, these are periodic arrays of two transparent dielectrics. The periodicity plays a crucial role in understanding the physical properties of both microstructures and macrostructures. One important aspect in photonic crystals is the formation of forbidden frequency bands in which electromagnetic (EM) modes spontaneous emission and zero-point fluctuations are all absent [9]. In this chapter, we deal with phononic crystals which are elastic composites made up of two materials with different elastic properties. In analogy to the case of phononic crystals, the emphasis will be on the existence of complete phononic band gaps for the elastic composites and their practical implications. The earliest papers on theoretical studies of phononic crystals are given in Refs. [3, 4, 10–12]. In Ref. [10], a periodic array of parallel rods of circular cross section embedded in a different background was considered. The intersection of these rods with perpendicular plane forms a two-dimensional lattice. Sigalas and Economou [10] investigated only the transverse polarization mode with displacement $\vec{u}(\vec{r}, t)$ parallel to the cylinders (and perpendicular to the Bloch wave vectors). The computations performed for Ni(Al) alloy cylinders in Al(Ni) alloy background exhibited absolute band gap extending throughout the Brillouin zone. Sigalas and Economou [10] also considered the mixed (longitudinal transverse) polarization modes for which $\vec{u}(\vec{r}, t)$ and the Bloch wave vectors are in the plane perpendicular to the cylinders. They found that Au cylinders in Be matrix exhibit a narrow, but complete gap, shared by both polarization. An elaborate theory of acoustic band structure in periodic composites of arbitrary dimensionality is presented in Ref. [4].

Analogous to the photonic crystals in the frequency range of a phononic band gap, vibrations, sound and phonons would be forbidden. From a practical point of view, a complete phononic band gap could be engineered to provide a vibrationless environment for high-precision mechanical devices in a given frequency range. Phononic crystals in the form of piezoelectric and pyroelectric composites have already found useful applications in transducers for pulse-echo medical ultrasonic imaging and for transmitting and receiving signals underwater [6, 11–14].

An adequate of a phononic crystal composite transducer requires a detailed understanding of elastic wave propagation in periodic structures, so that the characteristic dimensions of the transducer disc and the composite may be correctly chosen. For such understanding, the availability of band structures is essential.

For acoustic devices based on periodic composites, the width of the band gaps and the midgap frequency (frequencies) play an essential role. For these elastic composites, the details of the gaps depend on the structure of the crystal lattice, on the average density and average elastic constant contrast C_{44} of the two constituent solids, on their density contrast and elastic constant contrast, on the filling fraction of one of the constituents and on the lattice constant. An elaborate study of such a complicated dependence is a major task.

Experimental studies on phononic crystals are given in Refs. [6–15], demonstrating the usefulness of acoustic waves in illustrating general features of wave propagation in inhomogeneous or random media.

8.3 Theory of Phononic Crystals—The Multiple Scattering Theory (MST)

The theory of phononic crystals will involve the calculations of acoustic wave propagation in periodic structures. The ultimate purpose is to find the existence of band gap in the periodic structures which is analogous to the photonic band gaps in photonic crystals, and the calculations have been performed using the plane wave (PW) method, which is based on the expansion of the periodic coefficients in the wave equations in Fourier sums. Study using the PW methods shows that band gap can exist under rather extreme conditions that concern mainly the elastic parameters (density, velocities) of the components of the composite, the volume fraction of one of the two components and the topology. However, the PW method is unable to describe composites with solid scatterers in a fluid.

Here, we shall follow the multiple scattering (MS) approach of Kafesaki and Economou [16] based on the well-known (in the band-structure electronic community) Korringa–Kohn–Rostoker (KKR) theory [17, 18].

Spherical scatterers embedded in a fluid host were considered by Kafesaki and Economou [16]. They start from the acoustic wave equation in a periodic medium:

$$\lambda(\vec{r})\nabla\left[\frac{1}{\rho(\vec{r})}\nabla P(\vec{r})\right] + \omega^2 P(\vec{r}) = 0 \tag{8.1}$$

where P = acoustic pressure, $\mathrm{p}(\vec{r})$ = mass density, ω = sound angular frequency, $\lambda = \rho\left(c_\mathrm{l}^2 - c_\mathrm{t}^2\right)$ = Lamé coefficient of the medium, $c_\mathrm{l}, c_\mathrm{t}$ = longitudinal and transverse sound velocities, respectively.

Equation (8.1) can be rewritten as

$$\nabla^2 P(\vec{r}) + \frac{\omega^2}{c_o} P(\vec{r}) + \omega^2\left[\frac{1}{c^2(\vec{r})} - \frac{1}{c_o^2}\right] P(\vec{r}) + \rho(\vec{r})\left[\nabla\frac{1}{\rho(\vec{r})}\right]\nabla P(\vec{r}) = 0 \tag{8.2}$$

which has the form

$$H_o(\vec{r})P(\vec{r}) + U(\vec{r})P(\vec{r}) = 0 \tag{8.3}$$

where $H_o(\vec{r})p(\vec{r}) = 0$, $H_o(\vec{r}) = \nabla^2 + \frac{\omega^2}{c_o^2}$ represents the wave equation in the absence of scatterers, and c_o is the wave velocity in the host material.

Equation (8.3) has the same form as the Schrödinger equation for the electron waves. This analogy shows that one can extend the KKR to the acoustic case. However, one has to beware of the important difference between the electronic case and the acoustic case. That is, the potential in the acoustic case has a δ function singularity at the surface of the scatterers due to the factor ∇p^{-1}. Thus, the contribution of the surface scattering to the volume integrals is not negligible as in the electronic case [18].

It can be shown that [19] in a periodic system Eq. (8.2) is equivalent to the following integral equation:

$$P(\vec{r}) = \int_U G\left(\vec{r} - \vec{r'}\right) V(\vec{r}) P\left(\vec{r'}\right) \mathrm{d}\vec{r'} \tag{8.4}$$

where V = volume of a unit shell, $V(\vec{r})$ = local potential.

The Green function $G\left(\vec{r} - \vec{r'}\right)$ is given by

$$G\left(\vec{r} - \vec{r'}\right) = \sum_n \mathrm{e}^{i\vec{k}\cdot\vec{R}_n} G_o\left(\vec{r} - \vec{r'} - \vec{R}_n\right) \tag{8.5}$$

G_0 is the Green's function [20] for the homogeneous equation $H_o(\vec{r})P(\vec{r}) = 0$:

$$G_o\left(\vec{r} - \vec{r'}\right) = -\frac{1}{4\pi} \frac{\mathrm{e}^{iK_o\left|\vec{r} - \vec{r'}\right|}}{\left|\vec{r} - \vec{r'}\right|}, \quad K_o = \frac{\omega}{c_o} \tag{8.6}$$

$V(\vec{r})$ is zero outside the unit shell centred at the origin of the coordinate system. It is related to U by $U(\vec{r}) = \sum_n V\left(\vec{r'} - \vec{R}_n\right)$, and the pressure field $P(\vec{r})$ obeys the Bloch's condition, $P\left(\vec{r} + \vec{R}_n\right) = \mathrm{e}^{i\vec{k}\cdot\vec{R}_n} P(\vec{r})$.

Taking into account that for acoustic waves the local potential V is nonzero only inside and at the surface of the scatterers (8.2), the integral over the unit shell in Eq. (8.4) is reduced to an integral over the volume of a scatterer ($r' \leq r_s$, r_s is the scatterer radius).

$$\int_V \mathrm{d}\vec{r'} = \lim_{\in \to 0+} \int_{\vec{r'} \leq r_s + \in} \mathrm{d}\vec{r'} \tag{8.7}$$

The limiting procedure in Eq. (8.7) ensures that we approach the surface of the sphere from inside, including the surface singularity.

By noticing that for nonoverlapping spheres and $\vec{r}, \vec{r'}$ inside a unit shell centred at the origin of the coordinate system, the function G obeys the equation

$$\nabla^2 G\left(\vec{r}-\vec{r'}\right)+K_o^2 G\left(\vec{r}-\vec{r'}\right)=\delta\left(\vec{r}-\vec{r'}\right) \tag{8.8}$$

and by the wave equation and the Gauss theorem, the volume integral in Eq. (8.7) can be transformed into a surface integral.

After some algebraic manipulations, one can find that

$$\lim_{r'\to r_s^+}\int_{s'}\left[P\left(\vec{r'}\right)\nabla_{r'}G\left(\vec{r}-\vec{r'}\right)-G\left(\vec{r}-\vec{r'}\right)\nabla_{r'}P\left(\vec{r'}\right)\right]\mathrm{d}\vec{s'}=\begin{cases}P\left(\vec{r'}\right) & \text{for } r>r_s\\ 0 & \text{for } r<r_s\end{cases} \tag{8.9}$$

where s' is a spherical surface of radius r', centred at the origin of the coordinates. $r'\to r_s^+$ in the above limit denotes that we approach the sphere surface from the outside. This is a direct consequence of (8.7), and it is very important for the acoustic case as the integrated functions are not continuous across the surface. The acoustic pressure is continuous, but its derivative has a step function discontinuity. Thus, the side limits do not coincide. The solution of Eq. (8.9) for $r<r_s$ gives the eigenfrequencies of our periodic system for each Bloch's vector $\vec{k}$. To obtain this solution, we use the fact that both the functions $G\left(\vec{r}-\vec{r'}\right)$ and $P\left(\vec{r'}\right)$ can be expanded in spherical functions of $\vec{r}$ and $\vec{r'}$:

$$G\left(\vec{r}-\vec{r'}\right)=\sum_{\ell m}\sum_{\ell' m'}\left[\begin{array}{c}A_{\ell m\ell' m'}\bar{j}_\ell(K_o r)\bar{j}_{\ell'}(K_o r')\\ +K_o j_\ell(K_o r)y_{\ell'}(K_o r')\delta_{\ell\ell'}\delta_{mm'}\end{array}\right]\times Y_{\ell m}(\vec{r})Y^*_{\ell' m'}\left(\vec{r'}\right) \tag{8.10}$$

for $r<r'$

$$\begin{aligned}P\left(\vec{r'}\right)\Big|_{r'\geq r_s}&=P^{\text{out}}\left(\vec{r'}\right)\\&=\sum_{\ell m}a_{\ell m}[j_\ell(K_o r')+t_\ell h_\ell(K_o r')]Y_{\ell m}\left(\vec{r'}\right)\end{aligned} \tag{8.11}$$

and second-kind spherical Bessel functions of order ℓ and $h_\ell=j_\ell+iy_\ell$.

Substituting Eqs. (8.10) and (8.11) into Eq. (8.9), we obtain the final multiple scattering equation:

$$\sum_{\ell' m'}[A_{\ell m\ell' m'}-K_o I_m\left(t_{\ell'}^{-1}\right)\delta_{\ell\ell'}\delta_{mm'}]a_{\ell' m'}=0 \tag{8..12}$$

The coefficients $A_{\ell m \ell' m'}$ in the above equations are called structure constants, and they depend on $\vec{K}$, ω and the lattice constants. The coefficients t_ℓ, relating the incident to the scattered field at each scatterer, can be calculated by solving a single-scattering problem.

Equation (8..12) can be rewritten as

$$\sum_{\ell' m'} A_{\ell m \ell' m'} a_{\ell' m'} = 0 \Leftrightarrow \sum_{L'} \Lambda_{LL'} a_{L'} = 0, \quad L \equiv (\ell, m) \tag{8.13}$$

which corresponds to a linear homogeneous algebraic system. The condition for this system to have nonvanishing solutions, $\det(\Lambda) = 0$, gives the eigenfrequencies of the periodic composite.

A careful analysis of the above equations show that the elastic parameters of the scattering material affect the calculation only through the scattering coefficients t_ℓ. t_ℓ can be calculated very easily and accurately for both solid and fluid scatterers. Thus, the method can be applied to both solid and fluid scatterers changing only the form of a single-scattering problem. This, however, is not the only advantage of the method. Its most important advantage is that it can be applied also in disordered system. It can treat system with positional as well as substitutional disorder.

8.3.1 Details of Calculation

The eigenmodes of a periodic system are obtained by requiring nonvanishing solutions for the linear homogeneous system (Eq. 8.13). Thus, one has to calculate the matrix X, the determinant of which has to be set equal to zero. The order of the matrix Λ depends on the number of the angular momentum term that we keep in the field function (8.11) in the calculations of Kafesaki and Economou [16]. They obtained good convergence by keeping the maximum number of $\ell = \ell_{\max} = 3$ or 4, while for the lower bands they had good convergence with $\ell_{\max}$ less than 3.

Another parameter of the problem is the size of the periodic system. Kohn and Rostoker [18] have considered a system of 400–500 lattice vectors in the direct as well as the reciprocal lattice with excellent convergence.

Among the calculational problems of the multiple scattering method, one worth mentioning is the problem of the spurious "roots". That is the sign changes of the determinant that do not correspond to actual eigenfrequencies of the system.

8.3.2 Discussion of Results

Figure 8.1 shows the band structure along the $L\ \Gamma$ and ΓX directions for an FCC periodic composite consisting of solid spheres in water host. The volume fraction of the spheres is f_s = 50%. Figure 8.1b shows the band structure for fluid spheres of

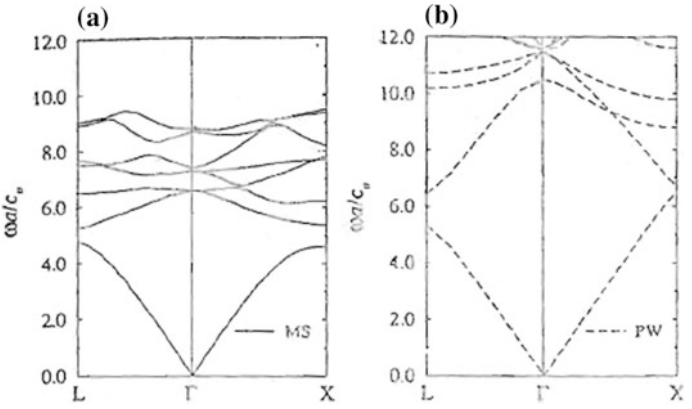

Fig. 8.1 Dispersion relation along the $L\Gamma$ and ΓX directions for an fcc periodic composite consisting of solid spheres in water. The parameters are as follows: $\frac{\rho_o}{\rho_n} = 1/2$, $\frac{c_o}{c_{ti}} = 1/2$, $\frac{\lambda_o}{\lambda_i} = 1/4$, $\frac{c_{li}}{c_{ti}} = 1/2$. Volume fractions of spheres $f = 50\%$. c_o is the wave velocity in the host and a the lattice constant. **a** Shows the result within MS method and **b** the same with PW and Eq. (15.3.1) [16]

the same λ and ρ as the solid ones and in the same periodic arrangement also in water host. Figure 8.1b shows the band-structure results for the same material combination using the plane wave (PW) method. The results are very different, which shows that the replacement of solid scatterers with fluids can change the band structure drastically.

The results for different material system consisting of glass spheres are shown in Fig. 8.2. This is in SC structure and glass volume fraction $f = 45\%$. Again here, the left panel is MS method result and the right is using PW method. Compared to

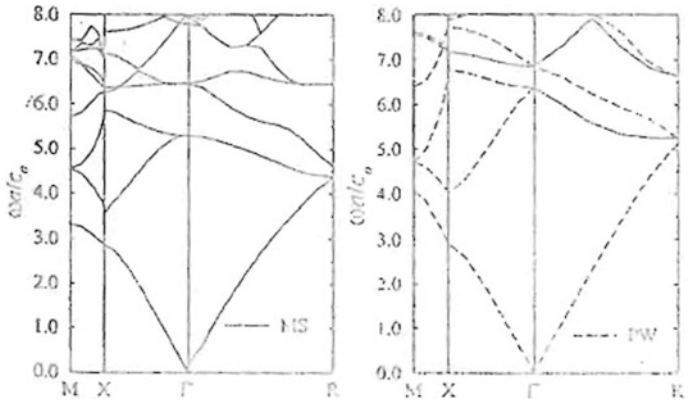

Fig. 8.2 Dispersion relation along the MX ΓR directions for a sc periodic composite consisting of glass spheres in water. Glass volume fraction $f = 45\%$. c_o is the wave velocity in the water and a the lattice constant [16]

Fig. 8.1, the difference between the MS result and the PW result is reduced. This means that reduction of the influence of the rigidity of the scatterers can be attributed to the larger velocity and density contrast between scatterers and host. The velocity and mainly the density contrast between scatterers and host are the most important parameters controlling the scattering and thus the propagation in the composite system. As these contrasts increase, other parameters as the rigidity of the scatterers become less important [21, 22].

8.4 Multiple Scattering Approach to Perfect Acoustic Lens

The multiple-scattering theory (MST) usually known as the KKR (Korringa, Kohn and Rostoker) approach [17, 18] was developed mainly for the calculation of electronic band structures although it originated from the study of classical waves including acoustic waves used by Liu et al. [23] to calculate the propagation of sound waves in periodic structures such as phononic crystals. The phononic crystals in this case are stainless steel balls immersed in water. They found theoretical and experimental agreement using ultrasound experiment of the observation of a sizable directional stopband in the transmission along (001) centred at about 0.65 units, coincides with unexpectedly directional gap along the Γ–x direction in the band structure. In the transmission along (111), they observed a narrow stopband at about 0.65 units, corresponding to the small gap at the L point in the band structure at the same frequency.

Other works on the studies on the existence and properties of phonon band gap are given in [4, 10]. These are due to Bragg scattering when the sound wavelength is comparable with the lattice constants. This leads to frequency bands where wave propagation is forbidden. This enables the understanding of how to achieve large complete band gaps in physically realizable materials and the mechanism of wave transport at band frequencies due to tunnelling [22]. Also, there has been relatively less attention paid to investigate how periodicity affects wave propagations over a wide range of frequencies outside the band gaps where novel refraction, diffraction and focusing effects may be possible.

At low sound frequencies, an effective continuum or medium approximation can be used to study the wave properties and accurately predict the wavespeed. In this frequency range, there is much common with the properties of low-frequency phonons in atomic crystals, where phonon focusing phenomena have been systematically studied [24]. However, at higher frequencies, much less is known about the behaviour of pass bands where the wavelengths can be much less than the lattice constant. Yang et al. have addressed this problem by theoretically and experimentally investigating the character of wave pattern and propagation in a 3D phonon crystal at frequency above the first complete band gap. They showed how a dramatic variation in wave propagation with both frequency and propagation direction can lead to novel focusing phenomena associated with large negative refraction. This is a different approach to negative refraction from that of

Veselago's work for the electromagnetic wave based on negative values of permittivity and permeability. They demonstrated the effect of negative refraction experimentally by using ultrasound technique to image the transmitted wave field and show that a flat crystal can focus a diverging incident beam into a sharp focal spot that can be seen remarkably far from the crystal.

They also calculated the field pattern theoretically using a Fourier imaging technique in which wave propagation through the crystal is accurately described by the 3D equifrequency surfaces predicted from the multiple scattering theory (MST) [25]. Their theoretical results also give an excellent explanation of the experimental data, showing how wave physics in the regime can be accurately modelled and how the theoretical structures on the equifrequency surfaces of phonon crystal can give rise to potential applications.

Zhang and Liu [26] first discussed the issue of negative refraction for acoustic waves in phononic crystals. They also repeated the observation of the negative refraction of the acoustic wave in phononic crystals, occurring at the frequencies with $\vec{S} \cdot \vec{k} > 0$ where $\vec{S}$ represents the Poynting vector. They considered a 2D phononic crystal consisting of infinite-length "rigid" or liquid cylinders embedded in a background, which has been studied extensively in Ref. [19–21]. Two types of phononic crystals were used by them: one is steel cylinders in air background, and the other is water cylinders in mercury background. The band structures of these two types of phononic crystals are plotted in Figs. 8.3a and 8.1b, respectively. Both of them were calculated by the MST (or Korringa–Kohn–Rostoker method given in Refs. [17, 18]).

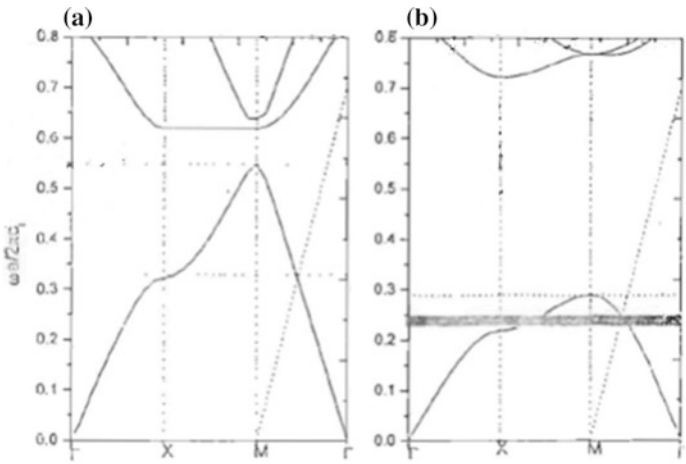

Fig. 8.3 **a** Acoustic band structures for a square lattice of steel cylinders in air background with cylinder radius $R = 0.36a$. **b** The acoustic band structures for a square lattice of water cylinders in mercury background with cylinder radius $R = 0.4a$. The light line shifted to M is shown in dashed line. Dot-dashed lines mark the region for negative refraction, and the shadow represents the AANR region [26]

To visualize and analyse refractive effects of the acoustic wave when it hits the above phononic crystal interfaces, Zhang and Liu [26] investigated the equifrequency surfaces (EFS) of the band structures just like the case for the electromagnetic waves in the photonic crystals because the gradient vector of constant-frequency contours in k-space gives the group velocities of the phononic modes. Hence, the propagation direction of energy velocity of acoustic wave can be reduced from them. The EFS can also be calculated using the MST or the Korringa–Kohn–Rostoker method. The features of the EFS for these two kinds of system within the first band are similar. Thus, only the results of water–mercury system with $R = 0.4a$ are shown in Fig. 8.4. The equifrequency surface contours at several relevant frequencies such as 0.05, 0.1, 0.2, 0.235 and 0.27 are demonstrated. It is clear that the lowest band has $\vec{S} \cdot \vec{k} > 0$ everywhere within the first Brillouin zone, meaning that the group velocity is never opposite to the phase velocity. The 0.05 and 0.1 contours are very close to a perfect circle, and the group velocity at any point of the contour is collimated with the k vector, indicating that the crystal behaves like an effective homogeneous medium at these two long wavelengths. The 0.2 contour is little bit distorted from a circle, and the 0.235 contour is convex around the M point due to a negative phononic "effective band". The conservations

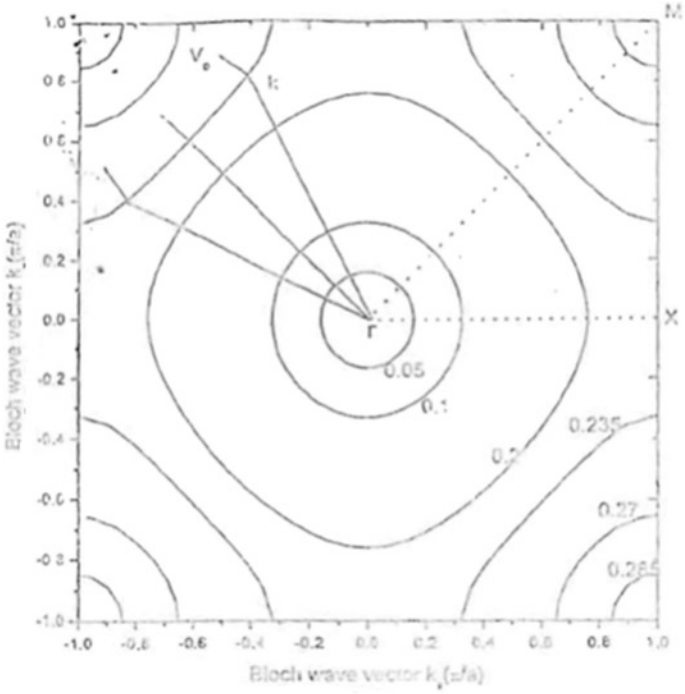

Fig. 8.4 Several constant-frequency contours of the first band of the 2D phononic crystal, which is composed of a square lattice of water cylinders in mercury background with $R = 0.4a$. The numbers in the figure mark the frequencies in unit of $2\pi\ c_l/a$ [26]

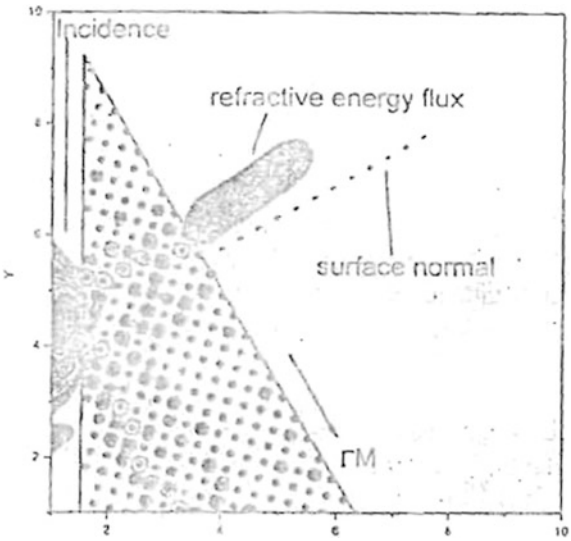

Fig. 8.5 Simulation of negative refraction. The boundaries of the sample are marked with black frame. The intensity of pressure field for incidence and refraction is shown in different shadows. A wedged sample considered here consists of water cylinders in mercury background with $R = 0.4a$ as shown on top of the figure. The frequency of incident wave is $\omega = 0.235(2\pi\, c_l/a)$ [26]

of the component along the surface of refraction would result in the negative refractions effect in some frequency region, marked as dotted lines in Fig. 8.5.

Furthermore, according to the analysis approach of [26, 27], the required condition for all-angle negative refraction (AANR) effect in some cases can be observed. Under these conditions, an acoustic beam incident on the ΓM surface with various incident angles will couple to a single Bloch mode that propagates into this crystal on the negative side of the boundary normal. Therefore, we can define a frequency region for the AANR by using these criteria.

From Fig. 8.5a, we noted that the AANR region is absent in the steel–air system, although the negative refractive region is very large. However, in the water–mercury system, the AANR region exists within the range of about 63 near $\omega = 0.24(2\pi c_l/a)$ (shadow region in Fig. 8.1b). This point differs for the two kinds of system. This difference is very important for the superlensing and focusing of acoustic waves in phononic crystals.

In order to test this theoretical analysis, Zhang and Liu [26] performed a numerical simulation to the two phononic crystals system based on the MST [28]. They used a 30° wedged sample which consisted of 238 water cylinders of $R = 0.4a$ in the mercury background with a square array. The shape of the sample and illustration of the refraction process are shown on the top of Fig. 8.5. The black frame marked the size of the sample. The wedged surface was the (11) surface when a slit beam of frequency $\omega = 0.235(2\pi c_l/a)$ with a half-width $wl = 2a$ incident normal to the left surface of the sample, it transports along the direction of incidence wave until it meets the wedge (11) interface of the sample, and then, a part of it will refract outside of the sample and the other reflects inside. There are two possibilities for the refracted wave. It may travel on the right side (positive refraction) or left side (negative refraction) of the surface normal. The simulation

results are plotted in Fig. 8.5. The field energy pattern of the incidence and refraction is shown in the figure. The arrows and text illustrate the various beam directions. It can be clearly seen that the density flux of the refractive wave outside of the sample travels on the negative refraction side of the surface normal. The refraction angle is consistent with the estimation from the wave vector space in Fig. 8.6. The simulation results show clearly that the negative refraction of the acoustic wave exists in the first band for the case with $\vec{S} \cdot \vec{k} > 0$. Similar phenomena have also been demonstrated in the steel–air system.

The concept of perfect lens or microsuperlens has been designed using the concept of negative refraction [29, 30] and fabricated with 2D photonic crystals [27].

Such a superlens can focus a point source on one side of the lens into a real point image on the other side even for the case of a parallel sided slab of material. The advantage of the superlens or perfect lens is the capability to defeat the diffraction limit or Rayleigh resolution criterion of wavelength divided by two. Such an image can be realized by flat slab instead of curved shapes, and thus, fabrications can be easier in principle. Zhang and Liu [26] demonstrated the design of such a perfect lens for sound waves which possesses the same advantage as that of optical system. They used a slab of the sample with $40a$ width and six layers thick. A continuous wave point source is placed at a distance $1.0a$ from the left surface of the slab. The frequency of the incident wave emitting from such a point source is $\omega = 0.24(2\pi c_1/a)$, chosen to be within the region where all-angle negative refractions may occur (Fig. 8.3b).

The MST method is used to calculate the propagations of an acoustic wave in such a system. The typical results of field pattern of pressure wave and their images across the slab sample are given in Fig. 8.6 The geometry of the phononic crystal

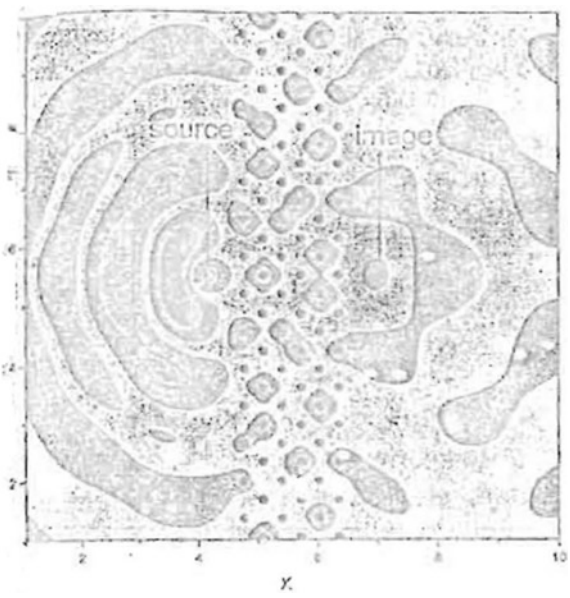

Fig. 8.6 Field pattern of pressure wave of a point source and its image across a six-layer slab at frequency ω = 0.24 (2π c_l/a). The system considered here consists of some water cylinders in mercury background with $R = 0.4a$. Dark and bright regions correspond to negative and positive values, respectively [26]

slab is also displayed. One can find quite a high-quality image formed on the opposite side of the slab. A closer look at the data reveals a transverse size (full size at half maximum) of the image spot as $0.6a$ (or $0.14\ \lambda$) at a distance of $1.0a$ from the right surface of the slab. The focusing size of the image depends on certain parameters such as the thickness of the slab and the distance between the source and the slab which is similar to the case of the optical system. The tuning of these parameters will produce a clearer acoustic image.

They also studied the effect on the image quality when the frequency of the sound wave is outside of the AANR region and system without the AANR region such as steel–air system. For these cases, the focusing phenomena are degraded. These show that the AANR is very important for the image formations.

This shows that negative refraction for acoustic wave in the 2D phonons crystal exists in a manner similar to that of optics.

8.5 Acoustic Metamaterials in a Broader Sense Beyond the Phononic Crystals (Ma and Sheng [31])

Metamaterial is a composite material. Its wave functionalities are a combination of manifestation of the local resonant constituent units. It is to be noted that the resonant frequency will be orders of magnitude larger than the physical dimension of the resonant unit due to its dependence on the restoring force due to the spring and the inertia of the mass. This is known as the sub-wavelength characteristic and is a common feature of metamaterials which have functionalities not found in nature.

In this chapter, the treatment is limited to the linear case; dealing only with infinitesimal amplitude sound wave, linear acoustic field equation is used. Acoustic metamaterials can be used to manipulate and control the propagation of acoustic waves described by the linear acoustic field equation which is derived from Newton's equation of motion, equation of continuity and the thermodynamic equation of state for adiabatic process as:

$$\nabla^2 P - \frac{\rho}{\kappa}\frac{\partial^2}{\partial t^2} P = 0 \tag{8.14}$$

where P = acoustic pressure, ρ = mass density, and κ = bulk modulus or compressibility. ρ and κ are the two constitutive parameters. The particle velocity is given by $v = \sqrt{\frac{\kappa}{\rho}}$.

In an acoustic metamaterial, the two constitutive parameters can have unusual values when considered in the effective medium sense, such as close to infinity, zero or negative. Such values imply acoustic wave characteristics that are usually not associated with ordinary composites. However, in acoustic metamaterials, such unusual features will occur due to local resonances of the constituent components.

They will be of "narrow band" in nature and occur only in the vicinities of the resonant frequencies.

Acoustic waves in fluids are longitudinal scalar waves. Acoustic waves in solids have two propagating modes, longitudinal scalar waves and transverse vector waves with polarization. In contrast, electromagnetic waves are transverse vector waves with two polarizations. However, there exists a close analogy between them since both are wave phenomena, and their wave equations have the same mathematical form. Their corresponding two constitutive parameters can be mapped as $\rho \rightarrow \epsilon$ and $\kappa \rightarrow \mu^{-1}$, where ϵ and μ are dielectric constant or permittivity and magnetic permeability, respectively. This also indicates that these two types of waves share much but not all of the underlying physics. This is the reason why negative refraction [32, 33], superlensing [34] and cloaking [35, 36] in acoustic metamaterials have developed in parallel with their counterparts in electromagnetic metamaterials.

In the subsequent section, one first analyses the local resonant structures that give rise to the unusual negative values of effective mass density and bulk modulus. For this purpose, a special class metamaterial known as decorated membrane resonators (DMRs) is chosen to demonstrate the negative effective values of the constitutive parameters, dispersions and the underlying physics. The diverse applications of acoustic metamaterials and emerging directions are then given.

8.6 Demonstration of Local Resonance Using the Spring-Mass Model and Dynamic Effective Mass [31]

There is a characteristic of the composite that is different from that of a rigid body. That is, the constituent components of a composite can display an inertial response. This can be mathematically illustrated as follows. First one considers a simple one-dimensional coupled oscillator with external excitation.

Mass M_1 will form a cavity. Mass M_2 is sliding inside the cavity without friction. The total force exerted on mass M_1 will be given by $F(\omega) + K(x_2 - x_1)$. The second term comes from the contact where the spring is connected to mass M_1. x_1, x_2 = displacements of M_1 and M_2, respectively.

The harmonic oscillator of M_2 is described by:

$$M_2\ddot{x}_2 = -K(x_2 - x_1), \tag{8.15}$$

With $\ddot{x}_{(1,2)} = -\omega^2\, x_{1,2}$, x_2 can be solved in terms of x_1. Then, F can be expressed in terms of x_1, as

$$F = [M_1 + (\omega_0^2 - \omega^2)]\ddot{x}_1 \tag{8.16}$$

where $\omega_0 = \sqrt{K/M_2}$, M_2 = the local resonance frequency, K = spring constant.

The inner structure of the system can be described by the system's apparent inertia, which possesses a frequency dispersion relation of

$$\overline{M}(\omega) = M_1 + K/(\omega_0^2 - \omega^2) \tag{8.17}$$

as plotted in Fig. 8.7b.

Due to the interesting fact that there are relative motions between the constituent components in a composite such as acoustic metamaterial, there can be a significant difference between the inertial response of the system $\overline{M}(\omega)$ and its static value. This is the reason for introducing the concept of dynamics effective mass to the system. Then, Newton's second law of motion can be rewritten as the system's inertial response $\overline{M}(\omega)$ can deviate significantly from its static value. That is why the dynamic effective mass is introduced into the system. This allows Newton's second law to be rewritten as: $F = \overline{M}(\omega)\ddot{x}_1$. The dynamics mass density ρ can be defined as

$$\overline{\rho} = \langle f \rangle / \langle \ddot{x} \rangle \tag{8.18}$$

where f = force density, x = unit cell displacement, and $\langle\ \rangle$ denotes averaging over the surface area of the unit cell under consideration.

The subject of effective mass is treated in Milton and Willis [37] and Mei et al. [38] on similar spring-mass system. Yao et al. [39] gave an experimental proof.

8.6.1 *Effective Mass Dispersion between Two Resonances*

A characteristic of acoustic metamaterial is mass density dispersion. This is known as antiresonance condition which takes place at a frequency between two resonances. It is of interest to calculate the average displacement of a sample with two resonances at frequencies ω_1 and ω_2. When the system is driven at a frequency ω between the two, both resonances will be excited but with opposite phases. The average displacement can cross zero at the antiresonance frequency $\tilde{\omega}$. Then $\langle \ddot{x} \rangle = -\omega_2 \langle x \rangle$ for harmonic motion. From Eq. (8.17), frequency dispersion can occur for the dynamic mass density. This is shown in Fig. 8.7b.

Acoustic metamaterial is an example of such composites with frequency dispersive properties. First, the acoustic metamaterial possesses local resonances. Ma

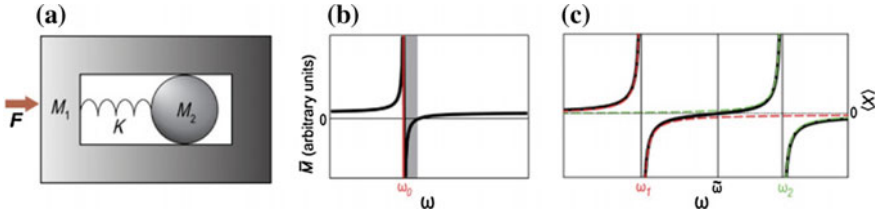

Fig. 8.7 Origin of anomalous constitutive parameters in acoustics [31]

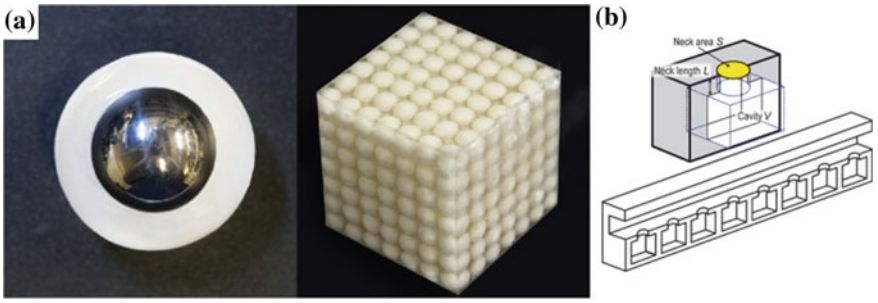

Fig. 8.8 Initial realizations of local resonant acoustic metamaterials [31]

and Sheng [31] proposed that the metamaterial be a matrix of silicone-coated metallic spheres embedded in epoxy [40]. Figure 8.8a shows image of a matrix and a unit cell. The relative motions of the constituents of the elementary building blocks will generate low-frequency resonances. The displacement of the metallic sphere will be related to the lowest frequency resonance of 400 Hz. The displacement of the silicone rubber layer is responsible for the second resonance at around 1350 Hz, with the metallic sphere almost at rest. The dynamic mass density ρ^{-} [41] will possess a strong frequency dispersion due to these resonances. This strong frequency dispersion can cause the effective dynamic mass density ρ^{-} to diverge to a very large value or with a negative value. Under such situations, the acoustic wave will be strongly attenuated within the structure yielding almost total reflection of the sound wave.

8.6.2 *Effective Bulk Modulus and Spatial Symmetry of the Resonances [31]*

Here, one considers the case of effective bulk modulus instead of the effective mass density to be frequency dependent. The Helmholtz resonator is an example of this. Here, the centre of mass is stationary and the deformation involves extension–compression motion. This is not like the dispersion in frequency of the effective mass density which is always associated with the displacement of the system's centre of mass.

Negative bulk modulus was experimentally demonstrated to be caused by the frequency dispersion of local resonances by Fang et al. [42]. They used an ultrasonic waveguide shunted by a chain of Helmholtz resonators which produce Helmholtz resonances due to the oscillation of the fluid in the neck section under the restoring force arisen from the expansion and compression of the fluid in the cavity. This is shown in Fig. 8.8b with the sample in sub-wavelength dimension.

The local resonances have spatial symmetrical properties. The effective bulk modulus and effective mass density characteristics are associated with these

symmetrical properties. The one-dimensional harmonic motion can be considered as the weighted superposition of symmetric and antisymmetric motions. This corresponds to the dipolar and monopolar resonant displacements, respectively. Li and Chan [43] use the Mie resonance of soft rubber spheres to analyse the relation between the symmetry of motion and acoustic response. They found out that dominantly expansive–compressive symmetry is generated by monopole symmetry, and this response is related to the bulk modulus. On the other hand, inertial response is due to the dipolar symmetry of motion. Also, modes with higher angular momenta have been studied and they produce interesting response for the elastic waves [44, 45].

8.6.3 Doubly Negative Mass Density and Bulk Modulus

There are several ways to achieve acoustic double negativity. Method one is to use only one resonator which can have different eigenmodes, each exhibiting the monopole resonance and dipole resonance separately. By tuning the frequency of the different eigenmodes, one can achieve simultaneous effective negative values of the bulk modulus and mass density. There are several examples based on this design. One is the Mie resonance of porous silicone rubber spheres producing negative refractive index [46]. Another is possible to achieve acoustic double negativity by overlapping the frequency responses with the above two symmetry types. There are several approaches to achieve this. First, a single resonator can have multiple eigenmodes exhibiting distinctive symmetries. With careful design, it is possible to tune the relative frequency of these eigenmodes to achieve double negativity [46]. Another example is the coupled membrane resonators [47]. The theoretical works on these approaches are given by Ding et al. [48], Christensen et al. [49] and Fok and Zhang [50]. Lee et al. [51–53] first showed experimentally acoustic double negativity. They used a sample that consists of a waveguide segmented by elastic membranes [53]. This enables frequency dispersion in the effective mass density. The same waveguide is also shunted by a series of side holes to produce frequency in the bulk modulus [54]. The acoustic double negativity is due to the overlap in the two dispersive frequency ranges. More recently, it is discovered that the interaction between identical symmetry type eigenmodes also leads to double negativity [54]. The following section on acoustic superlens will have more details on this.

8.7 Membrane-Type Acoustic Metamaterials [31]

An example of a group of acoustic metamaterials that can exhibit effective mass density frequency dispersion over certain frequency ranges, typically audible frequency ranges of 50–2000 Hz and double acoustic negativity, is decorated double membrane resonators (DMRs) [31]. Here, the membranes are light and thin and

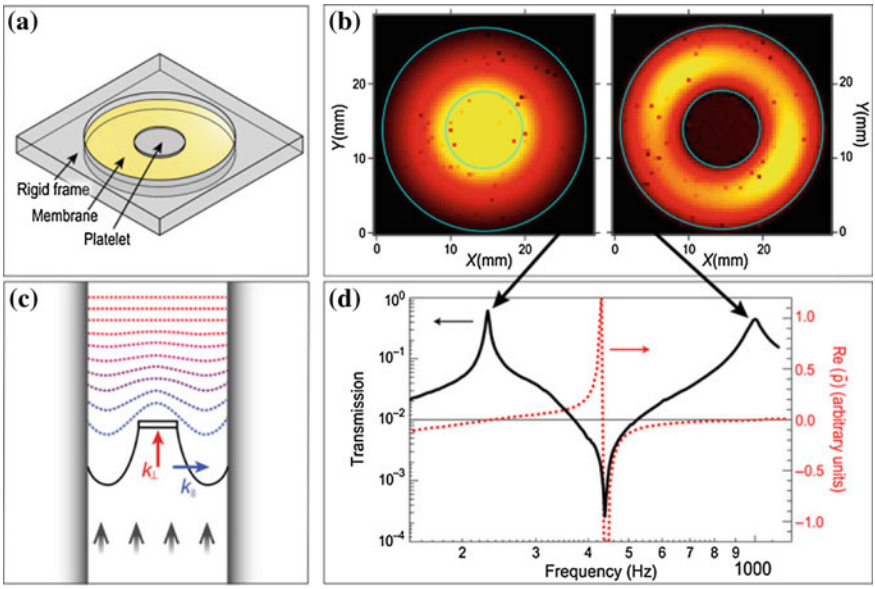

Fig. 8.9 Single membrane with negative effective mass density [31]

hence with high application potentials. Figure 8.9a shows an example of DMR with a flexible membrane of only sub-millimetres thick and several centimetres width fixed on a rigid film. In order to be modelled as a spring-mass oscillator, a rigid platelet is attached to the centre of the membrane. The proper restoring force for oscillations is given by a uniform prestress. The spring will be equivalent to membrane and the central platelet equivalent to the mass [55]. Next, one analysed the response of the DMR. This will be represented by the normal displacement profile $W(x)$.

The scattering characteristics of the DMR can be observed by the dipole symmetry of the local resonance. This gives rise to the frequency dispersion of the effective mass density $\overline{\rho}$. This is due to the membrane's thin nature. The compressitivity of the membrane is required in the high frequency region. The dipole symmetry is the nature of the low-frequency eigenmodes. Usually, two eigenmodes will occur below 1 kHz. Normal displacement profiles are plotted in Fig. 8.9b.

8.7.1 Normal Displacement Decomposition and Relationship to Propagative and Evanescent Modes

For the purpose of analysis, one writes the normal displacement $W(\boldsymbol{x})$ as the sum of two components, the surfaced averaged portion and the variation term on the normal displacement:

$$W(x) = \langle W \rangle + \delta W(x) \tag{8.19}$$

where $\langle W \rangle$ = surface-averaged normal displacement and is given by

$$\langle W \rangle \equiv \frac{1}{\pi R^2} \int_0^{2\pi} \int_0^R W(r, \varphi) r \mathrm{d}r \mathrm{d}\varphi \tag{8.20}$$

and R = DMR's radius, r and φ = radial and azimuthal coordinate, respectively.

The whole picture of piston-like motion is described by $\langle W \rangle$, and $\delta W(\boldsymbol{x})$ only represents the high spatial frequency portion. The Fourier wave vector parallel to the plane of the membrane k_{11} will describe the spatial variation of $\delta W(\boldsymbol{x})$. The magnitude of this wave vector will obey the inequality$/k_{11}/ \geq 2\pi/R$.

Acoustic wave in air obeys the following dispersive relation:

$$k_{\parallel}^2 + k_{\perp}^2 = \left(\frac{2\pi}{\lambda}\right)^2 \tag{8.21}$$

where $k_{\perp}$ = normal component of the wave vector and λ = wavelength.

From (8.21), normal displacement is continuous across the membrane–air interface, $\lambda \gg R$ at the relevant frequencies, and k_{11} is imaginary. This shows that $\delta W(\boldsymbol{x})$ will couple only to evanescent waves. On the contrary, $\langle W \rangle$ is constant and will couple to propagating wave. Hence, the Fourier k_{11} components will have a distribution that will peak at $k_{11} = 0$. These are schematically shown in Fig. 8.9c.

Evanescent waves are nonpropagating and located at nearfield. In the far field, DMR will be concerned only with $\langle W \rangle$, which describes piston-like motion [38, 47].

8.7.2 *Effective Mass Density and Impedance of the Membrane Resonator*

The effective mass density can be derived from the previous section's description of propagation mechanism as:

$$\overline{\rho} = (1/\omega^2 \overline{d}) \frac{\langle P \rangle}{\langle W \rangle} \tag{8.22}$$

where $\overline{d}$ = mean thickness, $\langle P \rangle$ = surface-averaged pressure difference on two sides of the membrane, and $\ddot{W} = -\omega_2 \langle W \rangle$ = surface-averaged acceleration.

Plotting the effective mass density as a function of frequency shows interesting results (Fig. 8.9d). $\overline{\rho}$ becomes zero at the DMR's eigenfrequencies. Also, it has positive sign and negative sign across the point. This also implies that there is a

phase difference of π on two sides of a resonance. A negative mass density also means that the system's acceleration is against the external force.

The next parameter to consider is the impedance of DMR. It can be defined as

$$Z = \langle P \rangle / \langle \dot{W} \rangle = i\langle P \rangle / \omega \langle W \rangle = -i\omega \overline{\rho}.\overline{d}. \tag{8.23}$$

The above equation shows that a near-zero value of the effective mass density implies that the effective impedance is well matched to the impedance of the air. This will enable an optimal coupling of the DMR with the incident sound. Further, if one expresses the effective mass density as: [56]

$$G = \langle W \rangle / \langle P \rangle = i/\omega Z = -1/(\omega^2 \overline{\rho} \overline{d}) \tag{8.24}$$

then a nonzero value of $\overline{\rho}$ will enable the normal displacement to diverge in the absence of dissipation. Hence, there will be a huge transmission peak as expected when $\overline{\rho}$ becomes zero (Fig. 8.9d).

Another interesting effect of the near-zero value of effective mass density is the phenomenon of supercoupling. This means an almost perfect through small paths during normal incidence [57–59]. Further, in the imaginary part of $\overline{\rho}$, the implying dissipation will be positive, if judged from the relation of $\overline{\rho}$ with Green's function and the impedance. The positive value can be further confirmed from its relation with the impedance where real part is associated with dissipation.

There is another interesting point known as antiresonance, which lies in the frequency range between the two resonance peaks. At this antiresonance frequency, $\langle W \rangle = 0$ causes $\overline{\rho}$ to diverge with a change in sign and the impedance to diverge, and the wave will be totally reflected. This is shown in Fig. 8.9d as a transmission drop near 440 Hz. This interesting property leads super thin and light weight reflective panels with exceptional capability to block low-frequency noise [55, 60–64].

$\langle W \rangle \rightarrow 0$ is due to the fixed boundary condition of the membrane. This causes $\overline{\rho}$ to be negatively divergent in the static limit. With a quasistatic force, this provides an infinite inertia of the system. The negative sign of the effective mass density is also a consequence of Newton's third law. This negative sign behaviour of $\overline{\rho}$ is also shown in other types of structures [51, 65]. For instance, a negative $\overline{\rho}$ in the low-frequency limit was recently demonstrated for liquid foam, which is equivalent to an array of flexible membranes [66].

8.7.3 *Effective Bulk Modulus of Two Coupled Membrane Resonators and Double Negativity*

In this section, the effective bulk modulus characteristics will be studied. For a thin membrane, the vibrations with the expansion and compression of the membrane

along the thickness direction will only occur at very high frequencies. These are monopolar vibrations giving anomalous values of the effective bulk modulus. One way to lower in monopolar resonant frequency is to couple two membranes to form a new DMR (Fig. 8.10a). This two coupled membrane resonator is similar to a single DMR as it also has two dipolar eigenmodes. Hence, it also possesses the characteristics of the effective mass density. It is to be pointed out that in this new structure, a third mode and a new mode are produced. Hence, the two membranes oscillate against each other. So, there are altogether three eigenmodes (Fig. 8.10b). The characteristics of the new mode lead to an effective bulk modulus $\overline{\kappa}$, and it is frequency dispersive (Fig. 8.10c, middle). This is because the DMR is pulsating with volume in compressive–expansive motions, while the centre of mass is kept stationary. Again $\overline{\kappa}$ approaches zero at the monopolar frequency and becomes negative at the higher frequency side of this eigenmode. Kafesaki and Economou [22] found that the monopole mode is situated near the dipolar antiresonance. The monopolar and dipolar modes of the DMR can be tuned independently. Since κ has a value almost zero, the two coupled membrane resonators with air space in between have a characteristic impedance Z which will be given by $z = \sqrt{\overline{\rho}\overline{\kappa}}$ and has a magnitude equal to that of air despite having a large $\overline{\rho}$.

The double negativity of $\overline{\rho}$ and $\overline{\kappa}$ will produce a real effective wave vector $\overline{k} = \omega\sqrt{\frac{\overline{\rho}}{\overline{\kappa}}}$. This implies a propagating wave.

The following is an analysis of how acoustic double negativity will give rise to a negative refractive index. Figure 8.10c will be referred. One will show that the real part of the effective index $\overline{n} = v_0/\sqrt{\frac{\overline{\kappa}}{\overline{\rho}}}$ will be negative where v_0 = speed of sound in air. Since $P \sim \overline{\kappa}\langle W\rangle$, $\overline{\kappa} \sim 1/G'$, and $\overline{\rho} = -1/G$, where G = Green's function. The sign of the imaginary part of G must be fixed. This shows that the imaginary parts of $\overline{\kappa}$ and $\overline{\rho}$ must be opposite in sign. The previous section shows that the imaginary

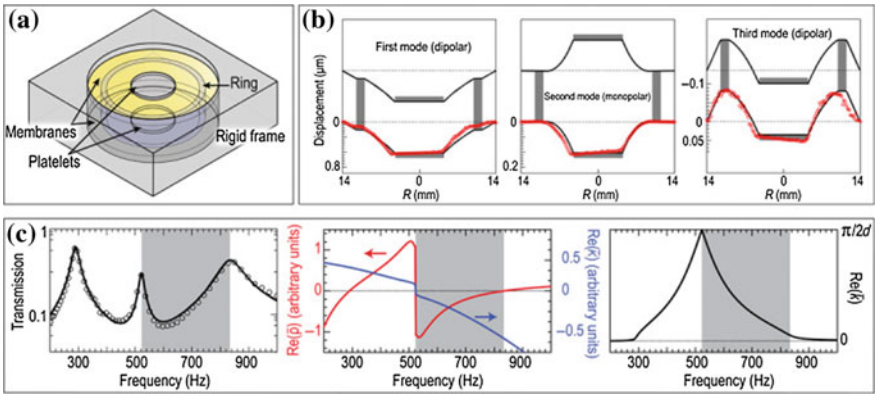

Fig. 8.10 Coupled membranes giving rise to both mass and modulus dispersions [31]

part of $\overline{\rho}$ is positive. This indicates that $\overline{\rho}$ should be in the second quadrant of the complex plane and $\overline{\kappa}$ in the third quadrant. It follows that $\overline{\rho}/\overline{\kappa}$ must be in the fourth quadrant. Also, the imaginary part of the refractive index will be positive if the sound is propagating forward, and as a consequence, the real part of the effective refractive index will be negative. Figure 8.10c (middle) shows $\overline{\kappa}$ and $\overline{\rho}$ negative in the grey-shaded region. This shows a negative refractive index in the finite frequency range.

8.8 Super-Resolution and Focusing Beyond the Diffraction Limit [31]

8.8.1 Resolution Limit and the Evanescent Waves

The double acoustic negativity enables the manipulation of acoustic wave. An important application is the enhancement of the resolution limit of acoustical imaging. The resolution limit is due to the dispersion relation $k^2 = (\omega/v)^2 = (2\pi/\lambda)^2$. The dispersion relation sets a limit on the magnitude of the real component k_{11}, the wave vector lying along the plane of the image.

With $k^2 = k^2_{\parallel} + k^2{}_{\perp}$, and for a negative value of $k^2{}_{\perp}$ or $k_{\perp}$ to be purely imaginary, one is able to increase the magnitude of k_{11} components to be larger than $2\pi/\lambda$. This will produce a smaller value of λ and hence enhance the image resolution. It is to be noted that the wave components with imaginary $k_{\perp}$ are evanescent waves which are nearfield waves and nonpropagating. They decay exponentially with distance away from the source. Hence, details of the source/scatterer are contained in the nearfield.

8.8.2 To Defeat the Diffraction Limit

Here, one will describe the achievement of sub-diffraction scale image resolution using acoustic metamaterials which manipulate the properties of the medium in the vicinity of the focal spot.

Sub-diffraction focusing was experimentally demonstrated by Lemoult et al. [67]. Their system consists of a two-dimensional square lattice of soda cans which act as acoustic cavity resonators. There will be interference between the resonating and the continuous fields giving rise to leaky modes in the system. These leaky modes are shown in Fig. 8.11a as polariton-like dispersion and Fano-like resonance profile. There is an interesting feature showing that below the band gap there is an almost flat dispersion. This indicates huge wave vector with a large density of states which is the cause of sub-diffraction intense focusing (Fig. 8.11b). Besides this, defect modes can also contribute to sub-wavelength diffraction. These can be

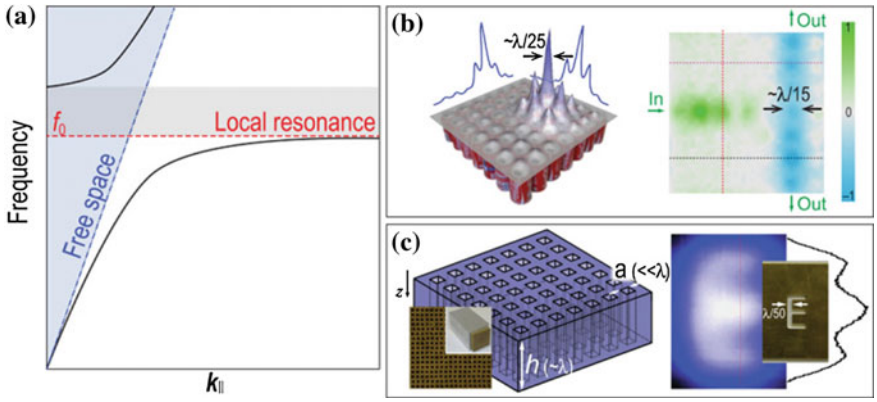

Fig. 8.11 Super-resolution with local resonances [31]

produced by blue-shifting some selected cavities "resonant frequency to the bulk band gap" (Fig. 8.11a, grey region).

Sofar one obtains the sub-wavelength diffraction focal spot by adding on extra wave vectors with the rescaling of the diffraction limit near the focus positions. To obtain a perfect image of a source, one needs to capture the nonpropagating evanescent wave which contains all the sub-wavelength diffraction information. The evanescent wave lies in the nearfield. Hence, one needs the acoustical imaging system to function in the nearfield region of the sound source, and with the acoustic lens made of metamaterial to capture the evanescent wave. In addition, defect modes can be created by blue-shifting the resonant frequency of some chosen cavities of the bulk structure so that they fall into the bulk band gap (Fig. 8.11a, grey region). As a result, the acoustic energy carried by these resonators was spatially confined in the lateral directions because there were no propagative modes within the bulk structure for these frequencies. Energy transport in the deep-sub-wavelength scale was thereby demonstrated by line defects, as shown in Fig. 8.11b [68].

In the above analysis, the sub-diffraction focal spot is made possible by the extra wave vectors supplied by rescaling the diffraction limit near the positions of the focus.

Next is to study the mechanism for retaining the evanescent modes. The method is to make use of the local resonances because the magnitude of k can be extended to huge values without altering the frequency. This is due to flat dispersion (Fig. 8.11a). This will introduce extra momenta and will sustain the evanescent waves. These Fabry–Perot resonances can be realized in waveguides with the length on the order of a wavelength or more but with cross-sectional dimension much less than the wavelength. The acoustical imaging system consists of an array of these waveguides placed in the nearfield of the source with each waveguide unit

capable of recording highly localized disturbances and conveys the information to the targeted locations. For such design of systems, acoustical images with sub-wavelength resolution have been obtained (Fig. 8.11c) [50, 51].

8.8.3 *Acoustic Superlens*

The superlens concept [69] which enables perfect imaging was proposed by Pendry [69] for electromagnetic waves. Here, a double negativity metamaterial (with negative permittivity and negative permeability) is used. This double negativity also produces negative refractive index. Snell's law shows that at the interface between a conventional material and a negative refractive index material, an obliquely incident wave from the side of the conventional material will bend to the same side of the surface normal, into the negative refractive index material. This is known as negative refraction. Negative refraction will enable a diverging wave to reconverge. It shows a rectangular slab of material that can be used as a lens. For such type pf lens, two foci will be generated by a point source: one within the slab and the other outside, on the other side of the slab [30] (Fig. 8.12a top).

Zhang et al. [70] demonstrated the first acoustic negative refraction using metamaterial. They built an interface between a normal material and a metamaterial, and negative refraction was shown which gave a negative refractive index with the source placed at one side of the interface; a focus was identified. The double negativity of the acoustic metamaterial amplifies the evanescent waves which carried the detailed information, and this enables the superlens (Fig. 8.12 bottom).

It is to be noted that singly negative metamaterial can also amplify the evanescent waves. This is due to the surface plasmons like resonance formation at the interface between the metamaterial and the normal material. This has been

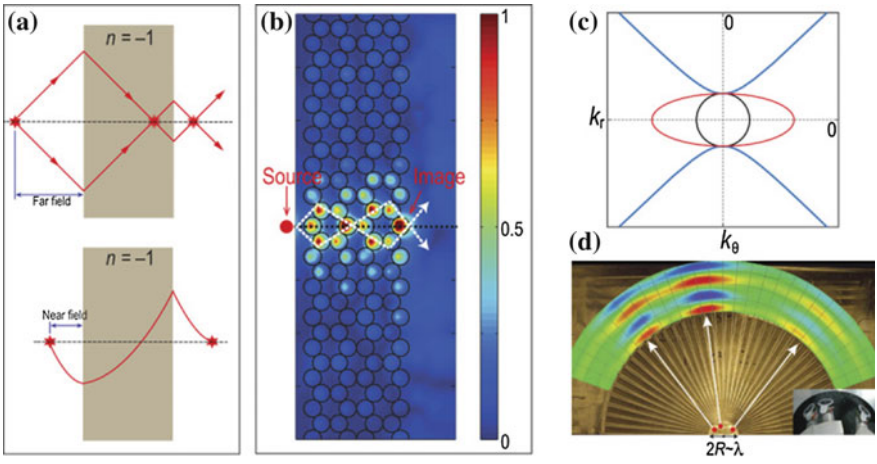

Fig. 8.12 Acoustic realization of superlens and hyperlens [31]

demonstrated by Park et al. [71]. They used a two-dimensional membrane array's negative effective mass density regime to amplify the evanescent waves, and super-resolution can be achieved [72]. Since this interfacial mode decays exponentially, from the interface, the lens has to be of sub-wavelength thickness.

Kaina et al. [54] also demonstrated an acoustic superlens made of doubly negative acoustic metamaterial. The principle used can be understood by the tight-binding model. The unit cell of the doubly negative acoustic metamaterial comprises two coupled Helmholtz-like cavity resonators which will generate monopolar modes and negative effective bulk modulus. The metamaterial is a two-dimensional lattice which consists of those unit cells. Coupling two eigenstates with identical eigenfrequencies will produce anticrossing and two modes with opposite symmetries separated by their resonant frequencies. One can adjust the coupling by introducing a slight mismatch in their eigenfrequencies or altering the distance between the resonances. This is equivalent to tuning the frequency and intensity of the dipolar modes. Two resonators out of phase will produce the dipolar mode. It is observed that within the negative effective bulk modulus band gap, there is a narrow transparency band with negative dispersion.

With the above design, it was experimentally demonstrated that a doubly negative flat lens can be fabricated with foci inside and outside the lens. It also showed that the evanescent waves can be amplified by the coupled resonators and sub-wavelength resolution can be achieved. Indeed the focal spot has a sharpness with amplitude full width at half maximum of of $\lambda/15$, three times smaller than the size of the image source which is $\lambda/5$ bandwidth. The reason for this additional sharpness arises from the superlens' doubly negative band which gives relatively flat dispersion, thus yielding extra wave vectors and high density of states.

The evanescent waves will decay once they leave the superlens [73]; in order to overcome this, one can build a far field superlens. For electromagnetic waves, this has been done by adding sub-wavelength structures such as corrugations or gratings [74, 75] which will provide additional wave vectors to bring the evanescent waves with lateral wave vectors larger than $2\pi/\lambda$ in magnitude back into the light cone of the free space propagating waves. This has yet to be done for the case of the acoustic waves.

8.8.4 *Acoustic Hyperlens [31]*

The acoustic hyperlens is an another approach to super-resolution [76]. The concept is based on a hyperbolic dispersion relation given by

$$\frac{k_\theta^2}{\overline{\rho}_r} + \frac{k_r^2}{\overline{\rho}_\theta} = \frac{\omega^2}{\overline{r}} \tag{8.24}$$

This dispersion relation has a hyperbolic shape. This is a consequence of the effective mass density being negative along the radial direction $\hat{r}$ but positive along

the azimuthal direction $\widehat{\theta}$. This yields $\overline{\rho_\theta}\ \overline{\rho_r} < 0$. This is illustrated in Fig. 8.12c. The relation is shown to be valid for acoustic wave [77–79]. Based on Eq. (8.2), the wave vector.

k_θ and/or k_r is no longer bounded and can take on arbitrarily large values. This means that the hyperbolic dispersion relation can be satisfied without any a dispersion which was shown to be possible for acoustic waves [77–79]. As a result, k_θ and/or k_r is no longer bounded and can, in principle, take arbitrarily large values. This means that the hyperbolic dispersion relation can be satisfied without any of the wave vectors to be imaginary.

This concept of acoustic hyperlens has been experimentally demonstrated by Shen et al. [79]. They fabricated a fan-shaped structure with alternating brass and air stripes lining along the $\widehat{\theta}$ direction (Fig. 8.6d).

In such a geometric structure, the effective mass density will be given as the arithmetic average of brass and air's mass density along the $\widehat{\theta}$ direction and also as the average of brass and air's inverse mass densities along the $\widehat{r}$ direction. Since there is a huge difference between brass and air's mass densities, the effective mass densities of brass and air can differ by a large ratio. Consequently, this geometric structure will have an elliptical equifrequency contour, with a large eccentricity. This enables access to huge wave vector components. The advantage of such a structure is that super-resolution can be achieved without the need for negative mass density and negative bulk modulus which are the outcomes of resonances, and hence is restricted over a narrow frequency range. The separation of the sound sources four to seven times smaller than the sound wavelength were shown to be clearly separated and magnified, measured outside the hyperlens. The measurements took place outside the hyperlens demonstrating successful conversion of evanescent waves into propagating waves. Besides the above experiments, an acoustic hyperlens using hyperbolic dispersion relation was also demonstrated using membranes made of metamaterials which generate negative mass density [79].

8.9 Coordinate Transformations

8.9.1 My Important Discovery of Negative Refraction is a Special Case of Coordinate Transformations or a Unified Theory for Negative Refraction and Cloaking

Here, we consider both cloaking and negative refraction under the umbrella theory of coordinate transformation or gauge invariance of the form of equations under coordinate transformations. This is a pattern of nature and is applicable to all equations of physics covering both Maxwell's equations and the acoustic equation

of motion. When the determinant of the direction cosines matrix (or transformation matrix) equals −1, one will have negative refraction or parity equals −1. Also, multiplying the original permittivity and the original permeability by the determinant value of −1 will produce negative values of the permittivity and the permeability. This shows that negative refraction is a special case of coordinate transformations used in cloaking problem when the determinant of the transformation matrix equals −1. This can be illustrated as follows:

$$\begin{pmatrix} v'_x \\ v'_y \\ v'_z \end{pmatrix} = \begin{pmatrix} \propto_1 & \propto_2 & \propto_3 \\ \beta_1 & \beta_2 & \beta_3 \\ \gamma_1 & \gamma_2 & \gamma_3 \end{pmatrix} \begin{pmatrix} v_x \\ v_y \\ v_z \end{pmatrix} \tag{8.25}$$

When the determinant of the direction cosines matrix on the right-hand side of (8.25) equals −1, we have

$$\vec{v'} = -\vec{v}. \tag{8.26}$$

Replacing the vectors by the examples of permeability and permittivity, we will have

$$\overrightarrow{\mu'_{lj}} = -\overrightarrow{\mu_{lj}} \text{ and } \overrightarrow{\varepsilon'_{il}} = -\overrightarrow{\varepsilon_{il}}. \tag{8.27}$$

This shows that negative refraction also produces negative permeability and negative permittivity.

Since this gauge invariance of the form of equation is a pattern of nature of all physics equations, it is also applicable to the acoustic case where the equivalence of the permittivity and permeability is the mass density and the bulk modulus or compressibility.

This also shows that cloaking material or component will become the lens in the special case of negative refraction and refraction is a special case of cloaking or the bending of light wave or sound wave when the path of wave propagation becomes linear from nonlinearity.

This shows that gauge invariance has a broader coverage and applications than Veselago [30]'s dispersion relation.

Further, we also introduce reflection invariance (or right–left symmetry) to explain negative refraction. In fact, $-\mu$ and $-\varepsilon$ can be considered as the mirror image of μ and ε and $-\rho$ and $-\kappa$ can be considered as the mirror image of ρ and κ. Again here, the concept of coordinate transformations is used.

Of course, it should be also mentioned here that gauge invariance approach to negative refraction removes the ambiguity caused by using the dispersion relation. Both positive and negative signs occur simultaneously due to the square root sign of the dispersion relation, and this has to be justified.

8.9.2 Acoustical Cloaking

Acoustical cloaking deals with the deflection or bending of sound wave and the control of the propagation and direction of sound wave according to our specified direction.

Again, Veselago [30]'s theory of using dispersion relation is not relevant here. We use coordinate transformations, a form of gauge invariance. That is, there is no change in the form of the acoustic field equation after the coordinate transformations or the acoustic field equation is gauge invariant subjected to coordinate transformations.

As an illustration, we quoted the results of Cummer and Schurig [80].

Cummer and Schurig [80] illustrated coordinate transformations for acoustics by using the linear acoustic equation for inviscid fluid:

$$j\omega p = -\kappa \nabla \cdot \vec{v}, \quad j\omega p\vec{v} = -\nabla p \tag{8.28}$$

where ω = angular frequency, v = sound velocity.

Next, he imposed a new set of curvilinear coordinates x', y' and z' on these equations. Using A as the Jacobian matrix of coordinate transformations from (x, y, z) to (x', y', z'), he expressed the gradient operation in the new primed coordinates as:

$$\nabla p = A^{\mathrm{T}} \nabla p = A^{\mathrm{T}} \nabla' p', \tag{8.29}$$

and the divergence operation can be expressed as

$$\nabla \cdot \vec{v} = \det(A) \nabla' \cdot \frac{A}{\det(A)} \vec{v} = \det(A) \nabla' \cdot \overrightarrow{v'} \tag{8.30}$$

With these expressions, the original Eq. (8.28) can be written in the new coordinates as

$$j\omega p' = -\kappa \det(A) \nabla' \cdot \overrightarrow{v'}$$

$$j\omega \det(A) \left(A^{T}\right)^{-1} \rho \left(A^{-1}\right) \overrightarrow{v'} = -\nabla' p' \tag{8.31}$$

which is in the same form as the original Eq. (8.28), but with the new medium parameters:

$$\kappa' = \det(A)\kappa, \quad \overline{\overline{\rho}} = \det(A) \left(A^{\mathrm{T}}\right)^{-1} \rho \left(A^{-1}\right). \tag{8.32}$$

Physically, this means that if one applies a coordinate transformations to a solution to Eq. (8.28) and changes the medium properties according to Eq. (8.31), the transformed fields are a solution to the acoustic equations in the new medium.

Acoustical cloaking can be classified as a form of acoustical imaging because by placing a metamaterial acoustical cloak on the object to be cloaked it will render its disappearance from one sight. The concept of acoustical cloaking also extended from electromagnetic cloaking [81, 82]. Electromagnetic cloaking uses concepts of gauge invariance from general relativity, that is, the form of the Maxwell's equations remains unchanged under arbitrary coordinate transformations with transformed permittivity and permeability values which are scaled by a common factor. Because of the nature of negative refraction of metamaterial, by cloaking the object with a metamaterial, the light rays will be deflected, stretched and bent and guided around the object and returned to their original trajectory.

However, due to the dispersion nature of the light, the cloaking effect is specific only to a single frequency and not broadband.

The concept of acoustical cloaking was extended to acoustics by Milton and Willis [37] and by Cummer and Schurig [80]. The analysis by Milton and Willis [37] indicated that the coordinate transformations approach cannot be extended to elastodynamic waves in solids in the fully general case or even for the special case of compressional waves in a fluid. However, a scattering theory analysis has shown that the cloaking solution exists for acoustic waves in fluids as three dimensions (Cummer and Schurig [80]) and by analogies with electromagnetics. It has been shown that 2D acoustic waves (Cummer and Schurig [80]) and 3D acoustic waves can be made as transformation invariant. The material parameters required to implement acoustic coordinate changes have also been obtained by Greenleaf et al. [83].

It has to be noted that the phenomenon of acoustical cloaking cannot be transplanted blindly from electromagnetic cloaking using analogy. As shown in section two of this chapter, Veselago [30]'s theory is not applicable to acoustic waves, and even for electromagnetic waves, it is valid only to isotropic case and not for anisotropic cloaking material which most cloaking materials are made of. Also, the acoustic metamaterial has to be derived using the theory of elasticity and not from dispersion relation as what used to derive the Yablonovitch [1]'s negative permeability and negative permittivity. Our gauge invariance approach can provide better physical understanding of negative refraction and cloaking. We also noted that acoustic negative refraction can be obtained from multiple scattering theory (MST) besides the approach of negative mass density and negative bulk modulus. This also confirms that negative refraction is a form of multiple scattering. The above analysis is also given in section two of this chapter.

Our idea of objection to use analogy between acoustic wave and electromagnetic wave is supported by Cummer and Schurig [80]. They pointed out that demonstrating the invariance through analogy of acoustic wave with electromagnetic wave masks some of the physics of the transformations approach particularly how vectors such as particle velocity and the pressure gradient change under transformation. Through an analysis of how power flow and constant phase surfaces must transform for completely general waves, they show that the velocity vector in acoustics must transform in a different way than the $\vec{E}$ and $\vec{H}$ vectors in electromagnetics. This

explains why Milton Willis's [37] elastodynamics analysis assumed that the acoustic velocity transforms like $\overrightarrow{E}$ and $\overrightarrow{H}$ did not result in acoustic equation transformation invariance. We feel that this further shows the intrinsic elastic properties of acoustic wave as different from the electromagnetics. The treatment of negative refraction using theory of elasticity approach by Lee et al. [84] and Gan [85]'s analysis on the gauge invariance of acoustic fields [85] further confirms this. An example of the fabricating of acoustical cloak is given by Cheng et al. [86].

8.9.2.1 Derivation of Transformation Acoustics

Here, we follow approach of Cummer et al. [87]. The fluid version of the linear acoustic field equations will be used:

$$\nabla p = i\omega\rho(\vec{r})\rho_0\vec{v} \tag{8.33}$$

$$i\omega p = \kappa(\vec{r})\kappa_0\nabla\cdot\vec{v} \tag{8.34}$$

where $\rho(\vec{r})$ and $\kappa(\vec{r})$ are the normalized density and bulk modulus, respectively, of the medium and are coordinate transform invariant. We will demonstrate how the acoustic $\vec{v}$ must transform by considering $\vec{v}$ in a nonorthogonal coordinate system described by coordinate q_1, q_2 and q_3 with unit vectors $\widehat{u}_1$, $\widehat{u}_2$ and $\widehat{u}_3$, respectively. Following Pendry [69] and letting $i = 1, 2, 3$

$$Q_i^2 = \left(\frac{\partial x}{\partial q_i}\right)^2 + \left(\frac{\partial y}{\partial q_i}\right)^2 + \left(\frac{\partial z}{\partial q_i}\right)^2 \tag{8.35}$$

$$\text{Area} = Q_1 dq_1 Q_2 dq_2 |\widehat{u}_1 \times \widehat{u}_2|$$

Figure 8.13 shows what happens when we apply the divergence theorem to an infinitesimal volume in this nonorthogonal coordinate system.

Deriving the net outward flux of $\vec{v}$ from this volume and setting it equal to the divergence of $\vec{v}$ times the infinitesimal volume, it can be shown that

$$\begin{aligned}(\nabla\cdot\vec{v})Q_1Q_2Q_3|\widehat{u}_1\cdot(\widehat{u}_2\times\widehat{u}_3)| = {} & \frac{\partial}{\partial q_1}[Q_2Q_3\vec{v}\cdot(\widehat{u}_2\times\widehat{u}_3)] + \frac{\partial}{\partial q_2}[Q_1Q_3\vec{v}\cdot(\widehat{u}_1\times\widehat{u}_3)] \\ & + \frac{\partial}{\partial q_3}[Q_1Q_2\vec{v}\cdot(\widehat{u}_1\times\widehat{u}_2)]\end{aligned} \tag{8.36}$$

Let $V_{\text{frac}} = |\widehat{u}_1\cdot(\widehat{u}_2\times\widehat{u}_3)|$ because this is the fraction by which a unit volume is compressed by the coordinate nonorthogonality and we use the conventional superscript (subscript) notation for contravariant (covariant) vector components using

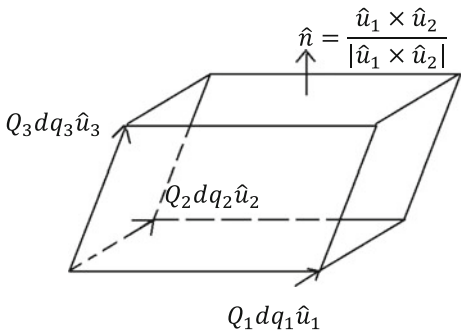

Fig. 8.13 Parallelepiped that defines an infinitesimal volume in the transformed coordinates. The area and unit normal of each face enter in the calculation of the net flux of a vector out of this volume [87]

$$\vec{v} \cdot (\hat{u}_2 \times \hat{u}_3) = v^1 \hat{u}_1 \times (\hat{u}_2 \times \hat{u}_3) \tag{8.37}$$

Equation (8.4) can be rewritten as

$$\begin{aligned}(\nabla \times \vec{v}) Q_1 Q_2 Q_3 V_{\text{frac}} = &\frac{\partial}{\partial q_1}\left(Q_2 Q_3 V_{\text{frac}} v^1\right) + \frac{\partial}{\partial q_2}\left(Q_1 Q_3 V_{\text{frac}} v^2\right) \\ &+ \frac{\partial}{\partial q_3}\left(Q_1 Q_2 V_{\text{frac}} v^3\right)\end{aligned} \tag{8.38}$$

Noting that the divergence in the transformed coordinates is defined by $\nabla_q \cdot \vec{v} = \frac{\partial v^1}{\partial q_1} + \frac{\partial v^2}{\partial q_2} + \frac{\partial v^3}{\partial q_3}$, we can write

$$\begin{aligned}(\nabla \cdot \vec{v}) Q_1 Q_2 Q_3 V_{\text{frac}} &= \nabla_q \cdot \left(V_{\text{frac}} \overline{\overline{Q}}_{per} \left[v^1 v^2 v^3\right]\right)^{\text{T}} \\ &= \nabla_q \cdot \vec{v}\end{aligned} \tag{8.39}$$

where

$$\overline{\overline{Q}}_{\text{per}} = \begin{bmatrix} Q_2 Q_3 & 0 & 0 \\ 0 & Q_1 Q_3 & 0 \\ 0 & 0 & Q_1 Q_2 \end{bmatrix} \tag{8.40}$$

and the transformed velocity vector $\vec{v}$ is given by

$$\vec{v} = V_{\text{frac}} \overline{\overline{Q}}_{\text{per}} \left[v^1 v^2 v^3\right]^{\text{T}}. \tag{8.41}$$

The per subscript on the tensor $\overline{\overline{Q}}_{\text{per}}$ is to denote that the diagonal elements transform each vector component by the product of the coordinate scaling factors perpendicular (more general, not parallel, for the case of nonorthogonal coordinates) to the direction of the vector component. Recall that our qualitative discussion above, summarized in Fig. 8.6, showed that this is precisely how the velocity vector must transform in a compressed wave in order for transformation

acoustics to work. Note that the elements of the volume vector $[v^1 v^2 v^3]^{\mathrm{T}}$ are the contravariant components of $\vec{v}$ in the nonorthogonal coordinate system, while the element of the vector $\vec{v}$ is the component in the original orthogonal coordinate system (Fig 8.14).

Multiplying (8.34) with $\lambda(\vec{r}) = 1$) by $Q_1 Q_2 Q_3 V_{\mathrm{frac}}$ and using (8.41) results in the equation in the transformed coordinates,

$$i\omega p = \kappa(\vec{q})\kappa \nabla_q \cdot \vec{v} \tag{8.42}$$

with

$$\kappa(\vec{q}) = (Q_1 Q_2 Q_3 V_{\mathrm{frac}})^{-1}. \tag{8.43}$$

This demonstrates the coordinate to function invariant of (8.34) provided that the bulk modulus is modified according to (8.43) and the velocity vector is transformed according to (8.42). More generally, this also shows how a vector must transform in order for the gradient operator to maintain its basis form.

Cummer et al. [87] derived how (8.33) and therefore the gradient operator transform under a coordinate change using the gradient theorem, and integrating ∇p along a short length in the q_1 coordinate directions, they find that

$$\nabla p \cdot Q_1 \hat{u}_1 = \frac{\partial p}{\partial q_1} = \left(\nabla_q p\right)^1. \tag{8.44}$$

The left-hand side contains the scaled covariant components of ∇p which must be converted to covariant components before it can be equated component-wise to $\nabla_q p$, the gradient in the transformed coordinates. They find that

$$\nabla_q p = \overline{\overline{Q}}_{\mathrm{par}} \overline{\overline{h}}^{-1} (\nabla p) \tag{8.45}$$

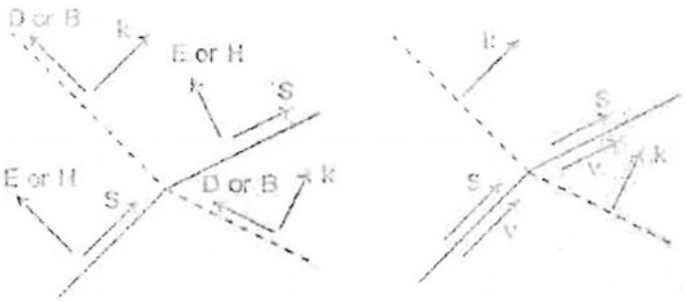

Fig. 8.14 Transformation of vectors in electromagnetic (left) and acoustic or compressional elastodynamic (right). The white converging arrows denote which component of each vector is compressed by coordinate transformations [87]

where $\overline{\overline{Q}}_{par}$ is the diagonal tensor containing coordinate scaling factors parallel to the direction of the vector component or

$$\overline{\overline{Q}}_{\text{par}} = \begin{bmatrix} Q_1 & 0 & 0 \\ 0 & Q_2 & 0 \\ 0 & 0 & Q_3 \end{bmatrix} \tag{8.46}$$

and

$$\overline{\overline{h}}^{-1} = \begin{bmatrix} \hat{u}_1 \cdot \hat{u}_1 & \hat{u}_1 \cdot \hat{u}_2 & \hat{u}_1 \cdot \hat{u}_3 \\ \hat{u}_2 \cdot \hat{u}_1 & \hat{u}_2 \cdot \hat{u}_2 & \hat{u}_2 \cdot \hat{u}_3 \\ \hat{u}_3 \cdot \hat{u}_1 & \hat{u}_3 \cdot \hat{u}_2 & \hat{u}_3 \cdot \hat{u}_3 \end{bmatrix}. \tag{8.47}$$

Note that this $\overline{\overline{h}}^{-1}$ is the same as $\overline{\overline{g}}^{-1}$ defined by Pendry [69]. They rename this tensor because they will use $\overline{\overline{g}}$ later to denote the metric tensor which is not quite the same as this $\overline{\overline{h}}$.

Finally, multiplying (8.33) (with $\rho(\vec{r}) = 1$) by $\overline{\overline{Q}}_{\text{par}}$, they find

$$p_q p = i\omega \overline{\overline{Q}}_{\text{par}} \overline{\overline{h}}^{-1} \rho_0 \vec{v} = i\omega \overline{\overline{Q}}_{\text{par}} \overline{\overline{h}}^{-1} \overline{\overline{Q}}_{\text{par}}^{-1} V_{\text{frac}}^{-1} \rho_0 \vec{v} \tag{8.48}$$

leaving us with the equivalent of (1) in fully transformed coordinates

$$\nabla_q p = i\omega \overline{\overline{\rho}} \rho_0 \vec{v} \tag{8.49}$$

with

$$\overline{\overline{\rho}} = \overline{\overline{Q}}_{\text{par}} \overline{\overline{h}}^{-1} \overline{\overline{Q}}_{\text{par}}^{-1} \overline{\overline{V}}_{\text{frac}}^{-1}. \tag{8.50}$$

Equations (8.42) and (8.49) show that the acoustic equations are fully transformation invariant with the modified material parameters in (8.43) and (8.50).

They further show that these experiments are equivalent to those shown by Naify et al. [63] purely by analogy with electromagnetics through the electric conductivity equation (Greenleaf et al. [88]) and those derived by Greenleaf et al. [83] for the general scale Helmholtz equation. Consequently, cloaking shell, concentrator and other devices that have been designed theoretically by electromagnetics can also be realized for acoustics provided that the bulk modulus and anisotropic effective mass density tensor can be realized in practice as specified by (8.43) and (8.50). This first principle derivation without using analogy shows explicitly in (8.41) how the acoustic velocity vector must transform under coordinate change, which as noted above is different from how the $\vec{E}$ and $\vec{H}$ field transform in electromagnetics. The scalar pressure is, however, not changed by the coordinate transformations, and thus, like phase fronts and power flow lines, it is simply deformed by any coordinate transformations.

8.9.2.2 Application to a Specific Example

We consider the spherical cloaking transformation [80] as illustrated in Fig. 8.7 and specified by $r' = a + r(b-a)/b$ where a and b are constants and $b > a$. This coordinate transformations is orthogonal and then $\overline{\overline{h}} = 1$ and $V_{\text{frac}} = 1$ which are good simplification. The Q_i length scaling factors are straightforward to calculate provided one realizes that the azimuthal and polar angles and not length, as in Cartesian coordinates and (8.35), must be modified slightly. The Q_i is defined by the ratio of infinitesimal lengths in the transformed and untransformed coordinates, and thus,

$$Q_r = \frac{\mathrm{d}r}{\mathrm{d}r'} = \frac{b}{b-a}, \quad Q_\phi = \frac{r\mathrm{d}\emptyset}{r'\mathrm{d}\phi'} = \frac{b}{b-a}\frac{r'-a}{r'} \tag{8.51}$$

$$Q_\Theta = \frac{r\sin\theta}{r'\sin\theta'}\frac{\mathrm{d}\theta}{\mathrm{d}\theta'} = \theta_\varphi \tag{8.52}$$

in agreement with the parameter found through other approaches by Greenleaf et al. [83] and Cummer et al. [89].

Thus Cummer et al. [87] showed $\vec{E}$ and $\vec{H}$ of electromagnetics transform differently from $\vec{v}$ of acoustic waves under coordinate transformations. It shows that a first principle analysis of the acoustic equation under arbitrary coordinate transformations confirms that the divergence operator is preserved only if velocity transforms in this physically correct way (Fig. 8.15).

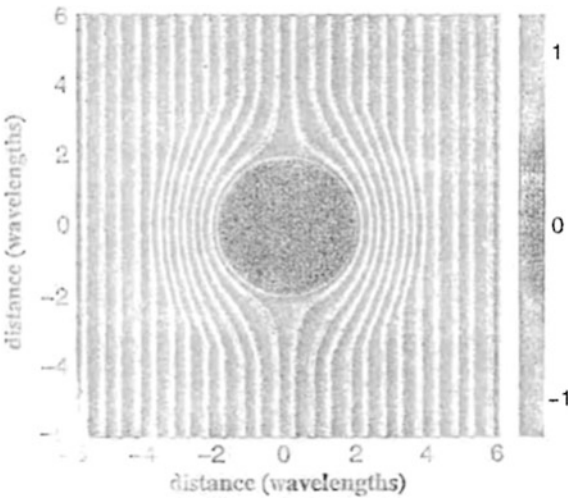

Fig. 8.15 Real part of the pressure field in the r–θ plane of the problem domain computed from the series solution. The plane wave is incident from the left [89]

8.9.3 Zero-Index Medium [31]

Zero-index medium (ZIM) [31] which has a refractive index near zero can be applied to acoustical cloaking with $\overline{n} \approx 0$; then $\Delta\varphi = \overline{k}d = \overline{n}\omega d/c \approx 0$ means no advance of phase inside the medium where d = propagating distance, ω = angular frequency and $\Delta\Phi$ = accumulated phase of the sound wave. The area/volume ratio of this type of material, from transformation acoustics, will be equivalent to a point with a measure of zero but with expansion in space [63]. This means that the wavefield inside such a medium will not change and will remain constant. The shape of the ZIM's boundary will determine the outgoing wavefront. This means that if viewed from outside, a scatterer will not generate any scattered wave if it is placed inside a ZIM and hidden [90].

A ZIM can generate other interesting effects. For instance, although a plane wave passing through a slab of ZIM with thickness d will accumulate no phase, the same wave when propagating through the background medium with refractive index n will advance in phase by $\Delta\varphi = n\omega d/c$. This will cause difference in the phases of the outgoing wave in these two different cases unless $d = 2\ m\pi c/n\omega$, where m = integer. This means that the cloaking effect would be lost through comparison of the two phases unless d fulfils the above relation.

Besides this, ZIM cloaking is limited only to normal incidence because total internal reflection will occur to the wave with oblique incident angles. There is some application of this interesting characteristic as shown below. First, one takes a prison made with ZIM and with two boundaries makes a nonzero angle. With an incoming wavefront at normal incidence to a boundary of the prism, total transmission through both prism interfaces is expected. However, a wave propagating in the opposite direction of the incident wave will be totally reflected by the prism due to nonzero incident angle. Thus, the restricted geometry of the prism gives rise to a symmetric transmission [91]. Another advantage is that ZIM's functionality is highly sensitive to the nature of defects. This is due to the boundary dependence of ZIM in the presence of acoustic waves. A defect with an acoustically soft boundary or $P = 0$ placed inside a ZIM will enable the wavefield inside to be zero everywhere giving rise to total reflection of incident wave [92–94]. This boundary dependence of the ZIM in the presence of sound wave can also be used to mitigate the transverse-longitudinal mode conversion of scatterers [95].

8.10 Space-Coiling and Acoustic Metasurfaces [31]

8.10.1 Incurring Large Phase Delays Within a Small Space

Acoustic waves are longitudinal waves. This is an advantage that can be tapped on for the design of the acoustic metamaterials. This will enable the acoustic waveguide to have no cut-off frequency. This advantage has been exploited by Liang and

Li [90] in their design using the space-coiling concept. This is a complex passage, with sub-wavelength cross section. This enables sound to propagate through passages that are much longer than their external dimension (Fig. 8.16a). The coiling up of passages produces a huge phase delay $\Delta\varphi = k_0 L$, where k_0 = wave number in the background fluid and L = "acoustic path". This type of geometric structure has been used in bass woofers or folded horn speakers [96]. Here, the phase and group velocities and hence the effective refractive index and dispersion relation can be tuned by adjusting the total length of the sound passage. This concept was experimentally proved [97–99].

The space-coiling design is easy to implement and also effective. This received much attention. Various functionalities such as high transmission [100, 101], absorption [102], one-way transmission [101] and zone plate focusing [100, 103–105] were demonstrated.

Cheng et al. [106] reported a fan-shaped design of space-coiling. The cylindrical-shaped unit cell with the winding air passage produces a high effective refractive index. This produces a multiple Mie resonances of angular momenta. Single negativity in the mass density and bulk modulus was shown. The strong Mie resonances produce a huge scattering cross section leading to high reflection with sparse units.

8.10.2 *Phase Manipulation with Acoustic Metasurfaces [31]*

Space-coiling design structures are useful for constructing acoustic metasurfaces, which are acoustic phase arrays with sub-wavelength thickness. They are capable of

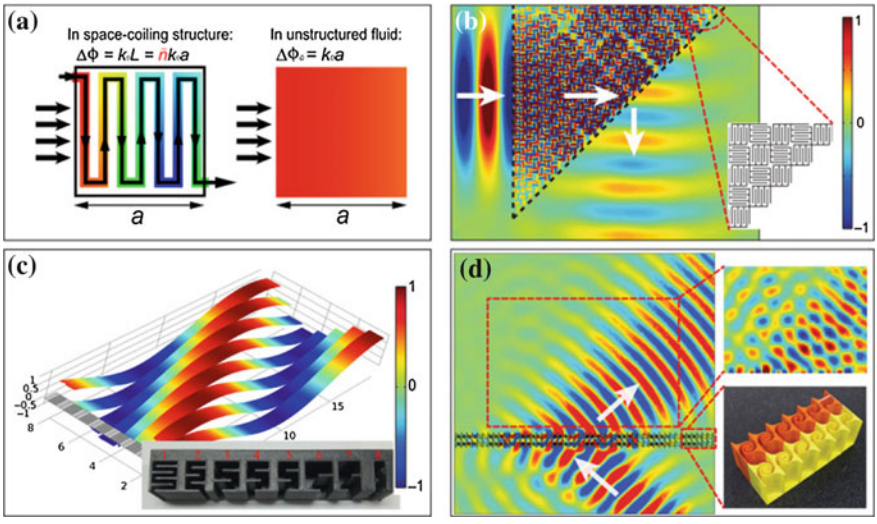

Fig. 8.16 Space-coiling and acoustic metasurfaces [31]

generating phase shift up to 2 π across a single layer. This phase shift supplies the incident wave with an extra momentum. This phase shift can cause the incident wave to reflect/refract at an abnormal angle due to the extra moment acquired. Li et al. [107] proposed a feasible design. Their reflective geometry is shown in Fig. 8.16c.l. Here, part of the incident wave that enters the coiled channels so that nonspecular reflected beam will be formed due to the laterally varying phase delay is acquired by the reflected wave. The wavefront of the nonspecular reflected beam is marked by red ridge as shown in Fig. 8.16c. Subsequent experiments [108] show interesting phenomena of negative refraction, focusing and surface wave conversion.

A weakness of this space-coiling design is the large impedance mismatch between the incident wave and the reflected wave. For sound transmission, besides phase shifts, impedance matching is also necessary to obtain optimal results. Some theoretical works [109, 110] have considered this. Some experimental works have target to resolve the impedance matching problem. One method is to use resonances to improve coupling [111, 112]. Another method is to improve impedance matching by adding on horn-like design [113, 114]. This is shown in Fig. 8.16d. With this addition of horn-like design, negative refraction was shown in transmission by using a lateral gradient in phase delay. However, these designs have to sacrifice the thickness of the devices. Their thickness is close to $\lambda/2$. Li et al. [107] also demonstrated exotic functionalities such as complex wavefront shaping in the formation of self-bending beams by imprinting spatial function to the phase profile generated by the metasurface. These performances will depend on the condition of the incident wave such as incident angle, beam shape, position and source geometry [108, 111].

8.11 Absorption [31]

Acoustic absorption is essential for noise reduction and sound insulation. The three principal mechanisms of absorption are dissipation, impedance matching and resonances. Friction will give rise to dissipation. So, sound absorbing materials are porous. Some common forms are fibreglass, mineral wools, sponges and cotton [115]. Impedance matching improves absorption by enhancing coupling of the incident acoustic energy with the absorbers. An example is gradient index material. Examples of gradient index materials are porous materials with varying filling density. Improvement in impedance matching can be obtained by cutting blocks wedge or conical shapes. Improved impedance matching and high energy density will produce resonances. An example is microperforated panels with back cavities [116].

The above methods will show good performance for a relatively broad and relatively high frequencies. They are less effective for low frequencies. This is due to quadratic dependence of attenuation on frequencies. An obvious way is to increase the thickness of the sound absorbing material which would be of the order

of a few wavelengths which can exceed 1 m for low-frequency sound as sound absorbing material. This is impractical. A way out is to use acoustic metamaterial as sound absorbing material. Sub-wavelength resonators can produce very high-level energy density. Since absorption is proportional to the product of energy density and absorption coefficient in the low-frequency regime, a small value of the absorption coefficient can be compensated by a large value of the energy density. This has been demonstrated by Maa [116]. They obtained large absorption by using sub-millimetre elastic membranes dotted by asymmetrically shaped rigid platelets. Figure 8.17a shows a concentration of large energy density within small regions near the perimeter of the rigid platelets due to the contrast in flexural rigidity. These regions are of sub-wavelength dimensions. This causes the decoupling of the high energy densities from the propagating modes, and so, only absorption can take place. Also, it has been shown that perfect impedance matching and high local energy density can take place simultaneously [117]. This can be achieved by adding a thin layer of sealed gas behind the DMR (Fig. 8.17b left), which will result in a new resonant mode by combining two low-frequency modes (Fig. 8.17b). Because the new resonant mode is a linear superposition of the two low-frequency eigenmodes, the two components of the normal displacements $\langle W \rangle$ and $\delta W(\boldsymbol{x})$ from Eq. (8.19) can be separately tunable. Thus, one can optimize $\langle W \rangle$ for perfect matching for air, and at the same time, $\delta W(\boldsymbol{x})$ can become very large so that all the incident wave energy will be absorbed (Fig. 8.17b right). This can lead to an extremely thin low-frequency narrow bandwidth total absorber.

There are also other forms of space-coiling design reported. One [102] is that sound was forced to travel a distance of $\lambda/4$ through a convoluted air passage and total reflection was reduced. This thin air passage, resembling a perforated plate, will be the absorbing medium. Also, broadband absorption was demonstrated by Jiang et al. [118]. This was done by stacking multiple quarter-wave resonators from optics. This is due to the destructive interference between counter-propagating waves. This will lead to the cancellation of outgoing waves, and total absorption can be achieved. Theoretical works have been done applying CPA to acoustics [119, 120]. They showed that stringent requirements are needed for geometry and material properties. For instance, Leroy et al. [120] showed high absorption in waterborne ultrasound using a sub-wavelength layer of resonant bubbles hollowed in a soft polymer film to cover a sound reflector.

Another method to obtain total absorption is by degenerating critical coupling. This can be done by using proper metamaterial design to obtain the exact degeneracy of two eigenmodes with different symmetric conditions [121]. The special advantage is the sub-millimetre thickness of the sound absorbing membrane made of acoustic metamaterial for low-frequency noise reduction compared with the tremendous thickness required for sound absorbing material for low-frequency applications.

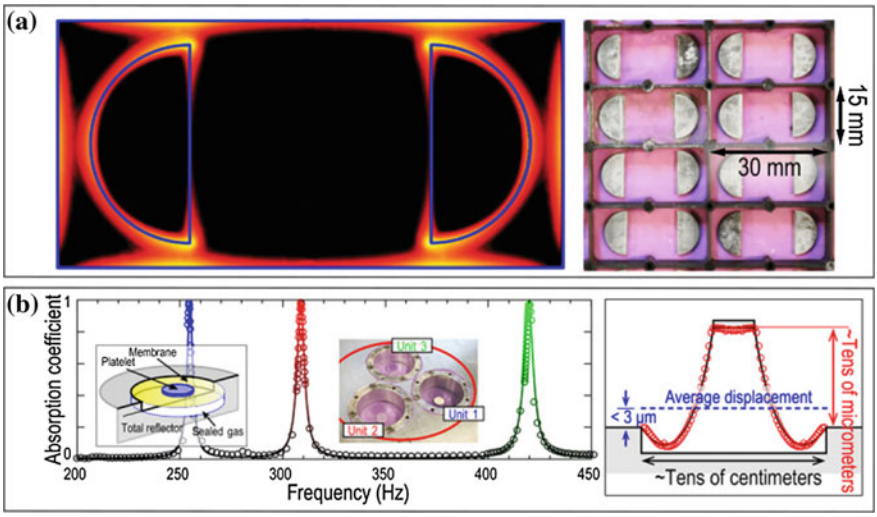

Fig. 8.17 Acoustic absorption by DMRs [31]

8.12 Sound Insulation Materials as Application of Complex Local Resonant Structures

8.12.1 Introduction

Noise pollution is an outcome of increasing population density, traffic flow and construction activities. There is increasing concern about inadequate sound insulation in buildings and the consequent implications for occupants' health and well-being both in the public sector and in the private sector. Indications from recent studies [122–124] show growing dissatisfaction from residents regarding the acoustic performance of their accommodation, reflected by an increasing number of noise nuisance complaints [124]. The problem is particularly evident in medium- to high-density housing situations. Acoustic intrusion commonly occurs at frequencies below 1 kHz which corresponds to the bass beat of music systems where human hearing has its highest sensitivity. The insulation in buildings for such low-frequency range using conventional methods will require thick sound absorbing material which is cumbersome and expensive. Acoustic metamaterial enables the sound insulation membrane with sub-millimetre thickness and for low-frequency noise absorption. This section will focus on the development of local resonant structures (LRS) as a form of metamaterials. Simple analytical models of single and multiresonant linear spring-mass systems will be used to study important design trade-offs and response characteristics such as bandwidth, band positioning and sound transmission loss during and after the frequency of localized resonance. New LRS specimens are then

subjected to dynamic, plane wave impedance tube and diffuse field testing methods, to indicate the performance of the metamaterial samples.

8.12.2 Sound Insulation

The purpose of sound insulation is to reduce sound transmission through the building. There are various conventional methods of sound insulation. One common way is the use of sound barriers which reflects sound transmission energy. For plane waves travelling though a medium, the quantity most commonly used for expressing the performance of a partition's sound insulation is the transmission loss TL or sound reduction index R. First defined in the 1950s [125], the sound reduction index is related to the transmission coefficient τ by:

$$R = 10\log_{10}\left(\frac{1}{\tau}\right). \tag{8.53}$$

The transmission coefficient is a frequency-dependent fraction of the incident sound energy and the transmitted sound energy through a medium. In the problem frequency range, reflection properties are dominated by the mass/area. This region may be approximated by the mass law equation:

$$R = 10\log_{10}\left[1 + \left(\frac{\pi f M \cos\theta}{\rho_a c_a}\right)^2\right] \tag{8.54}$$

where M is the mass per area, ρ_a is the density of air, c_a is speed of sound, f is the frequency, and θ is the angle of incidence. The sound reduction index is maximized when sound is transmitted at normal incidence.

8.12.3 Application of Acoustic Metamaterials to Sound Insulation [126]

Acoustic metamaterials are artificial composites with periodic structures and possess properties which can be artificially manipulated, that is, with properties not found in nature. They are inhomogeneous in nature and thus with a nonuniform composition engineered to provide properties which may not be readily available in nature. These inhomogeneous materials have a nonuniform composition. Klironomos and Economou [127] showed that the presence of inhomogeneity in a material can influence the propagation of waves in periodic material structures. These materials have been developed by John [128] and Kushwaha et al. [129] in the areas of electromagnetics and acoustics, respectively. Metamaterials can form

band gaps enabling the material to prevent wave transmission in specific frequency ranges of electromagnetic, elastic or acoustic waves in any direction. The band gap can be created by two mechanisms [130]: (1) Bragg scattering and (2) localized resonance. Analysis of large-scale acoustic Bragg scattering was first realized in 1995 by Martinez-sala et al. [131] where he described the sound transmission properties of a large open air sculpture in Madrid. This sculpture consisted of a periodic crystal-like arrangement of tall metal rods. Band gap behaviour of these structures is due to the phenomena of wave diffraction and interference created by the high-density rods acting as scattering reflectors. In order to create an acoustic band gap in the audible range using Bragg scattering, the internal structure of the material needs to be large. Because of the existence of Bragg scattering, it is required that the lattice constant/arrangement be a minimum of half the wave length of the incident sound wave [132]. For low-frequency wavelengths in order of metres, this is simply too large to be practical for insulation applications.

Liu et al. [133] in 2000 created band gap by localized resonances. Here, localized resonances were created by a three-component acoustic metamaterial, including a host material with polymer-coated rigid inclusions. The frequency of the band gap is dictated by the resonant frequency of the resonators and is independent of periodicity and symmetry. LRS use internal resonances to alter the effective properties of the material at different frequencies. One such property is the ability to inhibit sound transmission in a targeted frequency range. Liu et al. [133] showed that when a significant improvement in sound transmission loss was found between 200 and 1000 Hz in a selected 100 Hz band. Using a unique LRS known as a local resonant sonic material LRSM.

Theoretically, Milton et al. [134], Yao et al. [135], Huang and Sun [136, 137], Gang et al. [138], Calius et al. [139] used the spring-mass model to explain the important features of the LRS. Starting with a simple resonator LRS, the model consisting of a mass attached to a spring is mounted on another two springs. Next, one applied point force P to the backing layer will represent the acoustic pressure applied by the sound field. First, the response of the system will be given as follows:

$$\begin{pmatrix} F \\ 0 \end{pmatrix} = \begin{bmatrix} k_0 + k_1 - m_0\omega^2 + i\omega c_1 & -k_1 - i\omega c_1 \\ -k_1 - i\omega c_1 & k_1 - m_1 + i\omega c_1 \end{bmatrix} \begin{pmatrix} x_0 \\ x_1 \end{pmatrix} \tag{8.55}$$

where F = total force, x = displacement, m = mass, c = damping coefficient and k = spring constant.

Rearranging and assuming no damping and solving the matrix, the system's effective mass (m_T) can be obtained as [134]:

$$m_T = \frac{F}{a_{m_0}} = m_0 + m_1\omega_1^2/(\omega_1^2 - \omega_0^2) \tag{8.56}$$

where F = externally applied force, a_{m_0} = acceleration of the host/layer, ω_1 = resonant frequency of the spring k_1 and mass m_1 when attached to a rigid base and can be found using:

$$\omega_1 = \sqrt{\frac{k_1}{m_1}} \tag{8.57}$$

By changing the spring stiffness k_1 or internal mass m_1, the resonant frequency and the amplitude may alter.

From the analysis of (8.56), at frequencies well below $f_1 = \omega_1/2\pi = 400$ Hz, the acceleration of the host material and resonator mass is close to equal, and the effective mass is approximately the sum of the components $m_T = m_0 + m_1$. At frequencies far above the resonance frequency, where $\omega \gg \omega_1$, the acceleration of the resonator mass approaches zero and the total effective mass becomes the host material only, where $m_T = m_0$. The frequency range most relevant here is frequencies around resonance. As ω approaches ω_1, the resonator mass and host components are in phase with each other. The acceleration of the host material drops towards zero, while the resonator mass acceleration is increasing. At $\omega = \omega_1$, the ratio of the resonator mass and host acceleration is at maximum and the host material is almost stationary. The host material has a large total effective mass, and therefore, sound transmission can be reflected well at this frequency. Frequencies immediately above resonance components become out of phase with each other, and it may be seen that the acceleration of both the host and resonator mass increases to a maximum. At this point, the ratio of the two components is zero. The result of this high acceleration in the host material is a decrease in the effective mass to almost zero and an increase in transmission though the structure. By substituting $m_T = 0$ and rearranging Eq. (8.56), it can be seen that the frequency at which this occurs is described by Yao et al. [135]:

$$\omega = \omega_1 \sqrt{(m_0 + m)/m_0}. \tag{8.58}$$

The biggest weakness in the LRS method is the limitation of the attenuation to a narrow range of frequencies, the detrimental effects, immediately after resonance, on transmission loss from the peak acceleration of the matrix material and to a lesser extent, the limiting effect of damping.

LRS performance is strongly affected not only by the characteristics of the resonator itself, but also more so by the way these local resonators are connected together to form the LRS. The realization of useful LRS-based applications depends on the combination of cost-effective materials and processes with modelling tools that enable design, analysis and optimization.

In the following section, a modelling-driven building block approach is used by Hall et al. [126] to develop LRS designs, with experimental verification at every level. The local resonant unit represented schematically by the spring-mass model provides the basic building blocks from which groups of resonant units are integrated to form layers which are combined to form panels. Here, a modelling

methodology is presented that predicts the transmission loss in an impedance tube and a full-scale room-to-room test facility. This modelling methodology is then used to explore the sensitivity of LRS performance to design parameters, with particular attention to broadening the transmission loss bandwidth and reducing detrimental effects outside this frequency band.

8.12.4 Modelling Methodology of the Localized Resonances Structures (LRS)

It is well known that complex mechanical systems can be represented by a combination of a large enough number of single degree-of-freedom SDOF sub-systems such as the one depicted schematically in the spring-mass model [140].

8.12.5 Experimental Methods of the Localized Resonance Structures (LRS)

Two different experimental methods were used to test the performance and validate the modelling approach by Hall et al. [126]. Plane wave testing and diffuse field testing laboratory-scale evaluations were performed using an impedance tube, which is suitable for testing single units or small groups of resonators and measuring the transmission and reflection of predominantly plane waves. Full-scale measurements were performed between reverberation rooms, which were suitable for testing relatively large specimens consisting of many resonators under diffuse sound field conditions.

8.12.6 Plane Wave Testing

Here, normal transmission loss measurements were performed using the impedance tube conforming the European Standard ISO 10534-2:2001 (E). Dimensions of the impedance tube followed that of the B&K type-4026 impedance tube. A 100-mm-diameter hollow cylinder made of medium density fibre (MDF) contains the resonator units being tested. Alternative resonator designs were attached to a backing plate that represented the matrix material of the LRS. The cylindrical LRS sample was suspended on two rubber rings between two parts of the impedance tube. A loud speaker generates plane wave sound that propagates down the first tube. Part of the signal is transmitted through the sample which is measured in the second tube using three microphones. Microphones 1, 2 and 3 are used to find the transmitted side complex wave constants A and B, while microphones 4, 5 and 6 are

used to find the receiving complex wave constants C and D. The receiving side of the impedance tube is in anechoic condition where reflections (D) are assumed to be near 0, and hence, the transmission coefficient is found to be near the ratio of A to C. The transfer coefficient may be found from $\tau = (AC - BD)/(AA - DD)$ where τ is the transmission coefficient. When τ is applied to $R = 20 \log_{10}(1/|\tau|)$, the sound reduction index may be found.

8.12.7 Diffuse Field Testing

Full-scale diffuse field testing was carried out by Hall et al. [126] in the room-to-room testing facility. It was developed according to ISO 140-3. Sound reduction index of the samples is measured in two reverberation rooms (202 and 208 m^3). The room-to-room testing facility was used by Hall et al. [126] for full-scale diffuse field testing and was designed to ISO 140-3. There is an adjustable gap between two well-insulated sliding doors that separate the two rooms. The test specimen is to fill this gap. A broadband pink noise source signal is then placed in one of the rooms. The spatial average sound pressure and reverberation time (RT) in the emitting and receiving rooms are then measured using 1/2″ B&K 4190 and 4165 microphones. The process is then repeated with the noise source in the other room. Data were processed in third octaves. In order to study the frequency response in more detail than third octaves, the spectrum was found by calculating the power spectral density (square of the magnitude of the Fourier transform of the signal) from the raw time domain pressure signals. The narrow band RT was found by interpolating the third octave RT results. The absorption area of the receiving room was found using:

$$A = 0.163V/T_{60} \tag{8.59}$$

where T_{60} is the reverberation time, V is the volume of the receiving room. The level difference (δL) of the specimen was then calculated from:

$$\delta L = 10 \log_{10}[P_0] - 10 \log_{10}[P_1] \tag{8.60}$$

where P_0 is the incident sound power and P is the radiated sound power. Under the assumption of diffuse sound fields in the transmitting and receiving rooms, the actual sound reduction index of the specimen may be found using:

$$Rd = \delta L + 10 \log_{10}\left[\frac{S}{A}\right] \tag{8.61}$$

where S is the area of the wall specimen. The single-layer panel consisted of 252 resonators attached to a 2.65 × 0.95 × 0.01 m plasterboard matrix layer using Loctite 401 adhesive. The accelerations perpendicular to the panel plane were also

measured, while the panel was subjected to pink noise. For each measurement, two PCB A353 B65 accelerometers were attached at any 2 of 9 different positions on the back of the panel using wax. The amplitude of the acceleration as a function of frequency at various locations were measured. These measurements also allowed the phase difference to be calculated between adjacent resonators. This testing method gives insight into the sound insulating performance of large-scale meta-material samples under a diffuse field.

8.12.8 Results

Experimental results are obtained and compared with theoretical calculations using the spring-mass model by Hall et al. [126] for single-frequency local resonant structures, parallel multi-frequency systems, series systems and series parallel systems.

8.12.9 Discussion

The results obtained for single-frequency LRS through both experimental observations and analysis indicate that when $\omega \leq \omega_1$, where ω_1 is the resonant frequency of the resonator, the LRS transmission loss is equal or greater than that of a homogeneous material with the equivalent mass area density. At frequencies approaching ω_1, the host material and resonator mass are in phase with each other. It may be seen that the acceleration of the resonator mass gradually increases in this frequency region, while the host material reduces the acceleration mass of the host material. The comparisons between modelling and experimental results, together with the experimental results obtained by Yao et al. [135], confirm that systems of linear spring-mass models can be used to obtain an accurate estimate of LRS sound transmission behaviour, whether it is in an impedance tube or between reverberant chambers. The key question for practical applications is how to maximize the frequency band over which the LRS is effective while also achieving a large enough increase in sound attenuation within that frequency range. Ideally, the LRS will have a multiplicity of resonances at frequencies that are so close together that the resonant peaks overlap. This can be achieved by designing systems of resonant units with incremental closely spaced frequencies and an appropriate amount of damping. Other researchers [141–143] have approached this problem by constructing multilayer LRS where each layer has a single resonance frequency, that is, the resonators in any given layer are all tuned to the same frequency, but this frequency is different from layer to layer. The limitation inherent in this approach is that increasing the system's bandwidth requires additional layers, each layer increases the thickness of the system, and building applications impose practical limits on the total thickness. So the question is whether sets of resonant units with

different but closely spaced resonant frequencies arranged in a single layer could produce a similar effect. The experimental and model results shown by Andrew Hall et al. [126] demonstrate that this is the case. When resonators are placed in parallel with only a small amount of damping, the band of increased attenuation becomes several times wider than the previous single resonator arrangement, but has a significantly lower peak magnitude. Similar to the single-frequency LRS, there is also a significant drop in the transmission loss after resonance due to a drop in the effective mass of the structure. Eventually, the LRS curve asymptotically approaches the host material mass law. One method of shaping the transmission loss curve and reducing the transmission loss dip around 1000 Hz is to use different masses in the resonators tuned to different frequencies. By tapering off the weights of the parallel resonator masses gradually from the bottom to the top over the LRS high TL band and with the addition of damping, the result is a smoothing effect over the TL dip after localized resonance. It has been already shown that practical methods of implementing these design features are possible and will be studied in future work. Single-frequency and parallel multifrequency LRS both consist of a single reflective layer with a specific effective mass spectra. In a series arrangement, a sound wave will interact with multiple reflective layers each with their own effective mass frequency spectra. A high attenuation band gap is shown. The magnitude of the attenuation approaches infinity when one increases the number of layers in the series. However, the width of the band gap given by the distance between its shoulders does not change significantly with the number of layers in series. These results show the condition for the full development of a band gap. That is, the inter-layer coupling spring has to be softer than the resonator spring or of equal stiffness. Also, the bandwidth will be wider for a softer inter-layer coupling relative to the resonator. In a multilayer system, the number of multiple transmission loss dips increases with the number of layers. This occurs outside the transmission band gap. Because these dips are the result of layer movement within the structure, increasing the damping factor significantly in the inter-layer coupling ($\zeta = 0.1 - 0.5$) reduces the adverse effects of these transmission loss dips while having no visible effect on the sound reduction index performance within the band gap. It is clear that combination of series and parallel arrangements is what yielded systems with the largest amount of attenuation over large bandwidths. Therefore, by designing a LRS system with the following elements: • several layers in series • offset spring stiffness between resonators and layers • damping between each layer, a stopband filter response is effectively created that has a wide enough bandwidth to be suitable for practical applications. Experimental verification of the model predictions has yet to be conducted. Implementations of this series–parallel LRS are still at the design stage due to the complexity of the problem when considering practical constraints such as structural integrity, construction materials and cost.

8.12.10 Conclusion

Local resonant structures (LRS) exhibit a significant improvement in sound attenuation over what can be achieved with a homogeneous material of similar mass, albeit in a limited frequency bandwidth. The magnitude of improvement is strongly dependent on the ratio of host:resonator mass, the damping of the resonator mass and the overall design of the LRS. To guide design, a modelling approach was developed based on the systems of interconnected single degree-of-freedom linear spring, mass and damper units, each of which represents one or a group of identical local resonators. Good correlation was obtained between modelling and various experimental methods showing that this modelling approach can be used to estimate both plane wave and diffuse field transmission through an LRS in the frequency domain of interest. Different LRS system configurations were analysed using this modelling method for the purposes of widening the frequency band of improved transmission loss, increasing the magnitude of transmission loss in this band and reducing adverse effects outside this band. Parallel systems were shown through modelling and testing to produce transmission loss gains over a much wider frequency range, with a reduction in the transmission loss dips at other frequencies by tapering the resonator mass distribution and damping across frequencies. Series resonators developed very high peak transmission loss, leading to transmission band gaps or stopbands. These complex designs need more detailed modelling and further experimental analysis to develop practical implementations. The realization of LRS applications requires the use of modelling to optimize the geometry, material properties, performance and cost of the materials, as well as to understand the tolerances of these variables. The ideal final outcome would be a cost-effective method for the fabrication and implementation of a local resonant metamaterial that satisfies the qualities described previously.

8.13 Emerging New Directions and Outlooks

Acoustic metamaterials have undergone tremendous further developments since they were first proposed and fabricated. This results in several new functionalities and has gone beyond the original definition of double acoustic and local resonant unit cells.

8.13.1 Elastic and Mechanical Metamaterials [31]

Acoustic metamaterial can be applied also to the study of structural elastic waves. This has been shown in the study using thin plates for the manipulation of elastic surface waves [144–147], cloaking [148–151] negative refraction [152–154] and

sub-diffraction focusing [154, 155]. Sofar, theoretical and numerical works on resonant elastic metamaterials have produced negative shear modulus and super-anisotropy. However, experimental investigations are rare. An interesting experiment by Brule et al. [156] drilled a rectangular array of boreholes into the ground surface to block low-frequency surface vibrations and hence mitigate the destructive effects of seismic waves.

Mechanical metamaterials in the form of pentamode metamaterials were proposed by Milton and Cherkaev [157] and Milton [158]. For this type of mechanical metamaterial, rigidity is maintained through point contacts between the tips of the elongated structural elements. For this type of structure, one can have a bulk modulus much larger than the shear modulus leading to the decoupling of the compression and transverse vibrations. This is because the bending and rotational motion about the point contacts encounter much smaller resistances. During the past few years, pentamode metamaterials have been successfully fabricated using technology of lithography and three-dimensional printing [157–162].

8.13.2 Acoustic Metamaterials as Rapidly Developing Field with Tremendous Potential

Recent developments on digitizing of metamaterials into binary units [163] can find applications in actively controllable metasurfaces and other functionalities more accessible. Acoustic metamaterial is a product and confirmation of the symmetric properties of the acoustic fields. This enables the manipulation and control of the acoustic fields. The local resonance aspect of acoustic metamaterials implies frequency dispersion and narrow frequency band limitation in the effectiveness. Broadening the frequency range of operation of acoustic metamaterials will enable a more diverse application of acoustic metamaterials. The application of acoustic metamaterials to acoustical imaging will extend application to ultrasound, such as, nondestructive testing and medical ultrasound. New concepts of “digitizing” metamaterials into binary units [163] have already made some promised functionalities more accessible, such as, actively controllable metasurfaces. Acoustic metamaterials have been used in underwater cloaking and antisubmarine works. Seismic metamaterials have been developed to protect buildings against earthquakes. Due to simple fabrication works, metamaterials can be used as sound insulation materials, a passive means as opposed to the electronic method of active noise cancellation. Recently, acoustic metamaterials have been used in selective perception in human audition [164].

References

1. Yablonovitch, E.: Inhibited spontaneous emission in solid-state physics and electronics. Phys. Rev. Lett. **58**, 2059–2062 (1987)
2. John, S.: Strong localization of photons in certain disordered dielectric superlattices. Phys. Rev. Lett. **58**, 2486–2489 (1987)
3. Sigalas, M., Economou, E.N.: Band structure of elastic waves in two dimensional systems. Solid State Commun. **86**, 141–143 (1993)
4. Kushwaha, M.S., Halevi, P., Dobrzynski, L., Djafari-Rouhani, B.: Acoustic band structure of periodic elastic composites. Phys. Rev. Lett. **71**, 2022–2025 (1993)
5. Yablonovitch, E., Gmitter, T.J.: Photonic band structure: the face-centered-cubic case. Phys. Rev. Lett. **63**, 1950–1953 (1989)
6. Martínez-Sala, R., Sancho, J., Sánchez, J.V., Gómez, V., Llinares, J., Meseguer, F.: Sound attenuation by sculpture. Nature **378**, 241 (1995)
7. Montero de Espinosa, F.R., Jiménez, E., Torres, M.: Ultrasonic band gap in a periodic two-dimensional composite. Phys. Rev. Lett. **80**, 1208–1211 (1998)
8. Chang, L.L., Esaki, L.: Semiconductor quantum heterostructures. Phys. Today **45**, 36 (1992)
9. Sheng, P. (ed.): Scattering and Localization of Classical Waves in Random Media. World Scientific, Singapore (1990)
10. Sigalas, M.M., Economou, E.N.: Elastic and acoustic wave band structure. J. Sound Vib. **158**, 377 (1992)
11. Kushwaha, M.S., et al.: Theory of acoustic band structure of periodic elastic composites. P. Rev. B **149**, 2313–2322 (1993)
12. Kushwaha, M. S., Halevi, P.: Band-gap engineering in periodic elastic composites. Appl. Phys. Lett. **64**, 1085–10900 (1994)
13. Economou, E.N., Sigalas, M.M.: Elastic and acoustic wave band structure. J. Acoust. Soc. Am. **95**, 1735 (1994)
14. Sanchez-Perez, J.V., et al.: Sound attenuation by a two-dimensional array of rigid cylinders. Phys. Rev. Lett. **80**, 5325 (1998)
15. Torres, M., Montero de Espinosa, F.R., Garcia-Pablos, D., Garcia, N.: Sonic band gaps in finite elastic media:surface states and localization phenomena in linear and point defects. Phys. Rev. Lett. **82**, 3054 (1999)
16. Kafesaki, M., Economou, E.N.: Multiple scattering theory for three-dimensional periodic acoustic composites. Phy. Rev. B. **60**, 11993–12001 (1999)
17. Korringa, J.: On the calculation of the energy of a Bloch wave in a metal. Physica (Amsterdam) **XIII**, 392 (1947)
18. Kohn, W., Rostoker, N.: Solution of the Schrondinger equation in periodic lattices with application to metallic lithium. Phys. Rev. **94**, 1111 (1951)
19. Ashcroft, N., Mermin, D.N.: Solid State Physics. Holt, Rinehart and Winston, New York (1976)
20. Economou, E.N.: Green's Functions in Quantum Physics. Springer, Berlin (1983)
21. Economou, E.N., Sigalas, M.M.: Stopband for elastic waves in periodic composite materials. J. Acoust. Soc. Am. **95**, 1734 (1994)
22. Kafesaki, M., Economou, E.N.: On the dynamics of locally resonant sonic composites. Phys. Rev. B **52**, 1113317 (1995)
23. Liu, Z., et al.: Elastic wave scattering by periodic structures of spherical objects: theory and experiment. Phy. Rev. B **62**(4), 2446–2457 (2000)
24. Yang, S., et al.: Biosensors on surface acoustic wave phononic band gap structure. Phy. Rev. Lett. **88**, 104301 (2002)
25. Wolfe, J.P.: Imaging Phonons: Acoustic Wave Propagation in Solids. Cambridge University Press, Cambridge, England (1998)
26. Zhang, X., Liu, Z.: Negative refraction of acoustic waves in two-dimensional phononic crystals. Appl. Phy. Lett. **85**(2), 341–343 (2004)

27. Luo, C., Johnson, S.C., Joannopuolos, J.D., Pendry, J.B.: All-angle negative refraction without negative refractive index. Phys. Rev. B **65**, 201104 (2002)
28. Luo, C., Johnson, S.C., Joannopuolos, J.D.: All-angle negatve refraction in a three dimensionally periodic photonic crystal. Appl. Phys. Lett. **81**, 2352 (2002)
29. Lai, Y., Zhang, X., Zhang, Z.Q.: Engineering acoustic band gaps. Appy. Phys. Lett. **79**, 3224 (2001)
30. Veselago, V.G.: The electrodynamics of substances with simultaneously negative values of ϵ and μ. Sov. Phys. Uspekhi **10**, 509–514 (1968)
31. Ma, G., Sheng, P.: Acoustic metamaterials: from local resonances to broad horizons. Sci. Adv. **2**(2) (2016)
32. Shelby, R.A., Smith, D.R., Schultz S.: Experimental verification of a negative index of refraction. Science **292**, 77–79 (2001)
33. Shalaev, V.M.: Optical negative-index metamaterials. Nat. Photon. **1**, 41–48 (2007)
34. Fang, N., Lee, H., Sun, C., Zhang, X.: Sub-diffraction-limited optical imaging with a silver superlens. Science **308**, 534–537 (2005) (PubMed)
35. Schurig, D., Mock, J.J., Justice, B.J., Cummer, S.A., Pendry, J.B., Starr, A.F., Smith, D. R.: Metamaterial electromagnetic cloak at microwave frequencies. Science **314**, 977–980 (2006) (PubMed)
36. Cai, W., Chettiar, U.K., Kildishev, A.V., Shalaev, V.M.: Optical cloaking with metamaterials. Nat. Photon. **1**, 224–227 (2007)
37. Milton, G.W., Willis, J.R.: On modifications of Newton's second law and linear continuum elastodynamics. Proc. Phys. Soc. A **463**, 855–880 (2007)
38. Mei, J., Ma, G., Yang, M., Yang, J., Sheng, P.: Acoustic Metamaterials and Phononic Crystals, pp. 159–199. Springer, New York (2013)
39. Yao, S., Zhou, X., Hu, G.: Experimental study on negative effective mass in a 1D mass–spring system. New J. Phys. **10**, 043020 (2008)
40. Liu, Z., Zhang, X., Mao, Y., Zhu, Y.Y., Yang, Z., Chan, C.T., Sheng, P.: Locally resonant sonic materials. Science **289**, 1734–1736 (2000)
41. Liu, Z., Chan, C.T., Sheng, P.: Analytic model of phononic crystals with local resonances. Phys. Rev. B **71**, 014103 (2005)
42. Fang, N., Xi, D., Xu, J., Ambati, M., Srituravanich, W., Sun, C., Zhang, X.: Ultrasonic metamaterials with negative modulus. Nat. Mater. **5**, 452–456 (2006)
43. Li, J., Chan, C.T.: Double-negative acoustic metamaterial. Phys. Rev. E. Stat. Nonlin. Soft Matter Phys. **70**, 055602 (2004)
44. Lai, Y., Wu, Y., Sheng, P., Zhang, Z.-Q.: Hybrid elastic solids. Nat. Mater. **10**, 620–624 (2011)
45. Wu, Y., Lai, Y., Zhang, Z.-Q.: Elastic metamaterials with simultaneously negative effective shear modulus and mass density. Phys. Rev. Lett. **107**, 105506 (2011)
46. Zui, C., Mondain-Monval, O.: Soft 3D acoustic metamaterial with negative index. Nat. Mater. **14**, 384–388 (2015)
47. Yang, M., Ma, G., Yang, Z., Sheng, P.: Coupled membranes with doubly negative mass density and bulk modulus. Phys. Rev. Lett. **110**, 134301 (2013)
48. Ding, Y., Liu, Z., Qiu, C., Shi, J.: Metamaterial with simultaneously negative bulk modulus and mass density. Phys. Rev. Lett. **99**, 093904 (2007)
49. Christensen, J., Liang, Z., Willatzen, M.: Metadevices for the confinement of sound and broadband double-negativity behavior. Phys. Rev. B **88**, 100301(R) (2013)
50. Fok, L., Zhang, X.: Negative acoustic index metamaterial. Phys. Rev. B **83**, 214304 (2011)
51. Lee, S.H., Park, C.M., Seo, Y.M., Wang, Z.G., Kim, C.K.: Acoustic metamaterial with negative density. Phys. Lett. A **373**, 4464–4469 (2009)
52. Lee, S.H., Park, C.M., Seo, Y.M., Wang, Z.G., Kim, C.K.: Acoustic metamaterial with negative modulus. J. Phys. Condens. Matter **21**, 175704 (2009)
53. Lee, S.H., Park, C.M., Seo, Y.M., Wang, Z.G., Kim, C.K.: Composite acoustic medium with simultaneously negative density and modulus. Phys. Rev. Lett. **104**, 054301 (2010)

54. Kaina, N., Lemoult, F., Fink, M., Lerosey, G.: Negative refractive index and acoustic superlens from multiple scattering in single negative metamaterials. Nature **525**, 77–81 (2015)
55. Yang, Z., Mei, J., Yang, M., Chan, N.H., Sheng, P.: Membrane-type acoustic metamaterial with negative dynamic mass. Phys. Rev. Lett. **101**, 204301 (2008) (PubMed)
56. Yang, M., Ma, G., Wu, Y., Yang, Z., Sheng, P.: Homogenization scheme for acoustic metamaterials. Phys. Rev. B **89**, 064309 (2014)
57. Park, J.J., Lee, K.J.B., Wright, O.B., Jung, M.K., Lee, S.H.: Giant acoustic concentration by extraordinary transmission in zero-mass metamaterials. Phys. Rev. Lett. **110**, 244302 (2013) (PubMed)
58. Jing, Y., Xu, J., Fang, N.X.: Numerical study of a near-zero-index acoustic metamaterial. Phys. Lett. A **376**, 2834–2837 (2012)
59. Fleury, R., Alù, A.: Extraordinary sound transmission through density-near-zero ultranarrow channels. Phys. Rev. Lett. **111**, 055501 (2013) (PubMed)
60. Yang, Z., Dai, H.M., Chan, N.H., Ma, G.C., Sheng, P.: Acoustic metamaterial panels for sound attenuation in the 50–1000 Hz regime. Appl. Phys. Lett. **96**, 041906 (2010)
61. Naify, C.J., Chang, C.M., McKnight, G., Nutt, S.: Transmission loss and dynamic response of membrane-type locally resonant acoustic metamaterials. J. Appl. Phys. **108**, 114905 (2010)
62. Naify, C.J., Chang, C.M., McKnight, G., Scheulen, F., Nutt, S.: Membrane-type metamaterials: transmission loss of multi-celled arrays. J. Appl. Phys. **109**, 104902 (2011)
63. Naify, C.J., Chang, C.M., McKnight, G., Nutt, S.: Transmission loss of membrane-type acoustic metamaterials with coaxial ring masses. J. Appl. Phys. **110**, 124903 (2011)
64. Ma, G., Yang, M., Yang, Z., Sheng, P.: Low-frequency narrow-band acoustic filter with large orifice. Appl. Phys. Lett. **103**, 011903 (2013)
65. Yao, S., Zhou, X., Hu, G.: Investigation of the negative-mass behaviors occurring below a cut-off frequency. New J. Phys. **12**, 103025 (2010)
66. Pierre, J., Dollet, B., Leroy, V.: Resonant acoustic propagation and negative density in liquid foams. Phys. Rev. Lett. **112**, 148307 (2014) (PubMed)
67. Lemoult, F., Fink, M., Lerosey G.: Acoustic resonators for far-field control of sound on a subwavelength scale. Phys. Rev. Lett. **107**, 064301 (2011) (PubMed)
68. Lemoult, F., Kaina, N., Fink, M., Lerosey, G.: Wave propagation control at the deep subwavelength scale in metamaterials. Nat. Phys. **9**, 55–60 (2013)
69. Pendry, J.B.: Negative refraction makes a perfect lens. Phys. Rev. Lett. **85**, 3966–3969 (2000) (PubMed)
70. Zhang, S., Yin, L., Fang, N.: Focusing ultrasound with an acoustic metamaterial network. Phys. Rev. Lett. **102**, 194301 (2009) (PubMed)
71. Park, C.M., Park, J.J., Lee, S.H., Seo, Y.M., Kim, C.K., Lee, S.H.: Amplification of acoustic evanescent waves using metamaterial slabs. Phys. Rev. Lett. **107**, 194301 (2011) (PubMed)
72. Park, J.J., Park, C.M., Lee, K.J.B., Lee, S.H.: Acoustic superlens using membrane-based metamaterials. Appl. Phys. Lett. **106**, 051901 (2015)
73. Podolskiy, V.A., Narimanov, E.E.: Near-sighted superlens. Opt. Lett. **30**, 75–77 (2005) (PubMed)
74. Liu, Z., Durant, S., Lee, H., Pikus, Y., Fang, N., Xiong, Y., Sun, C., Zhang, X.: Far-field optical superlens. Nano Lett. **7**, 403–408 (2007) (PubMed)
75. Zhang, X., Liu, Z.: Superlenses to overcome the diffraction limit. Nat. Mater. **7**, 435–441 (2008) (PubMed)
76. Jacob, Z., Alekseyev, L.V., Narimanov, E.: Optical hyperlens: Far-field imaging beyond the diffraction limit. Opt. Express **14**, 8247–8256 (2006) (PubMed)
77. Christensen, J., García de Abajo, F.J.: Anisotropic metamaterials for full control of acoustic waves. Phys. Rev. Lett. **108**, 124301 (2012) (PubMed)
78. García-Chocano, V.M., Christensen, J., Sánchez-Dehesa, J.: Negative refraction and energy funneling by hyperbolic materials: an experimental demonstration in acoustics. Phys. Rev. Lett. **112**, 144301 (2014) (PubMed)

79. Shen, C., Xie, Y., Sui, N., Wang, W., Cummer, S.A., Jing, Y.: Broadband acoustic hyperbolic metamaterial. Phys. Rev. Lett. **115**, 254301 (2015) (PubMed)
80. Cummer, S.A., Schurig, D.: One path to acoustic cloaking. New J. Phys. **9**, 45 (2007)
81. Schurig, D., et al.: Metamaterial electromagnetic cloak at microwave frequencies. Science **314**, 977–980 (2006)
82. Pendry, J.B., Schurig, D., Smith, D.R.: Controlling electromagnetic fields. Science **312**, 1780–1782 (2006)
83. Greenleaf, A., Kurylev, Y., Lassas, M., Uhlmann, G.: Comment on "scattering theory derivation of a 3D acousgtic cloaking shell". http://aixiv.org/abs/0801.3279vl.,2008
84. Lee, S.H., et al.: Composite acoustic medium with simultaneously negative density and modulus. In: Proceedings of ICSV17, Cairo, Egypt, July 2010
85. Gan, W.S.: Gauge invariance approach to acoustic fields. In: Akiyama, I. (ed.) Acoustical Imaging, vol. 29, pp. 389–394. Springer, The Netherlands (2007)
86. Cheng, Y., Xu, J.Y., Liu, X.J.: One-dimensional structured ultrasonic metamaterials with simultaneously negative dynamic density and modulus. Phys. Rev. B **77**, 045134 (2008)
87. Cummer, S.A., Rahm, M., Schurig, D.: Material parameters and vector scaling in transformation acoustics. New J. Phys. **10**, 115025–115034 (2008)
88. Greenleaf, A., et al.: Anisotropic conductivities that cannot be detected by EIT. Physiol. Meas. **24**, 413–419 (2003)
89. Cummer, S.A., et al.: Scattering theory derivation of a 3D acoustic cloaking shell. Phy. Rev. Lett. **100**, 024301 (2008)
90. Liang, Z., Li, J.: Extreme acoustic metamaterial by coiling up space. Phys. Rev. Lett. **108**, 114301 (2012)
91. Li, Y., Cheng, J.C.: Unidirectional acoustic transmission through a prism with near-zero refractive index. Appl. Phys. Lett. **103**, 053505 (2013)
92. Nguyen, V.C., Chen, L., Halterman, K.: Total transmission and total reflection by zero index metamaterials with defects. Phys. Rev. Lett. **105**, 233908 (2010)
93. Wu, Y., Li, J.: Total reflection and cloaking by zero index metamaterials loaded with rectangular dielectric defects. Appl. Phys. Lett. **102**, 183105 (2013)
94. Wei, Q., Cheng, Y., Liu, X.-J.: Acoustic total transmission and total reflection in zero-index metamaterials with defects. Appl. Phys. Lett. **102**, 174104 (2013)
95. Liu, F., Liu, Z.: Elastic waves scattering without conversion in metamaterials with simultaneous zero indices for longitudinal and transverse waves. Phys. Rev. Lett. **115**, 175502 (2015)
96. Klipsch, P.W.: A low frequency horn of small dimensions. J. Acoust. Soc. Am. **13**, 137–144 (1941)
97. Liang, Z., Feng, T., Lok, S., Liu, F., Ng, K.B., Chan, C.H., Wang, J., Han, S., Lee, S., Li, J.: Space-coiling metamaterials with double negativity and conical dispersion. Sci. Rep. **3**, 1614 (2013)
98. Xie, Y., Popa, B.-I., Zigoneanu, L., Cummer, S.A.: Measurement of a broadband negative index with space-coiling acoustic metamaterials. Phys. Rev. Lett. **110**, 175501 (2013)
99. Frenzel, T., Brehm, J.D., Bückmann, T., Schittny, R., Kadic, M., Wegener, M.: Three-dimensional labyrinthine acoustic metamaterials. Appl. Phys. Lett. **103**, 061907 (2013)
100. Molerón, M., Serra-Garcia, M., Daraio, C.: Acoustic Fresnel lenses with extraordinary transmission. Appl. Phys. Lett. **105**, 114109 (2014)
101. Li, Y., Liang, B., Zou, X.-Y., Cheng, J.-C.: Extraordinary acoustic transmission through ultrathin acoustic metamaterials by coiling up space. Appl. Phys. Lett. **103**, 063509 (2013)
102. Cai, X., Guo, Q., Hu, G., Yang, J.: Ultrathin low-frequency sound absorbing panels based on coplanar spiral tubes or coplanar Helmholtz resonators. Appl. Phys. Lett. **105**, 121901 (2014)
103. Li, Y., Liang, B., Tao, X., Zhu, X.-F., Zou, X.-Y., Cheng, J.-C.: Acoustic focusing by coiling up space. Appl. Phys. Lett. **101**, 233508 (2012)

104. Li, Y., Yu, G., Liang, B., Zou, X., Li, G., Cheng, S., Cheng, J.: Three-dimensional ultrathin planar lenses by acoustic metamaterials. Sci. Rep. **4**, 6830 (2014)
105. Tang, K., Qiu, C., Lu, J., Ke, M., Liu, Z.: Focusing and directional beaming effects of airborne sound through a planar lens with zigzag slits. J. Appl. Phys. **117**, 024503 (2015)
106. Cheng, Y., Zhou, C., Yuan, B.G., Wu, D.J., Wei, Q., Liu, X.J.: Ultra-sparse metasurface for high reflection of low-frequency sound based on artificial Mie resonances. Nat. Mater. **14**, 1013–1019 (2015)
107. Li, Y., Liang, B., Gu, Z.-M., Zou, X.-Y., Cheng, J.-C.: Reflected wavefront manipulation based on ultrathin planar acoustic metasurfaces. Sci. Rep. **3**, 2546 (2013)
108. Li, Y., Jiang, X., Li, R.-Q., Liang, B., Zou, X.-Y., Yin, L.-L., Cheng, J.-C.: Experimental realization of full control of reflected waves with subwavelength acoustic metasurfaces. Phys. Rev. Appl. **2**, 064002 (2014)
109. Mei, J., Wu, Y.: Controllable transmission and total reflection through an impedance-matched acoustic metasurface. New J. Phys. **16**, 123007 (2014)
110. Peng, P., Xiao, B., Wu, Y.: Flat acoustic lens by acoustic grating with curled slit. Phys. Letters A. **378**(45), 3389–3392 (2014)
111. Tang, K., Qiu, C., Ke, M., Lu, J., Ye, Y., Liu, Z.: Anomalous refraction of airborne sound through ultrathin metasurfaces. Sci. Rep. **4**, 6517 (2014)
112. Li, Y., Jiang, X., Liang, B., Cheng, J.-C., Zhang, L.: Metascreen-based acoustic passive phased array. Phys. Rev. Appl. **4**, 024003 (2015)
113. Xie, Y., Konneker, A., Popa, B.-I., Cummer, S.A.: Tapered labyrinthine acoustic metamaterials for broadband impedance matching. Appl. Phys. Lett. **103**, 201906 (2013)
114. Xie, Y., Wang, W., Chen, H., Konneker, A., Popa, B.-I., Cummer, S.A.: Wavefront modulation and subwavelength diffractive acoustics with an acoustic metasurface. Nat. Commun. **5**, 5553 (2014)
115. Arenas, J.P., Crocker, M.J.: Recent trends in porous sound-absorbing materials. J. Sound Vib. **44**, 12–17 (2010)
116. Maa, D.-Y.: Potential of microperforated panel absorber. J. Acoust. Soc. Am. **104**, 2861–2866 (1998)
117. Ma, G., Yang, M., Xiao, S., Yang, Z., Sheng, P.: Acoustic metasurface with hybrid resonances. Nat. Mater. **13**, 873–878 (2014)
118. Jiang, X., Liang, B., Li, R.-Q., Zou, X.-Y., Yin, L.-L., Cheng, J.-C.: Ultra-broadband absorption by acoustic metamaterials. Appl. Phys. Lett. **105**, 243505 (2014)
119. Wei, P., Croënne, C., Chu, S.T., Li, J.: Symmetrical and anti-symmetrical coherent perfect absorption for acoustic waves. Appl. Phys. Lett. **104**, 121902 (2014)
120. Leroy, V., Strybulevych, A., Lanoy, M., Lemoult, F., Tourin, A., Page, J.H.: Superabsorption of acoustic waves with bubble metascreens. Phys. Rev. B **91**, 020301 (2015)
121. Piper, J.R., Liu, V., Fan, S.: Total absorption by degenerate critical coupling. Appl. Phys. Lett. **104**, 251110 (2014)
122. Stansfeld, S.A., Matheson, M.P.: Noise pollution: non-auditory effects on health. Br. Med. **68**, 243–257 (2003)
123. Nivison, M.E., Endresen, I.M.: An analysis of relationships among environmental noise, annoyance and sensitivity to noise, and the consequences for health and sleep. J. Behav. Med. **16**(3) (1993)
124. City, Melbourne.: Proposed Amendments to Part F5 of the Building Code of Australia (BCA). City of Melbourne
125. London, A.: Transmission of reverberant sound through single walls. J. Res. Nat. Bureau Stand. **42**(605) (1949)
126. Hall, A.J., Calius, E.P., Dodd, G., Wester, E.: Modelling and experimental validation of complex locally resonant structures. In: Proceedings of 20th International Congress on Acoustics, ICA 2010, 23–27 Aug, Sydney, Australia

127. Klironomos, A.D., Economou, E.N.: Elastic wave band gaps and single scattering. Solid State Commun. **105**(5), 327–332 (1998). ISSN 0038-1098. doi:10.1016/S0038-1098(97)10048-5
128. John, S.: Localization of light. Physics Today, **44** (1991)
129. Kushwaha, M.S., Halevi, P., Dobrzynski, L., Djafari-Rouhani, B.: Acoustic band structure of periodic elastic composites. Phys. Rev. Lett. **71**(13), 2022–2025 (1993). ISSN 0031-9007
130. Liu, Z., Chan, C.T., Sheng, P.: Threecomponent elastic wave band-gap material. Phys. Rev. B, **65**(16), 165, 116 (2002). doi:10.1103/PhysRevB.65.165116
131. Martinez-Sala, R., Sancho, J., Sanchez, J.V., Gomez, V., Llinares, J., Meseguer, F.: Sound attenuation by sculpture. Nature, **378**(6554), 241–241 (1995). http://dx.doi.org/10.1038/378241a0
132. Fung, K.-H.: Phononic band gaps of locally resonant sonic materials with finite thickness. Master's thesis, The Hong Kong University of Scienc and Technology (August 2004)
133. Liu, Z., Mao, Y., Zhu, Y., Chan, C.T., Sheng, P.: Locally resonant sonic materials. Science, **289**(5485), 1734–1736 (2000). ISSN 1095-9203
134. Milton, G.W, Willis, J.R. On modifications of Newton's second law and linear continuum elastodynamics. Proc. R. Soc. A **463** (2007)
135. Yao, S., Zhou, X., Hu, G.: Experimental study on negative mass in a 1D mass-spring system. N. J. Phys. **10**(4), 043,020 (11 pp) (2008)
136. Huang, H.H., Sun, C.T.: Wave attenuation mechanism in an acoustic metamaterial with negative effective mass density. N. J. Phys. **11**(1), 013,003 (15 pp) (2009)
137. Huang, H.H., Sun, C.T., Huang, G.L.: On the negative effective mass density in acoustic metamaterials. Int. J. Eng. Sci. **47**(4), 610–617 (2009). ISSN 0020-7225. doi:10.1016/j.ijengsci.2008.12.007
138. Gang, W., Yao-Zong, L., Ji-Hong, W., DianLong, Y.: Formation mechanism of the low-frequency locally resonant band gap in the two-dimensional ternary phononic crystals. Chin. Phys. **15**(2), 407–411 (2006)
139. Calius, E., Bremaud, X., Smith, B., Hall, A.: Negative mass sound shielding structures (2009) (in press)
140. Suzuki, H.: Resonance frequencies and loss factors of various single-degree-of-freedom systems. J. Acoust. Soc. Jpn. (E) **21** (2000)
141. Ho, K.M., Cheng, C.K., Yang, Z., Zhang, X.X., Sheng, P.: Broadband locally resonant sonic shields. Appl. Phys. Lett. **83**(26), 5566–5568 (2003). doi:10.1063/1.1637152
142. Yang, Z., Dai, H.M., Chan, N.H., Ma, G.C., Sheng, P.: Acoustic metamaterial panels for sound attenuation in the 50–1000 Hz regime. Appl. Phys. Lett. **96**(4), 041906 (2010). doi:10.1063/1.3299007
143. Zhi-Ming, L., Sheng-Liang, Y., Xun, Z.: Ultrawide bandgap locally resonant sonic materials. Chin. Phys. Lett. **22**(12), 3107 (2005)
144. Oudich, M., Li, Y., Assouar, B.M., Hou, Z.: A sonic band gap based on the locally resonant phononic plates with stubs. New J. Phys. **12**, 083049 (2010)
145. Oudich, M., Senesi, M., Assouar, M.B., Ruzenne, M., Sun, J.-H., Vincent, B., Hou, Z., Wu, T.-T.: Experimental evidence of locally resonant sonic band gap in two-dimensional phononic stubbed plates. Phys. Rev. B **84**, 165136 (2011)
146. Rupin, M., Lemoult, F., Lerosey, G., Roux, P.: Experimental demonstration of ordered and disordered multiresonant metamaterials for lamb waves. Phys. Rev. Lett. **112**, 234301 (2014)
147. Zhu, R., Liu, X.N., Huang, G.L., Huang, H.H., Sun, C.T.: Microstructural design and experimental validation of elastic metamaterial plates with anisotropic mass density. Phys. Rev. B **86**, 144307 (2012)
148. Farhat, M., Guenneau, S., Enoch, S.: Ultrabroadband elastic cloaking in thin plates. Phys. Rev. Lett. **103**, 024301 (2009)
149. Farhat, M., Guenneau, S., Enoch, S., Movchan, A.B.: Cloaking bending waves propagating in thin elastic plates. Phys. Rev. B **79**, 033102 (2009)

150. Stenger, N., Wilhelm, M., Wegener, M.: Experiments on elastic cloaking in thin plates. Phys. Rev. Lett. **108**, 014301 (2012)
151. Colombi, A., Roux, P., Guenneau, S., Rupin, M.: Directional cloaking of flexural waves in a plate with a locally resonant metamaterial. J. Acoust. Soc. Am. **137**, 1783–1789 (2015)
152. Zhu, R., Liu, X.N., Hu, G.K., Sun, C.T., Huang, G.L.: Negative refraction of elastic waves at the deep-subwavelength scale in a single-phase metamaterial. Nat. Commun. **5**, 5510 (2014)
153. Dubois, M., Farhat, M., Bossy, E., Enoch, S., Guenneau, S., Sebbah, P.: Flat lens for pulse focusing of elastic waves in thin plates. Appl. Phys. Lett. **103**, 071915 (2013)
154. Dubois, M., Bossy, E., Enoch, S., Guenneau, S., Lerosey, G., Sebbah, P.: Time-driven superoscillations with negative refraction. Phys. Rev. Lett. **114**, 013902 (2015)
155. Rupin, M., Catheline, S., Roux, P.: Super-resolution experiments on lamb waves using a single emitter. Appl. Phys. Lett. **106**, 024103 (2015)
156. Brûlé, S., Javelaud, E.H., Enoch, S., Guenneau, S.: Experiments on seismic metamaterials: Molding surface waves. Phys. Rev. Lett. **112**, 133901 (2014)
157. Milton, G.W., Cherkaev, A.V.: Which elasticity tensors are realizable? J. Eng. Mater. Technol. **117**, 483–493 (1995)
158. Milton, G.W.: The Theory of Composites. Cambridge University Press, Cambridge (2002)
159. Kadic, M., Bückmann, T., Stenger, N., Thiel, M., Wegener, M.: On the practicability of pentamode mechanical metamaterials. Appl. Phys. Lett. **100**, 191901 (2012)
160. Bückmann, T., Stenger, N., Kadic, M., Kaschke, J., Frölich, A., Kennerknecht, T., Eberl, C., Thiel, M., Wegener, M.: Tailored 3D mechanical metamaterials made by dip-in direct-laser-writing optical lithography. Adv. Mater. **24**, 2710–2714 (2012)
161. Zheng, X., Lee, H., Weisgraber, T.H., Shusteff, M., DeOtte, J., Duoss, E.B., Kuntz, J.D., Biener, M.M., Ge, Q., Jackson, J.A., Kucheyev, S.O., Fang, N.X.: Ultralight, ultrastiff mechanical metamaterials. Science **344**, 1373–1377 (2014)
162. Bückmann, T., Thiel, M., Kadic, M., Schittny, R., Wegener, M.: An elasto-mechanical unfeelability cloak made of pentamode metamaterials. Nat. Commun. **5**, 4130 (2014)
163. Della, G.C., Engheta, N.: Digital metamaterials. Nat. Mater. **13**, 1115–1121 (2014)
164. Xie, Y., Tsai, T.-H., Konneker, A., Popa, B.-I., Brady, D.J., Cummer, S.A.: Single-sensor multispeaker listening with acoustic metamaterials. Proc. Natl. Acad. Sci. U.S.A. **112**, 10595–10598 (2015)

Chapter 9
Application of Acoustic Metamaterial to Time-Reversal Acoustics

Abstract Time reversal acoustics is based on the time reversal symmetry of the acoustic fields. A detailed description of the acoustic field equation showing the time reversal symmetry property of S the solution is given. A geometric structure of a metamaterial for both an electromagnetic wave and acoustic wave is given. Then, the geometric structure of the metamaterial to implement time reversal acoustics is given. Time reversal acoustics has been successfully applied to non-destructive testing, medical ultrasound imaging, and underwater acoustics. The advantage of using metamaterial in time reversal acoustics is that it supports modes which radiate spatial information of the near field of a source efficiently in the far field.

9.1 Time-Reversal Symmetry Property of Acoustic Field-Basic Principle of Time-Reversal Acoustics

One will start with the linear acoustic field equation of an acoustic pressure field $p(\mathbf{r}, t)$ in an inhomogeneous medium, which will be valid for a lossless fluid medium with compressibility $\kappa(\boldsymbol{r})$ and density $\rho(\mathbf{r})$ that vary with space and local sound velocity as $c(\mathbf{r}) = (\rho(\boldsymbol{r})\kappa(\boldsymbol{r})^{-1/2}$, one obtains for the propagation equation of an acoustic pressure field $p(\mathbf{r}.t)$ in the transient regime [1]:

$$\nabla \cdot \left(\frac{\nabla p}{\rho}\right) - \frac{1}{\rho c^2}\frac{\partial^2}{\partial t^2}p = 0 \tag{9.1}$$

For propagation in the x direction, the solution will be given by $p = \exp j(\omega t - kx)$. Time-reversal symmetry property of the acoustic field means that replacing t by $-t$ is another solution of the equation. This means the solution will consist a right propagating wave as well as a left propagating wave. A further illustration of the principle of time-reversal symmetry can be shown as follows. The simple case of the reflection and transmission of the plane sound wave at the straight interface of two media with different densities is considered. Let the incident sound pressure field be $p(r,t)$ and the amplitude of the reflected wave be R and the amplitude of the transmitted wave be T. Hence, there will be three different

W.S. Gan, *New Acoustics Based on Metamaterials*, Engineering Materials,
https://doi.org/10.1007/978-981-10-6376-3_9

waves to be considered: the incident wave, the reflected wave and the transmitted wave. The next step is to show the application of the time-reversal symmetry property of the acoustic field. That is the process can be time reversed by reversing the sound wave vector direction. The time-reversed solution will be $p(r, -t)$ and by substitution into the acoustic equation of wave motion will show that it is also a solution of the wave equation.

If one defines the amplitudes of the reflected and transmitted waves for the incident wave coming out of medium two as R' and T' then using principle of superposition for the two incident waves one at medium 1 and one at medium 2 can lead to the generation of four waves, two propagating in medium 1 with amplitude $R^2 + \mathrm{TT}'$, and two propagating in medium 2 with total amplitude $\mathrm{RT} + \mathrm{TR}'$. A simple calculation of the reflection and transmission coefficients R, T, R' and T' will give:

$$R^2 + \mathrm{TT}' = 1 \tag{9.2}$$

$$R + R' = 0 \tag{9.3}$$

The above example shows the acoustic wave equation has time-reversal symmetry property.

The above outcome of time-reversal symmetry can be generalized to other forms of acoustic fields beside the simplest form of plane waves and also to other structures of inhomogeneities.

It is to be noted that Eqs. (9.2) and (9.3) are only valid for propagating waves. That is, the reflected and transmitted waves have real wave numbers. Evanescent wave or nonpropagating wave will not obey Eqs. (9.2) and (9.3). Usually, the incident wave will contain both propagating wave and evanescent wave. Thus, evanescent wave cannot be time reversed due to the undefined direction of propagation [2]. The evanescent wave can be produced by an incident sound wave being scattered by a medium whose bulk modulus $\kappa(\mathbf{r})$ contains spatial frequency components of dimension smaller than the wavelength. The evanescent wave can also be produced sound wave incident at specific angles. If the incident wave is of finite bandwidth then some information will be lost during the time-reversal process. Thus, time-reversal process has limitation due to the presence of both propagating and evanescent waves.

9.2 Experimental Implementation of Time-Reversal Acoustics

Time-reversal symmetry property of acoustic field enables one to focus through an inhomogeneous medium. The acoustic pressure field can be time reversed and re-emitted. This process can be used to focus through inhomogeneous media on a reflecting target that behaves as an acoustic source after being isonified. Fink et al.'s [3] work is the first application of time-reversal acoustics to acoustical imaging.

Time-reversal acoustics enables the focusing of a wave on a target, stationary or moving through an inhomogeneous medium. This is an important problem to solve in acoustics. In order to experimentally implement this concept, Fink et al's. [3] time-reversal mirror (TRM) is made of an array of piezoelectric transducers. These transducer elements can both receive and transmit an instantaneous measurement of the temporal pressure wavefront. They also have linear property. The experimental procedure is as follows. Digital signal processing plays a major role in time-reversal process and the construction of the time-reversal mirror (TRM). It also enables focusing through an inhomogeneous medium. The technique used is known as the adaptive time-delay technique. The spatial-temporal matched filter is used to describe the pulse wave time-reversal focusing inhomogeneous propagation transfer function between the array and the target. This enables reciprocity in the inhomogeneous medium. Optimal inputs are also provided to the transducer elements. The construction of the time-reversal mirror (TRM) is as follows. It is a 1D or 2D transducer array. Each element is connected to an individual electronic circuit, which includes a receiving amplifier, A/D converter, a programmable transmitter and a storage memory. The programmable transmitter is the most important element of the electronic circuitry because it synthesizes the time-reversed version of the stored signal.

Thus, the TRM is able to detect the pressure field located at a position r_i. with a transducer array. The signals are then digitized and stored over the time interval T. This acoustic pressure field is retransmitted in a reversed temporal chronology by the same transducer array. This enables transmission of $p(r_i, T - t)$, the time-reversal process converts the divergent wave into a convergent wave focusing onto the same source. This process is valid even in an inhomogeneous medium. The conventional mirror produces a virtual acoustic image of a real object whereas the TRM produces a real acoustic image of a virtual object/source. This time-reversal process can be extended to focusing on a reflective target, which can be isonified to become an acoustic source.

9.3 Ultrasonic Focusing in Inhomogeneous Media

9.3.1 Adaptative Time-Delay Focusing Techniques

To put the principle of time-reversal acoustics into practice, Fink et al. [3] design the time-reversal mirror (TRM), which is based on signal processing technique. The TRM is made of transducer arrays. Each element of the transducer element acts as a receiver of the acoustic signal. They are then digitized. There is time delay between signals from neighbouring array elements, and this is calculated using cross-correlation formula. These time delays will be used to calculate the optimal time-delay characteristic required to focus on the source. Here, the focusing of sound waves in an inhomogeneous medium is based on the electronic method of using a set of delay that can exactly compensate the spherical curvature of the signals that are received by the transducer array. The delay lines allow the signals to

be brought into phase before their summation. Also, the acoustic source can be passive, like a target reflecting an incident wave.

The inhomogeneous medium is an aberrating medium. Here, the alignment of the signals does not obey the spherical character of the time-reversal mirror (TRM). This necessitates the compensating time delay. The correct time delay can be calculated from the time shift of the peak of the cross-correlation between signals from neighbouring transducers [4, 5]. There is a second technique, which is using for the case of an aberrating medium; the signals are no longer aligned by the spherical delay characteristic. Here, one needs to superimpose a compensating time delay. The correct time delays are determined by the time shift corresponding to the peak of the cross-correlation between signals from neighbouring transducers [4, 5]. There is a second technique, which is using the time-delay law [6]. Here, it deals with the maximization of the energy of the summed signals. These two methods are similar because they achieve the maximization of the cross-correlation between all pairs of signals simultaneously to achieve the energy maximization [7]. However, both methods unable to achieve optimal focusing. This will be illustrated by real-life situations later in this chapter. When the aberrator-array probe distance increases, the adaptive delay-line focusing technique will not work [7]. Then, it will need a more general approach to take into consideration all the information recorded such as shape variation and time-delay characteristic.

Results will vary. There are various problems to be solved. The first is the nature of the reflective target that one is focusing. The point-like target is the ideal target, and this is the source of the spherical wave, which will be distorted during propagation through the inhomogeneous aberrating medium. In a real situation, the medical ultrasound imaging takes place in the near field and the sources are not point-like. For instance, the liver or the kidney stone has a finite size. The scattered signals from such targets will be different from one transducer element to the other and thus the cross-correlation will vary.

In usual practical situations, the region to be scanned does not contain the highly reflective target, in the scanning of the abdomen, there is sound velocity variation throughout the region causing degrading in the focusing of low megahertz ultrasonic waves. This will result in multiple scattering in the region instead of single scattering from a highly reflective target. Here, the calculation of the adequate focusing time-delay law for such multiple scattering media can be done using the cross-correlation technique [4–7]. This is based on the summation of individual echoes reflected on each scatterer. The Van Cittert Zernike theorem [8] states that the sound field propagates with a spatial correlation width that increases proportionally to the propagation distance. This property can be applied to the optimal focusing is neighbouring transducer elements can receive a highly correlated signal if they are sufficiently far from the scattering region [8, 9]. These signals will be shifted by the aberrating layer, and the proper delay will be found by the cross-correlation technique. This will put the targeted nature under control. The next problem to resolve will be the nature of the inhomogeneous medium. Here, the cross-correlation technique has its limitations. This is due to its assumption of all the effects of the inhomogeneity on the spherical wavefront can be summed up as a

simple distortion of the wavefront shape. This amounts to that the inhomogeneity of the medium only modifies the propagation delay between the source and the transducer. This means that time-delay characteristics are sufficient for the optimal transducer array. This assumption fails for medical ultrasound imaging as the imaging is in the near field and the inhomogeneities are spread over the whole volume of the region to be scanned. Sound wave propagates through such an inhomogeneous medium due to diffraction, refraction and multiple scattering. Its temporal and spatial shape will be distorted and also delayed. Also, the adaptive delay-line focusing technique fails when the aberrator-array probe distance increases [7]. In this case, the time-reversed process has to take into account all the information recorded on the medium that is the shape variation and the time-delay characteristics.

9.3.2 The Time-Reversal Cavity

The solution $p(\mathbf{r}, t)$ of the wave equation is determined by the initial boundary conditions and acoustic source. The purpose of the experiment is to generate the dual solution of $p(\mathbf{r}, -t)$. Due to causality consideration, $p(\mathbf{r}, -t)$ is not experimentally valid and generation of $p(\mathbf{r}, T - t)$ has to be implemented instead.

It is difficult to generate the time-reversed solution experimentally. First, the pressure $p(\mathbf{r}, t)$ has to be measured during the whole time-reversed period T for the whole 3D volume. The pressure field vanishes for $t > T$ and then retransmit in all the volume $p(r, T - t)$. This method is unrealistic because the whole volume with transmit-receive probes has to be sampled.

Here, Huygens' Principle produces a more realistic solution to the time-reversal process. The acoustic pressure field at any point of a 3D volume problem can be reduced to a 2D surface problem because the acoustic pressure field form and its normal derivative at any point of a closed surface can predict the wave field at any point of the volume [10]. This concept is used to treat the focusing on a target in an inhomogeneous medium as follows. An inhomogeneous medium will distort the spherical wavefront of a point-like source. To fabricate, a time-reversal mirror (TRM) has to assume that one is able to measure the acoustic pressure field and its normal derivative at any point on the closed surface. Step two, one will make use of Huygens' Principle to assume that the secondary sources (monopole and dipole) can be created on the surface corresponding to the time reversal of the signals measured during step one. Due to the creation of the secondary sources, the acoustic pressure field is time reversed and back propagated inside the surfaced, but interaction with the inhomogeneities of the medium will cause distortion on the wavefront.

This will cause the time-reversed pressure field to refocus on the initial sound source [11, 12]. This will provide better focusing than the correlation technique. The reason is that here, there is no assumption that the inhomogeneities are located near the transducer array and that the time delay due to inhomogeneity is reduced to only a time delay under such conditions, it can be shown [11, 12] that the time-reversed pressure field is focused to only a varying from one transducer

element to another. However, the resolution will be restricted by the finite spectral bandwidth. This is due to the fact that spatial scales of inhomogeneities smaller than the minimum wavelength will be blurred. Hence, generation of $p(\mathbf{r}, T - t)$ is not perfect throughout the whole volume.

9.3.3 Time-Reversal Mirror

The time-reversal mirror (TRM) is difficult to fabricate in practice as the time-reversal cavity is only an ideal concept for focusing through an inhomogeneous medium. The greatest difficulty is for surrounding the focal region by an array of transducers. For acoustical imaging with applications to ultrasound nondestructive testing and medical ultrasound, usually, the pulse-echo mode imaging mode is used. This means that it is necessary to place the probe on one side of the region to be scanned. This imaging mode is important and has the advantage of focusing only from an array of transducers. Here, the time-reversal cavity will become the time-reversal mirror (TRM). Although the TRM is open, its capability to focus through an inhomogeneous medium is comparable with that of a closed cavity.

The TRM can be prefocused in 1D or in 2D or a plane mirror. Even in focusing through homogeneous media, the TRM has limitations same as those with conventional focusing using the delay-line technique. These are: (1) diffraction effects will still be there resulting in the image of a point becoming a spot with dimensions depending on the wavelength. This is equivalent to low-pass filter on the spatial frequency spectrum of any wave field, (2) a point spread function (PSF) with width related to the angular aperture of the mirror observed from the focal point due to the limited dimension of the TRM, (3) the time-delay law of classical time-delay focusing has to be applied to the temporal sampling of the data recorded and transmitted by the TRM. To avoid secondary lobes, a maximum rate of T/8 with T = central period is needed [5, 13]. Grating lobes will be produced by the spatial sampling of the TRM using an array of transducers. This can be avoided if the array pitch of the order $\lambda/2$, λ = central wavelength of the pressure field is used. This is not necessary with a spherical or cylindrical TRM prefocused on the regional interest.

9.3.4 Focusing with a Time-Reversal Mirror

The mechanism of time-reversal focusing by a time-reversal mirror (TRM) can be understood as follows. First, the acoustic field propagates through the inhomogeneous medium from the mirror to the target. The acoustic wave will be multiply scattered by the target and is distorted. This scattered field is then recorded by the transducer array. Next, the transducer array synthesizes the time-reversed field. The time-reversed field then back propagated through the inhomogeneous aberrating medium and refocused on the target. The TRM has a limitation when applied to a

strongly inhomogeneous medium. This is due to multiple scatterings in all directions. This will cause distortion in the wavefront as experimentally demonstrated [14]. This is a weakness of the TRM compared to the closed cavity. It is also necessary to perform the measurement over a long interval due to the slow decay of the multiple scatterings. On the other hand, when dealing with weak inhomogeneities, which give rise to single scattering and first born approximation can be used and the TRM will compensate exactly for the time-reversal wavefront over shorter time duration and optimal focusing can be achieved by recording the time-reversal of the field recorded on only one plane.

9.3.5 Signal Processing used in Time-Reversal Method

The time-reversed mechanism can also be interpreted in terms of electronic engineering and signal processing can be used. In terms of signal processing language, time-reversal focusing through the inhomogeneous medium is equivalent to first derive the inhomogeneous propagation transfer function between the time-reversed mirror elements and the target. Then the spatial-temporal matched filter is obtained for the transfer function. Hence, the time-reversed-focusing technique is related to the matched filter principle of signal processing. The analogy between the time-reversed-focusing and the matched filter principle of electronics is shown by that using the matched filter principle for a linear system with the output signal of impulse response $h(t)$ will be maximised by an input signal in the form $h(-t)$ [15]. The energy of the input signal produces the impulse response.

The principle of time-reversal symmetry is valid for any lossless inhomogeneous medium and is valid for any size of the geometry and sampling pitch of the transducer elements. Our aim of using the TRM is to maximise the acoustic pressure at the target location by providing inputs to the transducer elements. First, the optimal transient signals from a set of transducer elements E_i located in r_i will be calculated. This signal will be focused on a point located in $r_{0.}$. The calculation will be done for the individual pressure fields produced by each transducer element E_i. This calculation in the transient regime is performed using the diffraction impulse theory.

9.3.6 The Iterative Time-Reversal Mode—an Automatic Target Selection

The TRM has the capability and the advantage to choose the duration of the signals to be time reversed and the origin by using the temporal window, which can select the data to be time reversed. The time-reversed process cannot be used to directly focus on one point when the medium contains several reflectors. For instance, when

there are two targets with different reflectivity illuminated by a short pulse, two wavefronts refocused on each target will be generated by the time-reversal of the echoes reflected from these targets. TRM produces two real acoustic images of the two reflections on themselves with the most reflective target giving the highest amplitude wavefront and the second target giving the weakest wavefront. In fact, what is described above is valid after neglecting the multiple scattering processes between the two targets. Multiple scattering processes can be avoided by selecting echoes within a particular time-reversed window. Then, the time-reversed process can be iterated [3, 16]. After the first time-reversal, the second target or the weakest target will reflect a wavefront more weakly. After several iterations, a wavefront focused on the most reflective target will be obtained after the convergence of the process. However, the convergence will occur only if the illumination of one target by the real acoustic image of the other target is avoided by choosing sufficient target separation [16, 17].

There is an existing contradiction between the concept of iteration and the physical principle of time-reversal symmetry. The complete time-reversal of an acoustic scene results in the time-reversed scene. Therefore, the iteration of the time-reversal operation gives stationary results, a contradiction with wavefield modification after each iteration. This can be explained as follows. A complete time-reversal operation requires a closed-time-reversal cavity surrounding the acoustic scene and a recording time T long enough to take into account all the multiple scattered waves. Here, one utilizes only a finite spatial aperture and short temporal windows. Hence, some information is lost. This information loss gives the iterative mode its target selection capabilities. Experimental results show the efficiency of the process on single wire targets [14]. In lithotripsy applications, the iterative mode allows the automatic selection of one of the kidney stones [14].

9.4 Some Practical Applications of Time-Reversal Acoustics

An example of the practical application of time-reversal acoustics is to medical ultrasound imaging to lithotripsy. The stone position can be imaged accurately with *X*-ray imaging. However, with ultrasound imaging it is difficult. There is sound speed variation through the inhomogeneities will distort and redirect the sound beam. Even more serious than this is breathing causes stone motion with amplitude up to 2 cm. Stone tracking is the first step to enable efficient therapy. These problems can be overcome by the time-reversal process, which can identify the target with the highest reflectivity such as the stone to be identified among other stones and organ walls. First, the transducer array will beam out an ultrasound to the whole region. The transducer array will receive the reflected field, time reversed and retransmit back to the source. The time-reversal process is iterated to enable the ultrasound beam to select the highest reflectivity. The whole process will converge

on one spot with dimension depending on the wavelength and the TRM geometry of the target is spatially extended. Hence, the last iteration will locate the target for stone destruction. It has to be mentioned that the frequency of the region of interest does not contain any highly reflective target.

Frequently, the region of interest does not contain any highly reflective target. Another example of practical application of time-reversal acoustics is the imaging of the abdomen where sound speed aberrations in the body can degrade the focusing characteristics of the ultrasonic beam at frequencies in the low-megahertz range. The advantage of time-reversal acoustics is that here, the single reflective target is replaced by the many scatterers that comprise the region being imaged. The cross-correlation technique can be used for the estimation of the adequate focusing time-delay law for such scattering media can be estimated for such scattering media [4–7]. This is an outcome of the remarkable property of the scattered pressure field that results from the summation of the individual echoes reflected on each scatterer. The Van Cittert Zernike theorem [8] states that the field propagates with a spatial correlation function width that increases proportionally to the propagation distance. The field propagates with a spatial correlation function width that increases proportionally to the propagation distance. This means that neighbouring transducers, as long as they are sufficiently far from the scattering region, will sense echographic signals that are highly correlated [8, 9]. These signals will be shifted by an aberrating layer and the proper delay can be determined by the cross-correlation technique. Sofar the problem of the targeted nature seemed to be solved. The nature of the inhomogeneous medium seems to be more critical. The underlying assumption of the cross-correlation technique is that all the effects of the inhomogeneity on the spherical wavefront added up as a simple distortion of the wavefront shape. That is, the aberration only modifies the propagation delay between the source and the elementary transducers. Knowledge of the proper time-delay characteristic is sufficient for accurate focusing in the receive or transmit modes. It is to be noted that this assumption is valid only when the aberration is thin and located very close to the array. In most medical applications, this assumption is incorrect, as one always work in the near field of the transducers and the inhomogeneities are distributed over the whole volume. Thus, a wave propagates in such an inhomogeneous medium is not only delayed, but also its spatial and temporal shape is also distorted through refraction, diffraction and multi-scattering.

In lithotripsy application, the stone is an extended target. An incident beam can induce acoustical resonances of the stone, and the wave reflected by the stone may contain different wavefronts resulting from these resonances [14]. This makes the time-reversal process a complicated one. Fortunately, in such situation, the time-reversal mirror is also efficient. It allows some matching of the new transmit waveform in order to produce stone resonances through the iterative time-reversed transmission. A simple explanation of this phenomenon can be given by a 1D experiment conducted with a plane transducer illuminating at normal incidence or a parallel face plate medium. In this experiment, the pulse-echo signal $e(t)$ reflected by the plate contains the multiple reflected waves generated in the resonant plate. For an ideal transducer excited by an electrical pulse $\delta(t)$, the signal $e(t)$ represents

the impulse response of the resonator. The time-reversal process will lead to a transmission of $e(-t)$. This is the optimal signal needed to excite the faceplate resonance This corresponds to the faceplate matched a filter that produces the maximum system response. These concepts can be extended with caution to 3D vibrating structure, the extended target, illuminated by 2D time-reversal mirrors. The theoretical modelling of this process is complex, and some simple physical ideas are provided here as guidelines. The vibration of a complex 3D structure is a linear combination of the different natural Fourier modes of the problem. Each mode is characterized by a wave vector K. In the case of the parallel face plate, there is only one mode with these modes if the corresponding wave vector directions are inside the angular aperture of the TRM. Besides, due to the array finite bandwidth, the phase conjugation of these modes will work only for wave vectors, whose modulus correspond to a frequency included in the transducer bandwidth. These concepts suggest the possibility of an automatic selection and excitation of some vibration modes of an object.

9.5 Sub-wavelength Focusing Using Far Field Time-Reversal for Electromagnetic Waves

Application of acoustic metamaterial to time-reversal mirror was based on the capability of the acoustic metamaterial to convert evanescent wave into propagating wave and thus achieving sub-wavelength image resolution limit at the far field. The procedure is as follows. First, one fabricates the acoustic metamaterial medium. Using the time-reversal symmetry property of the acoustic wave equation of motion, one is able to focus back into the initial source position from the far field. With the time-reversal symmetry property between the propagating wave and the evanescent wave, one is able to obtain a sub-wavelength resolution at the focal spot. Thus, if one places the sources with impulse response at a distance from the TRM much smaller than the wavelength in the acoustic metamaterial medium, one is able to focus independently on each of them. This will enable the conventional diffraction limit to be defeated.

The availability of the sub-wavelength information in the free space radiation is due to the resonance enhancement of the eigenmode of the broadband source placed at the near field of the medium. This enables sub-wavelength image resolution. This will occur during the conversion of the evanescent wave into propagating wave by the acoustic metamaterial.

Lerosey et al's. [18] experiment for electromagnetic waves using metamaterial for TRM is performed in an anechoic chamber. It is performed as follows. The central frequency used is 2.45 GHz. The bandwidth is 100 MHz. There is a receiver array consists of 8 antennas located in the anechoic chamber. Each antenna is surrounded by a microstructure consisting of a random distribution of almost parallel thin copper wires. Hence, the focusing points are in the far field of the TRM.

The evanescent waves will be converted into propagating waves after scattering by the thin copper wires. A TRM consisting of eight commercial bipolar antennae is placed in the far field at a distance of ten wavelengths from the receiving array. The TRM will be a virtual far field time-reversal cavity. The conventional image diffraction limit is defeated in this manner.

The principles of the above experiment can be described as follows. The broadband incident field is decomposed into high-spatial frequency components upon scattering of the random distribution of thin copper wire. A sub-wavelength focusing around the source location is created from time-reversal symmetry outcome of the time-reversal scattering process. These propagating waves are propagated back from the far field in the time-reversed process. On the other hand, the initial evanescent waves around the focus are created by spatial reversibility and reciprocity after each propagating wave interacts with the random distribution of copper thin wires.

9.6 Extension of Above Concept to Acoustics

Due to the many similarities in wave properties between electromagnetic waves and acoustic waves, the above method of converting evanescent waves into propagating waves and sub-wavelength focusing can be extended to acoustic waves. The acoustic metamaterials consist of basic unit cells with properties that can be manipulated and controlled. These unit cells have resonant character and are of sub-wavelength size. The effective medium theory is used here. There are several examples of the unit cells of acoustic metamaterials such as split-ring resonator (SRR), complimentary SRR and parallel cut wires. The effective parameters of the acoustic metamaterial are obtained by averaging the acoustic field across one unit cell. Acoustic metamaterial with negative effective mass density and negative effective modulus has been successfully fabricated and they produce negative refractive index [19].

There are several proposals on experiments on sub-wavelength focusing in acoustics. Here, the experiment of Lemoult et al. [20] is given. They achieved sub-wavelength focusing in the far field with wavelength much smaller than the sound wavelength in air. Helmholtz resonators are used as unit cells. An array of soda cans is used in the far field. The theoretical concept of the resonant metamaterial given in the previous section is used. The experiment demonstrates that the array of cans excited in resonant periodic modes in sub-wavelength spatial period. The incident waves are from commercial computer loudspeaker and are diffraction limited. These sub-wavelength resonant modes are Bloch modes with radiation patterns depending on their wave vectors. The outcome is one is able to obtain in the far field sub-wavelength focusing of sub-diffraction wave field of broadband sound. The capability is focusing on sound into spots as small as 1/25th of sound wavelength in the air and a position resolution of the centre to centre distance between the soda cans of up to 1/15th of sound wavelength.

Their experimental set-up is shown in Fig. 9.1. Figure 9.2 shows the array of cans surrounded by loudspeakers. The experiment demonstrated that incident monochromatic and diffraction limited sound fields can generate sub-diffraction resonant modes over the whole array of soda cans. Sub-wavelength focal spots can be produced. Time-reversal is used to focus sound from an array of sensors into one point. This is equivalent to summing up all the modes with zero relative phase at this specific position to create a spatio-temporally focused wave. To extend this to the broadband source, by adding up various presenting modes coherently at a specific time and a given location while they add up incoherently at other positions and other times.

Their experiments have been performed at several locations using the ensemble of Helmholtz resonators and the eight computer loudspeakers. It is also shown that focusing sound using an array of cans results in much thinner foci than with a single can.

They also discovered a key property for the design of high-performance actuators. That is the sub-wavelength focusing of acoustic pressure fields can lead to strong enhancement of the acoustic displacement.

Lemoult et al's. [20] experiment has made some discoveries of fundamental interests. First is that sub-wavelength pressure fields can create enhanced acoustic displacements with numerous potential applications, especially to the design of sensors and actuators. Second, with the advantage of dispersion, it allows one to independently address many sensors with their temporal signatures and a few

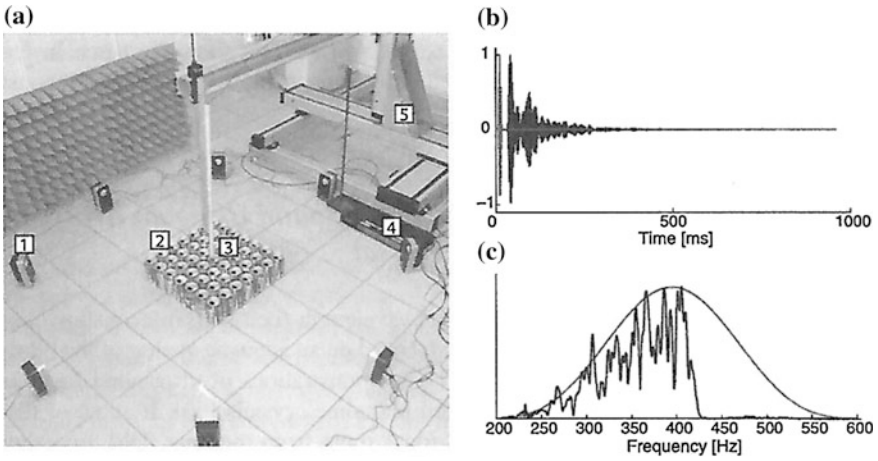

Fig. 9.1 Experimental set-up. **a** A picture of the set-up utilized in the experiment. Eight commercial computer speakers (1) are controlled using a multichannel sound card (4) and create sounds that excite an array of Helmholtz resonators (i.e. soda cans) (2). Mounted on a 3D moving stage (5), a microphone (3) records the pressure over the array of cans. **b** Typical emitted pulse (red) and measured pressure (blue) on top of one can. **c** The spectrum of the original pulse (red) and average spectrum of the pressure measured every can of the array (blue) (Lemoult et al. [20])

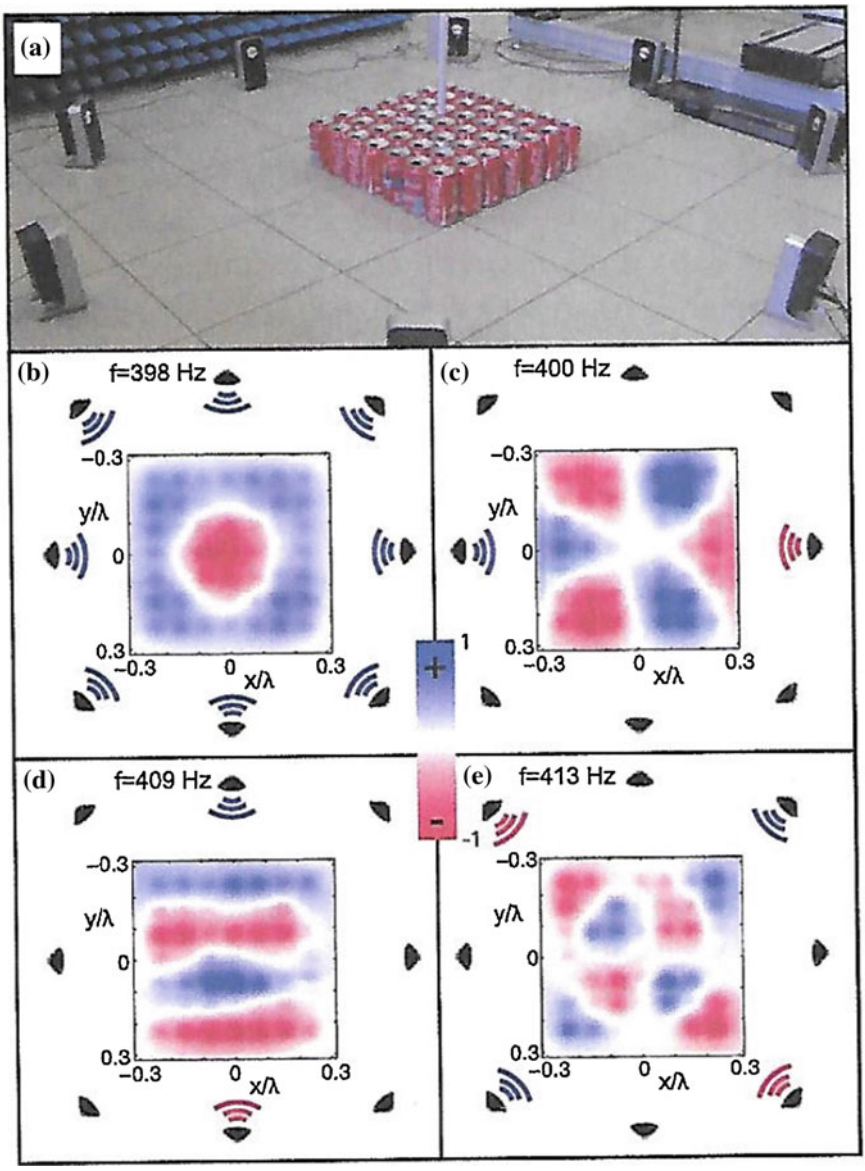

Fig. 9.2 Sub-wavelength modes. **a** A close view of the array of cans surrounded by the 8 computer speakers. The speakers are placed more than one wavelength away from the cans so that evanescent waves are negligible at this distance. **b** A sub-wavelength mode measured at 398 Hz when the speakers are used to generate a monopolar radiation pattern, this mode is already sub-wavelength, with a $\lambda/4$ spatial period. **c** A mode corresponding to a horizontal dipolar pattern at 400 Hz. **d** A vertical dipolar wave field created with the speakers results in a $\lambda/3$ spatial period mode at 409 Hz. **e** A quadripolar far field pattern excites a deep sub-wavelength mode at 413 Hz (Lemoult et al. [20])

sources. Third, it produces the capability of engineering a matrix of sensors and actuators that are arranged on a sub-wavelength scale.

Lemoult et al's. [20] results can be extended to a broad frequency spectrum of resonators and even generalized to elastic waves in solids. There are many potential applications such as the design of arrays of actuators, micro-mechanical actuators at any frequency (or audible sound control, for audible sound generation).

The sub-wavelength image resolution of the resonant acoustic metalens is useful in acoustical imaging. This is known as superresolution, which enables the projection on the far field the near-field information of a source regardless of its spatial variations.

References

1. Morse, P.N., Ingard, K.U.: Theoretical Acoustics. McGraw-Hill, New York (1968)
2. Nieto-Vesperinasand, M., Wolf, E.: Phase conjugation and symmetries with wave fields in free space containing evanescent components. J. Opt. Soc. Am. **2**(9), 1429–1434 (1985)
3. Fink, M., Prada, C., Wu, F., Cassereau, D.: Selffocusing with time reversal mirror in inhomogeneous media. In: 1989 Proceedings IEEE Ultrasonic Symposium 1989, vol. 2, pp. 681–686. Montreal, PQ, Canada
4. Flax, S.W., O'Donnell, M.: Phase aberration correction using signals from point reflectors and diffuse scatterers: basic principles. IEEE Trans. Ultrason., Ferroelectr. Freq. Control **35**, 758–767(1988)
5. O'Donnell, M., Flax, S.W.: Phase aberration correction using signals from point reflectors and diffuse scatterers: measurements. IEEE Trans. Ultrason. Ferroelectr. Freq. Control **35**, 768–774 (1988)
6. Nock, L., Trahey, G.E., Smith, S.W.: Phase aberration correction in medical ultrasound using speckle brightness as a quality factor. J. Acoust. Soc. Am. **85**, 1819–1833 (1989)
7. Mallart, R., Fink, M.: Sound speed fluctuations in medical ultrasound imaging. Comparison between different correction algorithms. In: Proceedings of the 19th International Symposium Acoustical Imaging (1991)
8. Mallart, R., Fink, M.: The Van Cittert-Zernike theorem in pulse-echomeasurements. J. Acoust. Soc. Am. **90**(5), 2718–2727 (1991)
9. Trahey, E., Zhao, D., Miglin, J.A., Smith, S.W.: Experimental results with a real-time adaptive ultrasonic imaging system for viewing through distorting media. IEEE Trans. Ultrason. Ferroelectr. Freq. Control **37**, 418–429 (1990)
10. Porter, R.P., Devaney, A.J.: Generalized holography and the inverse source problems. J. Opt. Soc. Am. **72**, 327–330 (1982)
11. Cassereau, D., Wu, F., Fink, M.: Limits of self-focusing using closed time-reversal cavities and mirrors-theory and experiment. In: 1990 Proceedings IEEE Ultrasonics Symposium, Hawaii, pp. 1613–1618 (1990)
12. Cassereau, D., Fink, M.: Time-reversal of ultrasonic fields, III. Theory of the closed time-reversal cavity. IEEE Trans. Ultrason. Ferroelectr. Freq. Control **39**, 579–592 (1992)
13. Kino, G.S.: Acoustics Waves, Signal Processing Series. PrenticeHall, Englewood Cliffs, NJ (1987)
14. Wu, F., Thomas J.L., Fink, M.: Timereversal of ultrasonic fields-part 11: experimental results. IEEE Trans. Ultrason. Ferroelectr. Freq. Control, 567–578 (1992)
15. Papoulis, A.: Signal Analysis. McGraw-Hill, New York (1984)
16. Prada, C., Wu, F., Fink, M.: The iterative time reversal mirror: a solution to selffocusing in pulse-echo mode. J. Acoust. Soc. Am. **90**, 1119–1129 (1991)

17. Prada, C.: Retournement temporal des ondes ultrasonores. These de doctorat de I'Universite Paris VII (1991)
18. Lerosey, G., et al.: Focusing beyond the diffraction limit with far field time reversal. Science **315**, 1120–1122 (2007)
19. Smith, D.R.: Composite medium with simultaneously negative permeability and permittivity. Phys. Rev. Lett. **84**, 4184–4187 (2000)
20. Lemoult, F., Fink, M., Lerosey, G.: Acoustic resonators for far field control of sound on a subwavelength scale. Phys. Rev. Lett. **107**, 064301 (2011)

Chapter 10
Underwater Acoustical Cloaking

Abstract Acoustical cloaking is the first example of sound propagation in curvilinear spacetime. Previous works are concerned only with the application of curvilinear coordinates to describe a stationary object's geometrical structure. The cloaking of underwater objects is an extension of the cloaking of objects in the air. This is more complex than cloaking in the air. The theory of sound propagation underwater is given. The form invariance of the Westervelt equation is shown. This enables the bending of sound around the object and the shielding of the object underwater. The application to anti-sonar work is described.

10.1 Acoustical Cloaking

Acoustical cloaking or the manifestation of invisibility objects is based on the form invariance of the acoustic field equation or the symmetry property of the acoustic field. This means that the acoustic field equation will remain in the same form under coordinate transformations. Acoustical cloaking has initiated a new field with much activities. This invention enables a hidden object undetectable under sound propagation by manipulating and controlling the direction of sound propagation around the object in the 3D space. The physics of cloaking underwater and cloaking in air is different in the effective parameters concerned. Chapter 2 of this book presents the subject of acoustical cloaking taking place in air. Here it is extended for acoustical cloaking taking place underwater. Cloaking underwater is not possible for light waves but realizable for sound waves. Acoustical cloaking in water is an entirely different field from acoustical cloaking in water.

One has to take note that the acoustic field equation for sound propagation underwater is different from that for sound propagation in the air. However, underwater acoustic wave equation also has form invariance property as acoustic field equation for sound propagation in air. To illustrate this, a theory for underwater sound propagation is given.

W.S. Gan, *New Acoustics Based on Metamaterials*, Engineering Materials,
https://doi.org/10.1007/978-981-10-6376-3_10

10.2 Propagation Theory

The underwater propagation of sound can be described mathematically by the homogeneous wave equation in the acoustic pressure P:

$$\frac{\mathrm{d}^2 P}{\mathrm{d}t^2} = c^2 \left(\frac{\partial^2 P}{\partial x^2} + \frac{\partial^2 P}{\partial y^2} + \frac{\partial^2 P}{\partial z^2} \right), \tag{10.1}$$

where c = sound velocity in water, using the appropriate boundary and medium condition for a particular problem.

There are two theoretical approaches to the solution of (10.1). One is the wave theory approach, and the other is the ray tracing or geometrical approach. For the wave theory approach, the solution of the wave equation is described in terms of characteristic functions called normal modes, each of which is a solution of the equation.

The wave theory approach takes account of wave nature of sound propagation in the sea such as the phenomena of diffraction and multiple scattering. The normal modes are combined additively to satisfy the boundary and source conditions of interest. The wave theory gives a formally complete solution. The result will show a mathematical solution suitable for computational purpose. Only in limiting cases, the analytical solutions exist. It presents computational difficulties in all but simplest boundary condition. However, it gives little insights on the distribution of energy of the sources in space and time and the solution is difficult to interpret. Normal mode theory is particularly suitable for description of sound propagation in shallow water. It is valid for all frequencies but practically is useful for low frequencies (few modes). The source function can be easily inserted. But it cannot easily handle real boundary conditions.

The ray theory approach is also known as ray acoustics or geometrical acoustics. Like geometrical optics, it does not handle diffraction problem. It has the following properties: (1) the existence of rays that describe the paths of propagation of sound wave. Rays are easily drawn. Sound distribution is easily visualized, (2) the concept of wavefronts, along which the phase or time function of the solutions, is constant. Real boundary conditions are inserted easily, for example, a sloping bottom. It is independent of the source. Ray acoustics is analogous to geometrical optics and it presents a picture of the propagations of sound in the sea in the form of the ray diagram. Rays can be drawn by hand using Snell's law. However, a ray-trace computer program is normally used. The ray theory does not provide an accurate solution when (a) the radius of curvature of the rays or (b) the pressure amplitude changes appreciably over the distance of one wavelength. In practice, ray theory is therefore restricted to high frequencies or short wavelengths if radius of ray curvature is larger than the wavelength or the sound velocity does not change much in a wavelength. It cannot be used for predicting the intensities of sound in shadow zones or caustics. An important book on theory of sound propagation in the sea is

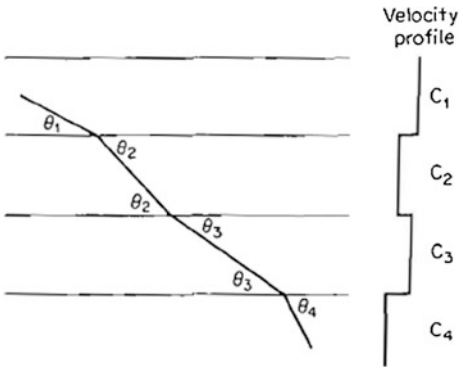

Fig. 10.1 Refraction in a layered medium

that of Brekhovskikh [1]. Brekhovskikh's book is based on the representation of the sea or the medium of sound propagates as a layered medium (Fig. 10.1).

Ray theory uses Snell's law which shows the analogies between sound waves and light waves. Snell's law describes the refraction of sound rays in a medium of variable velocity. Snell's law states that in a medium consisting of constant velocity layers (Fig. 10.1), the grazing angles θ_1, θ_2, … of a ray at the layer boundaries are related to the sound velocities c_1, c_2, … of the layers by

$$\frac{\cos\,\theta_1}{c_1} = \frac{\cos\,\theta_2}{c_2} = \frac{\cos\,\theta_3}{c_3} = \cdots = \text{a constant for any one ray.} \tag{10.2}$$

When $\theta = 0°$, the ray constant becomes the reciprocal of the sound velocity in the layer in which the ray becomes horizontal. This expression is the basis of ray computation used by most analogue and digital computers, since it enables a particular ray to be "traced out" by following it through the successive layers into which the velocity profile may have been divided. In a layered medium having layers with constant velocity, the rays consist of a series of straight-line segments joined together, in effect, by Snell's law.

10.3 Reflection and Scattering from the Sea Surface

The sea surface is both a reflector and a scatterer of sound and has a profound effect on sound propagation in the sea where the sound or receiver lies at shallow depth. If the sea surface were perfectly smooth, it would form an almost perfect reflector of sound. The intensity of sound reflected from the smooth sea surface would be very nearly equal to that incident upon it. The reflection loss, equal to $10\log(I_r/I_i)$, where I_r and I_i are the reflected and incident intensities of an incident plane wave, would be closely equal to zero decibels. In real situations, the sea is somewhat rough, and the loss on reflection is found to be no longer zero. A criterion for the roughness or smoothness of the surface is given by the Rayleigh parameter, defined

as $R = kH \sin\theta$, where k = wave number = $2\pi/\lambda$, H = rms "wave height" (crest to trough) and θ is the grazing angle. When $R \ll 1$, the surface is primarily a reflector and produces a coherent reflection at the specular angle equal to the angle of incidence. When $R \gg 1$, the surface acts as a scatterer, sending incoherent energy in all directions. With certain theoretical assumption, the amplitude reflection coefficient μ of an irregular surface defined as the ratio of the reflected or coherent amplitude of the return to the incident amplitude can be shown to be $\mu = \exp(-R)$. When $R \gg 1$, the return from the surface is incoherent scattering, instead of coherent reflection with a distribution throughout space depending upon the nature of the surface roughness.

10.4 Reflection and Scattering from the Sea Bottom

The sea bottom is a reflecting and scattering boundary of the sea having a number of characteristics similar to the sea surface. However, its effects are more complicated because of its diverse and multilayered composition. An example of this similar behaviour is the fact that the sea bottom casts a shadow or produces a shadow zone, in the upward-refracting water above it in the depths of the deep sea.

The reflection of sound from the sea bed is vastly more complex than that from the sea surface. First, the bottom is more variable in its acoustic properties because it may vary in composition from hard rock to soft mud. Secondly, it is often layered, with a density and a sound velocity that change gradually or abruptly with depth. For these reasons, the reflection loss of the seabed is less easily predicted than that of the sea surface.

10.5 Sea Bottom—Reflection Loss

The reflection loss of sound incident at an angle to a plane boundary between two fluids was worked out by Rayleigh [2]: If a plane wave is incident at grazing angle θ, upon the boundary between fluids of density ρ_1 and ρ_2 and of sound velocity c_1

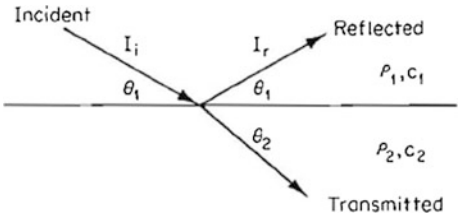

Fig. 10.2 Reflected and transmission rays at a discontinuity between two media

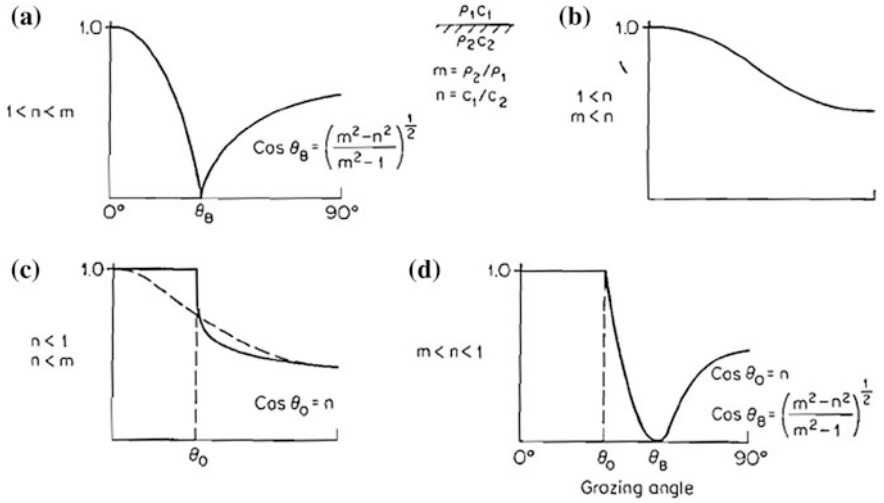

Fig. 10.3 Ratio of reflected to incident intensities for four combinations of conditions of sound velocities and densities in lossless media separated by a plane interface. The dashed curve in © shows the effect of an attenuation lower medium (From Brekhovskikh [1], Fig. 10.7)

and c_2 as shown in Fig. 10.2, then by the Rayleigh formula, the intensity of the reflected wave I_r is related to the intensity of the incident wave I_i by

$$\frac{I_r}{I_i} = \left[\frac{m\sin\theta_1 - n\sin\theta_2}{m\sin\theta_1 + n\sin\theta_2}\right]^2 = \left[\frac{m\sin\theta_1 - (n^2 - \cos^2\theta_1)^{1/2}}{m\sin\theta_1 + (n^2 - \cos^2\theta_1)^{1/2}}\right]^2, \tag{10.3}$$

where following the citations of Brekhovskikh [1] $m = \frac{\rho_1}{\rho_2}$ and $n = \frac{c_1}{c_2}$.

Figure 10.3, adapted from Brekhovskikh [1], shows the behaviour of the loss with grazing angle for four different conditions on m and n. Of these four, the most common condition for natural bottom is probably that of Fig. 10.3c, in which a critical angle θ_0 exists such that complete or total reflection occurs (zero loss) at grazing angles less than critical. In many soft mud bottoms, the sound velocity is less than that in the water above, and an angle of intromission θ_B may exist, as in Fig. 10.3a.

So far, absorption has not been brought into picture. All bottom materials are to some extent absorptive, and the effect of absorption is to smooth out the variation of loss with angle, so as to eliminate, or obscure, the sharp changes occurring at the critical angle θ_0 and the angle of intermission θ_B. An example of the effect of absorption is the dashed curve as shown in Fig. 10.3c.

Many measurements of sound attenuation in sediments have been made [3]. They show that the attenuation coefficient of compressional waves in marine sediments is related to frequency by

$$\alpha = kf^n, \tag{10.4}$$

where α is in decibels per metre, f is the frequency in kilohertz and k and n are empirical constants.

If the bottom in the most simple model is taken to be a homogeneous absorptive fluid with a plane interface, then the three bottom parameters that determine the reflections loss are its density, sound velocity and attenuation coefficient. If the bottom happens to be a sedimentary material, these quantities are related to and determined by the porosity of the sediment.

However, a number of complications to this simple model occur in the real world. First of all, the ocean flow is not a perfectly plane interface so that scattering as well as reflection takes place. In a very rough area, such as the Mid-Atlantis Ridge, scattered sound dominates the bottom return. As a result, some sound is sent by the bottom in all directions and the "beam pattern" of the bottom return shows no appreciable lobe or peak in the specular direction.

10.6 Westervelt Equation

A common equation for use in underwater acoustics is the Westervelt equation:

$$\nabla^2 p - \frac{1}{c_0^2}\frac{\partial^2}{\partial t^2}p + \frac{\delta}{c_0^4}\frac{\partial^3}{\partial t^3}p = -\frac{\beta}{\rho_0 c_0^4}\frac{\partial^2}{\partial t^2}p^2, \tag{10.5}$$

where p = sound pressure, c_0 = small signal sound speed, δ = sound diffusivity, μ = shear viscosity, μ_B = bulk viscosity, γ = thermal conductivity, c_v, c_p = specific heat at constant volume and pressure, respectively.

$$\delta = \frac{1}{\rho_0}\left(\frac{4}{3}\mu + \mu_B\right) + \frac{\gamma}{\rho_0}\left(\frac{1}{c_v} - \frac{1}{c_p}\right). \tag{10.6}$$

It is of interest to note that the Westervelt also has the form invariance property. That is, by replacing the μ, μ_B and ρ by their negative values, there is no change in the form of the equation. This confirms that coordinate transformations is applicable to the Westervelt equation. Also the status of viscosity in underwater is equivalent to that of bulk modulus in solids.

To study the difference between underwater cloaking and cloaking in the air, one needs to understand the difference in properties between the two host media, water and air. When performing cloaking in the air, one has the advantage that most materials used as inclusions have large effective mass compared with that of air and very high speed of mass anisotropy can be achieved due to the very low density and very high compressibility of air. However, this also gives rise to the limitation that it is very difficult to fabricate an acoustic metamaterial that is lighter and more

compressible than air. Water on the other hand is more compressible and less dense than most solid inclusion. Hence, it is difficult to attain high effective mass density and high effective stiffness with water as a host medium. However, it has been recorded in the literature that closed-cell metal foam which enables gas-filled materials demonstrating masses less than that of the water host.

The above shows that the achievable effective parameters are difficult for using air and water as host media. An example is that in air, it is easy to achieve a density component that is very large at the inner edge of the shell, but it is difficult to do so for water.

10.6.1 Coordinate Transformations on the Westervelt Equation

Coordinate transformations on the Westervelt can be done by following the procedure below:

Here, we follow approach of Cummer et al. [4]. The fluids version of the linear acoustic field equations will be used:

$$\nabla p = i\omega\rho\left(\overrightarrow{r}\right)\rho_0\overrightarrow{v}, \tag{10.7}$$

$$i\omega p = \kappa\left(\overrightarrow{r}\right)\kappa_0\nabla\cdot\overrightarrow{v}, \tag{10.8}$$

where $\rho\left(\overrightarrow{r}\right)$ and $\kappa\left(\overrightarrow{r}\right)$ are the normalized density and bulk modulus, respectively, of the medium and are coordinate transform invariant. We will demonstrate how the acoustic $\overrightarrow{v}$ must transform by considering $\overrightarrow{v}$ in a nonorthogonal coordinate system described by coordinates q_1, q_2 and q_3 with unit vectors $\hat{u}_1$,$\hat{u}_2$ and $\hat{u}_3$, respectively. Following Pendry et al. [5] and letting $i = 1, 2, 3$

$$Q_i^2 = \left(\frac{\partial x}{\partial q_i}\right)^2 + \left(\frac{\partial y}{\partial q_i}\right)^2 + \left(\frac{\partial z}{\partial q_i}\right)^2, \tag{10.9}$$

$$\hat{n} = \frac{\hat{u}_1 \times \hat{u}_2}{|\hat{u}_1 \times \hat{u}_2|},$$

$$\text{Area} = Q_1 dq_1 Q_2 dq_2 |\hat{u}_1 \times \hat{u}_2|.$$

Figure 10.4 shows what happens when we apply the divergence theorem to an infinitesimal volume in this nonorthogonal coordinate system.

Deriving the net outward flux of $\overrightarrow{v}$ from this volume and setting it equal to the divergence of $\overrightarrow{v}$ times the infinitesimal volume, it can be shown that

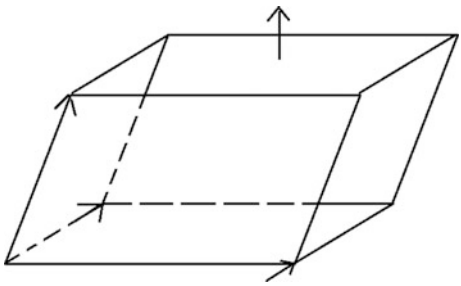

Fig. 10.4 The parallelepiped that defines an infinitesimal volume in the transformed coordinates. The area and unit normal of each face enters in the calculation of the net flux of a vector out of this volume (From Cummer et al. [4])

$$(\nabla \cdot \vec{v}) Q_1 Q_2 Q_3 |\hat{u}_1 \cdot (\hat{u}_2 \times \hat{u}_3)| = \frac{\partial}{\partial q_1}[Q_2 Q_3 \vec{v} \cdot (\hat{u}_2 \times \hat{u}_3)] + \frac{\partial}{\partial q_2}[Q_1 Q_3 \vec{v} \cdot (\hat{u}_1 \times \hat{u}_3)] + \frac{\partial}{\partial q_3}[Q_1 Q_2 \vec{v} \cdot (\hat{u}_1 \times \hat{u}_2)]. \tag{10.10}$$

Let $V_{\text{frac}} = |\hat{u}_1 \cdot (\hat{u}_2 \times \hat{u}_3)|$, because this is the fraction by which a unit volume is compressed by the coordinate nonorthogonality, and we use the conventional superscript (subscript) notation for contravariant (covariant) vector components using

$$\overrightarrow{v} \cdot (\hat{u}_2 \times \hat{u}_3) = v^1 \hat{u}_1 \times (\hat{u}_2 \times \hat{u}_3). \tag{10.11}$$

equation (10.10) can be rewritten as

$$(\nabla \times \overrightarrow{v}) Q_1 Q_2 Q_3 V_{\text{frac}} = \frac{\partial}{\partial q_1}(Q_2 Q_3 V_{\text{frac}} v^1) + \frac{\partial}{\partial q_2}(Q_1 Q_3 V_{\text{frac}} v^2) + \frac{\partial}{\partial q_3}(Q_1 Q_2 V_{\text{frac}} v^3). \tag{10.12}$$

Noting that the divergence in the transformed coordinates is defined by $\nabla_q \cdot \overrightarrow{v} = \frac{\partial v^1}{\partial q_1} + \frac{\partial v^2}{\partial q_2} + \frac{\partial v^3}{\partial q_3}$, we can write

$$\nabla_q \cdot (V_{\text{frac}} \overline{\overline{Q}}_{\text{per}} [v^1 v^2 v^3]^{\text{T}} = \nabla_q \cdot \widetilde{v}, \tag{10.13}$$

where

$$\overline{\overline{Q_{\text{per}}}} = \begin{bmatrix} Q_2 Q_3 & 0 & 0 \\ 0 & Q_1 Q_3 & 0 \\ 0 & 0 & Q_1 Q_2 \end{bmatrix} \tag{10.14}$$

and the transformed velocity vector $\widetilde{v}$ is given by

$$\widetilde{v} = V_{\text{frac}} \overline{\overline{Q}}_{\text{per}} [v^1 v^2 v^3]^{\text{T}}. \tag{10.15}$$

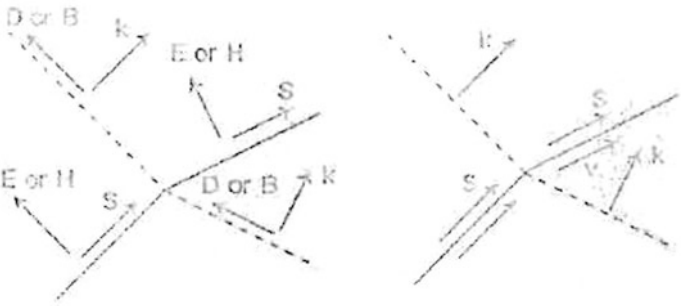

Fig. 10.5 The transformation of vectors in electromagnetic (left) and acoustic or compressional elastodynamic (right). The white converging arrows denote which component of each vector is compressed by the coordinate transformations (From Cummer et al. [4])

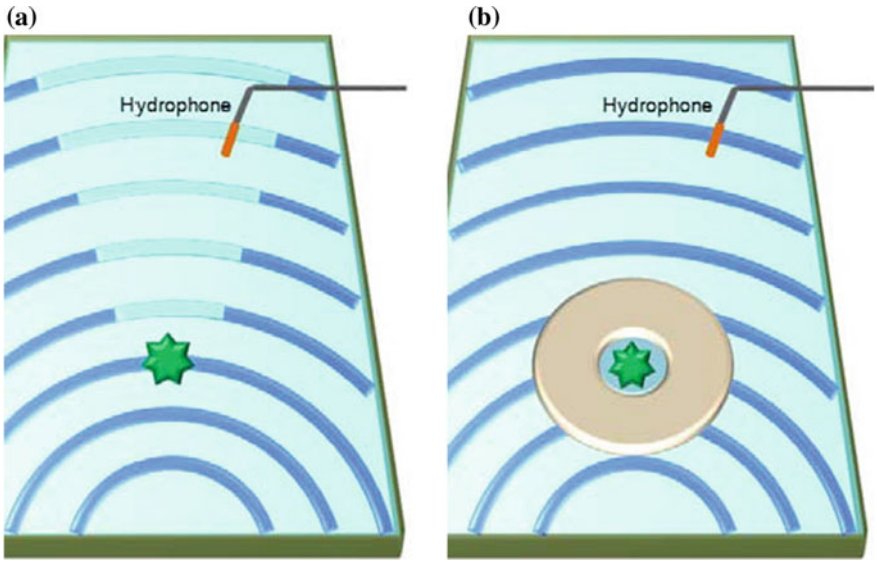

Fig. 10.6 Schematic diagram of the experimental set-up. A burst of monotonic signal with a width of twenty periods was used to drive the transducer as an underwater point source in the water tank. One needle-sized hydrophone detected the ultrasonic signals in the immediate environment of **a** the object and **b** the cloaked object (Zhang et al. [6])

The per subscript on the tensor $\overline{\overline{Q}}_{\text{per}}$ is to denote that the diagonal elements transform each vector component by the product of the coordinate scaling factors perpendicular (more general, not parallel, for the case of nonorthogonal coordinates) to the direction of the vector component. Recall that our qualitative discussion above, summarized in Fig. 10.6, showed that this is precisely how the velocity vector must transform in a compressed wave in order for transformation

acoustics to work. Note that the elements of the volume vector $[v^1 v^2 v^3]^{\mathrm{T}}$ are the contravariant components of $\overrightarrow{v}$ in the nonorthogonal coordinate system while the element of the vector $\overrightarrow{v}$ is the component in the original orthogonal coordinate system (Fig. 10.5).

Multiplying (10.8) (with $\lambda\left(\overrightarrow{r}\right) = 1$) by $Q_1 Q_2 Q_3 V_{\mathrm{frac}}$ and using (10.14) results in the equation in the transformed coordinates,

$$i\omega p = \kappa(\vec{q})\kappa\nabla_{\mathrm{q}} \cdot \overrightarrow{v} \tag{10.16}$$

with

$$\kappa(\overline{q}) = \left(Q_1 Q_2 Q_3 V_{\mathrm{frac}}\right)^{-1}. \tag{10.17}$$

This demonstrates the coordinate to function invariant of (10.8) provided that the bulk modulus is modified according to (10.17) and the velocity vector is transformed according to (10.16). More generally, this also shows how a vector must transform in order for the gradient operator to maintain its basis form.

Cummer et al. [4] derived how (10.7) and therefore the gradient operator transform under a coordinate change using the gradient theorem and integrating ∇p along a short length in the q_1 coordinate directions, they find that

$$\nabla p \cdot Q_1 \hat{u}_1 = \frac{\partial p}{\partial q_1} = \left(\nabla_q p\right)^1. \tag{10.18}$$

The left-hand side contains the scaled covariant components of ∇p which must be converted to covariant components before it can be equated component-wise to $\nabla_q p$, the gradient in the transformed coordinates. They find that

$$\nabla_q p = \overline{\overline{Q}}_{\mathrm{par}} \overline{\overline{h}}^{-1} (\nabla p), \tag{10.19}$$

where $\overline{\overline{Q}}_{\mathrm{par}}$ is the diagonal tensor containing coordinate scaling factors parallel to the direction of the vector component or

$$\overline{\overline{Q}}_{\mathrm{par}} = \begin{bmatrix} Q_1 & 0 & 0 \\ 0 & Q_2 & 0 \\ 0 & 0 & Q_3 \end{bmatrix} \tag{10.20}$$

and

$$\overline{\overline{h}}^{-1} = \begin{bmatrix} \hat{u}_1 \cdot \hat{u}_1 & \hat{u}_1 \cdot \hat{u}_2 & \hat{u}_1 \cdot \hat{u}_3 \\ \hat{u}_2 \cdot \hat{u}_1 & \hat{u}_2 \cdot \hat{u}_2 & \hat{u}_2 \cdot \hat{u}_3 \\ \hat{u}_3 \cdot \hat{u}_1 & \hat{u}_3 \cdot \hat{u}_2 & \hat{u}_3 \cdot \hat{u}_3 \end{bmatrix}. \tag{10.21}$$

Note that this $\overline{\overline{h}}^{-1}$ is the same as $\overline{\overline{g}}^{-1}$ defined by Pendry et al. [5]. They rename this tensor because they will use $\overline{\overline{g}}$ later to denote the metric tensor which is not quite the same as this $\overline{\overline{h}}$.

Finally, multiplying (10.1) (with $\rho(\vec{r}) = 1$) by $\overline{\overline{Q}}_{\text{par}}$, they find

$$p_q p = i\omega \overline{\overline{Q}}_{\text{par}} \overline{\overline{h}}^{-1} \rho_0 \overrightarrow{v} = i\omega \overline{\overline{Q}}_{\text{par}} \overline{\overline{h}}^{-1} \overline{\overline{Q}}_{\text{par}}^{-1} V_{\text{frac}}^{-1} \rho_0 \overrightarrow{v}, \tag{10.22}$$

leaving us with the equivalent of (10.7) in fully transformed coordinates:

$$\nabla_q p = i\omega \overline{\overline{\rho}} \rho_0 \overrightarrow{v} \tag{10.23}$$

with

$$\overline{\overline{p}} = \overline{\overline{Q}}_{\text{par}} \overline{\overline{h}}^{-1} \overline{\overline{Q}}_{\text{par}}^{-1} \overline{\overline{v^{-1}}}_{\text{frac}}. \tag{10.24}$$

Equations (10.16) and (10.23) show that the acoustic equations are fully transformation invariant with the modified material parameters in (10.17) and (10.24).

They further show that these experiments are equivalent to those shown by Chen and Chan [7] purely by analogy with electromagnetics through the electric conductivity equation [8] and those derived by Greenleaf et al. [9] for the general scale Helmholtz equation. Consequently, cloaking shell, concentrator and other devices that have been designed theoretically by electromagnetic can also be realized for acoustics provided that the bulk modulus and anisotropic effective mass density tensor can be realized in practice as specified by (10.17) and (10.24). This first principle derivation without using analogy shows explicitly in (10.14) how the acoustic velocity vector must transform under coordinate change, which as noted above is different from how the $\vec{E}$ and $\vec{H}$ field, transform in electromagnetics. The scalar pressure is, however, not changed by the coordinate transformations and, thus like phase fronts and power flow lines, is simply deformed by any coordinate transformations.

10.7 A Practical Example of Underwater Acoustical Cloaking

10.7.1 Principle of Underwater Acoustic Cloaking

As one can see from above section that sound propagation in water undergoes different mechanisms from sound propagation in air and so underwater cloaking will be a different treatment from cloaking in the air. To tackle the problem of underwater acoustical cloaking, underwater acoustic cloaking [6] used a different

approach from that of acoustic cloaking in the air. It is based on the acoustic transmission line approach using the analogy between the electronic circuit elements and the lumped acoustic elements. The basic geometry of the cloak is of cylindrical shape. It consists of an array of sub-wavelength cavities and connecting channels with spatially designed geometry. The acoustic wave equations describing ultrasound propagation through the electronic networks will be replaced by the telegraph's equations. The fluid motion will be analogous to the current flow in the electronic circuit. The transmission line approach has the advantage of (a) simple geometric structure, (b) scaling, (c) ease of manufacturing (d) low loss, (e) broadband using nonresonant constituents and (f) potential to extend to large number of other acoustic devices based on transformation.

The 2D acoustic metamaterial cloak will squeeze the cylindrical region of $0 < r < R_2$ into an annular region of $R_1 < r' < R_2$. r and r' are the radial coordinates in the original and transformed region, respectively. The sound wave will be smoothly bent inside the cloak and will be excluded from the extended volume without perturbation of external field.

The distributed acoustic system will be described by the 2D telegrapher's equations. The warping of space will follow the distribution of shunt capacitor and serial inductor in the annular region given as:

$$L_r = \rho_w \frac{\Delta r}{2S_r}, \tag{10.25}$$

$$L_\Phi = \rho_w r \frac{\Delta \Phi}{2S_\Phi} \left(\frac{r - R_1}{r}\right)^2, \tag{10.26}$$

$$C = 2\Delta r S_\Phi \beta_w \left(\frac{R_2}{R_{2-R_1}}\right)^2. \tag{10.27}$$

10.7.2 Geometric Structure of the Underwater Acoustic Cloak

The above parameters are used for the fabrication of the underwater acoustic cloak. The transmission line approach is used. The underwater cloak is implemented by a network of anisotropic acoustic transmission line making use of the analogy between the lumped element of the transmission line and the parameters of the acoustic equation of motion. First one will start with the building blocks of this network. The acoustic cloak consists of sixteen homogeneous concentric cylinders. The first cylinder next to the inner lining of the cloak is divided into 32 units around the circumference. From the first to the fourth layer, the spacing along the radial direction is $\lambda/7$, $\lambda/8$, and $\lambda/9$, respectively, in the outward direction, where λ = sound wavelength in water. From the fifth layer onwards to the sixteenth layer, the

layers are evenly spaced with distance equal to $\lambda/10$ along the radial direction. The size of each unit cell is only $\lambda/10$. Also the first cylinder next to the inner lining of the cloak consists of 32 unit cells around the circumference. The size of the unit cell is smaller than $\lambda/10$ along the circumference of direction. From the second layer onwards, the number of unit cells is doubled to 6 and further increased to 128 from the sixth layer.

10.7.3 Experimental Procedure

To start the experiment, the whole metamaterial structure is placed in water [6]. This structure behaves like an anisotropic lumped transmission line for incoming underwater ultrasound. The equivalence of the acoustic lumped elements to the transmission line elements works as follows. Here, the acoustic capacitor $C = V/\rho_w C_w^2$ is equivalent to the cavity with large volume in centre, and the serial inductors are $L_r = \rho_w l_r/S_r, L_\Phi = \rho_w l_\Phi/S_\Phi$, [10–14] equivalent to the channels connecting it to the four neighbouring cavities. The transmission line cloak is realized by tailoring the geometry of the building blocks given in Fig. 10.2c with the spatially varying profile given by the above relation. Reroutes the path of underwater sound around the cloaked object without significant scattering.

As an analysis, aluminium is chosen as material for the cloak. Aluminium has acoustic impedance eleven times that of water. From the elasticity of aluminium, one can infer that at low frequencies most of the acoustic energy will be confined in the fluid where the excitation comes from [13]. Also ultrasound propagates through aluminium may increase the energy loss by the cloaking material [14].

The experiment will demonstrate the performance of the underwater acoustic cloak. First the object is placed in the water tank. Then, the acoustic pressure of the propagating ultrasound is measured with and without the presence of the cloak (Fig. 10.6). The object to be cloaked is a steel cylinder. The radius of this cylinder is equal to the inner radius of the cloak. The metamaterial network is machined on the side of the cloak. The side of the cloak was placed against the bottom of the tank. The steel cylinder is surrounded with the metamaterial cloak. A spherical-shaped transducer as a point source generates the ultrasound waves. In order to map the spatial acoustic pressure field distribution in 2D *xy* direction, a hydrophone is mounted on a linear translation stage by stepping the hydrophone in small increments and recording the acoustic pulse signal from the water at every step. Fig. 10.8a shows the experimental results. The results show the effect of cloaking. Without the cloak and with the steel cylinder standing alone, there is considerable shadowing and scattering at 60 kHz. With the presence of the cloak, the cloak together with the hidden cylinder becomes invisible because the wave trajectory was restored behind the cloak with diminutive distortion in the cylinder

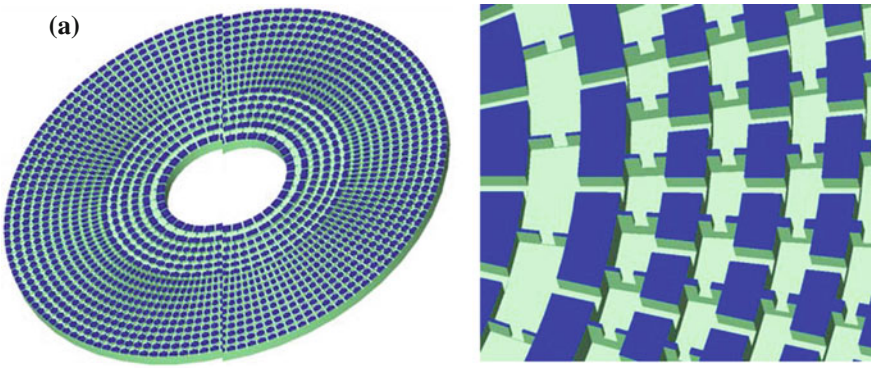

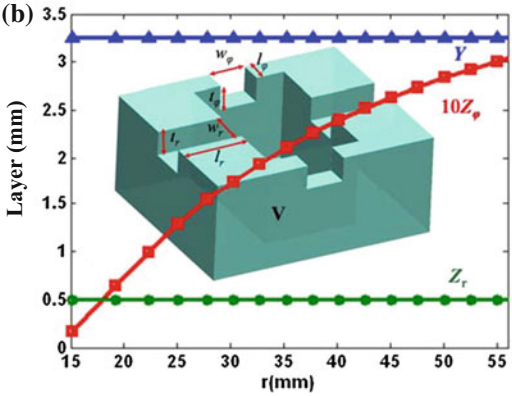

(c)

Layer (mm)	$l_r(mm)$	l_Φ(mm)	V(mm^3)
1	2.05	0.10	3.00
3	1.37	0.22	2.29
5	1.24	0.41	2.06
7	1.24	0.30	2.06
9	1.24	0.41	2.06
11	1.24	0.52	2.06
13	1.24	0.63	2.06
15	1.24	0.74	2.06

L ©

Fig. 10.7 A 2D acoustic cloak for underwater ultrasound waves. (a) The configuration of the acoustic cylindrical cloak synthesized by an acoustic transmission line, namely serial inductors and shunt capacitors. The inset is the expanded view of the network. The cavities with large volume work as shunt capacitors and those cavities are connected by narrow channels that act as the serial inductors. (b) One building block of the acoustic circuit, each unit cell consists of one large cavity in the centre with channels connecting to the four neighbouring blocks. The reduced cloaking parameters are used in the design. The serial impedance Z, shunt admittance Y have constant value and Z_ϕ increases as radius changes from $R1$ = 13.5 mm to the $R2$ = 54.1 mm. (c) The geometry parameters of the building blocks in the layers with odd number are presented in the table. The depth and width t_r, w_r and t_ϕ, w_ϕ of the channels along radial and angular directions have constant values of 0.5 mm (Zhang et al. [6])

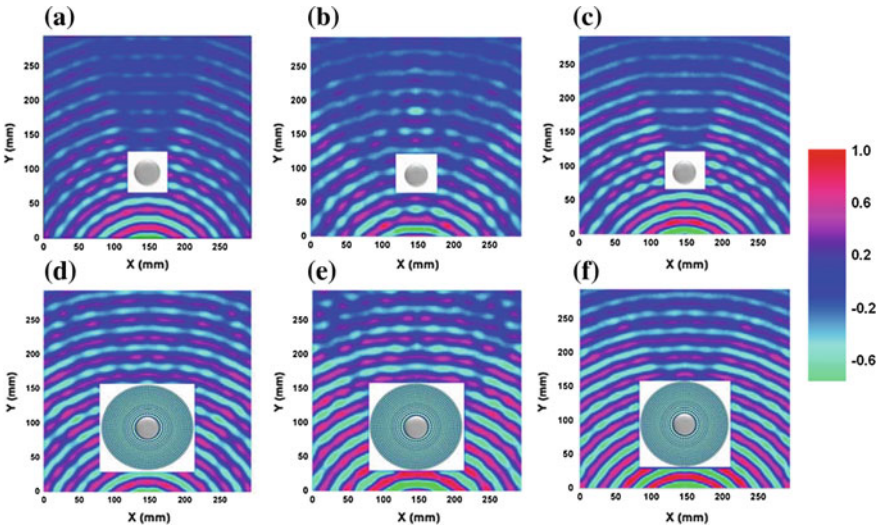

Fig. 10.8 Measured pressure field mappings of the bare steel cylinder and the cloaked steel cylinder illuminated with a point ultrasound source. The cloak lies in the centre of the water tank and surrounds the steel cylinder. The scattering field patterns of the bare steel cylinder at **a** 60 kHz **b** 52 kHz and **c** 64 kHz. The pseudo colormaps in the immediate environment of the cloaked steel cylinder at **d** 60 kHz **e** 52 kHz and **f** 64 kHz (Zhang et al. [6])

wavefronts. The very small attenuation of the transmitted fields observed on the exit side of the cloak showed the low loss nature of the metamaterial cloak (Fig. 10.7).

Figure 10.8b–f show the acoustic wavefield distribution with and without cloaking at 52 and 60 kHz. This demonstrates the broadband nature of the cloak. The unit cells of the metamaterial cloak are nonresonant in nature. An example of the acoustic wavefield distribution at 52 and 60 kHz are given in Fig. 10.8b–f for cases with and without cloak by Zhang et al. [6] to demonstrate with broadband from 40 to 80 kHz. Below 40 kHz, the scattering from object with radius 13.5 mm is negligible. At the 80 kHz end, there are limitations by two factors. One is the transmission line model will break down at around 120 kHz when the unit cell size is about one quarter wavelength. The upper frequency limit can be extended by using smaller unit cells. The other factor is the cutoff frequency at 80 kHz. This is due to the low pass topology of the circuit network. This problem can be resolved by modifying the geometry of the building block.

The improvement on the performance of the underwater cloak was further investigated by Zhang et al. [6]. They conduct a number of measurements over different frequencies. For these experiments, they measured the peak values of the acoustic pressure along the wavefronts below the underwater cloak.

The cloaking performance is measured quantitatively by the average visibility of the object. It is defined as

$$\overline{\Upsilon}=\frac{1}{h}\sum_{j=1}^{n}\Upsilon_j, \tag{10.28}$$

where $\Upsilon_j = \left(P_{\max,j} - P_{\min,j}\right)/\left(P_{\max,j} + P_{\min,j}\right)$, $P_{max,j}$ and $P_{min,j}$ are the maximum and minimum peak values, respectively, and numbered by j.

An example of the measured peak pressure at 60 kHz long one wavefront in the exit side of the object for with cloak and without cloak are shown in Fig. 10.9. The measurement results for the free space case when there is neither object nor cloak in the water tank is plotted as reference. It is shown that there is small modulation in the amplitude along one wavefront. Figure 10.9b shows the comparison of the averaged visibility of the cloaked objet over all wavefronts on the exit side with the case of an uncloaked cylinder. This comparison shows the underwater acoustic cloak has good performance of shielding effectiveness over a broad frequency range even with impedance mismatch at the outer interface of the cloak. The visibility is 0.62 for the bare steel cylinder but reduced to 0.32 for the cloaked cylinder at 60 kHz. This shows significant reduction in shadowing and scattering.

Theoretically, the averaged visibility should be zero when there is no scattering and shadowing. However, in practice due to the presence of noise in the measure, the averaged visibility still has a small value for the free space as shown in Fig. 10.9b. The above results show that the transmission model consisting of a network of lumped circuit elements for the underwater cloak is workable. The unit cell of this acoustic metamaterial is nonresonant in nature and can be valid for a broad frequency range.

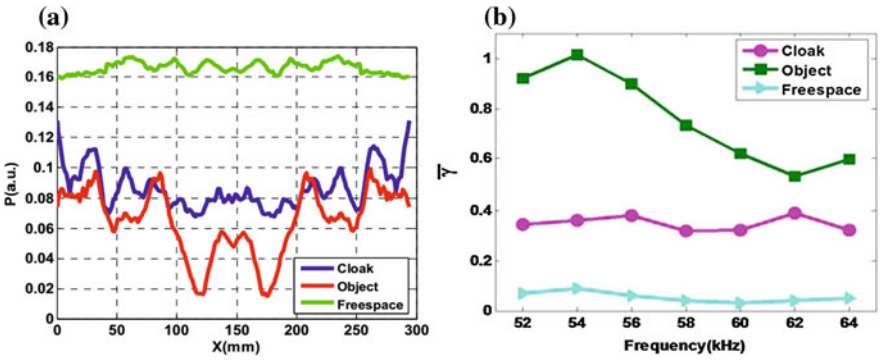

Fig. 10.9 Frequency dependence of the averaged visibility of the steel cylinder with and without the acoustic cloak. (a) The measured peak values of the pressure field along the wavefront lies between y = 100 mm and y = 170 with and without cloak at 60 kHz. The green line plot is the reference case when there is no object in the water tank. (b) Plot of the averaged visibility. The experimental results measured with and without cloak are marked by the magenta circles and green square, respectively. The reference visibility when there is no object is marked by blue triangular (Zhang et al. [6])

10.8 Application of Underwater Acoustical Cloaking

Underwater acoustic cloaking can be applied to shield submarines from sonar. It will need further works to scale up the above underwater acoustic cloak to the size that can be applied to deroute the sonar.

References

1. Brekhovskikh, L.M.: Waves in Layered Media. Academic Press Inc., New York (1960)
2. Rayleigh, L.: The Theory of Sound, vol. 2. Dover Publications Inc, New York (1945)
3. Hamilton, E.L.: Compressional wave attenuation in marine sediments. Geophysics **37**, 620 (1972)
4. Cummer, S.A., Rahm, M., Schurig, D.: Material parameters and vector scaling in transformation acoustics. New J. Phys. **10**, 115025–115034 (2008)
5. Pendry, J.B., Schurig, D., Smith, D.R.: Controlling electromagnetic fields. Science **312**, 1780 (2006)
6. Zhang, S., Xia, C., Fang, N.: Broadband acoustic cloaking for ultrasound waves. Phys. Rev. Lett. **106**, 024301 (2011)
7. Chen, H., Chan, C.T.: Acoustic cloaking in three dimensions using acoustic metamaterials. Appl. Phys. Lett. **91**, 183518 (2007)
8. Greenleaf, A., et al.: Anisotropic conductivities that cannot be detected by EIT. Physiol. Meas. **24**, 413–419 (2003)
9. Greenleaf, A., Kurylev, Y., Lassas, M., Uhlmann, G.: Comment on "scattering theory derivation of a 3D acoustic cloaking shell". http://aixiv.org/abs/081.39279v1
10. Stewart, G.W.: Acoustic wave filters. Phys. Rev. **20**, 528 (1922)
11. Beranek, L.L.: Acoustics. McGraw-Hill, New York (1954)
12. Kinsler, L.E.: Fundamentals of Acoustics. Wiley, New York (1982)
13. Fuller, C.R., Fahy, F.J.: Characteristics of wave propagation and energy distributions in cylindrical elastic shells filled with fluid. J. Sound Vib. **81**(4), 501–518 (1982)
14. Lamb, H.: Manchester Literary and Philosophical Society-Memoirs and Proceedings, vol. 42, no. 9 (1898)

Chapter 11
Seismic Metamaterials

Abstract The seismic metamaterial is an application of the cloaking of objects to shielding of buildings and large objects from seismic waves. This enables the bending of seismic waves away from the structures. The detailed theory and adaptation to the required situation are given. This is an example of the scaling up the capability of the acoustical metamaterials from nanometre size to building scale.

11.1 Introduction

The sudden release of huge amount of energy from the earth's crust will give rise to earthquakes which produce seismic waves. A **seismic metamaterial** is a metamaterial that is designed to counteract the adverse effects of seismic waves on artificial structures, which exist on or near the surface of the earth. As of 2009, seismic metamaterials were still in the development stage. More than a million earthquakes are recorded each year, by a worldwide system of earthquake detection stations. The propagation velocity of the seismic waves depends on density and elasticity of the earth materials. In other words, the speeds of the seismic waves vary as they travel through different materials in the earth. The two main components of a seismic event are body waves and surface waves. Both of these have different modes of wave propagation.

Computations showed that seismic waves travelling towards a building could be directed around the building, leaving the building unscathed, by using *seismic metamaterials*. The very long wavelengths of earthquake waves would be shortened as they interact with the metamaterials; the waves would pass around the building so as to arrive in phase as the earthquake wave proceeded, as if the building was not there. The mathematical models produce the regular pattern provided by metamaterial cloaking. This method was first understood with electromagnetic cloaking metamaterials—the electromagnetic energy is in effect directed around an object, or hole, and protecting buildings from seismic waves employs this same principle.

Giant polymer-made split ring resonators combined with other metamaterials are designed to couple at the seismic wavelength. Concentric layers of this material would be stacked, each layer separated by an elastic medium. The design that

W.S. Gan, *New Acoustics Based on Metamaterials*, Engineering Materials,
https://doi.org/10.1007/978-981-10-6376-3_11

worked is ten layers of six different materials, which can be easily deployed in building foundations. As of 2009, the project is still in the design stage.

11.2 Electromagnetics Cloaking Principles for Seismic Metamaterials

For seismic metamaterials to protect surface structures, the proposal includes a layered structure of metamaterials, separated by elastic plates in a cylindrical configuration. A prior simulation showed that it is possible to create concealment from electromagnetic radiation with concentric, alternating layers of electromagnetic metamaterials. That study is in contrast to concealment by inclusions in a split ring resonator designed as an anisotropic metamaterial [1].

The configuration can be viewed as alternating layers of "homogeneous isotropic dielectric material" A with "homogeneous isotropic dielectric material" B. Each dielectric material is much thinner than the radiated wavelength. As a whole, such structure is an anisotropic medium. The layered dielectric materials surround an "infinite conducting cylinder". The layered dielectric materials radiate outwards, in a concentric fashion, and the cylinder is encased in the first layer. The other layers alternate and surround the previous layer all the way to the first layer. Electromagnetic wave scattering was calculated and simulated for the layered (metamaterial) structure and the split ring resonator anisotropic metamaterial, to show the effectiveness of the layered metamaterial [1].

11.3 Acoustical Cloaking Principles for Seismic Metamaterials

The theory and ultimate development for the seismic metamaterial is based on coordinate transformations achieved when concealing a small cylindrical object with electromagnetic waves. This was followed by an analysis of acoustic cloaking, and whether or not coordinate transformations could be applied to artificially fabricated acoustic materials [2].

Applying the concepts used to understand electromagnetic materials to material properties in other systems shows them to be closely analogous. Wave vector, wave impedance and direction of power flow are universal. By understanding how permittivity and permeability control these components of wave propagation, applicable analogies can be used for other material interactions [3].

In most instances, applying coordinate transformations to engineered artificial elastic media is not possible. However, there is at least one special case where there is a direct equivalence between electromagnetics and elastodynamics. Furthermore, this case appears practically useful. In two dimensions, isotropic acoustic media and isotropic electromagnetic media are exactly equivalent. Under these conditions, the isotropic characteristic works in anisotropic media as well [3].

It has been demonstrated mathematically that the 2D Maxwell equations with normal incidence apply to 2D acoustic equations when replacing the electromagnetic parameters with the following acoustic parameters: pressure, vector fluid velocity, fluid mass density and the fluid bulk modulus. The compressional wave solutions used in the electromagnetic cloaking are transferred to material fluidic solutions where fluid motion is parallel to the wave vector. The computations then show that coordinate transformations can be applied to acoustic media when restricted to normal incidence in two dimensions [3].

Next, the electromagnetic cloaking shell is referenced as an exact equivalence for a simulated demonstration of the acoustic cloaking shell. Bulk modulus and mass density determine the spatial dimensions of the cloak, which can bend any incident wave around the centre of the shell. In a simulation with perfect conditions, because it is easier to demonstrate the principles involved, there is zero scattering in any direction.

11.4 Seismic Cloak Would Minimize Earthquake Damage

Seismic invisibility cloaks can shield vulnerable buildings from damaging earthquakes. A group of researchers in France under Guenneau [1] have been testing experimentally an early prototype of such seismic cloak. The concept could be extended to protect sensitive facilities such as nuclear power plants from earthquake damage by creating protective cloaks or barriers that divert earthquake energy away (Fig. 11.1).

Traditionally, earthquake engineering, a study of insulating the building from earthquake, is based on the dissipation and damping of energy when the building is hit by shock waves. Now with the arrival of seismic metamaterials in France, Sebastien Guenneau [1] and colleagues at the Institut Fresnel and the geoengineering company Ménard modify the condition and structure of the ground around the building to shield it from the seismic waves. This forms a seismic cloak for the building from the propagating earthquake. Preliminary tests on the effectiveness of seismic cloak are also carried out.

Their work is an example of the application of acoustic metamaterials, an extension of electromagnetic metamaterial. The concept of metamaterial was proposed by Victor Veselago in 1968. Experimentally, electromagnetic metamaterial was built in 2000 by David Smith of Duke University, USA. Subsequently, John Pendry et al. also developed coordinate transformations method known as transformation optics which forms the mathematical basis of cloaking.

11.4.1 Transformation Seismology

Coordinate transformations introduced from Einstein's theory of general relativity into electromagnetic waves enables the bending and the shielding of the object away from the electromagnetic wave, making the object invisible. Guenneau et al. [1] applied

Fig. 11.1 Putting the cloak to the test (after Stephane Brule of Menard)

transformation optics to seismology. Here, the propagation and the scattering of electromagnetic waves take place. In this chapter, sound waves or seismic waves and transformation acoustics are used instead. The interchange of the kinetic energy and the elastic energy contained in sound wave propagation and the potential energy stored in the deformation of the earth's crust takes place. The analogy between electromagnetic wave and sound wave is manifested as the soil mass density is equivalent to the electric permittivity and the elastic modulus is equivalent to the magnetic permeability. So transformation seismology is analogous to transformation optics.

The practical implementation of this theory in a seismic cloak workable for all types of destructive seismic waves is extremely difficult. Now, both the soil mass density and the elastic modulus of the surroundings will be controlled simultaneously. To satisfy the anisotropic nature requirement of the cloak, the elastic moduli have to be different in different directions. This is the same requirement as for the electromagnetic cloak. For the electromagnetic cloak, the solution is to fabricate a 2D cloak instead of a 3D cloak. For the seismic waves, the same method is applied to seismic cloak for earthquake shielding using the same principle that seismic wave is only propagating in 2D across the earth's surface.

The above hypothesis has been tested by Stéphane Brûlé et al. at Ménard. The following experiment was performed to test the effectiveness of the seismic cloak. A source vibrating at 50 Hz, the upper limit of the earthquake surface wave, was buried just below the surface of a sedimentary basin. Sensors were placed several metres away to record the earth's speed of vibration. Strong oscillations were recorded. Then, they bored holes at strategic positions with 5 m depth to modify the elastic modulus and mass density of the soil based on their calculations. Sensors were again placed on some regions on the other side of the bore holes, recorded less than 20% of the oscillation amplitude. This demonstrated that the seismic cloak in the form of the modified elastic modulus and mass density of the soil can shield off much of the seismic energy.

It is to be noted that the seismic cloak would require the similar space to the region being cloaked. Also, a potential weakness of the present cloak showed that the seismic waves not transmitted will be reflected. Hence, the next step should be to build a full cloak that will control the seismic wave propagation and will not damage neighbouring buildings.

11.5 A Practical Example of a Seismic Cloak

For the last fifteen years, cloaking technology has been an intensive area of research and development. The capability of hiding objects from incident waves has numerous practical applications. One of them is in the shielding of buildings from seismic wave possibility. The function of the seismic cloak which is surrounding the building and its foundation is to steer seismic wave around the building structures. Several groups have been involved in this work (Fig. 11.2).

One group, the collaboration of Sang-Hoon Kim of the Mokpo N Maritime University in South Korea and the Australian National University showed that the metamaterials can instead dissipate seismic energy by the conversion of the propagating waves into nonpropagating evanescent waves which will also die down exponentially in travelling. This is done by analysing and calculating the properties of the metamaterials and designing the unit cells which consist of repeating concrete cylinders of 18 m

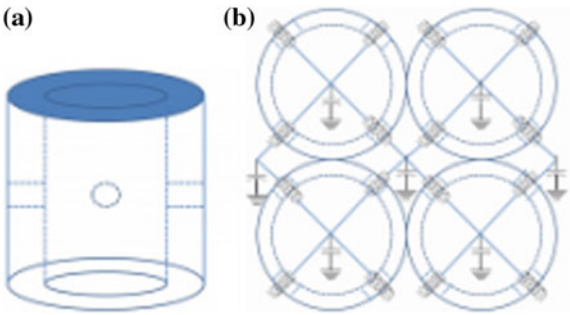

Fig. 11.2 A Seismic Cloak **a** A sample of a meta-cylinder with 4 side holes. The size of the cylinder is less than the wavelength of the surface waves. **b** A combined form of the 4 meta-cylinders. An electrical analogy is shown (after Kim and Das [4])

diameter with four perpendicular holes in its sides [Fig. 11.2]. The building will be surrounded by these cylindrical shells with varying size placed some 60 m across. This will absorb seismic energy over a range of wavelengths. This seismic cloak will be in the form of big structure which has to be constructed only around isolated buildings. Hence, this will not benefit the neighbouring buildings. The cost is high but not prohibitive. So the seismic cloak will be essential for structures of importance to society such as nuclear reactors, dams, power plants, airports and oil refineries.

There is still an outstanding issue of how to handle the seismic energy that is dissipated. It is necessary to have a convincing proof that the concrete seismic cloak can handle the tremendous seismic energy released and dissipated during big earthquakes.

11.6 Seismic Waveguide Made of Metamaterials

Kim and Das [4] have developed a new method of an earthquake-resistant design to support conventional seismic designs using acoustic metamaterials. They suggest a simple and practical method to reduce the amplitude of a seismic wave exponentially. Their device is an attenuator of a seismic wave. Constructing a cylindrical shell-type waveguide that creates a stopband for the seismic wave, they convert the wave into an evanescent wave for some frequency range without touching the building they want to protect.

11.6.1 Introductory Theory on Seismic Waves

As mentioned in above section, Kim and Das [4] have developed a new method of earthquake-resistant seismic metamaterial using acoustic metamaterials. Their device is equivalent to an attenuator of seismic wave. They construct a cylindrical shell-type waveguide that creates a stopband for the seismic wave. The seismic wave was converted into an evanescent wave for same frequency range without touching the building they will protect. Earthquake produces seismic waves. These seismic waves that possess large amplitudes and low frequencies cause great hazards to extensive life and property such as the collapse of dams, bridges and power plants. Hence, seismic capabilities are highly relevant to public safety, and huge amount of researches have gone into establishing practical analysis and design works for them. Several earthquake-proof engineering methods have been proposed, but still they are not so successful. Seismic waves are a kind of inhomogeneous acoustic wave with various long wavelengths. There are two types of seismic waves: body waves and surface waves. The body waves are the P (primary) and S (secondary) waves, and the surface waves are the R (Rayleigh) and L (love) waves. Surface waves travel slower than body waves, and their amplitudes decrease exponentially with the depth. It travels about 1–3 km/sec with various varieties

within the depth of a wavelength [2, 5]. The wavelengths are in the order of 100 m, and the frequencies are about 10–30 Hz. These frequencies are at the low end of the spectrum and are just below the audible frequency. During earthquake, the Rayleigh wave or surface wave decays slower than body waves and will be there for a long duration due to their very low frequencies or infrasonic frequencies. Also, they are of very high intensity and is a field of nonlinear acoustics. Hence, they are more destructive than body waves. This surface wave or Rayleigh wave can exist only in a homogeneous medium with boundaries and homogeneity. Rayleigh waves are transverse waves [2, 5]. The motion during earthquake observed at the ground surface is mainly Rayleigh waves or R waves. During earthquake, there is another type of waves known as L waves. They are polarized shear waves through the elastic layer. L waves have both transverse and longitudinal components. Most people feel the horizontal shifting of the earth during earthquake. This is due to the presence of the L waves.

However, the cloaked seismic waves are still destructive to the buildings behind the cloaked region. Recent development of acoustic metamaterials research opens a new direction to control the seismic waves. Sang-Hoon Kim et al. [4] proposed a different approach. Their solution is based on that metamaterial acts as an attenuate shifting or by using negative modulus and by converting the destructive seismic wave into evanescent wave using the imaginary velocity of stopband of the seismic waves.

There are several ways to represent the scale of the earthquake. The most common one is the Richter scale which is based on the amplitude of the seismic waves. It is defined as:

$$M = \log\left(A/A_0\right) \tag{11.1}$$

where A = maximum amplitude of the seismic wave and A_0 = maximum amplitude of the background vibration and order of μm. The seismic measuring equipment provides a transformed magnitude of the intensity. The strength of earthquake can be also measured in terms of the peak ground acceleration (PGA) which is expressed in closed form. Here, Sam Lee et al's. [4] work is based on the reduction of the amplitude of the seismic wave using seismic metamaterials.

11.6.2 Negative Modulus

The elasticity of the medium can produce acoustic waves. Elasticity is usually measured in terms of the elastic moduli which are: (1) Young's modulus, Y, which is one dimensional and is defined by

$$\mathrm{Y} = \frac{\Delta P l}{\Delta l}, \tag{11.2}$$

where ΔP = stress and l = the length. (2) shear modulus, G, is a two dimensional for a surface wave and is defined by

$$G = \frac{\Delta P}{\Delta x/h} \tag{11.3}$$

where Δx = horizontal shift and h = height of the object. (3) bulk modulus, or compressibility κ, which is three-dimensional one for body wave and is defined by

$$k = -\frac{\Delta P}{\frac{\Delta V}{V}}. \tag{11.4}$$

The earth crust as a seismic medium can be considered as an accumulation of infinite number of elastic plates. Although the seismic surface wave is not pure two-dimensional, its velocity is mainly dependent upon the density, ρ, and shear modulus, G, of the seismic medium.

Seismic wave is a form of acoustic wave and hence follows the acoustic field equation derived as follows. Assuming time dependence and propagation in the plane wave time dependence, e^{jwt} and propagation in a two-dimensional flat spacetime, one has first the Newton's second law:

$$\nabla_s p = i\omega\rho v \tag{11.5}$$

where p = acoustic pressure, v = particle velocity and ∇_s = Laplace operator at the surface.

and the continuity equation written as:

$$i\omega p = G\nabla_s \cdot v \tag{11.6}$$

where ∇s is the Laplacian operator at the surface, p is the pressure, ω is the angular frequency of the wave, and v is the velocity. Combining (11.5) and (11.6) yields the acoustic field equation:

$$\nabla_s^2 p + \frac{\omega^2}{v^2} p = 0 \tag{11.7}$$

where ω = angular frequency of the sound wave.

The particle velocity of the seismic wave is:

$$v = \sqrt{\frac{G}{p}} \tag{11.8}$$

The physics of the conversion of propagating seismic waves into dissipating evanescent waves is as follows. The seismic metamaterial will produce negative bulk modulus. This yields an imaginary velocity. The refractive index $n = \frac{v_0}{v} =$

$v_0\sqrt{\rho/G}$ where v_0 = background velocity also becomes imaginary and thus in turn produces a negative wave number k as $k = 2\pi n/\lambda$. The imaginary value of the wave vector makes the amplitude of the seismic wave decaying or dissipating, giving rise to the evanescent wave. This is known as the noise attenuator or noise barrier. The impedance $z = \rho v = \sqrt{\rho G}$ also becomes imaginary and absorptive.

Acoustic metamaterials with negative bulk modulus and negative mass density have been investigated and fabricated for other frequency range other than the infrasonic or seismic frequency range [6–8]. The key component used is the Helmholtz resonator. An array of Helmholtz resonators is used to produce negative bulk modulus. The resonance of the Helmholtz resonator gives rise to the negative bulk modulus at some specific frequency ranges. Within this frequency range, sound intensity decays exponentially and the propagating sound wave is converted into the evanescent wave.

In general, the elastic material is described by three independent elastic moduli components: G, B, and therefore, sometimes the G is replaced by a linear combination of G, B, and the Lamé constant [2, 5], but it will not change the structure of the theory. Acoustic waves from the modulus share fundamental properties of sound waves. From the formalism of electromagnetic response in metamaterials, effective electric permittivity and effective magnetic permeability show negative values at some specific frequency ranges around resonances [9]. The Helmholtz resonator is a realization of an electrical resonance circuit by mechanical correspondence. It is known as that the plasmon frequency in metals or in an array of metal wires produces the electric permittivity as [10]:

$$\varepsilon = \varepsilon_0\left[1 - \frac{\omega_p^2}{\omega(\omega + i\Gamma)}\right] \tag{11.9}$$

where ω_p is the plasma frequency and Γ is a loss by damping. With the analogy between electromagnetic wave and the acoustic wave, Eq. (11.2) is analogous to the Faraday's law and Eq. (11.3) is analogous to the Ampere's law. Also, the inverse of the elastic modulus in acoustic wave is analogous to the permittivity of the electromagnetic wave. With the structural loss, the effective shear modulus,

G_{eff}, is given similarly with the general form of the bulk modulus as [11–15]:

$$\frac{1}{G_{eff}} = \frac{1}{G}\left[1 - \frac{F\omega_0^2}{\omega^2 - \omega_0^2 + i\Gamma\omega}\right] \tag{11.10}$$

where ω_0 is the resonance frequency and F is a geometric factor [10, 16].

11.6.3 Seismic Attenuator

One can build an attenuator or an earthquake-proof barrier of a seismic wave by filling up many resonators under the ground around the building that we want to protect. Then, the amplitude of the seismic wave that passed the waveguide is reduced exponentially by the imaginary wave vector at the frequency ranges of negative modulus. Mixing up many different kinds of resonators will cover many different corresponding frequency ranges of the seismic waves. If one assumes that the plain seismic wave of wavelength λ propagates in x-direction, the amplitude of the wave reduces exponentially as:

$$Ae^{ikx} = Ae^{i2\pi nx/\lambda} = A\exp\left(-2\pi/n/x/\lambda\right) \tag{11.11}$$

Let the initial seismic wave, that is, before entering the waveguide, have amplitude A_i and magnitude M_i, and final seismic wave, that is after leaving the waveguide, have amplitude A_f and magnitude M_f, then following the Eqs. (11.1) and (11.11), one obtains:

$$A_f = A_i\exp\left(-2\pi/n/x/\lambda\right) \tag{11.12}$$

which shows the amplitude of the seismic wave reduces exponentially as passing through the waveguide of metamaterials.

One can rewrite Eq. (11.12) with the definition of the magnitude given in Eq. (11.1) as:

$$A_0 10^{M_i}\exp\left(-2\pi/n/x/\lambda\right) = A_0 10^{M_f} \tag{11.13}$$

Taking logarithms both sides of Eq. (11.13), one obtains the width of the waveguide, $x \to \Delta x$, as

$$\Delta x = \frac{\ln 10}{2\pi}\lambda\Delta M//n/ = 0.366\,\lambda\Delta M//n/ \tag{11.14}$$

where $\Delta M = M_i - M_f$.

For example, if the refractive index is $n = 2$ and the wavelength of the surface wave is $\lambda = 100$ m, one will need the waveguide of the width $\Delta x \simeq 18$ m to reduce $\Delta M = 1$. If the aseismic level of the building is $M = 5$ and the width of the waveguide surrounding the building is about 60 m, then the effective aseismic level of the building is increased to $M = 8$. Therefore, a high refractive index material is desirable for a narrow waveguide.

In civil engineering, earthquake proofing methods must be practical. That is easy to construct and clear to manufacture, and the resonator must be easy to build. Kim and Das [4] designed an example of a resonator shown in Fig. 11.2. The size of the cylinder can be estimated from the analogy between mechanical pipes and electric

circuits. Hence, a tube or a pipe with open ends corresponds to an inductor, and a closed end corresponds to a capacitor [16, 17].

$$L=\frac{\rho l'}{S}\ ,\ C=\frac{V}{\omega v^2} \tag{11.15}$$

where ρ = density inside the volume, l' = effective length, S = area of the cross-section, V = volume and v = velocity inside.

From Eq. (11.15), the resonant frequency is given as

$$\omega_0 \sim \frac{1}{\sqrt{LC}}=\sqrt{\frac{Sv}{l'v}} \tag{11.16}$$

In the meta-cylinder, l' is the effective length which is given by $l' \simeq l + 0.85d$ [17], where l = length of the hole or thickness of the cylinder, and d = diameter of the hole.

The shape of the meta-cylinder is neither necessary to be circular nor to have 4 holes. It could be any form of a concrete box with several side holes. Cubic or hexagonal boxes would be fine. Various kinds of resonators may cover various kinds of resonance frequencies of the seismic waves. An energy dissipation of the seismic waves will take place inside the waveguide, and the absorbed energy will turn into sound and heat. This makes the temperature of the waveguide increasing depending on the magnitude of energy that arrives at the waveguide.

Hence, a supportive method is proposed for aseismic design. It is not to add another aseismic system to a building but to construct an earthquake-proof barrier around the building to be protected. This barrier or attenuator is a seismic waveguide which reduces exponentially the amplitude of the dangerous seismic waves.

By controlling the width and refractive index of the waveguide, one can upgrade the aseismic range of the building as needed in order to defend it, at will, without touching it. This would be the big advantage of the waveguide or attenuator method. This method will be effective for isolated buildings because one needs some areas to construct the aseismic shell. This method will be applicable to sensitive buildings such as power plants, dams, airports, nuclear reactors, oil refining complexes, long-span bridges and express railroads.

References

1. Farhat, M., Guenneau, S., Enoch, S., Movchan, A.B.: Phys. Rev. B **79**, 033102 (2009)
2. Gioncu, V., and Mazzolani F.M.: Earthquake Engineering for Structural Design, p. 223. Spon, New York (2010)
3. Farhat, M., Guenneau, S., Enoch, S.: Phys. Rev. Lett. **103**, 024301 (2009)
4. Kim, S.H., and Das, M.P.: Seismic Waveguide Of Metamaterials, Mod. Phys. Lett. B **26**, 1250105, physics. (2012)

5. Villaverde, R.: Fundamental Concepts of Earthquake Engineering, Chaps. 4, 5. CRC, New York (2009)
6. Wu, Y., Lai, Y., Zhang, Z.Q.: Phys. Rev. B **76**, 205313 (2007)
7. Wu, Y., Lai, Y., Zhang, Z.Q.: Phys. Rev. Lett. **107**, 105506 (2011)
8. Zhou, X., Hu, Z.: Phys. Rev. B **79**, 195109 (2009)
9. Pendry, J.B., Holden, A.J., Robbins, D., Stewart, W.J.: J IEEE Trans. Microw. Theory tech. **47**, 2075 (1999)
10. Caloz, C., Itoch, T.: Electromagnetic Metamaterials, Chap. 1. Wiley, New York (2006)
11. Fang, N., Xi, X., Xu, J., Ambati, M., Srituravanich, W., Sun, C., Zhang, X.: Nature **5**, 452 (2006)
12. Cheng, Y., Xu, J.Y., Liu, X.J.: Appl. Phys. Lett. **92**, 051913 (2008)
13. Cheng, Y., Xu, J.Y., Liu, X.J.: Phys. Rev. B **77**, 045134 (2008)
14. Lee S.H., Park, C.M., Seo, Y.M., Wang, Z.G., and Kim, C.K.: J. Phys. Condensed Matter, **21,** 175704 (2009)
15. Lee, S.H., Park, C.M., Seo, Y.M., Wang, Z.G., Kim, C.K.: Phys. Rev. Lett. **104**, 054301 (2010)
16. Ding, C., Hao, L., Zhao, X.: J. Appl. Phys. **108**, 074911 (2010)
17. Beranek L.L.: Acoustics, Chaps. 3, 5. McGraw-Hill, New York (1954)

Chapter 12
Application of Acoustic Metamaterials to Finite Amplitude Sound Wave

Abstract First, the application of finite amplitude wave to acoustical cloaking is given. This is an extension of coordinate transformations from the linear acoustic field equation to nonlinear acoustic field equation which also shows form invariance. Then, metamaterial is applied to two examples of nonlinear acoustics. First to acoustic radiation force. Metamaterial enables a negative radiation force. Previous work on negative acoustic radiation force has the limitation only to Bessel beam. The second example is to apply to force of levitation. Metamaterial enables the control and manipulation of the force of levitation and allows for the levitation and suspension of larger objects.

12.1 Introduction

In 2007, Gan [1] introduced symmetry properties to acoustic fields. This has been confirmed by the successful fabrication of the acoustic metamaterials, various applications of time reversal acoustics [2], the scale invariance properties of the turbulence field which is basically acoustic field [3] and that the phonon is a Goldstone mode [4]. Acoustic metamaterials give rise to several novel applications such as negative refraction [5], acoustical cloaking [6], sound insulation [7], acoustic waveguides [8]. It would be of great interest to extend to the new field of the application of finite amplitude wave to acoustic metamaterials. In this paper, the Burgers equation is applied to acoustical cloaking. Also, acoustical metamaterial is applied to the acoustic radiation force (ARF) which has application in acoustical imaging and drug delivery and the force of levitation which are based on intense sound waves which are finite amplitude sound waves. The force of levitation is the outcome of the balance of the upward thrust of the ARF and the downward pull of the gravitational force. The metamaterial with a negative mass density will produce a repulsive gravity and also the ARF travelling in an opposite direction, that is, towards the sound source instead of travelling in the same direction of sound propagation as in conventional material. Since the repulsive gravity is related to general relativity, this will be the first application acoustical metamaterial to general relativity. The introduction of general relativity will bring nonlinear acoustics to the next level.

W.S. Gan, *New Acoustics Based on Metamaterials*, Engineering Materials,
https://doi.org/10.1007/978-981-10-6376-3_12

12.2 Acoustical Cloaking

Acoustical cloaking is the first introduction of acoustics to curvilinear space-time. Previously, all associations of acoustics with curvilinear space-time are only the use of curvilinear coordinates to describe the geometrical shape of certain structure of interest. They are not concerned with the propagation or bending of sound wave in curvilinear space-time. Acoustical cloaking is based on the form invariance or symmetry property of the acoustic equation of motion. The basic mathematics here is coordinate transformation which is also used in the derivation of the nonlinear field equations of general relativity. The Burgers equation will be used here:

$$\frac{\partial p}{\partial t} + p\nabla p = d\nabla^2 p \tag{12.1}$$

where p = acoustic pressure, d = diffusion coefficient or viscosity.

For simplification, the one-dimensional x-direction propagation is chosen with sinusoidal wave,

$p = i(\omega t - kx)$. Then,

$$j\omega p + p^2(-jk) = d(-k^2 p) \tag{12.2}$$

To start with, the acoustic pressure p must transform by considering p in a nonorthogonal coordinate system described by coordinates q_1, q_2, q_3 with unit vectors $\overrightarrow{u_1}, \overrightarrow{u_2}, \overrightarrow{u_3}$, respectively. Following Pendry et al. [6] and letting i = 1, 2, 3:

$$Q_i^2 = \left(\frac{\partial x}{\partial q_i}\right)^2 + \left(\frac{\partial y}{\partial q_i}\right)^2 + \left(\frac{\partial z}{\partial i}\right)^2 \tag{12.3}$$

The divergence theorem is applied to an infinitesimal volume in this nonorthogonal coordinate system. Deriving the net outward flux of p from this volume and setting it equal to the divergence of p times the infinitesimal volume, it can be shown that

$$\begin{aligned}(\nabla \cdot p)Q_1Q_2Q_3/\overrightarrow{u_1}\cdot\left(\overrightarrow{u_2}\times\overrightarrow{u_3}\right)/ = {} & \frac{\partial}{\partial q_1}\left[Q_2Q_3p\cdot\left(\overrightarrow{u_2}\times\overrightarrow{u_3}\right)\right] \\ & + \frac{\partial}{\partial q_2}\left[Q_1Q_3p\cdot\left(\overrightarrow{u_1}\times\overrightarrow{u_3}\right)\right] + \frac{\partial}{\partial q_3}\left[Q_1Q_2p\cdot\left(\overrightarrow{u_1}\times\overrightarrow{u_2}\right)\right]\end{aligned} \tag{12.4}$$

Let $V_{\text{frac}} = /\overrightarrow{u_1}\cdot\left(\overrightarrow{u_2}\times\overrightarrow{u_3}\right)$ because this is the fraction by which a unit volume is compressed by the coordinate nonorthogonality and the conventional superscript (subscript) notation for contravariant (covariant) vector components using

$$p \cdot \left(\overrightarrow{u_2} \times \overrightarrow{u_3}\right) = p^1 \overrightarrow{u_1} \cdot \left(\overrightarrow{u_2} \times \overrightarrow{u_3}\right) \tag{12.5}$$

Then, Eq. (12.4) can be rewritten as

$$(\nabla \cdot p) Q_1 Q_2 Q_3 V_{\text{frac}} = \frac{\partial}{\partial q_1}\left(Q_2 Q_3 V_{\text{frac}} p^1\right) + \frac{\partial}{\partial q_2}\left(Q_1 Q_3 V_{\text{frac}} p^2\right) + \frac{\partial}{\partial q_3}\left(Q_1 Q_2 V_{\text{frac}} p^3\right) \tag{12.6}$$

Noting that the divergence in the transformed coordinates is defined by $\nabla_q \cdot p = \frac{\partial p^1}{\partial q_1} + \frac{\partial p^2}{\partial q_2} + \frac{\partial p^3}{\partial q_3}$, then

$$\nabla_q \cdot \left(V_{\text{frac}} \overline{\overline{Q_{\text{per}}}}\right) \left[p^1 p^2 p^3\right]^{\text{T}} = \nabla_{q \cdot p} \tag{12.7}$$

where

$$\overline{\overline{Q_{\text{per}}}} = \begin{bmatrix} Q_2 Q_3 & 0 & 0 \\ 0 & Q_1 Q_3 & 0 \\ 0 & 0 & Q_1 Q_2 \end{bmatrix} \tag{12.8}$$

and the transformed acoustic pressure is given by

$$p = V_{\text{frac}} \overline{\overline{Q_{\text{per}}}} \left[p^1 p^2 p^3\right]^{\text{T}} \tag{12.9}$$

The "per" subscript on the tensor $\overline{\overline{Q_{\text{per}}}}$ is to denote that the diagonal elements transform each vector component by the product of the coordinate scaling factors perpendicular (more general, not parallel, for the case of nonorthogonal coordinates) to the direction of the vector component.

The p in (12.9) is same as the p given by (12.1).

12.3 Acoustic Radiation Force

The concept of acoustical tweezers was introduced by Wu [9] and this triggers off an increasing interest on ARF. Acoustic tweezers are under the field of acoustophoresis.

In acoustophoresis, ARF is used in the contactless manipulation, separation and trapping of small particles and cells [10]. Two-dimensional tweezers have been achieved in lab-on-a-chip devices [11] and by using circular phase arrays [12].

Over the last century, single-beam acoustical tweezer has also been developed using a tightly focused beam [13]. Force exerted by a plane or a spherical wave on a suspended sphere in a nonviscous fluid has been extensively investigated over the last century [14–20], based on the partial-wave expansion of the incident and the scattered waves and the axial radiation force exerted on a sphere by a planar piston beam [21, 22], a spherically focused beam [23], Bessel beams [24], [25–27], and a

Gaussian [28] beam. In all these studies, the sphere is located on the axis of the beam, and for focused beams, the analysis was restricted to the sphere placed in the focus point.

The design of a single-beam acoustical tweezers will require an analysis of how the radiation force on the sphere behaves in the vicinity of the transducer's focus point. So far, this analysis has been done only for $ka \gg 1$, the geometric scattering region [29] where k = incident wave number and a = sphere's radius. For other regimes such as Rayleigh scattering ($ka \ll 1$) and resonant scattering ($ka \sim 1$), the ARF can be computed using the partial-wave expansion method [30]. Here, the radiation force exerted on a suspended sphere is expressed in terms of the beam-shape and the scattering coefficients [31]. Each beam-shape coefficient (BSC) is the complex amplitude of an incident partial-wave, while the scattering coefficients are obtained from the acoustic boundary conditions across the sphere's surface. The scattering coefficient is related to the mechanical properties of the scatterer, while the BSCs carry information on the geometry of the incident beam.

The radiation force produced by a spherically focused transducer on a sphere arbitrarily located in the host medium can be obtained by calculating the BSC with respect to the particle's position. There are several numerical schemes to compute the BSC include the mid-point integral rule [31, 32] and the discrete spherical harmonics transform (DSHT) [33, 34], which is based on the discrete Fourier transform and several other quadrature methods to compute BSCs in the context of optical computing [35]. Both the mid-point integral rule and DSHT method require that the incident pressure amplitude should be sampled over a virtual sphere which encloses the beam propagation region, containing the spherical target. For highly oscillating functions, the mid-point integral rule requires a large number of sampling points to ensure proper converge of the BSC computation while the DSHT method renders more accurate results with less sampling points, it may develop numerical errors related to aliasing due to undersampling and spectral leakage caused by function domain truncation.

In order to circumvent numerical approximations for the calculation of ARF, an exact method is proposed here based on the partial-wave expansion method [30, 34] and the translational addition theorem [36]. A similar method has been used to exactly calculate the radiation pressure generated by the electromagnetic wave [37]. The proposed method is used to calculate the radiation force produced by a spherically focused transducer on a silicone-oil droplet. The incident beam is generated by a biomedical focused transducer with a driving frequency of 3.1 MHz, and an F-number of 1.6ARF is computed along the beam's axis and on the transducer's focal plane using closed expression of the BCS with respect to the beam focal point [38]. Both resonant and Rayleigh scattering regimes are considered. The results obtained from the Rayleigh regime are compared with those from Gorkov's theory [18]. A significant deviation is noted in the axial radiation force when ultrasound absorption inside the droplet is taken into account. In addition, transverse trapping is obtained in both the Rayleigh and the resonant scattering regimes. However, simultaneous axial and transverse trapping occurs only for droplets in the Rayleigh scattering regime.

The following is a specific application with an example of the procedure for the derivation of the ARF on a sphere.

Consider an acoustic beam of arbitrary wavefront with angular frequency ω and propagating in an inviscid infinite fluid. The fluid has ambient density ρ_0 and speed of sound c_0. The acoustic beam is described by the excess of pressure p as a function of the position vector r, with respect to a defined coordinate system. The time-dependence e^{-iwt} is suppressed for the sake of simplicity. A spherical scatterer with radius a, density ρ_1 and speed of sound c_1 is placed in the ultrasound beam path.

A spherically focused transducer with diameter $2b$ and curvature radius z_0 is used to produce a focused beam. The origin of the coordinate system O is set at the transducer's focus. When the centre of the sphere coincides with O, the scattering of the incident beam is referred to as the on-focus scattering configuration [38].

In this on-focus scattering formalism, the normalized amplitude of the incident pressure beam can be described in spherical coordinates $\mathbf{r} = re_r\,(\theta, \phi)$, where e_r is the radial unit-vector, θ and ϕ are the polar and the azimuthal angles, respectively.

The incident pressure partial-wave expansion is given by [38]:

$$p_i = \sum_{n,m} a_n^m j_n(kr) Y_n^m(\ominus, \Phi) \tag{12.10}$$

where $k = \omega/c_0$, j_n = nth-order spherical Bessel function and Y_n^m = spherical harmonic function of nth-order and mth-degree. Here, the amplitude is normalized to the pressure magnitude p_0.

ARF is produced when acoustic waves illuminate on objects and is the result of momentum exchange between the object and the incident field. In most cases, ARFs are positive as acoustic waves usually push objects towards the propagating direction. Negative ARFs occur when acoustic waves pull the objects continuously towards the wave source direction. Negative ARFs have more applications than positive ARFs such as in particle manipulation and in acoustic levitation. ARF has applications in acoustical imaging [39] and biomedical applications in microfluids [40] and in the force of levitation [41] The ARF is due to intense sound and so the finite amplitude wave has to be used.

The ARF on a general object in an ideal fluid is:

$$F_i = \int_{SR} \left[-\frac{\rho v^2}{2} + \frac{\rho}{2c^2}\frac{\partial \phi^2}{\partial t} + \rho\left(v_i v_j\right) \right] \mathrm{d}S_j \tag{12.11}$$

where ρ = mass density, v = particle velocity, c = sound velocity and ϕ = scalar potential.

This will give an upward acoustic pressure on the object. If the object is made of acoustic metamaterial of negative mass density, the ARF will be negative. The

thrust on the object will be in opposite in direction. That is will be downward instead. Also, negative radiation force has been observed by Marston [42] but it is restricted only to Bessel beams.

12.4 Application of Acoustical Metamaterials to Force of Levitation [41] in the Presence of General Relativity and Gravitational Force

Levitation is a process demonstrated by Einstein's theory of general relativity and the effect of gravitational force. It happens when the upward thrust of the ARF balances the downward gravitational pull. Levitation can be realized by various physical means, such as ARF, aerodynamic force, electrostatic force, and magnetic force. Acoustic levitation enables the suspension of an object in air or in fluid. In this chapter, only one-dimensional levitation methods utilizing high-intensive ultrasonic sound waves will be discussed. An acoustic wave can exert an ARF force on objects immersed in the wave field. These forces are normally weak, but they can become quite substantial when high-intensity sound wave is used due to the nonlinear characteristics. These ARFs can become large enough to levitate substances against gravitational force. This technique is known as acoustic levitation or ultrasonic levitation, and the sound waves used are in the ultrasonic frequency range (higher than 20 kHz).

The recent successful detection of gravitational wave enhances the status of general relativity. Here, general relativity will be applied to nonlinear acoustics. This will bring nonlinear acoustics to the next level. An obvious application will be to the force of levitation [41]. Acoustic levitation enables the suspension of an object in the air or in the fluid. This will occur when the upward thrust of the acoustic pressure on the object is equal to the downward force of gravity. To understand acoustic levitation, both nonlinear acoustics and general relativity have to be used. This will introduce general relativity into nonlinear acoustics and show the role and the effect played by general relativity in nonlinear acoustics.

This will be the second application of sound propagation in curvilinear space-time. The first application is acoustical cloaking.

The presence of a negative mass density will produce a negative ARF. Marston [42] produced a negative ARF using Bessel beams. The advantage of using acoustic metamaterial for producing negative ARF is without the restriction to Bessel beams. In addition, negative mass density will produce a negative mass which in turn will produce a negative force of gravity or a repulsive force of gravity. This will enable the use of acoustic metamaterials on space flight.

12.4.1 Modelling of the Proposed Levitation System [41]

Zhao et al. [41] proposed an acoustic levitation system to levitate a relatively large object (a few times of the sound wavelength in air) of disc shaped. A circular plate vibrating in its flexural vibration mode is chosen as the sound radiator to obtain a large sound radiation surface. The sound field can be simplified and described as follows: the circular disc vibrates in its flexural vibration mode and generates the sound, and radiator (a circular disc) vibrates in its flexural vibration mode and generates a sound beam in front. The sound beam propagates forward and is reflected by a rigid surface, the object to be levitated, placed perpendicular to the sound beam at a distance of L away from the radiator. An acoustic wave field resulted from multiple reflections is formed between two surfaces. The acoustic field becomes a standing wave when L is equal to multiple times of half wavelength of sound. Excessive pressure on the rigid surface is generated by the acoustic field.

In the Zhao et al. [41] system, a piezoelectric Langevin type transducer driven in its first longitudinal mode ($\lambda/2$) at 20 kHz is used to generate ultrasonic vibrations. A stepped horn ($\lambda/2$) is attached to magnify the vibration amplitude of the transducer. An aluminium plate of diameter 120 mm is used as sound radiator. The plate is screwed into the horn. To match one of the plate's asymmetric flexural modes of vibration, the axial resonant frequency of horn and transducer, the plates thickness is chosen so that the corresponding natural frequency of the free vibrating plate appears at 20 kHz. By properly matching the thickness, flexural modes of vibration with one, two and three nodal circles have been constructed. A plate with two modals has been formed experimentally, a good compromise between mechanical strength and achievable vibration amplitude. After assembly, the resonant frequency of the entire system (transducer, horn and plate) appears at about 19 kHz. It is slightly depending on the input power. The resonant frequency of the system can be tracked during operation by using an Adaptive Phase Locked Loop control algorithm (APLL) is used.

An experimental set-up is used to measure the acoustic levitation force produced by the disc levitation system. A schematic diagram of the experimental set-up is shown in Fig. 12.1. An aluminium plate with the same diameter as the radiation plate is positioned in opposite to the radiator. This sound-reflecting plate is mounted on a vertical linear stage through a load cell for being able to measure the vertical force acting on the reflector directly. Using the linear stage, the reflector will be positioned freely between the contact position and a distance of about 40 mm above the radiator. A laser interferometer is installed to measure the exact vertical position of the reflector.

A common compact disc (CD) is chosen as the object to be levitated. It has the same diameter as the vibrating plate, with a thickness of 1.3 mm and a mass of 16 g. A stable levitation state is observed when the input power reaches about 30 W The CD then rests without any instable vertical motion above the flexural plate. The maximum vibration amplitude of the excitation system occurs at the centre of the flexural plate and is about 25 μm at 19 kHz for this level of power. This is

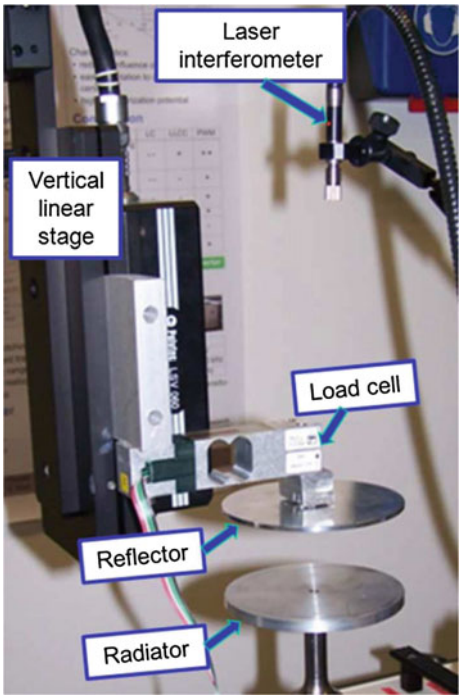

Fig. 12.1 Experiment set-up for measuring the ARF (Zhao and Wallaschek [41])

measured by the laser vibrometer. It is noted that the CD in this experiment is at a position slightly higher than half a wavelength above the peak of the levitation force, where the acoustic levitation force equals the gravitational force of the CD. This is different from the common radiator-reflector-type systems, in which small particles are levitated at positions slightly below the pressure nodes of the standing wave. Stable levitation could not be achieved at one wavelength or higher positions with the proposed experimental set-up due to the quickly dropped levitation force.

12.4.2 Computation of the Acoustic Levitation Force

The cylindrical coordinates (r, Θ, z) is used here to describe the sound radiator which is a circular plate with constant thickness, where r = radius from the centre of the sound radiator, θ = angle of that radius and z = length in the direction normal to the plane of the radiator.

The formulation is that of the transverse vibration of a circular plate: one has the following general solution for the plate equation:

$$Z(r,\Theta,t) = \left[a_{ij}J_i\left(\frac{\lambda_{ij}r}{\alpha}\right) + b_{ij}I_i\left(\frac{\lambda_{ij}r}{\alpha}\right)\right]\cos i\theta\ \cos 2\pi t \tag{12.12}$$

where $Z(r, \theta)$ = the displacement of the mid-surface of the plate, a = radius of the circular plate, f = natural frequency of the related mode shape, i, j = the number of nodal diameters and nodal circles, not counting the boundary, respectively. J_i and I_i = Bessel function and modified Bessel function of the first kind relatively, and i order. a_{ij} and b_{ij} = constants which are determined to within an arbitrary constant by the boundary conditions and mode number. λ_{ij} = dimensionless frequency parameter related to the boundary conditions on the plate, the plate geometry and Poisson's ratio.

Zhao et al. [41] have derived the Rayleigh radiation pressure from the vibrating circular plate as:

$$p_{ra} = Z(r)^2\frac{v_0^2}{4(\sin h^2\alpha' L + \sin^2 kL)}\rho_0 \tag{12.13}$$

where V_0 = surface vibration amplitude, ρ_0 = ambient density, L = distance between object to be levitated and the radiator and α' = increased absorption coefficient of finite amplitude wave.

Zhao et al. [41] have been able to levitate a compact disc of radius of 6 cm to a height of 2 cm or around half the sound wavelength. The levitated object is shown in Fig. 12.2.

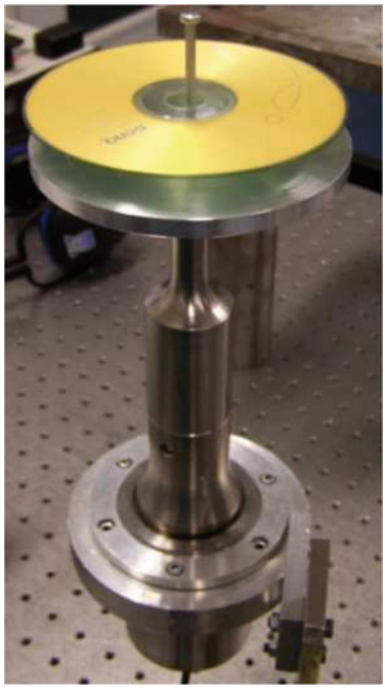

Fig. 12.2 Stable levitation of CD at half wavelength ($\lambda/2$) above the radiator. The central pin (screwed into the flexural plate) is used only for centring the plate in radial direction (Zhao and Wallaschek [41])

The effect of negative mass density of acoustical metamaterial will modify the balancing condition of the force of levitation. This will enable the control and manipulation of the force of levitation and enable the levitation or suspension of larger object. Negative ARF will travel in a direction towards the sound source instead of in the same direction of sound propagation as in conventional material. Also, negative mass density will produce repulsive gravity. A new balanced condition can be evaluated based on the use of acoustic metamaterials. This will enable the levitation of heavier objects. Also, this will open the door of the application of acoustic metamaterials on space flight. This will be the first application of acoustic metamaterial to general relativity.

12.5 Conclusions

Extension of metamaterials to nonlinear acoustics will enable novel applications in acoustical cloaking, acoustical radiation force and to levitation of a heavier object. The introduction of metamaterial to general relativity with the concept of repulsive gravity will enable the use of acoustic metamaterials on space flight. Acoustic force of levitation taking account of gravitational force and general relativity is the second application of sound propagation in curvilinear space-time after acoustical cloaking.

References

1. Gan, W.S.: Gauge invariance approach to acoustic fields. In: Akiyama, I. (ed.) Acoustical Imaging, vol. 29, pp. 389–394. Springer, Berlin (2007)
2. Fink, M.: Time reversal of ultrasonic fields—Part I. Basic principles. IEEE Trans. Ultrasons. Ferroelectr. Freq. Control **39**(5), 1–12 (2006)
3. Kolmogorov, A.N.: The local structure of turbulence in incompressible viscous fluids for very large Reynolds numbers. Proc. USSR Acad. Sci. **30**, 299–303 (1941)
4. Goldstone, J.: Field theories with superconductor solutions. Nuoco Cimento **19**, 154–164 (1961)
5. Veselago, V.G.: The electrodynamics of substance with simultaneous negative values of ε and μ. Sov. Phys. Uspekhi **10**(4), 509–514 (1968)
6. Pendry, J.B., Schurig, D., Smith, D.R.: Controlling electromagnetic field. Science **312**, 1780–1782 (2006)
7. Goffaux, C., Maseri, F., Vasseur, J.O., Djafari-Rouhani, B., Lambin, Ph: Measurements and calculation of the sound attenuation by a phononic band gap structure suitable for an insulation partition application. Appl. Phys. Lett. **83**, 281 (2003)
8. Gan, W.S.: Acoustical Imaging: Techniques and Applications for Engineers, Wiley, USA, pp. 397–398 (2012)
9. Wu, J.: Acoustical tweezers. J. Acoust. Soc. Am. **89**, 2140–2143 (1991)
10. Lenshof, A., Magnusson, C., Laurell, T.: Acoustofluidics 8: applications of acoustophoresis in continuous flow microsystems. Lab Chip **12**, 1210–1223 (2012)

11. Shi, J.,. Ahmed, D., Mao, X., Lin, S., Lawit, A., Huang, T.: Acoustic tweezers: patterning cells and microparticles using standing surface acoustic waves (SSAW). Lab Chip **9**, 2890–2895 (2009)
12. Courtney, C.R.P., Ong, C.K., Drinkwater, B.W., Wilcox, P.D.: Manipulation of microparticles using phase controllable ultrasonic standing waves (EL). J. Acoust. Soc. Am. **128**, 195–199 (2010)
13. Lee, J., Teh, S., Lee, A., Kim, H., Lee, C., Shung, K.: Single beam acoustic trapping. Appl. Phys. Lett. **95**, 073701 (2009)
14. King, L.V.: On the acoustic radiation pressure on spheres. Proc. R. Soc. A. **147**(861), 212–240 (1934)
15. EmbletonT, F.W.: Mean force on a sphere in a spherical sound field. I. (Theoretical). J. Acoust. Soc. Am. **26**, 40–45 (1954)
16. Yosioka, K., Kawasima, Y.: Acoustic radiation pressure on a compressible sphere. Acustica **5**, 167–173 (1955)
17. Westervelt, P.J.: Acoustic radiation pressure. J. Acoust. Soc. Am. **29**, 26–29 (1957)
18. Gorkov, L.P.: On the forces acting on a small particle in an acoustic field in an ideal fluid. Sov. Phys. Dokl. **6**, 773–775 (1962)
19. Nyborg, W.L.: Radiation pressure on a small rigid sphere. J. Acoust. Soc. Am. **42**, 947–952 (1967)
20. Hasegawa, T., Yosioka, K.: Acoustic-radiation force on a solid elastic sphere. J. Acoust. Soc. Am. **46**, 1139–1143 (1969)
21. Hasegawa, T., Kido, T., Takeda, S., Inoue, N., Matsuzawa, K.: Acoustic radiation force on a rigid sphere in the near field of a circular piston vibrator. J. Acoust. Soc. Am. **88**(3), 1578–1583 (1990)
22. Mitri, F.G.: Near-field single tractor-beam acoustical tweezers. Appl. Phys. Lett. **103**(11), 114102 (2013)
23. Chen, X., Apfe, R.: Radiation force on a spherical object in an axisymmetric wave field and its application to the calibration of high-frequency transducers. J. Acoust. Soc. Am. **99**, 713–724 (1996)
24. Marston, P.L.: Axial radiation force of a Bessel beam on a sphere and direction reversal of the force. J. Acoust. Soc. Am. **120**, 3518–3524 (2006)
25. Mitri, F.G.: Acoustic scattering of a high-order Bessel beam by an elastic sphere. Ann. Phys. **323**, 2840–2850 (2008)
26. Mitri, F.G.: Langevin acoustic radiation force of a high-order Bessel beam on a rigid sphere. IEEE Trans. Ultrason. Ferroelectr. Freq. Control **56**, 1059–1064 (2009)
27. Azarpeyvand, M.: Acoustic radiation force of a Bessel beam on a porous sphere. J. Acoust. Soc. Am. **131**, 4337–4348 (2012)
28. Zhang, X., Zhang, G.: Acoustic radiation force of a Gaussian beam incident on spherical particles in water. Ultras. Med. Biol. **38**, 2007–2017 (2012)
29. Lee, J., Shung, K.K.: Radiation forces exerted on arbitrarily located sphere by acoustic tweezer. J. Acoust. Soc. Am. **120**, 1084–1094 (2006)
30. Silva, G.T.: An expression for the radiation force exerted by an acoustic beam with arbitrary wavefront. J. Acoust. Soc. Am. **130**, 3541–3545 (2011)
31. Silva, G.T.: Off-axis scattering of an ultrasound Bessel beam by a sphere. IEEE Trans. Ultrason. Ferroelectr. Freq. Control **58**, 298–304 (2011)
32. Mitri, F.G., Silva, G.T.: Off-axial acoustic scattering of a high-order Bessel vortex beam by a rigid sphere. Wave Motion **48**, 392–400 (2011)
33. Silva, G.T., Lobo, T.P., Mitri, F.G.: Radiation torque produced by an arbitrary acoustic wave. Europhys. Phys. Lett. **97**, 54003 (2012)
34. Silva, G.T., Lopes, J.H., Mitri, F.G.: Off-axial acoustic radiation force of repulsor and tractor Bessel beams on a sphere. IEEE Trans. Ultras. Ferroel. Freq. Control **60**, 1207–1212 (2012)
35. Gouesbet, G., Letellier, C., Ren, K.F., Gréhan, G.: Discussion of two quadrature methods of evaluating beam-shape coefficients in generalized Lorenz-Mie theory. Appl. Opt. **35**, 1537–1542 (1996)

36. Martin, P.A.: Multiple Scattering Interaction of Time-Harmonic Waves with N Obstacles, Chap. 3. Cambridge University Press, Cambridge, UK (2006)
37. Moine, O., Stout, B.: Optical force calculations in arbitrary beams by use of the vector addition theorem. J. Opt. Soc. Am. B **22**, 1620–1631 (2005)
38. Edwards, P.L., Jarzynski, J.: Scattering of focused ultrasound by spherical microparticles. J. Acoust. Soc. Am. **74**, 1006–1012 (1983)
39. Williams, E.G.: Fourier Acoustics: Sound Radiation and Nearfield Acoustical Holography, Chap. 6. Academic Press Inc., San Diego, CA (1999)
40. Magnusson, A., Laurell, T.: Acoustofluidics 8: Applications of acoustophoresis in continuous flow microsystems. Lab Chip **12**, 1210–1223 (2012)
41. Zhao, S., Wallaschek, J.: A standing wave acoustic levitation system for large planar objects. Arch. Appl. Mech. **81**(2), 123–139 (2014)
42. Marston, P.L.: Axial radiation force of a Bessel beam on a sphere and direction reversal of the force. J. Acoust. Soc. Am. **120**, 3518–3524 (2006)

Chapter 13
Acoustical Imaging on a Curvilinear Spacetime

Abstract First is the introduction to the subject. Then, there are the usual applications to the theory of general relativity. Two examples of applications to acoustical imaging are given: vibrography and elasticity imaging.

13.1 Introduction

So far, all the theories and equations for acoustical imaging are based on a flat spacetime or Minkowski spacetime. The transpose to a curvilinear spacetime [1] will enable a nonlinear treatment and more accurate calculation of the energy and momentum besides the add-on of the gravitational force term. This is because the curvature of the spacetime is very sensitive to a slight change in the energy and momentum of the system. This will enable the more accurate calculation of the acoustic intensity used in the formation of acoustical images and also provide more information. Since high frequencies acoustical imaging is a branch, it is necessary to consider the curvilinear spacetime platform. As an illustration, two acoustical imaging modalities, vibrography and elasticity imaging, are analysed. Einstein, in his original paper on the theory of general relativity [1], specially singled out hydrodynamics as a field of fundamental physics for extension to the curvilinear spacetime. Acoustics is related to hydrodynamics and fluid dynamics, hence is of particular relevance here. This will enable more accurate and correct calculation of the acoustic radiation force (ARF) and stress energy and enable better image resolution. Vibrography and elasticity imaging are not only frequencies dependent based on the classical Rayleigh image resolution criterion but also on the precise calculation of the energy and momentum of the system which includes the gravitational force.

W.S. Gan, *New Acoustics Based on Metamaterials*, Engineering Materials,
https://doi.org/10.1007/978-981-10-6376-3_13

13.2 The Usual Applications of the Theory of General Relativity

So far, the applications of the theory of general relativity are to astrophysics and cosmology and to plasma physics related to cosmology and to fission. These are areas related either to the large mass size or to intense energy where nonlinear aspects of physics are concerned. It is to be noted that in nonlinear acoustics when finite amplitude sound wave or intense sound field is involved with, the relativistic treatment is necessary. It will be reduced to the linearized, nonrelativistic treatment when the sound field is weak. An example where relativistic treatment is particularly relevant is the calculation of the ARF which is intense sound field. A further support of this argument is the force of levitation. The acoustic levitation occurs when the ARF balances the gravitational force. This shows the relevance of the theory of general relativity which is used to calculate the gravitational force.

Another area in nonlinear acoustics which will need relativistic treatment is sonoluminescence or sonofusion. This is the release of tremendous heat energy when the bubble breaks up analogous to the release of tremendous heat energy when the atoms break up. The relativistic treatment of the elastic energy exerted by the skin of the bubble before it collapses will enable a more accurate determination of the heat energy released. In the following sections, two examples of acoustical imaging related to the curvilinear spacetime treatment are given.

13.3 Vibrography

The principle of vibrography is a form of acoustical imaging based on the ARF. The derivation of ARF is from the Navier–Stokes equation of fluid dynamics. To enable the curvilinear spacetime and a relativistic formulation of the ARF, one will start with the procedure of the derivation of the ARF from the Navier–Stokes equation. The theory of the ARF relies on a perturbation expansion of the acoustics fields in the fluid. The main results of the perturbation theory are summarized here. The ultrasound perturbations on a quiescent fluid are considered to first and second order in density ρ, pressure p and velocity u (1st denotes first order and 2nd denotes second order):

$$\rho = \rho_0 + \rho_1 + \rho_2 \tag{13.1}$$

$$p = p_0 + c_0^2 \rho_{1\text{st}} + p_{2\text{nd}} \tag{13.2}$$

$$u = u_{1\text{st}} + u_{2\text{nd}} \tag{13.3}$$

where c_0 = speed of sound in the fluid, and $p_{1st} = c_0^2 \rho_{1st}$. Neglecting viscosity in the bulk fluid, the first-order Navier–Stokes equations are:

$$\partial_t \rho_{1st} = -\rho_0 \nabla . u_{1st} \tag{13.4a}$$

which is the continuity equation

$$\rho_0 \partial_t u_{1st} = -c_0^2 \nabla \rho_{1st} \tag{13.4b}$$

One assumes time-harmonic fields,

$$\rho_{1st} = \rho_{1st}(\vec{r}) e^{-i\omega t} \tag{13.5a}$$

$$p_{1st} = p_{1st}(\vec{r}) e^{-i\omega t} \tag{13.5b}$$

$$u_{1st} = u_{1st}(\vec{r}) e^{-i\omega t} \tag{13.5c}$$

and introduces the velocity potential ϕ_{1st},

$$u_{1st}(\vec{r}) = \nabla \phi_1(\vec{r}) \tag{13.6a}$$

$$p_{1st}(\vec{r}) = \mathrm{i}\rho_0(\omega)\phi_1(\vec{r}) \tag{13.6b}$$

$$\rho_{1st}(\vec{r}) = \mathrm{i}\rho_0(\omega/c_0^2)\phi_1(\vec{r}) \tag{13.6c}$$

The velocity potential fulfils the Helmholtz wave equation:

$$\nabla^2 \phi_{1st} = \frac{1}{c_0^2} \partial_t^2 \phi_1 = -\frac{\omega^2}{c_0^2} \phi_1 \tag{13.7}$$

which forms the starting point for the scattering theory to calculate the ARF acting on the particle.

As an illustration, one will take the case of the ARF for the case of an oscillating sphere. The ARF can be calculated as the surface integral of the averaged second-order pressure and the momentum flux tensor at a fixed surface just outside the oscillating sphere. Using the first-order Navier–Stokes equation and the first-order Helmholtz wave equation, the ARF can be derived as:

$$U_{rad} = \int \mathrm{d}a \{ \langle p_{2nd} \rangle \vec{n} + \rho_0 \langle (\vec{n}.\overrightarrow{u_{1st}}\overrightarrow{u_{1st}}) \rangle \} \tag{13.8}$$

where a = diameter of sphere $\ll \lambda$ = sound wavelength, p_{2nd} = second-order acoustic pressure, ρ_0 = density of sphere, and u_{1st} = 1st order particle velocity = $\nabla \phi_{1st}$, where ϕ_{1st} = 1st order acoustic potential, and $\phi_{1st} = \phi_{in} + \phi_{scat}$ where ϕ_{in} = velocity potential of incident sound field, and ϕ_{scat} = velocity potential of scattered sound field, and

$$\langle p_{2\text{nd}} \rangle = \frac{1}{2}\kappa_0 \langle p_{1\text{st}}^2 \rangle - \frac{1}{2}\rho_0 \langle u_{1\text{st}}^2 \rangle$$

For the curvilinear spacetime, the momentum equation and the continuity equation are as follows:

$$(e+p)\frac{\mathrm{D}u}{\mathrm{D}\tau} = -\nabla p - u\frac{\mathrm{D}p}{\mathrm{D}\tau} \quad \text{(momentum equation)} \tag{13.9}$$

$$u^\mu \nabla_\mu e = -(e+p)\nabla_\mu u_\mu \quad \text{(continuity equation)} \tag{13.10}$$

Solving (13.9) and (13.10), one will be able to obtain p and u. Substitution in (13.8) will provide the ARF.

It is also of interest to study the difference between Eq. (13.10), the continuity equation for the curvilinear spacetime, and the Eq. (13.4a), the continuity equation for the flat spacetime.

For flat spacetime, the momentum equation is given by:

$$\frac{\mathrm{D}u_j}{\mathrm{D}t} = \frac{\partial T_{ij}}{\partial x_j} - \rho g_j \tag{13.11}$$

13.4 Elasticity Imaging

Elasticity imaging is another modality of acoustical imaging where stress tensor and strain tensor are involved. Usually, the Hooke's law gives a linear relationship between the stress tensor and the strain tensor. The weakness of this law is that it fails for intense stress. A common approach for the extension to nonlinear elasticity is to start with the linear first-order Hooke's law and extend to include second-order, third-order and higher-order elastic constants. Our treatment of using the theory of general relativity is that it starts with the nonlinear strong field case and reduces to the linear weak field as an approximation. This will be more accurate method and includes all the necessary information.

For the curvilinear spacetime, the stress tensor can be given as:

$$T_{\mu\nu} = (e+p)u_\mu u_\nu + p g_{\mu\nu} \tag{13.12}$$

where e = total energy density and $g_{\mu\nu}$ = metric.

For weak field limit, or the flat spacetime limit, $u_i \ll 1$, $e \gg p$, $e \sim \rho$, and $g_{\mu\nu} = 1$, and (13.12) reduces to

$$T_{\mu\nu} = \rho u_\mu u_\nu + p \tag{3.13}$$

where ρ = rest frame mass energy density.

Reference

1. Einstein, A: The foundation of the general theory of relativity. Ann. Phys. **354**(7), 769 (1916)

Chapter 14
Transport Theory is Key Foundation of Theoretical Metamaterials Design—Metamaterial is Artificial Phase Transition

Abstract An introduction to transport theory and transport properties followed by the discovery that metamaterial is in fact artificial phase transition. Singularity behaviour of the transport properties at the critical point of phase transition is given. Then, there is the use of the transport properties to explore new forms of metamaterials. Metamaterials as artificial phase transition is a breakthrough to a new world of artificial materials.

14.1 Transport Theory, Transport Properties and Discovery of Metamaterial is in Fact Artificial Phase Transition

Recently, Gan discovered that metamaterial is in fact an artificial phase transition. In this chapter, it will illustrate that the double negativity of permeability and permittivity of electromagnetic metamaterial and the double negativity of effective bulk modulus and effective mass density of acoustic metamaterial are in fact, artificial phase transition from positive phase material to negative phase material. The transport properties here are as follows: permeability, permittivity, effective bulk modulus and effective mass density. Phase transition enables a breakthrough to a world of new materials. The Nobel physics award in 2016 to topological phase transition enhanced the status of phase transition. Transport theory will play the role of key foundation of theoretical materials design. Transport theory describes transport phenomena which in turn are governed by transport properties. Transport properties are key constituents of phase transition. Examples of transport properties are as follows: binary diffusion coefficients, electrical conductivity, diffusion coefficients, thermal conductivity, thermal diffusion coefficients, viscosity, permeability, porosity, dipole moment, polarizability of molecules, rotational relaxation time and Lenaerd-Jones well depth, etc.

In 1966, Gan coined the term transport theory during his Ph.D. work at the physics department of Imperial College London. His Ph.D. thesis, Transport Theory in Magnetoacoustics [1] (1969, Imperial College London), is the first to introduce

W.S. Gan, *New Acoustics Based on Metamaterials*, Engineering Materials,
https://doi.org/10.1007/978-981-10-6376-3_14

transport theory into condensed matter physics. Throughout the years, there have been tremendous developments in transport theory as described by Vijay Shenoy's lectures [2]. The most important developments took place in electronic transport theory and in quantum transport theory which includes fractional quantum Hall effect, Anderson localization, Onsager relation, etc. Today, transport theory is the key foundation of theoretical materials design. It is the most important theory in condensed matter physics. The status of transport theory in condensed matter physics is equivalent to that of the Yang Mills theory [3] in particle physics. In 1967, Philip Warren Anderson and Volker Heine coined the term condensed matter physics when they changed the name of the solid state theory group to condensed matter theory group at the Cavendish Lab, Cambridge, to combine solid state physics with liquid state physics and to reflect the important role of phase transition. Gan's Ph.D. thesis [1] also is the first to introduce statistical mechanics approach to ultrasound propagation in semiconductors in the presence of high magnetic fields and at low temperatures instead of the usual method of electron–phonon interaction and phonon–phonon interaction of many body theory. His Ph.D. thesis included the calculation of the magnetoconductivity tensor and the ultrasound attenuation coefficient which are transport properties. Thus, his Ph.D. thesis also played a role in the founding of the field of condensed matter physics. Today, condensed matter physics group is the largest group in terms of membership in the American Physical Society. This shows the importance of condensed matter physics.

14.2 Discovery of Metamaterial is Artificial Phase Transition and Singularity Behaviour of the Transport Properties of Metamaterials at the Critical Point of Phase Transition

Based on transport properties, one can discover other forms of metamaterials beyond the electromagnetic metamaterial and the acoustic metamaterial. Also, there is no need to use analogy to extend the electromagnetic metamaterial to the acoustic metamaterial because this is based on the fundamental and first principle of the

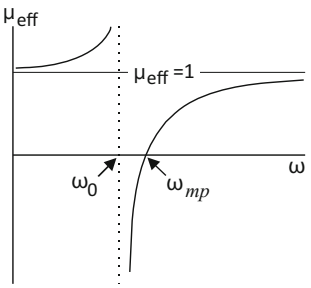

Fig. 14.1 Singularity behaviour of permeability in magnetism at the critical point of phase transition [4]

problem, the transport properties. Also, it is of interest to note that the transport properties have singularity or divergent behaviour at the critical point of phase transition. The plots of the transport properties versus frequencies show a hyperbolic shape of rising to a very high value and then a sudden drop to a huge negative value followed by a gradual rise in the negative region. This can be illustrated by Figs. 14.1, 14.2, 14.3 and 14.4.

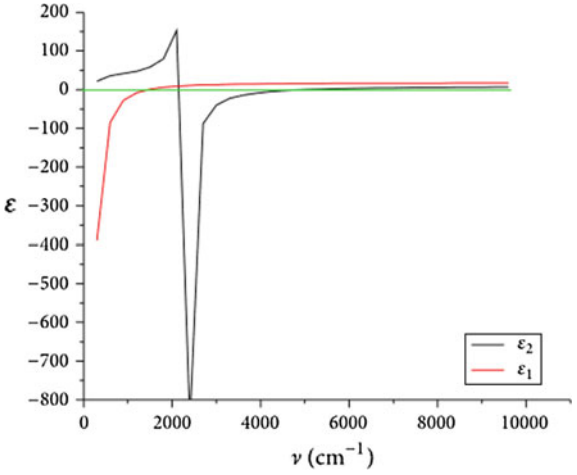

Fig. 14.2 Singularity behaviour of permittivity in high temperature superconductivity at the critical point of phase transition [5]

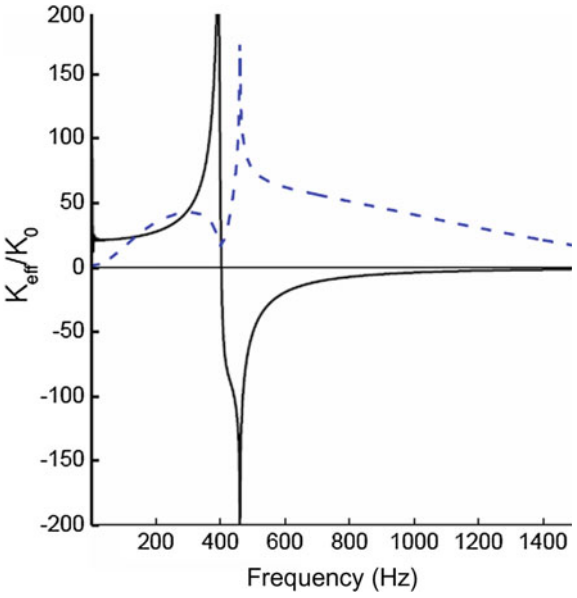

Fig. 14.3 Singularity behaviour of the bulk modulus at the critical point of phase transition or resonance frequency [6]

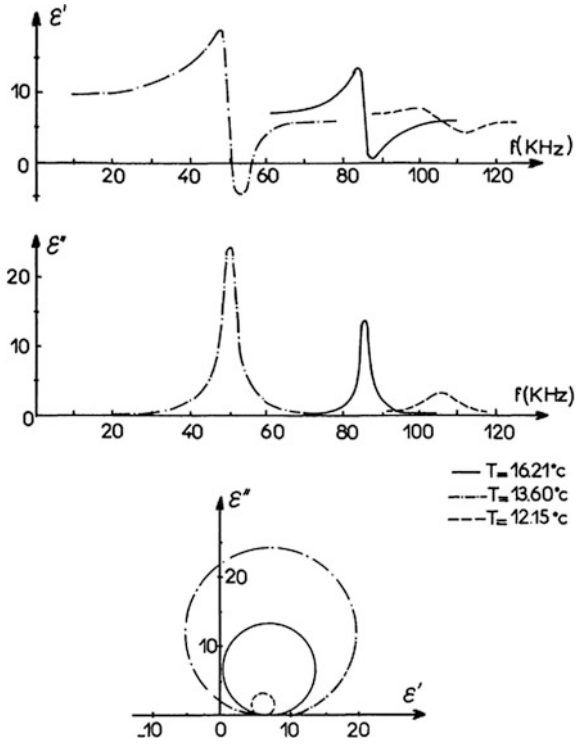

Fig. 14.4 Typical piezoelectric resonance curves and corresponding Cole-Cole diagram for a low frequency acoustic resonance mode observed in the sample $T_{\propto}$ above and below the transition temperature $T_c = 13.43\,^{\circ}\mathrm{C}$ [7]

It will be of interest to note that the second-order phase transition such as magnetization also has a singularity at the point of condensation or phase transition. This helps to support that metamaterial has phase transition characteristics.

14.3 Use of Transport Properties to Explore New Forms of Metamaterials

The double negativity of electromagnetic metamaterial and acoustic metamaterial and the singularity of the dielectric response function of high temperature superconductivity are first examples of the use of transport properties to discover new forms of metamaterials.

14.3.1 Artificial Elasticity

The singularity behaviour of the effective bulk modulus at the resonance frequency or critical point of phase transition can be exploited to fabricate acoustic metamaterial [6]. Here, there is a sudden increase in the effective bulk modulus to a very high value at the resonance frequency followed by a sudden drop to very high negative value and a gradual increase in value in the negative region. This singularity behaviour can be exploited to fabricate acoustic metamaterial using the geometric structure of split-ring resonator (SRR) with the unit cell made of elastic material. This enables the control and manipulation of the elasticity of the material. This is artificial elasticity.

14.3.2 Artificial Magnetism

Pendry et al.'s [4] paper on magnetism from conductors and enhanced nonlinear phenomena is an example of artificial magnetism. Here, the permeability, which is a transport property, shows a singularity behaviour at the critical point of phase transition with a sudden rise in the resonance frequency to positive infinite value followed by a sudden drop to negative infinite value and then a gradual rise in the negative region. The negative values of permeability are used to fabricate the negative electromagnetic metamaterial using the SRR geometric structure as the unit cell of the metamaterial, and the material of the unit cell is made of magnetic material. This enables the achievement of an electromagnetic metamaterial experimentally and the manipulation and control of magnetism. This is artificial magnetism.

14.3.3 Artificial High Temperature Superconductivity

Smolyaninov and Smolyaninova [5] proposed that high temperature superconductivity can be achieved using metamaterial. This is because dielectric response function governing electron–electron interaction can be used to increase the critical temperature of high temperature superconductivity according to Kirzhnits et al. [8]. It is found that the dielectric response function, which is a transport property, has singularity behaviour (hyperbolic shape) at the resonance frequency or the critical point of phase transition. The dielectric response function versus frequencies plot shows a sudden increase to high positive value and then a sudden drop to large negative value followed by a gradual increase in value in the negative region. This behaviour can be exploited in the fabrication of high temperature superconductor by using a geometric structure of SRR for the unit cell made of high temperature superconductor.

This enables one to manipulate and control high temperature superconductivity. Hence, the name high temperature superconductivity metamaterial.

14.3.4 Artificial Piezoelectricity

Piezoelectricity is an important phenomenon in acoustics. It provides the physical basis for almost all practical applications of acoustic fields. This is because they provide an effective means for electrically generating and detecting acoustic vibrations. It is found by Legrand [7] that the permittivity also has a singularity behaviour at the resonance frequency or point of phase transition with a sudden increase to a very high value followed by a sudden drop to negative value then a gradual increase in value in the negative region. This singularity behaviour can be used to fabricate artificial piezoelectricity by using SRR as a geometric structure of the unit cell made of piezoelectric material. This will enable the manipulation and control of piezoelectricity. This is artificial piezoelectricity.

14.3.5 Artificial Ferromagnetism

In ferromagnetism, according to Mayer [9], there is some sort of mathematical singularity at the condensation point. The transport property of ferromagnetism is magnetization or dipole moment. It is of interest to investigate the singularity behaviour of the dipole moment at the critical point of phase transition or condensation point. There will be a temperature dependence of the dipole moment besides the frequencies dependence. One will have to plot the dipole moment versus the frequencies at a series of temperatures. There will be no singularity behaviour of the dipole moment versus frequencies plots at other temperatures. However, at the critical temperature of second-order phase transition, there will be a hyperbolic shape behaviour of the dipole moment versus frequencies plot similar to that of the cases of the artificial elasticity, artificial magnetism and artificial piezoelectricity.

14.4 Metamaterial as Artificial Phase Transition as Breakthrough to a New World of Artificial Materials

Double-negativity electromagnetic metamaterial and double-negativity acoustic metamaterial are manifestations of artificial magnetism and artificial elasticity. This will be a starting point for the exploration of various new artificial materials based on metamaterial and phase transition. Immediate examples are artificial

piezoelectricity and artificial ferromagnetism. This will open to a new world of artificial materials based on other transport properties besides permeability, permittivity, effective bulk modulus and effective mass density.

14.5 Conclusions

Transport theory has come a long way with tremendous development in condensed matter physics since the term was coined by me in 1966. It has now become the key foundation of theoretical materials design. Hence, it has become the most important theory in condensed matter physics.

References

1. Gan, W.S.: Transport Theory in Magnetoacoustics. Ph.D. thesis, Imperial College London, 1969 (published as a Google Book)
2. Shenoy, V.B.: Transport Theory. Lecture Notes. SERC School on Condensed Matter Physics (2006)
3. Yang, C.N., Mills, R.: Conservation of isotopic spin and isotopic gauge invariance. Phys. Rev. **96**(1), 191–195 (1954)
4. Pendry, J.B., Holden, A.J., Robbins, D.J., Stewart, W.J.: Magnetism from conductors & enhanced nonlinear phenomena. IEEE Trans. Microw. Theory Tech. **47**(11), 2075–2084 (1999)
5. Smolyaninov, I.I., Smolyaninova, V.N.: Is there a metamaterial route to high temperature superconductivity. arxiv.org/pdf/1311.3277 (2014)
6. Sharma, B., Sun, C.T.: Acoustic metamaterial with negative modulus and double negative structure. arxiv.org/pdf/1501.02833.5
7. Legrand, J.F.: Ferroelastic and ferroelectric phase transition in a molecular crystal: tanance. 2. Phenomenological model and piezoelectric resonance study of the soft acoustic mode. J. Phys. **43**, 1099–1116 (1982)
8. Kirzhnits, D.A., Maksimov, E.G., Khomskii, D.I.: The dependence of superconductivity in terms of dielectric response function. J. Low Temp. Phys. **10**, 79 (1973)
9. Mayer, J.E., Mayer, M.G.: Statistical Mechanics. Wiley (1940)